

**DEVELOPING A SYSTEM TO INVESTIGATE AGE-RELATED
DIFFERENCES IN THE REAL-TIME UTILIZATION OF DYNAMICALLY
CHANGING EXTERNAL CUES DURING NAVIGATION**

by

Adam Ward Lester

Copyright © Adam Ward Lester 2019

A Dissertation Submitted to the Faculty of the
GRADUATE INTERDISCIPLINARY PROGRAM IN NEUROSCIENCE

In Partial Fulfillment of the Requirements
For the Degree of

DOCTOR OF PHILOSOPHY

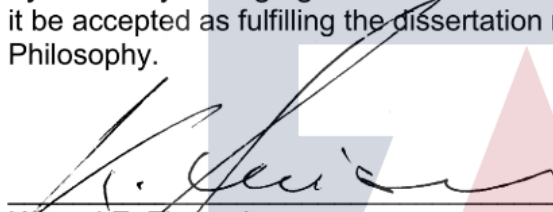
In the Graduate College

THE UNIVERSITY OF ARIZONA

2019

THE UNIVERSITY OF ARIZONA
GRADUATE COLLEGE

As members of the Dissertation Committee, we certify that we have read the dissertation prepared by Adam Ward Lester, titled Developing a system to investigate age-related differences in the real-time utilization of dynamically changing external cues during navigation and recommend that it be accepted as fulfilling the dissertation requirement for the Degree of Doctor of Philosophy.




Konrad E. Zinsmaier Date: 12/14/2018



Carol A. Barnes Date: 12/14/2018



Lynn Nadel Date: 12/14/2018



Stephen L. Cowen Date: 12/14/2018




A. David Redish Date: 12/14/2018

Final approval and acceptance of this dissertation is contingent upon the candidate's submission of the final copies of the dissertation to the Graduate College.




I hereby certify that I have read this dissertation and recommend that it be accepted as fulfilling the dissertation requirement.



Dissertation Committee Chair: Konrad E. Zinsmaier Date: 12/14/2018

I hereby certify that I have read this dissertation prepared under my direction and recommend that it be accepted as fulfilling the dissertation requirement.



Dissertation Research Supervisor: Carol A. Barnes Date: 12/14/2018

STATEMENT BY AUTHOR

This dissertation has been submitted in partial fulfillment of the requirements for an advanced degree at the University of Arizona and is deposited in the University Library to be made available to borrowers under rules of the Library.

Brief quotations from this dissertation are allowable without special permission, provided that an accurate acknowledgement of the source is made. Requests for permission for extended quotation from or reproduction of this manuscript in whole or in part may be granted by the head of the major department or the Dean of the Graduate College when in his or her judgment the proposed use of the material is in the interests of scholarship. In all other instances, however, permission must be obtained from the author.

SIGNED: Adam Ward Lester

ACKNOWLEDGEMENTS

I would like to start by individually thanking my committee members for the invaluable intellectual energy and time they invested to help get me to this point. Thank you to **David Redish** for bringing his encyclopedic knowledge of the computational theories surrounding navigation research to bear against this work, and **Lynn Nadel**, who, after his long and distinguished career, not only tolerated but kindly corrected every unchecked grammatical error included in the first draft of this thesis. Thank you as well to **Stephen Cowen**, who always made himself available for impromptu discussions, and **Konrad Zinsmaier**, whom I have long admired for his unique style of mentorship that blends equal parts no-nonsense skepticism and genuine kind-heartedness. Finally, I feel a tremendous amount of gratitude to my advisor **Carol Barnes** for making me accountable for my ideas and challenging them at those times when I was being stubborn or myopic in my thinking, while also being a consistent source of support, intellectual perspective, and renewed optimism during those periods when my confidence was shaken. I feel extremely grateful to have found a home her lab and could not have asked for a better advisor, mentor and role model for what is achievable when one sets their mind and heart to a goal.

I also must thank the many other individuals in the lab who have guided and mentored me in one form or other through this process. Thank you to **Rachel Samson** and **Peter Lipa**, both of whom readily shared so much of their practical experience and knowledge when I was first learning the ropes. Thank you as well to **Sara Burke**, who has been a voice of reason and guidance through the years, and **Andrew Maurer**, whose tough love approach to mentorship fostered my intellectual curiosity while also teaching me to stand firm and ‘pull no punches’ when defending my ideas. To my lab sibling **Daniel Gray**, whose ability to calmly balance the many demands inherent to the graduate experience has been a useful, and sometimes comic, contrast to my more manic and hyper-focused temperament. To our other lab brother **Colin Kyle**, who has been a great resource for esoteric and out-of-the-box approaches to analysis. Finally, to our newest member **Sahana Srivathsa**, whose passion and enthusiasm has helped reinvigorate my own excitement and temper some of my late-stage dissertation curmudgeonliness.

It is hard to imagine how this dissertation work could have been completed without the help of all the hardworking and dedicated undergraduate students who I have had the pleasure of mentoring over the years: **Colton Blum**, **Ali Gilliland**, **Kaitlyn Martin**, **Surbhi Patel**, **Robert Screen**, **Jessica Burkhart**, and **Sandra Arnautovic**. I feel a particularly large debt of gratitude to **Adele Kapellusch**, who was involved with the project from the start and, I must say, really spoiled me in terms of expectations for any students that came after by consistently going above and beyond what was expected, while being the embodiment of patience

and kindness through it all.

I have been fortunate enough to be in a lab with a large and truly capable administrative and technical support team. Thank you to **Luann Snyder, Michelle Albert, Michelle Carroll, Marc Zempare** and **Natalie Carey**, who have made so much of my graduate research experience an easier and more fluid process. Thank you also to **Michael Montgomery** for keeping the servers and computers humming along and to **Kim Bohne** for the effort and ocular strain she has invested in building our microdrives as well as the creativity and enthusiasm she has shown as we have worked to design a 'bigger better mousetrap'.

It is often easy to forget that there is a world beyond the lab, particularly during those fevered periods completing a project or knuckling down to make a deadline. Thankfully I have had many loving and understanding people throughout this time who have reminded me to keep some balance and take time out for the other things in life, while also weathering my absences when I occasionally ignored their sage advice (and texts). To my mother, **Cynthia Lester**, whose love and unwavering support I have always been able to rely on. Throughout my life she has encouraged my passions, whatever direction they happened to pull me, and her playful and often sardonic sense of humor has helped me to see the comedy in even the most difficult periods. To my late stepfather, **Allen Jackson**, who I wish I had the opportunity to tell now, with the perspective of time, how grateful I am for the role he filled in my life and the impact he had on shaping the person I am today. To **Zenara** and **Lili**, who have blessed me with the opportunity to experience the joys of being in the father role myself. I am deeply grateful to them both for reminding me how to have fun and be present, and for giving me a chance to take a break and play. It has been such a pleasure to watch the two of them grow into the amazing people they have become and I am so proud of them both.

TABLE OF CONTENTS

LIST OF FIGURES	9
ABSTRACT	11
CHAPTER 1: INTRODUCTION	14
1.1. Spatial cues and frames of reference	15
1.2. Cognitive representations of space	18
1.3. Spatial processing within the entorhinal-hippocampal system	22
1.4. Assessing and dissociating navigational strategies	28
CHAPTER 2: AGE-RELATED CHANGES IN SPATIAL NAVIGATION	30
2.1. Age-related changes in spatial information processing during active navigation	30
2.2. Age-related changes in plasticity and synaptic signaling	35
2.3. Age-related alterations in the creation, consolidation and retrieval of memory traces	43
2.3.1. Place learning and cognitive mapping	44
2.3.2. Route-based learning and hippocampal sequences	49
2.3.3. Consolidation of spatial memories	56
2.4. Age-related differences in spatial navigation performance and strategy selection	59
2.5. Alterations in spatial processing and navigation in age-related neuropathology	64
2.6. Conclusions	71
CHAPTER 3: DEVELOPING A NOVEL SYSTEM FOR ASSESSING DYNAMIC VISUAL CUE CONTROL OF NAVIGATION BEHAVIOR IN RODENTS	73
3.1. Introduction	73
3.1.1. Differentiating the role of allothetic and idiothetic feedback in navigation and spatial representation networks	73
3.1.2. Stability of spatial representations	78
3.1.3. The time-course of spatial representation updating	82
3.1.4. Assessing navigation in virtual reality environments	85
3.1.5. Aims and design principles	86
3.2. Materials and methods	88
3.2.1. Subjects	88
3.2.2. Instantaneous Cue Rotation apparatus design	89
3.2.3. Fixed feeder reward system	91
3.2.4. Mobile feeder reward system	92
3.2.5. Software	95
3.2.6. Instantaneous Cue Rotation experiment	96
3.2.7. Training on the Instantaneous Cue Rotation task	98
3.2.8. Testing on the Instantaneous Cue Rotation task	101
3.2.9. Data analysis	102

3.2.10. Statistical analysis	104
3.3. Results	105
3.3.1. Training on the Instantaneous Cue Rotation task.....	105
3.3.2. Goal navigation performance on the Instantaneous Cue Rotation task.....	107
3.3.3. Influence of visual cue rotation on overall running behavior .	113
3.4. Discussion.....	120
3.4.1. Summary of salient results	120
3.4.2. Design considerations	122
3.4.3. Performance differences on the fixed feeder and mobile feeder versions of the Instantaneous Cue Rotation task.....	127
3.5. Conquering confounding odor cues	134
CHAPTER 4: ASSESSING OLD AND YOUNG RATS ON THE INSTANTANEOUS CUE ROTATION TASK	139
4.1. Introduction	139
4.2. Methods	151
4.2.1. Age comparison of behavioral performance on the Instantaneous Cue Rotation task.....	151
4.2.2. Attractor network-based model of the Instantaneous Cue Rotation task.....	152
4.3. Results	156
4.3.1. Age-related differences in goal navigation performance.....	156
4.3.2. Age-related differences in visual cue control of overall running behavior	162
4.3.3. Model of directional representation updating during simulated instantaneous cue rotation.....	170
4.4. Discussion.....	180
4.4.1. Summary of salient results	180
4.4.2. Age-related differences in the Instantaneous Cue Rotation task	182
4.4.3. Implications of the behavioral findings within the context of the proposed computation model and existing electrophysiological findings	190
CHAPTER 5: ONGOING WORK AND FUTURE DIRECTIONS FOR INVESTIGATING AGE-RELATED CHANGES IN ENTORHINAL- HIPOCAMPAL SPATIAL UPDATING.....	199
5.1. Pilot MEC and CA1 recordings assessing realignment following manual rotation of visual cues.....	206
5.1.1. Material and methods	208
5.1.2. Results	211
5.1.3. Discussion	215
5.2. Developing technologies for simultaneous hippocampal and MEC recording	222

CHAPTER 6: SUMMARY AND CONCLUSIONS	232
6.1. Summary of the thesis	232
6.2. Conclusions	238
REFERENCES	246

LIST OF FIGURES

Figure 1.1: Navigation within different spatial reference frames.	18
Figure 1.2: Spatially-modulated cells and the entorhinal-hippocampal network.	22
Figure 2.1: Neurophysiological changes with age.	34
Figure 2.2: Correspondence of age-related navigational deficits in rodents and humans in cognitive mapping.	45
Figure 2.3: Route and sequence learning.	51
Figure 2.4: Correspondence of age-related navigational deficits in rodents and humans: Strategy preferences.	64
Figure 2.5: Alzheimer’s disease-related grid cell dysfunction in mice and humans.	67
Figure 3.1: Schematic of the Instantaneous Cue Rotation apparatus.	90
Figure 3.2: Reward delivery systems for the fixed and mobile feeder versions of the Instantaneous Cue Rotation task.	92
Figure 3.3: Reward schedule for the fixed and mobile feeder versions of the Instantaneous Cue Rotation task.	94
Figure 3.4: Instantaneous Cue Rotation (ICR) task overview.	97
Figure 3.5: Procedure for quantifying behavioral realignment.	103
Figure 3.6: Goal navigation performance and accuracy on the Instantaneous Cue Rotation task.	106
Figure 3.7: Comparison of running velocity at all positions along the track between the two versions of the task.	109
Figure 3.8: Effects of cue rotation on running velocity preceding goal arrival.	113
Figure 3.9: Comparison of behavioral realignment following cue rotation for the two versions of the task.	116
Figure 3.10: Time-course of behavioral realignment following cue rotation.	118

Figure 4.1: Delayed realignment of aged place fields in response to allothetic and idiothetic mismatch.	144
Figure 4.2: Ring attractor model of head direction encoding.	147
Figure 4.3: Overview of the head direction cell model.	151
Figure 4.4: Goal navigation performance in old and young rats.	156
Figure 4.5: Goal navigation accuracy in old and young rats.	158
Figure 4.6: Age-related differences in goal-related running velocity.	160
Figure 4.7: Age-related differences in behavioral realignment following cue rotation.	162
Figure 4.8: Magnitude and time-course of behavioral realignment in young and aged rats.	168
Figure 4.9: Influence of allothetic and idiothetic input on directional updating in the head direction network model.	171
Figure 4.10: Time-course of realignment in the head direction network model following visual cue rotation.	172
Figure 4.11: Effects of combined idiothetic error and allothetic rotation in the head direction network model.	175
Figure 4.12: Comparison of attractor network realignment with varying levels of idiothetic error.	179
Figure 5.1: Histology from CA1 and MEC implanted rats.	210
Figure 5.2: Example visual cue rotation-induced firing field realignment following rotation of the running enclosure.	212
Figure 5.3: Example of delayed realignment of MEC head direction cells following cue rotation.	215
Figure 5.4: Optimizing tetrode configurations for the target regions of interest.	225
Figure 5.5: Initial designs for a dual-bundle drive.	227
Figure 5.6: Modified Neuralynx Halo-18 microdrive and Cube2 wireless recording system.	231

ABSTRACT

Successful navigation depends critically upon two broad categories of sensory information, environmental (allothetic) and self-motion (idiothetic). Both the hippocampus and the medial portion of the entorhinal cortex (MEC) are critical for spatial navigation and contain functionally distinct sub-networks of spatially-modulated cells. These cells are characterized by their tuning to different spatial sensory-perceptual features of the environment and all utilize both allothetic and idiothetic cues to anchor and update their spatial firing to generate a comprehensive and dynamic representation of space. As with older adults, aged rats show pronounced impairments on a number of different spatial navigation tasks and these impairments are accompanied by a bias toward relying on egocentric over allocentric navigation strategies. Similarly, the hippocampus and MEC are also highly susceptible to age-associated changes. The influence visual allothetic cues exert on hippocampal place cell spatial tuning is diminished and delayed in aged animals. Two plausible and non-exclusive explanations that could account for these age-related alterations in allothetic processing are 1) circuit disruptions caused by known age-related functional and anatomical changes in the entorhinal-hippocampal processing pathway or 2) degraded sensory-perceptual information resulting from well-established age-related deficits across multiple sensory domains. Either of these possibilities could have the effect of either slowing allothetic cue processing or weakening the

ability of these cues to influence firing field alignment. Within this context, this thesis was conceived with the aim of investigating the degree and timing with which young and aged animals utilize allothetic and idiothetic feedback to update their internal representation of space and calibrate their behavioral output. A large focus of this thesis is given to the incremental design and piloting of a number of novel technologies. Foremost among the methodological contributions of this study is the development of an augmented reality behavioral apparatus, termed the Instantaneous Cue Rotation (ICR) arena, which utilizes projected visual cues to allow for rapid remote control of all symmetry breaking visual features in the environment as rats actively engage in a visual-cue based goal navigation task. The results of extensive behavioral piloting of old and young rats validate both the ICR rotation manipulation as well as the mobile reward delivery system. This system traverses the track in tandem with the rat, enabling food based spatial reinforcement while preventing food-related olfactory cues from becoming associated with any specific location. In parallel with this work, microdrive technology was developed to enable simultaneous recording from both MEC and CA1 which is discussed along with results from single-region hippocampal and MEC implanted rats assessed in the context of a cue rotation manipulation conceptually similar to the that of the ICR. Finally, the results of the behavioral study suggest that in young rats the cue rotation exerts reliable but incomplete control over running behavior. In aged rats, by comparison,

the cues exert an overall less pronounced influence on running behavior, consistent with known age-related deficits in allothetic processing. When assessed on a lap-by-lap basis, it was found that the behavior of both young and aged rats became progressively more aligned with the cues over the first few laps following cue rotation. These findings suggest a progressive realignment of behavior from an egocentric to an allocentric reference frame which is reminiscent of the reported progressive realignment of place field firing in response to conflicting spatial feedback.

CHAPTER 1: INTRODUCTION

The world's population is aging at an unprecedented rate.

According to the WHO, the number of people aged over 60 is set to rise to 2 billion by 2050, all of whom will have to cope with some form of either normative or pathological cognitive decline. While a large body of research into cognitive aging has focused on functions such as memory and attention, relatively few studies have investigated changes in spatial navigation. This is surprising because key structures of the brain's navigation circuit are particularly vulnerable to the deleterious consequences of aging. Hence, detection of navigational deficits should provide a distinct metric for assessing age-related cognitive decline. Furthermore, recent breakthroughs in understanding the cellular components of basic navigational circuits in a variety of species, including rodents, bats and nonhuman primates, provide the opportunity to distinguish those network changes that occur as a result of normative aging processes from those imposed by specific neuropathological conditions.

In surveys, older people indeed report substantial declines in navigational capabilities (Burns, 1999), which can severely restrict mobility and social participation. Self-reported difficulties and objective tests are consistent with the observations of altered spatial cognition in all species examined. For example, older humans show deficits in tasks designed to test spatial navigation (e.g., Moffat, 2009) as do nonhuman primates (e.g.,

Rapp et al., 1997), dogs (e.g., Head et al., 1995), rats (e.g., Barnes, 1979) and mice (e.g., Bach et al., 1999) and these problems cannot be explained solely by general, age-related declines in cognitive (e.g., reduced processing speed) or motor functioning. The following sections will provide an introduction to the behavioral and neural mechanisms that subserve navigation in order to provide a framework for a more detailed discussion of the navigational impairments which occur in old age.

1.1. Spatial cues and frames of reference

Across a broad range of species, including humans, navigation is one of the most fundamental behaviors. The operations that subserve navigation depend on a multitude of ongoing cognitive functions and processes. Navigation depends on perceiving spatial information from multiple sensory cues that can be broken down, broadly, into two distinct categories. The first, *idiothetic* cues, signal information about movements of the body. Idiothetic cues include those derived from vestibular, proprioceptive and locomotor feedback, all of which can be used to keep track of one's position and orientation. Following primary sensory processing, these cues are first integrated in brainstem nuclei to yield estimates of angular and linear movement velocity. In primates, idiothetic (i.e., self-motion) information is further processed in parietal/superior temporal cortices. The second class, *allothetic* cues, signal information about things external to the organism. Allothetic cues include objects or

environment features, which typically are stable spatial reference points such as landmarks and extended boundaries that can be used to determine one's position and orientation relative these external spatial cues. In primates, these cues are predominantly derived from visual perception, but other species also make heavy use of non-visual cues (i.e., auditory, olfactory and tactile stimuli). Following primary sensory processing, these cues are first integrated in brainstem nuclei to yield estimates of angular and linear movement velocity. Similarly, optic flow arising from visual perception also provides idiothetic information to the organism. Both types of idiothetic cues are further processed in parietal/superior temporal cortices, thus providing an integrated percept of self-motion.

Within the category of allothetic (i.e., environmental) cues is an additional classification of exteroceptive cue types that include local (i.e., proximal) cues and distal cues. The precise definitions of these classifications can vary depending on experimental condition, era in which the experiment was conducted, and individual preference (for review of these considerations, see Knierim & Hamilton, 2011). Broadly defined, *local* cues are those that are near and physically accessible to the rat, such as the behavioral enclosure. Conversely, *distal* cues are distant and physically inaccessible, such as the walls of the recording room.

The mammalian brain uses these multisensory spatial cues to build up a variety of spatial representations. Again, these representations are

typically conceptualized within the framework of two broad categories that are commonly used to characterizing what spatial reference frame an animal is operating in. An *allocentric* reference frame describes situations in which spatial information, such as the position of a landmark, is encoded with respect to other objects in the environment (**Figure 1.1A**). Allocentric representations are independent of the position of the navigator and do not change as the navigator moves through space. The prototypical allocentric navigation task is wayfinding, whereby one must the plan a novel route through a familiar space. An *egocentric* reference frame, in contrast, describes situations in which spatial information is encoded relative to the navigator (**Figure 1.1B**). The prototypical egocentric navigation task is route navigation, which can be solved using egocentric navigation strategies and codes such as make a left at landmark x. In the simplest terms, an allocentric reference frame is independent of the position of the navigator and does not change as the navigator moves through space while an egocentric reference frame involves representations of locations that are encoded relative to the navigator. Importantly, egocentric reference frames can be informed by both idiothetic and allothetic cues such as is the case for optic flow, in which visual sensory perceptual information (e.g., allothetic cues) carry information about egocentric-based movement.

1.2. Cognitive representations of space

As previously described, the mammalian brain uses idiothetic and allothetic cues to build up a variety of spatial representations. The first window into such representations came from O'Keefe and Dostrovsky's observation (1971) that the firing properties of rodent hippocampal principal cells are tuned to the region of space an animal is in. These *place cells* inspired ideas about how space provides a scaffold for integrating multimodal features of a given experience or episode. Cells with similar, although not necessarily identical, properties have subsequently been found in a number of mammalian species including mice (e.g., McHugh et al., 1996), bats (e.g., Ulanovsky and Moss, 2007),

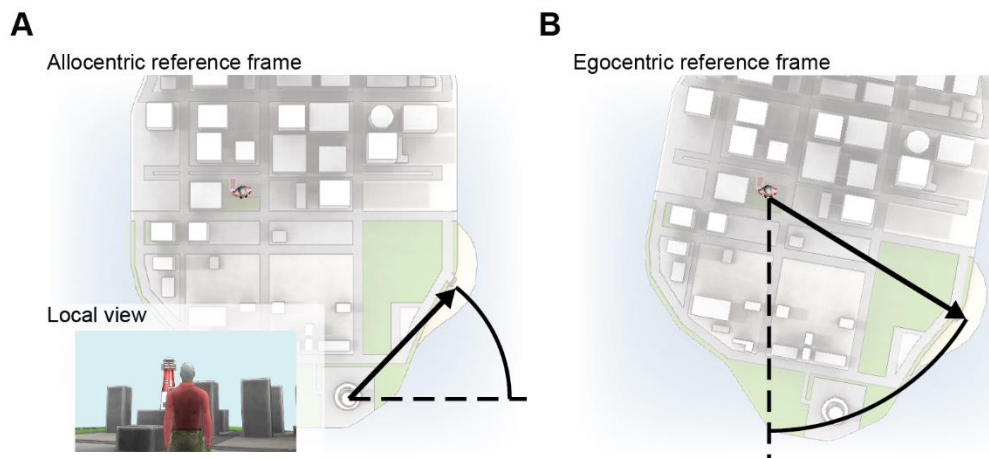


Figure 1.1: Navigation within different spatial reference frames.

(A) An example of an *allocentric* reference frame. The position of a landmark (i.e., beach), is encoded with respect to *allothetic* cues in the environment (e.g., lighthouse). The dashed line represents the allocentric reference direction that is fixed with respect to the dominant geometric boundary, and the solid arrow represents the allocentric direction to other features in the space. The *local view* of the observer is also shown, illustrating the available sensory inputs within the visual field of view of the observer's current position and orientation. **(B)** An example of an *egocentric* reference frame in which space is encoded with respect to *idiothetic* cues including distance and direction from the observer. The dashed line represents the egocentric reference direction, which is aligned to the orientation of the observer, and the arrow denote the egocentric self-to-object distance and direction.

humans (e.g., Ekstrom et al., 2003) and non-human primates (e.g., Feigenbaum and Rolls, 1991). O'Keefe and Nadel (1978) went on to describe how space and navigation through it anchors our daily experiences within the hippocampus to create a cognitive map.

An ever broadening catalogue of functionally distinct sub networks of spatially-modulated neurons have been identified that collectively constitute what O'Keefe and Nadel (1978) originally referred to as the cognitive map of space (**Figure 1.2A**). First, *head direction* cells signal the orientation of an organism's head in the horizontal plane (Taube et al., 1990a). These cells were first observed in the dorsal presubiculum by Ranck (1985) and later in a network of structures including thalamic nuclei, mammillary bodies, parasubiculum, retrosplenial and entorhinal cortices (for review, see Taube, 2007). Neuroimaging studies have provided corresponding evidence for head direction coding in humans (Shine et al., 2016). Additionally, distance and direction to boundaries are signaled by *border cells* or *boundary vector cells*, which have been found in entorhinal cortex, subiculum, pre- and parasubiculum (Solstad et al., 2008; Lever et al., 2009; Boccara et al., 2010). More recently, *grid cells* have been found in entorhinal cortex, subiculum, pre- and parasubiculum (Fyhn et al., 2004; Solstad et al., 2008; Lever et al., 2009; Boccara et al., 2010) in several species, including rats (Hafting et al., 2005), primates (Jacobs et al., 2013), bats (Yartsev et al., 2011). Additionally, there is indirect evidence for grid cells in humans (Doeller et al., 2010). Grid cells

fire in multiple locations in the environment forming a repeating hexagonal grid-like pattern that spans the entirety of the environment. One of the most recent cell type to be added to the pantheon of spatially-modulated neurons is the *speed cell* (Kropff et al., 2015). Speed cells have been identified in the hippocampus and MEC. These cells are not influenced by external features of an environment but instead their firing rate varies as a function of an animal's running speed.

Collectively, place, grid, head direction and speed cells are part of the neural substrate of a cognitive map. All are thought to contribute to the computations required for successful navigation and the generation of an integrated internal representation of space. While the firing of all these cell subtypes is likely influenced by both allothetic and idiothetic cues, each may utilize these cues differently to perform distinct computational functions. With respect to idiothetic cues, vestibular information is required for robust and stable place cell spatial representations (Stackman et al., 2002; Ravassard et al., 2013). Additionally, angular vestibular information is necessary for directional tuning in head direction cells (Stackman and Taube, 1997; Muir et al., 2009) and, even in the absence of other spatial feedback, is sufficient for their initial generation (Shinder and Taube, 2011). A subset of grid cells also show heading and velocity modulation (Sargolini et al., 2006; Kropff et al., 2015). In addition, various features of grid fields are environment invariant (Fyhn et al., 2007) and MEC lesions have recently been shown to impair linear distance estimation in rats

(Jacob et al., 2017a). Together these qualities of the grid network suggest that grid cells may be preferentially influenced by idiothetic cues (Redish and Touretzky, 1997; Redish, 1999; McNaughton et al., 2006; Kropff et al., 2015). Importantly, the spatial tuning of head direction (Taube et al., 1990b) and grid cells (Hafting et al., 2005; Chen et al., 2016; Pérez-Escobar et al., 2016) is also dependent on allothetic cues. Furthermore, the rotation of visual cues has been shown to induce a proportional rotation in place cells (e.g., O'Keefe and Conway, 1978), head direction cells (e.g., Taube et al., 1990b), grid cells (e.g., Hafting et al., 2005) and border cells (e.g., Solstad et al., 2008). As such, visual cues are important for aligning internal spatial representation to an allocentric reference frame (Gallistel, 1990). Finally, environment geometry dictates not just border cell spatial firing, but also a number of spatial features of grid field organization (Barry et al., 2007; Derdikman et al., 2009; Krupic et al., 2015; Stensola et al., 2015). In summary, spatial processing is subserved by diverse sub-networks of functionally specialized cells that utilize a complex mixture of idiothetic and allothetic cues to generate an information-rich representation of space.

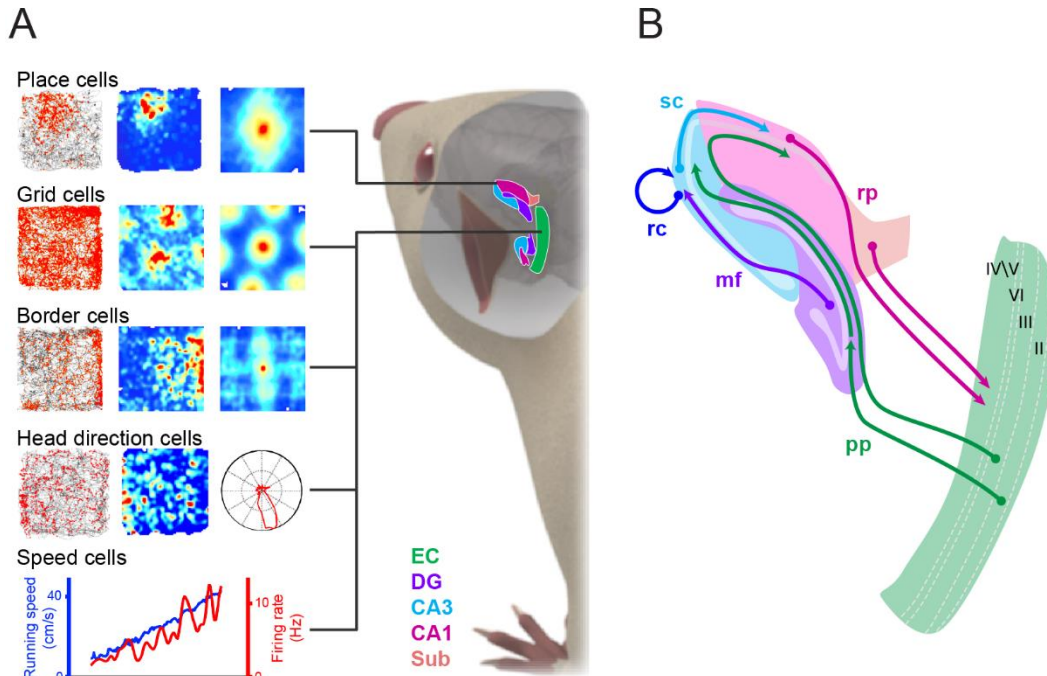


Figure 1.2: Spatially-modulated cells and the entorhinal-hippocampal network.

(A) Sagittal view of the rat brain showing the sub-regions of the hippocampus and entorhinal cortex along with representative firing fields of the various types of spatially-modulated cells within these regions. The speed cell graph shows running speed and cell firing rate by position and was adapted from Kropff et al. (2015). All other spatially modulated units were recorded from rats traversing a 50 cm by 50 cm square enclosure. Recordings were collected from two separate rats, one of which was implanted over either intermediate CA1 or medial entorhinal cortex. Graphs on the left show running trajectory (black) and firing position for each spike (red). Graphs in the center show firing rate maps, with firing rate indicated by colors ranging from cool to warm. Graphs on the right show 2D spatial autocorrelation or head direction tuning. **(B)** Schematic illustrating the major entorhinal-hippocampal and intrahippocampal projections. EC: entorhinal cortex; DG: dentate gyrus; Sub: subiculum; pp: perforant path; mf: mossy fibers; rc: recurrent collaterals; sc: Schaffer collaterals; rp: return projections from CA1 to EC.

1.3. Spatial processing within the entorhinal-hippocampal system

Evidence from anatomical, neurophysiological and modeling studies suggest that the individual sub-networks of the greater entorhinal-hippocampal system have some degree of regional specialization, not just with respect to the types of spatial information their constituent cells encode, but also in terms of the spatial and mnemonic computations these

sub-networks perform. In order to understand how sensory-perceptual input is processed into the various abstracted spatial/mnemonic representations generated by the entorhinal-hippocampal system it is important to first consider the anatomical organization and inter-regional pathways through which sensory-perceptual information is processed (**Figure 1.2B**). The entorhinal cortex (EC) provides the majority of neocortical input to the hippocampus and is segregated into two main sub-regions. These include the medial entorhinal cortex (MEC) and the lateral entorhinal cortex (LEC), each of which have characteristically different patterns of neocortical connectivity. Notably, the MEC is preferentially connected with postrhinal, occipital and parietal cortex, while the LEC is strongly connected with perirhinal, insular and prefrontal areas (Insausti et al., 1997; Burwell and Amaral, 1998, 1998). Multi-modal sensory-perceptual information reaches the hippocampus from EC via the perforant path, which is organized such that principle cells of layer II EC projects to dentate gyrus (DG) and CA3 while layer III EC cells project to CA1 (for review, see Witter and Amaral, 2004). Each of the hippocampal subregions are, in turn, connected in a predominantly unidirectional manner with DG granule cells sending sparse, powerful and divergent afferents to CA3 through the mossy fiber pathway, while CA3 projects to CA1 via the Schaffer collateral pathway. Finally, CA1 and subiculum send return projections to deep layers IV/VI of EC allowing for bidirectional information flow.

Based on theoretical models (Marr, 1971; McNaughton and Morris, 1987; O'Reilly and McClelland, 1994; Treves and Rolls, 1994; Redish, 1999), and experimental work (Guzowski et al., 2004; Lee et al., 2004a; Leutgeb et al., 2004; Vazdarjanova and Guzowski, 2004), each hippocampal subregion is thought to perform distinct operations related to the encoding and retrieval of spatial representations. The dentate gyrus (DG) with its disproportionately large population of granule cells receives minimally overlapping projections from the entorhinal cortex that could serve to expand the representational space in downstream CA3 principal cells (Marr, 1971). This process of *pattern separation* decorrelates cortical inputs in order to minimize the overlap between neurons recruited to encode successive memory traces. This allows for maximally dissimilar network projection to CA3 pyramidal cells, increasing memory storage efficiency (Marr, 1971). Alternatively, *pattern completion* enables reinstatement of a previously encoded spatial/mnemonic representation in the presence of partial or degraded input (Marr, 1971; McNaughton and Morris, 1987). The anatomical implementation of this process is thought to involve the autoassociative connections of CA3 principal cells. These connections functionally couple coactive cells at the time of encoding so that later activation of a sufficient subset will propagate to all members of the cell assembly resulting in a complete, or near complete, reinstatement of the learned pattern. When confronted with sensory-perceptual input patterns that have some degree of feature

overlap with a previously experienced environment, the network must determine if the similarity in input patterns indicates that the current environment is the same as a previously experienced environment or, alternatively, signals that the navigator is experiencing a new, although perceptually similar, environment. The bias of the network to resolve this input ambiguity by either pattern completing to a stored representation or pattern separating to a new and distinct map likely depends on the degree of feature overlap (O'Reilly and McClelland, 1994; Redish, 1999; Guzowski et al., 2004; Yassa and Stark, 2011). In either instance, the representation generated by CA3 that is fed forward to CA1, will not necessarily match the signal relayed by the EC. It has been proposed that CA1 may act as a *comparator* of the modified CA3 representations, and the direct and relatively unmodified cortical sensory input it receives directly from layer III of the entorhinal cortex (Hasselmo et al., 1995; Vinogradova, 2001), providing the final hippocampus-processed output back to the neocortex through its major return pathway.

Several converging lines of evidence suggest that MEC may be the primary anatomical locus of a *path integration* operation (Redish and Touretzky, 1997; Redish, 1999; McNaughton et al., 2006), whereby an animal's current position can be continually updated on the basis of idiothetic cues alone through the integration of distance and heading information (Mittelstaedt and Mittelstaedt, 1980; Gallistel, 1990). The real-time speed and heading signals carried by MEC speed and head direction

cells, as well as a subset of grid cells, are ideally suited for path integration computations (Sargolini et al., 2006; Kropff et al., 2015). Furthermore, speed cell tuning is environment invariant as are various features of grid cell firing fields (Fyhn et al., 2007). Considered together, these qualities of the MEC network, coupled with the finding that lesioning of MEC, but not hippocampus, results in impaired estimations of linear distance (Jacob et al., 2017a), provide compelling support for the MEC's role in path integration operations. Importantly, most path integration tasks also require an estimate of the distance and heading of a goal location (i.e., vector towards an allothetic landmark), which has been linked to hippocampal/entorhinal and parietal computations (Wolbers et al., 2007; Chadwick et al., 2015; Sarel et al., 2017). As such, visual cues are important both for aligning internal spatial representations to an allocentric reference frame as well as to correct for path integration errors that accumulate over time and space (Mittelstaedt and Mittelstaedt, 1980; Gallistel, 1990; Benhamou, 1997; Redish, 1999).

Finally, several well characterized slow and fast oscillations are believed to play an important role in coordinating the neuronal firing in the entorhinal-hippocampal system. These oscillations are present in the recorded local field potential (LFP), which provides information about synchronized population activity in the form of summed extracellular currents present in a local volume of brain tissue. One of the most prominent of these cross-regional LFP oscillations is the theta rhythm

(Vanderwolf, 1969; Buzsàki and Eidelberg, 1983; O'Keefe and Recce, 1993). These theta oscillations are thought to be critical for synaptic plasticity (Huerta and Lisman, 1995; Pavlides et al., 1988) and coordination of episodic and spatial memories (Hasselmo, 2005a; O'Keefe and Burgess, 2005a). Interestingly, the spatially tuned cells in MEC and hippocampus tend to fire at distinct and different phases of the local theta rhythm, suggesting that theta may coordinate semi-independent computations in different subdivisions of the entorhinal-hippocampal system (Buzsàki and Eidelberg, 1983; Mizuseki et al., 2009; Jeewajee et al., 2014). For instance, it has been suggested that theta oscillations could segregate the encoding and retrieval of episodic memories by partitioning entorhinal-hippocampal and intrahippocampal processing by within distinct phases of theta (Hasselmo, 2005a; O'Keefe and Burgess, 2005b). MEC and hippocampus are also coupled by a fast gamma oscillation (70-140 Hz), whereas CA1 and CA3 show increased synchronization in a slower gamma band (30 – 60 Hz) (Colgin et al., 2009). Collectively, these findings suggest that various slow and fast oscillations could subserve information transfer by providing a temporal window that can pace neural excitability and allow for segregation of neuronal information processing within the hippocampus (Skaggs et al., 1996; Hasselmo et al., 2002; Hasselmo, 2005a; Dragoi and Buzsàki, 2006; Diba and Buzsàki, 2008; Sirota et al., 2008), and across the entorhinal-hippocampal network (Mizuseki et al., 2009; Mitchell and Ranck Jr, 1980).

1.4. Assessing and dissociating navigational strategies

Humans and other animals face a variety of navigation tasks on a daily basis. Both the navigation strategies and neural computations employed to solve these tasks critically depend on the availability of environmental cues and the agent's knowledge of the space, the location of the destination, and the path to the destination (Wiener et al., 2009; Wolbers and Wiener, 2014). Importantly, because any strategy is likely the consequence of the complex interactions between various characteristics of the spatial context and the individual participant, it is difficult to design a task that is inherently egocentric or allocentric without taking into account the behavior and cognitive processes of the navigator (Ekstrom et al., 2014). For instance, older humans and other animals will differ from younger individuals in the strategic approaches used to solve even the simplest two choice T-maze or Y-maze (Barnes et al., 1980; Rodgers et al., 2012). Nevertheless, some tasks may lend themselves to egocentric strategies such that the adoption of one strategy over the other will more readily result in success.

To conclude, successful everyday navigation is a particularly complex behavior relying on a range of perceptual, mnemonic and executive computations. It requires the integration of different types of spatial information, the selection of the appropriate navigation strategy and, if circumstances change, switching between strategies. Moreover, navigation typically involves coordinating a number of different sub-tasks

or processes. Given this complexity, age-related declines in navigation likely result from a multitude of mechanisms as will be discussed in the next chapter.

CHAPTER 2: AGE-RELATED CHANGES IN SPATIAL NAVIGATION

2.1. Age-related changes in spatial information processing during active navigation

The cognitive map is a high level and abstract representation of space that is fundamentally derived from the integration of various multimodal sensory streams. As a consequence, successful navigation is contingent on the quality of perceptual information that informs those downstream computations responsible for generating the spatial tuning of the many spatially-modulated cells described. Even though older adults are known to experience various changes in visual perception (e.g., visual acuity; contrast sensitivity), perceiving the position of static external objects is unimpaired. For example, older adults outperform younger participants in the perception of egocentric distances (4-12m) in an outdoor environment, because they show less compression of space at longer distances (Bian and Andersen, 2013). These results are in line with other studies showing intact perception of surface slant in old age (Norman et al., 2009), which is an important cue for distance perception. Similarly, other studies found no impairment when older participants estimated the distance between two external objects (Norman et al., 2015), demonstrating that neither egocentric nor allocentric distance perception are significantly affected by age.

In contrast to the preserved perception of static spatial relationships, older adults exhibit subtle deficits in perceiving self-motion

direction and speed. For example, Warren and colleagues (Warren Jr et al., 1989) found a small but significant age-related decline of about 1-2° in the ability to perceive heading direction, and subsequent studies have reported similar results with a range of optic flow stimuli (Kavcic et al., 2011; Lich and Bremmer, 2014). Importantly, such deficits are also observed when self-motion is computed from body-based cues and used to regulate walking speed (Roditi and Crane, 2012; Lalonde-Parsi and Lamontagne, 2015). Note, however, that self-motion perception in everyday navigation is normally based on body-based and visual cues simultaneously, and older adults appear to at least partially compensate for the unisensory deficits by recalibrating the relative weights given to each cue type (Bates and Wolbers, 2014; Lalonde-Parsi and Lamontagne, 2015).

Age-related deficits in idiothetic perception have been linked to several mechanisms. First, neuron loss or reduced GABAergic inhibition in areas VIP and MT/MST (Lich and Bremmer, 2014) increase the level of noise and decrease the directional tuning of motion sensitive neurons (Liang et al., 2010). Such deficits can be further amplified by altered eye movement behavior (Dowiasch et al., 2015), which changes the way older adults sample the outside world. Secondly, epidemiological, physiological and histopathological studies have shown that vestibular function declines with age (Anson and Jeka, 2015). While the vestibular system is known for its role in maintaining balance and postural control, increasing evidence

demonstrates important connections between the vestibular system and spatial navigation in humans (Brandt et al., 2005), as has been previously reported in rodents (Potegal et al., 1977). In rodent model studies, disruption of vestibular inputs results in reduced place cell spatial tuning (Stackman et al., 2002) and a complete loss of directional tuning of anterior thalamic head direction cells (Stackman and Taube, 1997). In addition, areas VIP and MT/MST also receive vestibular input, hence vestibular damage could also alter the computation of idiothetic speed and direction in cortical structures.

Even though age-related deficits in space perception appear to be absent for static cues and relatively subtle for self-motion cues, older adults often show striking difficulties in path integration tasks. For example, after moving about in an unfamiliar environment, they underestimate travelled distances and turns, and are less accurate when returning to the start of a journey. This has been shown when navigation is based either on visual or non-visual cues (Allen et al., 2004; Mahmood et al., 2009; Adamo et al., 2012; Harris and Wolbers, 2012). Given that both idiothetic and allothetic information is used to compute position and orientation in all the spatially-modulated cells described above, the particular vulnerability of the hippocampus and other medial temporal lobe structures to the deleterious consequences of aging (Barnes, 1979; Burke and Barnes, 2006; Lister and Barnes, 2009; Stranahan et al., 2010) could result in compromised computations of position and orientation. In fact,

even though there is mixed evidence regarding an association between age-related changes in hippocampal volume and memory function (Van Petten, 2004), several studies have reported changes in place cell firing characteristics. For example, old rats show differences in the stability of their cognitive maps as assessed by ensemble recordings of hippocampal neurons (Barnes et al., 1997; Schimanski et al., 2013). CA1 hippocampal pyramidal cells in aged rats occasionally generate a new and distinct place cell representation for a familiar environment (Barnes et al., 1997; Schimanski et al., 2013), and these cells take significantly longer to begin to show consistent spatial firing, even in familiar environments (Hok et al., 2012).

Changes in spatial working memory are a further likely source of impaired positional coding in old age. For example, aged rats show deficits on a working memory versions of the Morris watermaze task, in which the inter-trial interval between training and testing of the hidden escape platform location is varied (Frick et al., 1995; Bizon et al., 2009). Spatial working memory depends not just on hippocampus but also on extra-hippocampal structures such as prefrontal cortex (Floresco et al., 1997). The medial prefrontal cortex monitors hippocampal output and stores location information to guide navigational behavior (Jones and Wilson, 2005; Wolbers et al., 2007). Neurons in medial prefrontal cortex undergo several changes in the course of normal aging, including a loss of NMDA receptors and there is increased inhibition of pyramidal cells due to

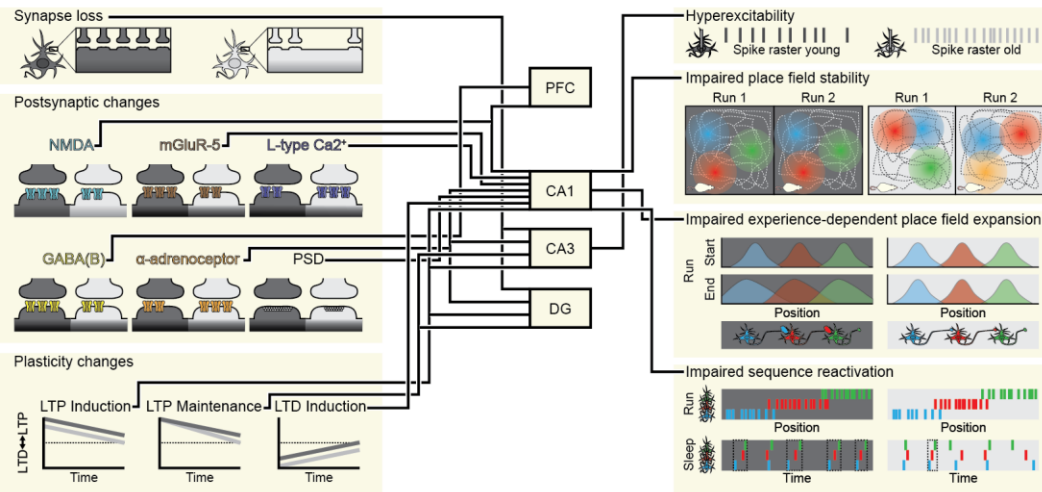


Figure 2.1: Neurophysiological changes with age.

Graphical overview of the major age-related neurophysiological changes discussed in the text. Examples from young animals are indicated in dark gray and those from age animals are indicated with light gray. NMDA, N-methyl-D-aspartate; mGluR-5, metabotropic glutamate receptor 5; GABA(B), gamma-amino butyric acid receptor B-type; PSD, postsynaptic density; LTP, long-term potentiation; LTD, long-term depression.

GABAergic changes (Carpenter et al., 2016; McQuail et al., 2016). As a consequence, compromised computations in medial prefrontal cortex can cause deficits in maintaining information about position and navigational goals in working memory, thus contributing to the navigational errors observed in both rodent and human studies.

Finally, changes in vestibular processing can affect the coding for position and orientation in old age. Age-related degeneration of the vestibular system is a multifactorial process, affecting the peripheral end-organs, the brainstem, the cerebellum and the cerebral cortex (Arshad and Seemungal, 2016). The vestibular nuclei of aged rats show a number of abnormal structural changes (Johnson and Miquel, 1974) as well as reduced levels of glutamate that could indicate a reduction in excitatory afferent drive (Liu et al., 2010). Given that vestibular signals convey information about translation and rotation of the body, age-related

changes of vestibular functioning will render idiothetic perception imprecise. This could explain why, for example, older adults are impaired when they are transported in a wheelchair and have to return to the starting location at the end of an outbound journey (Allen et al., 2004; Adamo et al., 2012). Importantly, such deficits are attenuated when the outbound path is experienced via active walking (Allen et al., 2004; Adamo et al., 2012), showing that motor efference copy and/or proprioceptive feedback can at least partially compensate for impaired vestibular processing. Furthermore, vestibular damage can induce pathology in downstream structures such as the hippocampus (Brandt et al., 2005), thus impacting the precision of positional computations in the place and grid cell systems. Finally, vestibular changes often induce problems with balance and postural control, which makes avoiding obstacles more difficult and increases the risk of falling. To counteract such deficits, older adults often employ more conservative adaptation strategies by taking slow, short and more frequent steps (Caetano et al., 2016) and by prioritizing walking control over concurrent cognitive tasks (Simieli et al., 2015). As a consequence, a reduced amount of attentional resources can be allocated to keeping track of both idiothetic and allothetic feedback, ultimately resulting in reduced navigation performance.

2.2. Age-related changes in plasticity and synaptic signaling

Aged animals undergo a number of changes in synaptic

communication and plasticity regulation (**Figure 2.1**). One key mechanism for storing spatial memories in the hippocampus is long-term potentiation (LTP), a sustained increase in synaptic strength (Bliss and Lømo, 1973). Similarly, long-term depression (LTD) provides a complimentary downregulation of synaptic strength which maintains the equilibrium of overall network excitability (Lynch et al., 1977; Levy and Steward, 1979). Donald Hebb first postulated that memories may be stored within a neural network, or cell assembly, through the selective modification of synapses between co-activated neurons (Hebb, 1949), and David Marr developed a theoretical model suggesting that the anatomical configuration of the hippocampus is well-suited to perform a rapid mnemonic function (Marr, 1971). The first empirical validation of these theories was accomplished by delivering patterned electrical stimulation to axons afferent to dentate gyrus (DG) granule cells, which resulted in strengthened synaptic weights (Bliss and Gardner-Medwin, 1973; Bliss and Lømo, 1973). It is now well-established that defects in plasticity mechanisms underlying both LTP in hippocampal and other circuits across the brain result in learning and memory deficits. The focus of this section will be on age-related changes in cell-to-cell signaling and transmitter systems within the hippocampus as they relate to LTP and LTD.

Assessing the functional properties of synapses is one way to examine how synaptic plasticity is altered in the aged nervous system. When robust high-frequency stimulation protocols have been used to

artificially induce LTP, many studies have reported an absence of age-related changes in hippocampal LTP induction, including those investigating perforant path-granule cell synapses (*in vivo awake*: Barnes, 1979; *in vitro*: Diana et al., 1994), CA3-CA1 Schaffer collateral synapses (*in vitro*: Landfield and Lynch, 1977; *in vivo anesthetized*: Landfield et al., 1978) and perforant path-CA3 pyramidal cell synapses (*in vivo anesthetized*: Dieguez and Barea-Rodriguez, 2004). Alternatively, the use of peri-threshold stimulation has been shown to unmask age-related LTP induction deficits in both dentate gyrus and CA1. For instance, when the combination of weak synaptic stimulation and direct depolarization of dentate gyrus granule cells was used to elicit LTP at perforant path-granule cell synapses of awake young and aged rats *in vivo*, aged synapses required larger depolarizations for LTP induction (Barnes et al., 2000), suggesting that aged animals have an increased threshold to induce LTP at these synapses. While aged neurons in CA1 do not show an increased threshold for LTP (Barnes et al., 1996), in the presence of peri-threshold stimulation, aged rats display lower levels of LTP induction than young rats (*in vitro*: Deupree et al., 1993; Moore et al., 1993; Rosenzweig et al., 1997). Age-related impairments in the maintenance of LTP have also been reported in dentate gyrus (*in vivo awake*: Barnes, 1979; Barnes and McNaughton, 1980, 1985) and CA3 (*in vivo anesthetized*: Dieguez and Barea-Rodriguez, 2004). Furthermore, Barnes (1979) found that aged rats with the most pronounced impairments in

spatial memory accuracy also showed significantly faster rates of LTP decay in dentate gyrus, indicating a direct relationship between age-related decline in LTP maintenance and spatial mnemonic performance.

One potential contribution to the LTP deficits reported for perforant path-granule cell synapses is the observation that granule cells in aged rats have a quarter fewer synaptic contacts from layer II medial entorhinal cortex (MEC) (Geinisman et al., 1992; **Figure 2.1**). The same MEC cells also project to the lacunosum moleculare layer of CA3, and older rats with spatial learning deficits show decreased levels of the presynaptic marker synaptophysin, suggesting there may be reduced synaptic input in CA3 as well (Smith et al., 2000). Because there is no loss of layer II MEC projection cells in old rats (Merrill et al., 2001), axons from these cells are thought to undergo pruning of their extensive collateral projections. In support of this model, the extracellularly recorded presynaptic fiber potential is smaller in the dentate gyrus of aged rats (Barnes and McNaughton, 1980). In addition, the size of the extracellularly recorded EPSP is smaller in old animals (Barnes, 1979; Barnes and McNaughton, 1980a; Yang et al., 2008) for equivalent stimulation strengths, which is consistent with reduced synaptic input. Additionally, older, memory-impaired human participants show reduced white matter volume in the vicinity of the perforant pathway (Rogalski et al., 2012), which is in line with the rodent data suggesting axon pruning. Although the total number of CA3 to CA1 Schafer collateral synapses is preserved with age

(Geinisman et al., 2004), these synapses do undergo a number of age-related changes. For instance, while the size of the unitary EPSPs at CA3-CA1 synapses of aged animals is comparable to what is seen in young animals (Barnes et al., 1997), aged animals show a reduction in the amplitude of Schafer collateral-induced field EPSPs in CA1 (Landfield et al., 1986; Barnes et al., 1992; Deupree et al., 1993). In addition, learning-impaired aged rats show significantly smaller postsynaptic densities in relation to young rats at CA3-CA1 synapses (Nicholson et al., 2004). When considered in conjunction with the electrophysiological findings, these results could be explained by a subset of synapses that become non-functional or silent in aged animals.

Advanced age is also accompanied by wide-ranging changes in the various transmitter systems which support cell-to-cell signaling and synaptic plasticity regulation. Glutamate is the predominant excitatory neurotransmitter in the mammalian nervous system. In the process of LTP induction, glutamate from presynaptic terminals binds AMPA receptors leading to a depolarization of the postsynaptic membrane. The change in membrane potential leads to an unblocking of NMDA receptors allowing for the influx of Ca^{2+} . The resulting rise in intracellular Ca^{2+} concentrations kicks off a cascade of enzymatic reactions that ultimately result in either LTP or LTD induction. While aged rats show elevated AMPA receptor-mediated currents for a given fiber potential amplitude in the granule cell layer of the dentate gyrus, NMDA receptor-mediated

currents are diminished (Yang et al., 2008). These reduced NMDA currents are consistent with a loss of NMDA receptors in the dentate gyrus of aged non-human primates (Gazzaley et al., 1996). For NMDA receptors in the mammalian hippocampus and prefrontal cortex the widely expressed modulatory subunit GluN2B has been shown to decline with age in rats (Sonntag et al., 2000; Dyall et al., 2007), mice (Zhao et al., 2009; Brim et al., 2013) and non-human primates (Bai et al., 2004). This subunit has slow channel kinetics allowing more Ca^{2+} influx over a longer time interval and expression levels of GluN2B have been linked directly to hippocampal-dependent memory (von Engelhardt et al., 2008; Brigman et al., 2010). Absence of the GluN2B results in impaired LTP (von Engelhardt et al., 2008; Brigman et al., 2010), whereas overexpression enhances LTP and memory performance (Tang et al., 1999; Cui et al., 2011). Additionally, glutamate binding to metabotropic glutamate receptors can facilitate the release of calcium through its action on inositol trisphosphate receptors. Memory-impaired aged rats also show reduced expression levels of postsynaptic metabotropic glutamate receptor 5 in CA1, accompanied by a loss in related downstream signaling molecules involved in LTP maintenance (Ménard and Quirion, 2012a).

While aged animals show diminished NMDAR-dependent LTP, voltage-dependent Ca^{2+} channel mediated LTP is greater in aged rats (Shankar et al., 1998; Boric et al., 2008) and mice (Robillard et al., 2011). The CA1 pyramidal cells of aged rats have elevated Ca^{2+} currents due to

a higher density of L-type Ca²⁺ channels (Thibault and Landfield, 1996). Interestingly, these channels do not appear to compensate for the loss of NMDA receptor function, but instead compound memory pathology as the administration of L-channel antagonists has been shown to reduce or even eliminate age-related memory decline in rats (Applegate and Landfield, 1988; Levere and Walker, 1992; Ingram et al., 1994; Riekkinen et al., 1997; Veng et al., 2003), rabbits (Solomon et al., 1995; Woodruff-Pak et al., 1997; Rose et al., 2007), non-human primates (Sandin et al., 1990) and humans (Ban et al., 1990; Trompet et al., 2008). It has been suggested that the overall disruption of Ca²⁺ homeostasis may actually shift the threshold for synaptic modification and bias aged synapses toward LTD and away from LTP (Foster and Norris, 1997). Consistent with this hypothesis, age-related LTD induction at CA3-CA1 synapses is elevated (Norris et al., 1996; Foster and Kumar, 2007). This age-related LTD enhancement can be reduced by blocking the release of intracellular Ca²⁺ stores (Kumar and Foster, 2005). Finally, glutamate binding to metabotropic glutamate receptors can facilitate the release of Ca²⁺ through its action on inositol trisphosphate receptors. Aged rats show an increased susceptibility to a specific form of LTD that relies on these metabotropic receptors (Kumar and Foster, 2007). Memory-impaired aged rats also show reduced expression levels of hippocampal post-synaptic metabotropic glutamate receptor 5 accompanied by a loss in related downstream signaling molecules involved in LTP maintenance (Ménard

and Quirion, 2012b).

Acetylcholine is an important neuromodulator for memory encoding and has been shown to facilitate hippocampal LTP (Huerta and Lisman, 1995; Adams et al., 2004; Hasselmo, 2006). The majority of cholinergic input to the hippocampus is provided by structures within the basal forebrain. Interrupting communication between these structures and the hippocampus disrupts idiothetic navigation (Gorny et al., 2002; Martin et al., 2007; Hamlin et al., 2013) and impairs hippocampal LTP (Ovsepian et al., 2004). In aged rats, cholinergic drive from the medial septum is reduced by approximately half in all three primary areas of the hippocampus including dentate gyrus, CA3 and CA1 (Shen and Barnes, 1996). This loss of cholinergic drive may stem from impaired muscarinic receptor function within the hippocampus itself (Lippa et al., 1985; Chouinard et al., 1995), or changes in gene regulation and intracellular signaling pathways within the cholinergic cells of the basal forebrain (Schliebs and Arendt, 2011).

Finally, the catecholamine transmitter systems, which include dopamine, serotonin and norepinephrine, have also been found to modify LTP in the hippocampus. There exists a large degree of variability in the age-related neurochemical changes reported for these systems in the hippocampus. It is evident, however, that aging results in some dysregulation that is likely to affect the dynamics of circuits critical for memory and navigation. For example, age-related spatial memory deficits

have been linked to hippocampal dopamine D1 receptor signaling deficits, which predominantly affect late phase LTP (Hersi et al., 1995 p.1; Bach et al., 1999). Aged rats also show reduced or functionally altered serotonergic 5HT receptors within the hippocampus (Gozlan et al., 1990; Nyakas et al., 1997; Topic et al., 2007). Finally, poor spatial memory retention performance in aged rats has been linked to an increase in α 1-adrenergic receptor density and altered α 2-adrenergic receptor binding in the hippocampus (Huguet and Tarrade, 1992; Topic et al., 2007).

2.3. Age-related alterations in the creation, consolidation and retrieval of memory traces

Beyond the deficits with creating online representations of spatial information, older adults have difficulties turning such representations into enduring long-term memory traces and retrieving them when necessary. For example, advanced age is often associated with substantial problems in learning the position of distal targets located beyond the current sensory horizon (Head and Isom, 2010; Lövdén et al., 2012). Similarly, human studies using a virtual analog of the Morris watermaze, have reported that older adults generally show slower learning rates (Daugherty et al., 2016) and are less accurate in locating the hidden platform (**Figure 2.2B**) and are less able to reproduce a map of the environment (Moffat and Resnick, 2002). Similar effects have been observed in studies with aged rodents (Barnes, 1979; Gage et al., 1984; Lindner, 1997; **Figure 2.2A**), and the

mechanisms underlying such deficits will be discussed in this section.

2.3.1. Place learning and cognitive mapping

In addition to deficits with forming spatial representations, inefficient retrieval from long-term memory can also contribute to a decline of navigational abilities (Iaria et al., 2009; Head and Isom, 2010). As mentioned above, old rats show distinct differences in the stability of their cognitive maps as assessed by ensemble recordings of CA1 hippocampal neurons (Barnes et al., 1997; Schimanski et al., 2013). Aged rats occasionally generate a new and distinct place cell representation for a familiar environment, suggesting they may be retrieving the incorrect map (Barnes et al., 1997; Schimanski et al., 2013) (**Figure 2.2C**). Specifically, the inability to represent an identical environment as the same place may arise due to a failure of pattern completion mechanisms to reinstantiate the correct representation (see **Chapter 1.3**). While there is no evidence of age-related changes in entorhinal-CA1 synapses, there is evidence that a greater proportion of CA3-CA1 synapses are functionally silent (see **Chapter 2.2**). These functionally silent synapses could result in a failure of CA3 to support CA1 in pattern completing to the correct representation, causing CA1 to instead generate a new map based on the direct cortical sensory input it receives from layer III entorhinal cortical projections. Alternatively, age-related decline in cholinergic modulation (Hasselmo et al., 1995) might reduce the relative influence of new information through the perforant path and favor the reactivation of stored cognitive maps in

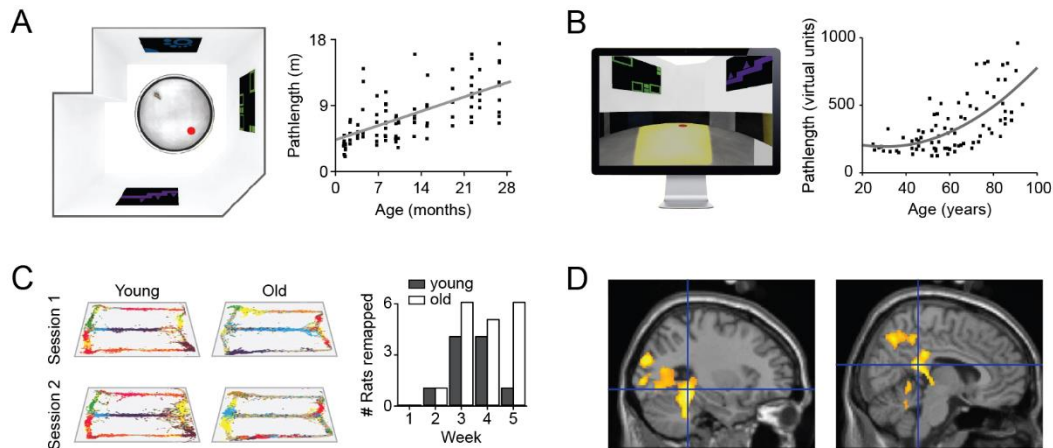


Figure 2.2: Correspondence of age-related navigational deficits in rodents and humans in cognitive mapping.

(A) Aged rats show reduced spatial navigation accuracy in the Morris watermaze task (Lindner, 1997) as measured by total distance swam (i.e., pathlength) to find the location of a submerged platform (shown in red). Rendering of a rat performing the Morris watermaze task in a room containing several orienting visual cues (left). Performance for rats from age 1.3 to 26.3 months old (right). **(B)** In a virtual Morris watermaze task (left), there was a non-linear relationship between age and total distance traveled in the virtual environment (Moffat and Resnick, 2002) in humans. As with a number of rodent aging studies (e.g., A), older adults took a longer time and traversed a greater linear distance in locating the hidden platform compared to younger adults. **(C)** Aged rats periodically generate new and distinct cognitive maps after repeated exposure to a familiar environment. Place field distributions are shown for one young and one old rat recorded over two consecutive episodes of running on a figure-8 maze (Barnes et al., 1997). Individual place cells are denoted with colored points. Place-field maps of young animals are highly correlated between consecutive exposures while aged animals occasionally showed uncorrelated firing, indicative of remapping. When the proportion of rats that remapped between morning and afternoon sessions was tracked over 31 days (Schimanski et al., 2013), maps were stable between sessions until day 14, when both age groups began to show periodic remapping episodes, with aged animals remapping more frequently. **(D)** In a neuroimaging study, older adults showed reduced activation in the hippocampus and parahippocampal gyrus and in the retrosplenial cortex compared to younger participants during virtual navigation (Moffat et al., 2006).

the CA3 auto-associative network that are then read out in CA1 resulting in the instantiation of old and incorrect maps.

Still another explanation for the remapping bias observed in aged rats is supplied by the three-mode place code model proposed by Redish (1999), which suggests that this phenomenon may arise from age-related LTP deficits. According to this model, upon initial exposure to an environment, the path integrator (e.g., putatively EC) drives place field

expression in CA3/CA1. At the same time, the CA3/CA1 representation becomes associated with both the path integrator representation and the various local view (i.e., allothetic) inputs sampled during the course of exploration. Upon reintroduction to the environment, the initial local view of the animal can be used to instantiate the stored CA3/CA1 place cell map that, in turn, resets the path integrator to bring it into alignment with the current positional coordinates. In parallel with this process, the DG compares the path integrator and local view inputs to provide a signal to downstream CA3/CA1 place codes about the similarity of the current and preceding experiences. Within this framework, impaired LTP may cause the aged hippocampal network to fail to associate local view and path integrator inputs with the CA3/CA1 place cell map generated during the first exposure to the environment (Redish et al., 1998; Redish, 1999). As a consequence, when revisiting the same environment, aged rats will fail to reset the path integrator to the correct starting coordinates consistent with the stored CA3/CA1 representation and the initial local view. The end result is that the mismatch in path integrator and local view feedback induces a change in the DG signal to CA3/CA1, causing the network to generate a new representation for an already experienced environment.

When recording place cells in CA3, Wilson et al. (2005) observed an opposite change from the remapping shown in CA1, in that aged rats exposed to distinct environments were often found to instantiate the same map for both. The tendency for aged CA3 place cells to perseverate to an

old and incorrect representation could result from a failure of upstream DG to dissociate similar sensory-perceptual features in the new and old environment (i.e., pattern separation; see **Chapter 1.3**). Given that the dentate gyrus/hilar region is particularly vulnerable in normal aging (Small et al., 2004; Yassa et al., 2011), coupled with the fact that aged rats display a drastic reduction in perforant path-granule cell synapses (Bondareff and Geinisman, 1976; Geinisman et al., 1977, 1986), it is likely that aging is accompanied by impaired pattern separation mechanisms. Consistent with this idea, aged humans with degraded perforant path integrity (Yassa et al., 2011) and patients with DG damage show poorer performance on discrimination tasks used to assess pattern separation (Baker et al., 2016). Similarly, the bias for aged rats to 're-use' an inappropriate map for different environments could also be a consequence of excessive pattern completion in CA3 (Wilson et al., 2006). If this is the case than aging may be accompanied by both defective encoding (i.e., pattern separation) as well as faulty recall mechanisms (i.e., pattern completion). There is evidence of hyperactivity of CA3 cells in older rats (Wilson et al., 2005) (**Figure 2.1**) and non-human primates (Thomé et al., 2015), as well as increased CA3 and DG activity linked to pattern separation/completion deficits in aged humans (Yassa and Stark, 2011). Given that the auto-associative connections in stratum radiatum of the CA3 network are unaffected by age (Smith et al., 2000), the hyperactivity of CA3 principal cells could bias this auto-associative network to

incorrectly re-instantiate a stored memory trace. Collectively, these changes would result in the network favoring the reactivation of stored cognitive maps, particularly under conditions in which new stimuli have a high degree of feature overlap with learned stimuli. On the behavioral level, corresponding data have been reported in older adults, who show increased pattern completion in situations when only partial cues of an environment can be seen (Head and Isom, 2010; Liu et al., 2011). Using a scene recognition task, Vieweg et al. (2015) observed a bias in older adults towards falsely classifying novel scenes as familiar ones, particularly when only some of the scene was visible. This bias could not be explained by an overall tendency to produce more false alarms, suggesting that new partial information triggered the recognition of learned items. Together with fMRI studies pointing to a reduced ability of the aging hippocampus to distinguish between similar stimuli (Yassa and Stark, 2011; Yassa et al., 2011), these data support the rodent literature in terms of a heightened, age-related tendency for pattern completion in CA3 (Wilson et al., 2005). As previously described, when exposed to input patterns that have some degree of feature overlap with a previously experienced environment, the bias to resolve contextual similarity/dissimilarity with either pattern separation or pattern completion depends on the degree of feature overlap (see **Chapter 1.3**). Overall, the findings discussed suggest that aged individuals may be biased both to over pattern complete and under pattern separate, requiring a greater

degree of feature dissimilarity to reconcile novel environments from those that have already been experienced (Wilson et al., 2006; Yassa and Stark, 2011).

Finally, in studies of human navigation, place learning and cognitive mapping have been shown to critically rely on retrosplenial computations (Morris et al., 1982; Hartley et al., 2003; Wolbers and Büchel, 2005; Goodrich-Hunsaker et al., 2010; Kolarik et al., 2016). Consequently, in human aging there has been great interest in the role of these structures in mediating age-related navigation impairments. For example, three studies have now reported quite consistent results demonstrating reduced or absent hippocampal, parahippocampal and retrosplenial activation (**Figure 2.2D**) in older as compared to younger adults during virtual navigation, despite quite different task demands across studies (Meulenbroek et al., 2004; Moffat et al., 2006; Antonova et al., 2009). This may suggest a lack of hippocampal recruitment or switching to extra-hippocampal strategies during spatial navigation in older participants, but could also result from sub-threshold activations or possibly from sparse coding (activations in a relatively smaller set of neurons) in older participants.

2.3.2. Route-based learning and hippocampal sequences

In contrast to the wealth of findings on age-related deficits in cognitive mapping or place-based navigation, fewer studies have investigated how aging affects route navigation. Route knowledge consists

of associations between local views of an environment and associated movements (**Figure 2.3A**). In humans, arguably the most frequently used navigation task is route navigation, and several studies have demonstrated declines in route learning in older adults (Wilkniss et al., 1997; Moffat et al., 2001; Head and Isom, 2010; Etchamendy et al., 2012). Similarly, route learning deficits are detected in older animals when using multi-compartment mazes, but can be partially ameliorated by systemic cholinergic treatment in both rats and mice (Ingram, 1988; Pistell et al., 2012). Successful route learning depends on a number of processes including the recognition of landmarks and places encountered during learning, knowledge about the sequence in which places/landmarks were encountered, the selection of landmarks that are navigationally relevant (i.e., those at decision points), and typically also the association of directional information with these landmarks. Moreover, successful navigation often requires retracing a recently travelled path to find the way back. Aging has been associated with less accurate binding of directional knowledge to landmarks (Head and Isom, 2010; Liu et al., 2011; Wiener et al., 2012; Zhong and Moffat, 2016) and impaired memory of the sequence in which landmarks were encountered (Wilkniss et al., 1997; Head and Isom, 2010; Wiener et al., 2012). Older adults are also more likely to point out salient landmarks than turns as providing the most useful information when learning novel routes (Lipman, 1991), and their ability to retrace a recently travelled route is impaired as compared to younger participants

(Liu et al., 2011; Wiener et al., 2012).

In terms of the underlying neural mechanisms, route learning and route navigation have been associated with caudate activation (Hartley et al., 2003) and caudate volume (Head and Isom, 2010). Furthermore, the caudate shows age-related neurodegenerative changes at similar rates to the hippocampus (Betts et al., 2016), which may explain aging-related declines in route navigation performance. On the other hand, it has also

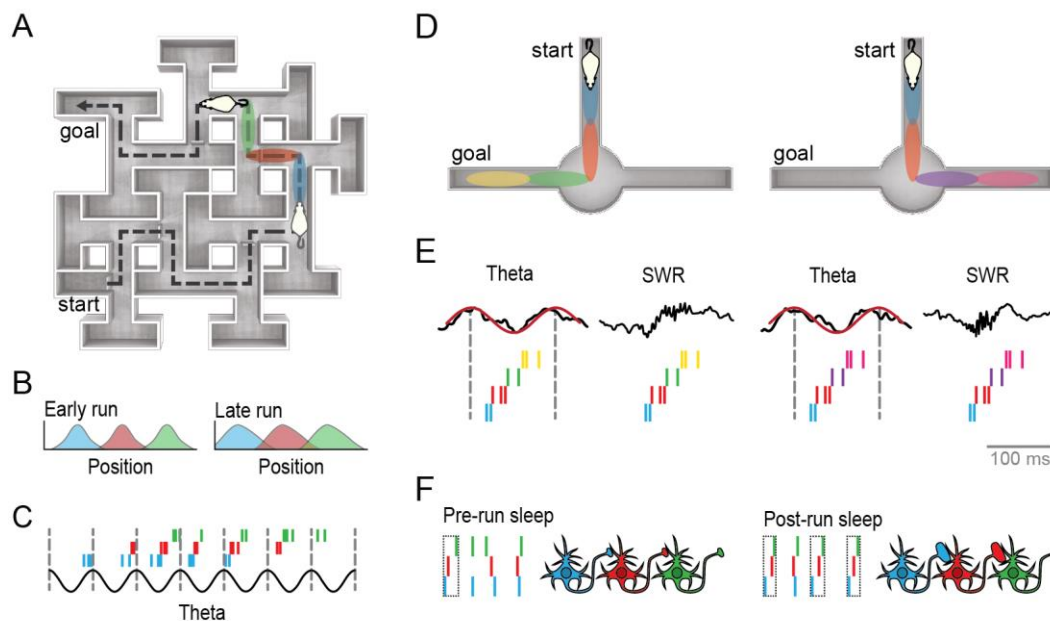


Figure 2.3: Route and sequence learning.

(A) An example route learning task for rats using the 14-unit T-maze, or Stone maze (adapted from Stone, 1929). Hatched lines indicate the learned route to a goal. In blue, red and green are the place fields of three neurons. (B) A sequence of three spatially adjacent place fields prior to (left) and following (right) behaviorally driven backwards expansion plasticity. (C) Raster plots showing spike timing for the same cells over multiple theta cycles illustrating phase precession. (D) Illustration of place field firing along two potential trajectories on a T-maze track. (E) Illustration of place cell sequential firing representing two potential trajectories shown in D played out within a single theta cycle or sharp-wave ripple (SWR) event. (F) Spike timing during slow wave sleep for three cells that were active during navigation. Sequences of activity that reproduce sequences observed during behavior are circled. The presence of backwards expansion increases the period of time over which adjacent place cells fire concurrently that may, in turn, facilitate sequential firing during rest and ultimately strengthen the synaptic weights of these cells. Strengthening the synaptic weights between cells with adjacent place fields could support both sequence and route learning. The deficits in backwards expansion and sequential replay in aged animals could, by extension, be responsible, at least in part, for route learning impairments.

been reported that older humans show preferentially greater fMRI activity in caudate nucleus while younger participants show greater hippocampal activity during virtual navigation (Konishi et al., 2013). This suggests that age-related deficits in route learning are likely not a consequence of caudate dysfunction. While route navigation is egocentric and procedural in nature, however, there is evidence that hippocampal computations may also be implicated in route navigation. For instance, the hippocampus has been shown to play an important role in processing information about the temporal order in which landmarks have been encountered (Rondi-Reig et al., 2006). One hippocampal-based mechanism that could contribute to age-dependent route learning deficits is experience-dependent place field expansion plasticity (Mehta et al., 2000; **Figure 2.3B**). Normally, even in familiar environments, the size of a CA1 place field is smaller on initial exposure to the environment on a given day. As the rat makes repeated traversals of a route, the place field becomes larger, and shifts backwards from the direction of movement (**Figure 2.1 and 2.3C**). For aged rats this phenomenon is attenuated (Shen et al., 1997; Ekstrom et al., 2001). In young rats, NMDA receptor blockade impairs both stimulation-induced LTP (Collingridge et al., 1983) and experience-dependent place field expansion plasticity, suggesting that age-related impairments in backward expansion likely arise from the dysregulation of NMDA receptor function previously discussed (see **Chapter 2.2**). Because this plasticity mechanism increases the size of place fields in the direction opposite to

the animal's trajectory of movement, it could provide a means of encoding sequences within cell assemblies (Blum and Abbott, 1996). Specifically, when place fields enlarge, the fields adjacent to each other will overlap to a greater degree following this expansion. The resultant longer periods of concurrent firing cause place fields with spatially-adjacent firing fields undergo an associative, temporally-asymmetric synaptic weight change that bias these cells toward firing in a specific sequence, which may act to more effectively link 'places' together.

A number of processes have been discovered that support place cell sequence reactivation during active navigation, which are believed to support real-time access to ensemble representations for retrospective and prospective spatial and mnemonic operations. For example, reactivation of ensemble place cell activity has been shown to occur over successive cycles of local field potential (LFP) theta oscillations (**Figure 2.3C**). During traversal through a given place field, place cell firing will process through phases of the LFP theta oscillation, such that the further through the field the animal passes, the earlier in the theta cycle the place cell fires (O'Keefe and Recce, 1993; Skaggs et al., 1996). During this theta *phase precession* there is a sequential updating of active cell assemblies such that the representation of the rats upcoming trajectory is played out sequentially within a compressed time scale of a single theta cycle. More recently, it has been shown that transient reactivation of cell sequences within a single theta cycle can project out over large distances

(Gupta et al., 2012) and tend to extend further preceding journeys to more distant goals (Wikenheiser and Redish, 2015a). Furthermore, in behavioral conditions in which rats must decide between two possible trajectories, such as two arms of a T-maze, theta sequences have been shown to trace out multiple options prior to the animal selecting a path (Johnson and Redish, 2007) (**Figure 2.3D and 2.3E**). These theta sequences are sometimes referred to as *theta sweeps* and have been shown to co-occur with vicarious trial and error behaviors, in which rats pause at a choice point and shift their orientation between multiple possible paths, suggesting these transient representations likely play a role in decision computations related to goal navigation. Sequence reactivation also occurs during episodes of sharp-wave ripple (SWR) activity that are characterized by a large deflection in the LFP immediately followed by a brief (~70 ms) high-frequency (140–240 Hz) oscillatory events (Buzsáki et al., 1992). SWR occur both during active navigation as well as during periods of sleep. The implications of sleep-related reactivation will be discussed further in the following section (see **Chapter 2.3.3**). Similar to theta sequences, in the context of active navigation, episodes of SWR ensemble reactivation are often referred to as *replay* events, and are believed to reflect possible future behaviors (Pfeiffer and Foster, 2013) (**Figure 2.3D and 2.3E**). Additionally, SWRs have been linked to the generation of novel un-experienced paths during spatial exploration (Gupta et al., 2010) and greater coordination of SWR replay is

predictive of goal navigation performance (Singer et al., 2013). Together, these findings suggest that SWR sequences may play a role in optimizing real-time goal-based navigation behavior. Finally, SWRs likely have a mnemonic function as disruption of SWRs during active navigation (Jadhav et al., 2012), or during post-training consolidation periods (Girardeau et al., 2009; Ego-Stengel and Wilson, 2010), has been shown to result in subsequent impairments in spatial memory performance. While theta sweeps have yet to be investigated in old and young animals, two related studies have shown evidence that aged rats show altered SWR activity during periods of active navigation as well as during periods of rest following a spatial navigation tasks (Wiegand et al., 2016; Cowen et al., 2018). During periods of rest, aged rats display a lower occurrence of SWR events and lower frequency ripple oscillations (Wiegand et al., 2016). During active navigation these age-related differences are not as evident, although aged rats do show a lower occurrence of SWR events after correcting for time spent at each location (i.e., decreased SWR rate; Cowen et al., 2018). Although ensemble sequence reactivation (i.e., SWR replay) was not examined in these studies, increased incidence of SWRs during task behavior has been shown to correlate with successful performance on working memory tasks (Dupret et al., 2010). This suggests that age-related reductions in sharp wave ripple occurrence could have meaningful effects on navigation behavior. For instance, reduced ripple occurrence in aged rats may decrease the number of

potential trajectories sampled during a given navigation experience leading to less optimal goal selection. This possible interpretation is consistent with observations that aged humans require longer acquisition periods to reduce their search path length in a virtual Morris watermaze task, in which a wide range of possible trajectories may be used to reach the hidden goal platform (Daugherty et al., 2016). Coupled with the findings that aged rats show impairments in sequence activation during rest (Gerrard et al., 2008) and display diminished backward field expansion that may reflect impaired online sequence encoding (Shen et al., 1997), these findings provide indirect evidence that waking sequence reactivation may be impaired with age. On the other hand, while memory for landmark locations in a virtual navigation task was found to be poorer in older compared with younger humans, both age groups improved to a similar degree following rest periods that might foster sequence reactivation, suggesting that waking sequence reactivation may be similarly efficient in older and younger adults (Craig et al., 2016). In light of the incongruities in the current literature and the absence of any direct comparison of ensemble sequence activity in old and young animals, it remains to be determined to what extent, if any, theta sweeps and waking SWR replay are altered with age.

2.3.3. Consolidation of spatial memories

Newly encoded spatial memories are typically fragile and, because they may decay, require additional maintenance processes. The concept

of memory consolidation, originally proposed by Muller and Pilzecker (Müller and Pilzecker, 1900), refers, in the broadest sense, to the process by which memories are stabilized over time. At the network level, one such process is the offline reactivation of assembly firing patterns that occurred during a previous period of active behavior. The recurrent collaterals of CA3 have long been thought to subserve an auto-associative function in the hippocampus, allowing for spontaneous replay of memories even in the absence of external input (Marr, 1971). As previously described, place fields with spatially-adjacent firing fields undergo synaptic weight changes that bias these cells to fire in sequential order. These sequences can be rapidly reinstated during active navigation through theta sweeps and sharp-wave ripple (SWR) replay (see **Chapter 2.3.2**) but are also preserved during 'off-line' periods, such that place cells that were activated sequentially during waking exploration will be more likely to fire in the same sequence during subsequent periods of sleep and wakeful resting. Such off-line replay events could help strengthen a given spatial representation within the hippocampus as well as coordinate the reactivation of multiple neocortical networks in order to consolidate new long-term memory traces (Wilson and McNaughton, 1994) (**Figure 2.3F**).

The reactivation of ensemble activity during sleep, which occurs during episodes of SWR events (i.e., sleep SWR replay), is hypothesized to coordinate the hippocampal-cortical 'transfer' of memories (Buzsáki, 1996). As previously described, the disruption of sharp-wave ripples

during rest periods following spatial tasks results in subsequent impairments in spatial memory performance (Girardeau et al., 2009; Ego-Stengel and Wilson, 2010). While cell pair reactivation in CA1 ensembles is equivalent in young and old rats (Gerrard et al., 2001), the temporal sequence of cell firing is disrupted in aging animals and is correlated with the fidelity of spatial memory (Gerrard et al., 2008) (**Figure 2.1**). These findings suggest that aging is accompanied by deficits in resting ensemble reactivation that could explain why aged rats show behavioral deficit in sequence learning (Winter, 1997; Oler and Markus, 1998). These resting sequence reactivation impairments may be a direct consequence of less reliable coordination of ensemble firing by SWRs. For example, CA1 cells of aged rats fire over a greater number SWR events than do those of young rats (Wiegand et al., 2016), which could indicate poorer segregation of ensemble sequence representations (Wikenheiser and Redish, 2015b). In addition, aged CA1 cells recorded in vitro show delayed activation relative to ripple onset (Kanak et al., 2013). In humans, sleep-dependent memory consolidation is also diminished with age (Spencer et al., 2007) but it is unknown at present whether this deficit affects the consolidation of spatial memories or the corresponding neural mechanisms that have implicated in rodent electrophysiological studies.

Finally, the previously discussed age-related changes in online sequence encoding during awake behavior may also play a role in subsequent resting sequence reactivation impairments. Waking SWR

associated reactivation events have been implicated in memory consolidation (Jadhav et al., 2012; Pfeiffer and Foster, 2013). These representations do not only reflect recent experience but also sometimes include path-sequences that were never experienced (Gupta et al., 2010). It has been suggested that both awake and resting SWRs may have distinct mnemonic functions, with waking SWRs supporting associates between possible trajectories and the value of their outcomes, while resting SWRs support neocortical memory consolidation (O'Neill et al., 2010; Carr et al., 2011). Furthermore, there is evidence that waking SWR sequences may carry higher fidelity representations of past experiences than those that occur during sleep, and may be more important for the evaluation of current decisions in the context of stored experiences (Karlsson and Frank, 2009; Tang et al., 2017). These findings suggest that even subtle age-related differences in waking SWR replay could have pronounced effects on navigation behavior. Future aging studies will be required to assess waking SWR replay in the context of route or goal learning navigation performance to determine if aging also results in compromised waking SWR sequences and what effect this may have on spatial memory-based navigation and consolidation.

2.4. Age-related differences in spatial navigation performance and strategy selection

Successful navigation not only requires the formation of spatial

representations and their retrieval from long-term memory, it often involves the computation of novel information, recombining information, or switching between different strategies or representations. For example, planning a novel route requires both the retrieval of cognitive maps from long-term memory as well as the computation of novel and viable path options from the current position to the destination. Aging humans are less efficient in using cognitive map-like knowledge for such route planning tasks, even if they have first successfully learned an environment (Iaria et al., 2009; Liu et al., 2011; Harris and Wolbers, 2014).

With respect to navigation strategies, aged rodents not only show more severe performance deficits in allocentric than in egocentric navigation tasks (Barnes et al., 1980; Rosenzweig et al., 2003), but they also exhibit spontaneous preferences for egocentric response strategies (**Figure 1.1A**) after being successfully trained on both allocentric and egocentric strategies (Barnes et al., 1980; Nicolle et al., 2003). This strategy bias is also reflected in the firing behavior of place cells. For example, when the starting position on a linear track is systematically varied with respect to the distance from the end of the track, CA1 place cells of both old and young rats tend to dynamically shift from being anchored to the starting location on the track (egocentric reference frame; **Figure 1.1B**), to aligning with the external room cues (Rosenzweig et al., 2003) (allocentric reference frame; **Figure 1.1A**). In older rats, this reference shift is delayed, suggesting the network itself is biased toward

maintaining an egocentric reference frame (Rosenzweig et al., 2003). Similar to rodents, aged humans have more difficulties in allocentric than in egocentric navigation tasks (Moffat et al., 2007; Iaria et al., 2009; Head and Isom, 2010) and accordingly show preferences for egocentric over allocentric navigation strategies (Bohbot et al., 2012; Rodgers et al., 2012)(**Figure 2.4B**) even if these strategies are maladaptive and result in navigational errors (**Figure 2.4C**) (Wiener et al., 2013). Shifts in navigation strategy use and preferences, away from allocentric strategies towards egocentric strategies, are accompanied by the use of different allothetic cues during navigation. In the virtual navigation Morris watermaze task, for example, older adults tend to rely more on proximal cues than distal cues or boundaries (Moffat and Resnick, 2002; Schuck et al., 2013). Thus, age-related shifts in preferences for navigation strategies are now well established for a number of species including humans.

In many situations, successful navigation also requires switching between different navigation strategies or frames of reference, for example when the available cues or task demands change. There is evidence that aging is accompanied by problems with navigation-related decisions as well as with detecting when a given behavioral strategy is no longer appropriate and adjusting behavior output accordingly (Etchamendy et al., 2012; Harris et al., 2012; Wiener et al., 2013; Breton et al., 2015). This ability is particularly problematic for aged humans and other animals when required to switch from an egocentric to an allocentric

strategy (**Figure 2.4C**), whereas switches from allocentric to egocentric strategies are less affected (Harris and Wolbers, 2012, 2014). For example, when tested on a virtual navigation task that dissociates spatial strategy use from response strategy use, which is egocentric and procedural in nature, aged humans took longer to learn the spatial version of the task and showed greater involvement of caudate nucleus over hippocampus (Konishi et al., 2013). Another study using a similar paradigm found that flexibility in switching from a response to a spatial strategy was positively correlated with hippocampal activation and negatively correlated with caudate activation, and that aged humans showed poorer flexibility in navigation strategy switching (Etchamendy et al., 2012). Age-related deficits with navigational strategy switching are likely linked to general strategy switching impairments, which are caused by changes in prefrontal and locus coeruleus (LC) functioning. In the LC, noradrenaline (NA) levels increase in response to changes in rewards associated with the current behavioral strategy (Aston-Jones and Cohen, 2005). Lower levels of NA have been found to alter gamma and theta oscillations in the local field potential as well as diminish theta sequence representations and vicarious trial and error behaviors (see **Chapter 2.3.2**), indicating a role for NA in navigation-related decision making (Amemiya et al., 2014; Amemiya and Redish, 2016, 2018). Furthermore, depletion of prefrontal NA by lesioning noradrenergic fibers projecting from LC to prefrontal cortex (PFC) or by infusion of a NA receptor antagonist

into medial PFC produces deficits in switching between different strategies (Tait et al., 2007a; Caetano et al., 2013). Aging degrades LC and disrupts NA function (Manaye et al., 1995; Grudzien et al., 2007) and the frontal cortical aging hypothesis suggests that various aspects of age-related cognitive decline may be attributable to PFC degradation (West, 1996; Pfefferbaum et al., 2005). There is ample evidence that PFC areas are involved in navigation strategy switching (Dias et al., 1996; Rich and Shapiro, 2009; Young and Shapiro, 2009; Caetano et al., 2013; Powell and Redish, 2016). While there are currently no animal model studies specifically exploring aged PFC function in the context of navigation strategy switching, both aged monkeys (Rapp, 1990; Gray et al., 2017) and rats (Beas et al., 2016) show reliable impairments on tasks assessing set shifting. Like navigation strategy switching, these set shifting paradigms require an animal to modify their behavior in response to changing task demands and are PFC-dependent (Birrell and Brown, 2000; Dalley et al., 2004; Tait et al., 2007b). Rodent studies show that these impairments are directly linked to decreased GABA(B) receptor expression in medial PFC (Beas et al., 2016) (**Figure 2.1**), but may also be a result of age-related decreases in PFC gray matter volume that is present in rats (Alexander et al., in press), non-human primates (Alexander et al., 2008) and humans (Storsve et al., 2014).

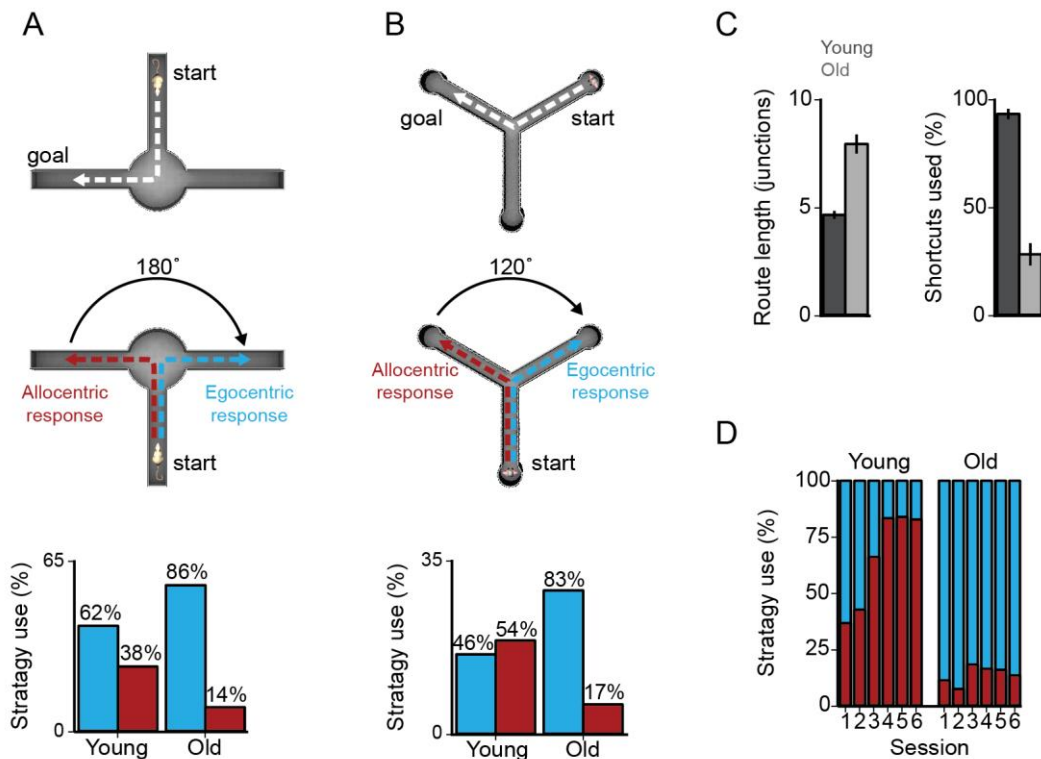


Figure 2.4: Correspondence of age-related navigational deficits in rodents and humans: Strategy preferences.

(A) In the T-maze task, an egocentric strategy was coded when a rat ‘turned right’ following 180° rotation of the start location and an allocentric strategy was coded when an animal moved to the same learned goal location relative to the external cues. Older rats overwhelmingly revealed an egocentric strategy on the probe trials (Barnes et al., 1980). (B) In the virtual Y-maze task, an egocentric strategy was coded when a human participant ‘turned right’ following displacement to a new starting location and an allocentric strategy was coded when the participant moved to the same learned goal location in absolute space (Rodgers et al., 2012). As with the rodent study (A), older adults spontaneously chose an egocentric strategy over an allocentric strategy compared to younger adults. (C) Similar results are observed in an environmental space task (top), in which older adults were impaired at switching from a learned route to a more optimal allocentric strategy, leading to increased route lengths and a reduced use of shortcuts (Harris and Wolbers, 2014). (D) Critically, in a task that distinguishes between allocentric and two egocentric (beacon/associative cue, not shown) strategies (bottom), older adults remain biased toward using an egocentric navigation strategy (Wiener et al., 2013). These results suggest that egocentric strategy preferences are difficult to overcome for older adults, even when they are maladaptive and lead to suboptimal task performance.

2.5. Alterations in spatial processing and navigation in age-related neuropathology

In the previous sections, the behavioral manifestations and putative

neural mechanisms of spatial navigation deficits were reviewed with a focus on normal aging, as contrasted with cognitive and brain aging that occurs in the absence of diagnosed neuropathology. Both neuroscientists and the lay public are intensely interested in pathological aging, with Alzheimer's disease (AD) being the second most feared disease of aging worldwide (Alzheimer's Association Worldwide Survey, 2014).

Behaviorally, AD manifests as a progressive cognitive decline often beginning with memory and progressing to other cognitive and perceptual domains as the disease advances (Weintraub et al., 2012). A common, though understudied aspect of AD is that of topographical disorientation. Even very early AD patients may become disoriented in their environment, a phenomenon that is more colloquially referred to as 'getting lost' or 'wandering'.

The early emergence of topographical disorientation in AD would be expected from the overlap of neural mechanisms of spatial computation with AD pathology, which prominently affects the perirhinal and entorhinal cortex, the hippocampus (Braak and Braak, 1995) and the retrosplenial cortex (Pengas et al., 2010). Motivated by this observation and also by the prospect of early detection and early intervention, there has been considerable recent interest in studying spatial navigation deficits in AD and in mild cognitive impairment (MCI), a condition hypothesized to be prodromal to AD. Serino et al. (2014) reviewed the extant literature and reported substantial navigation impairments in AD

and MCI in tasks that emphasized both allocentric and egocentric processing (Serino et al., 2014). Interestingly, one study tested asymptomatic young and aged humans on a virtual navigation task that includes both a hippocampus-dependent spatial component and a caudate-dependent response-based component. It was found that carriers of the Apolipoprotein E (APOE) ϵ 2 allele had more gray matter in the hippocampus and tended to use a hippocampus-dependent strategy to a greater extent than carriers of the ϵ 4 allele, which is a genetic risk factor of AD (Konishi et al., 2016). Consistent with these findings, ϵ 2 allele carriers have been shown to have larger hippocampal volume as compared to ϵ 4 allele carriers (Alexopoulos et al., 2011) while symptomatic AD patients have been shown to have greater gray matter volume in the caudate nucleus (Persson et al., 2018). Another study showed relatively specific deficits in AD patients for translating an allocentric reference frame to an egocentric reference frame (Pai and Yang, 2013), an ability thought to rely on the retrosplenial cortex (Byrne et al., 2007). Based in part on these findings, the earliest deficit in preclinical AD may be in the conversion between allocentric to egocentric coordinate systems (Serino and Riva, 2013). Moreover, deficits in route learning performance in early AD have been associated with hypometabolism in the retrosplenial cortex, thalamus and parietal cortex (Pengas et al., 2012). Mokrisova et al. (2016) showed that deficits in path integration in AD and MCI were mediated in part by changes in hippocampal, entorhinal and parietal cortex volumes.

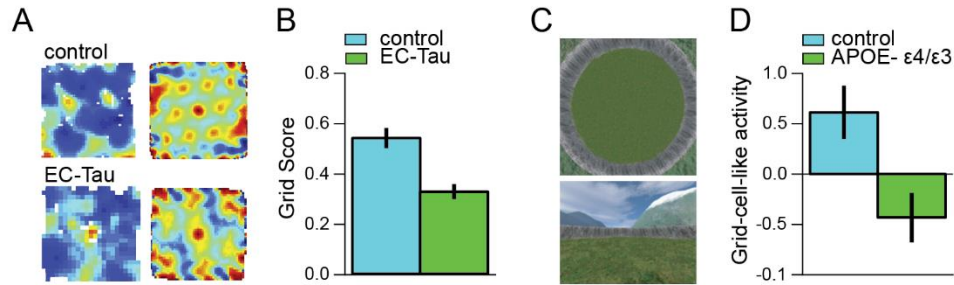


Figure 2.5: Alzheimer's disease-related grid cell dysfunction in mice and humans.

(A) Firing rate map (left panels) and spatial autocorrelograms (right panels) are shown for an example grid cell recorded from a control mouse and a grid cell from an age-matched mouse expressing a human tau mutation (EC-Tau; Fu et al., 2017). (B) The EC-Tau mice who formed mature tangles also had impaired grid cell function at 30+ months of age. (C) Top-down (top panel) and first-person (bottom panel) view of a virtual reality environment used to test memory performance and grid cell function in young controls and young human adults at risk of developing AD (i.e., those carrying the APOE-ε4 allele)(Kunz et al., 2015). (D) fMRI was used to assess a correlate of grid cell activity in the entorhinal cortex, and the pattern of activity suggested disrupted grid cell-like representations in the at risk population.

Cumulatively, these findings suggest that changes in the 'navigation circuit' may be a predominant and early consequence of AD and manifest as behavioral deficiencies in spatial navigation.

With respect to entorhinal cortex, tau deposition has been found to impair grid cell function and to cause navigation deficits in a transgenic mouse model of AD (Fu et al., 2017). Impaired grid cell-like properties have also been reported in young adults who were carriers of the APOE ε4 allele (Kunz et al., 2015), suggesting that physiological changes in grid cell networks may appear very early in adulthood (**Figure 2.5**). In addition to the APOE ε4 gene, a negative influence of other genetic risk factors for AD on navigation skill has been observed among carriers of the VL variant of the TOMM40 gene (Laczó et al., 2015) and the T polymorphism of the KIBRA gene (Schuck et al., 2013). Given that old, memory-deficient rats

show improved memory following pharmacological treatments that manipulate KIBRA activity (Huentelman et al., 2009), KIBRA pathways may be promising therapeutic targets for cognitive enhancement in normative aging, and potentially in attenuating AD-related memory deficits.

Given that healthy older individuals show impairments in various navigational computations, it is not surprising that those individuals with MCI, early AD or who are at genetic risk for AD show still more profound impairments. A major limitation in the current literature, however, is the dearth of prospective longitudinal studies examining whether navigation assessment in healthy elderly can be used as a predictor of future AD or MCI onset on an individual basis, as this is critical to early diagnosis and intervention. One such study (Laczo et al., 2010) demonstrated that amnesic MCI converters (compared with the nonconverters) showed higher deficits in both egocentric and allocentric navigation tasks, suggesting that spatial navigation testing may help predict the conversion to AD among MCI patients.

Another aspect of potential clinical utility of navigation assessment is for purposes of treatment and intervention. In this domain, spatial navigation tasks have been used as both an outcome variable (to assess the efficacy of clinical/pharmacologic intervention) and also as an intervention for possible cognitive/neural training. Pharmacological treatment of early AD with cholinergic agonists to reverse AD-related

acetylcholine depletion has been found to enhance navigation performance in early AD (Hort et al., 2014) and to increase navigation-related hippocampal activation in MCI (Grön et al., 2006). In addition, behavioral interventions in the form of cognitive training may enhance cognitive performance in healthy elderly and also delay the onset or ameliorate the symptoms of dementia. For example, the habitual use of video games or virtual reality task with incorporate specific regionally dependent navigation strategies have been shown to preferentially activate specific brain regions (Iaria et al., 2003; Bohbot et al., 2012; Konishi and Bohbot, 2013; Konishi et al., 2013) and can even alter region specific gray matter volume (West et al., 2015). Furthermore, these types of virtual reality tasks may be used to identify individuals with preclinical risk factors for AD (Konishi et al., 2016). The utility of cognitive training to enhance cognitive function is an area of some controversy as it is clear that participants improve on virtually all trained domains, but generalization of this training to other cognitive domains or to real world tasks (i.e., transfer) has been less consistent (Noack et al., 2014). Lövdén et al. (2012) found that navigation training improved navigation performance in younger and older adults and also prevented the age-related hippocampal volume loss that would have occurred over the training interval. In another study of the same participants, increases in cortical thickness in the precuneus and parietal lobe were observed only in younger trained participants, with no effect of navigation training on

cortical thickness observed in the older participants (Wenger et al., 2012). The navigation training in this study showed little transfer to other, non-trained cognitive domains. In contrast, Mitolo et al. (2017) found that route learning training enhanced route learning performance up to 3 months post-training and also improved visuo-spatial working memory, indicating transfer to an important cognitive domain. Finally, a one-month spatial training in middle aged adults (40-55 years) has been shown to improved performance on a maze learning task and to decrease activation in the hippocampus and parahippocampal gyrus (Hötting et al., 2013), a finding that the authors attributed to reduced cognitive effort required post-training.

Researchers and clinicians have just begun to incorporate navigation tasks into clinical research and practice. Navigation assessment has potential utility as a predictor of future AD, as an outcome measure in behavioral and pharmacological intervention studies, and as a cognitive training task. Spatial navigation may prove to be particularly useful in these domains because of its known dependence on the highly plastic brain systems that may be both benefitted by training but also vulnerable to AD pathology. Currently, however, this field is hampered by the absence of agreement on a 'gold standard' navigation task, or set of tasks, to be used in clinical settings that are quick to administer, require minimal training, have established population norms, and meet quality criteria for diagnostic tests.

2.6. Conclusions

A progressive loss of navigational abilities in old age is now a well-established fact both in rodents and humans. Given that spatial navigation is a complex cognitive operation, deficits can arise at multiple processing stages. These include difficulties with computing spatial information from incoming sensory cues, deficits with forming stable and distinct memory traces of spatial information, and challenges arising during planning and control of navigational behavior. The research discussed in this section show that the deficits likely include alterations both in specialized spatial computations, such as idiothetic processing, as well as a broad range of other cognitive domains. As a consequence, age-related navigational deficits are best understood as reflecting a combination of impaired spatial coding as well as other learning and memory problems that will also affect non-spatial behaviors.

Despite the wealth of aging studies discussed, several important problems remain to be addressed. For example, the majority of the aging literature, particularly in humans, is based on cross-sectional studies. Longitudinal studies can be challenging to implement and are accompanied by their own limitations, including participant attrition and shared historical effects (Campbell and Stanley, 1963). Replication of existing findings using a longitudinal design would, however, aid in separating true age-related change from confounding cohort effects and enable more precise identification of the variables driving potential decline.

Moreover, while it is known that the scale of space in which navigation takes place affects the exact cognitive processes involved in navigation (Wolbers and Wiener, 2014; Meilinger et al., 2016), it is currently unknown whether aging differentially affects navigation in, and spatial representations of, environments at different spatial scales. It is also unknown if and how key systems such as the entorhinal grid cell system are affected in healthy aging, which makes it difficult to pinpoint the exact reasons why older adults may find it difficult to keep track of their position. Critically, such studies are also needed to harness the clinical potential of spatial navigation.

Given the current interest in developing functional biomarkers to detect people at risk for dementia, and the fact that key structures of the navigation circuit are among the first cortical structures affected by AD pathology, assessing navigational abilities might contribute to the detection of preclinical stages of AD. Moreover, navigational indicators could prove to be sensitive outcome measures - or cognitive endpoints - in clinical trials testing novel therapeutic approaches. This, however, requires the development of standardized, validated assessment protocols, which are not available at present. Excitingly, the recent advent of affordable, high quality virtual reality technology opens up completely new possibilities for developing ecologically valid assessments of navigational functions and for training navigational computations.

CHAPTER 3: DEVELOPING A NOVEL SYSTEM FOR ASSESSING DYNAMIC VISUAL CUE CONTROL OF NAVIGATION BEHAVIOR IN RODENTS

3.1. Introduction

3.1.1. Differentiating the role of allothetic and idiothetic feedback in navigation and spatial representation networks

As previously discussed in Chapter 1.1, spatial navigation is generally studied in the context of two broad categories of spatial information, allothetic cues (e.g., visual, auditory, tactile or olfactory environmental landmarks) and idiothetic cues (e.g., vestibular, kinesthetic and optic flow self-motion feedback). During active navigation, both of these information streams are drawn upon to generate and continuously update an animal's internal representation of space. A number of studies have attempted to dissociate the unique roles of allothetic and idiothetic cues in the context of navigation strategy, navigational accuracy and the instantiation and maintenance of an internal cognitive representation of space. These two forms of information interact in a complex manner such that both are informed by, but do not necessarily depend upon, the other. For instance, rodents will utilize external visual cues to navigate to a learned goal location (e.g., O'Keefe and Conway, 1980; Suzuki et al., 1980) but can also perform such tasks in the absence of any visible cues (Mittelstaedt and Mittelstaedt, 1980; Etienne, 1992).

A number of approaches have been developed to artificially

introduce a mismatch in allothetic and idiothetic feedback in order to dissociate their respective influence on navigation and spatial cognition. One means of generating this mismatch is to hold allothetic cues constant while altering idiothetic cues either by varying angular vestibular feedback or relative running distance (Sharp et al., 1995; Gothard et al., 1996; Redish et al., 2000; Rosenzweig et al., 2003). A more common and tractable approach is, instead, to manipulate allothetic feedback by altering the salient visual cues in an environment. One well established experimental paradigm for doing this is to have animals perform a navigation task in an environment that contains a single dominant orienting landmark (e.g., a large white cue card), then rotate the cue while the animal is absent from the environment and re-assess the animal's behavior with the cue in its new position (Muller and Kubie, 1987). Rotation of visual cues has been shown to cause a comparable rotation in the goal locations visited by rats on a radial eight-arm maze (Suzuki et al., 1980), plus maze arena (O'Keefe and Speakman, 1987) and in the Morris watermaze (Wörtwein et al., 1995; McGauran et al., 2004). The cue rotation manipulation has also been used extensively to assess the degree to which the firing location and orientation of different classes of spatially-modulated cells are anchored to external environmental cues. These cells are classified based on their tuning to location, heading, environmental boundaries, running speed or some combination of spatial features (see **Chapter 1**). Rotation of visual cues causes a proportional

rotation in place cells, head direction cells, and border cells (e.g., Hafting et al., 2005; O'Keefe & Conway, 1978; Solstad et al., 2008; Taube et al., 1990b). Cue rotation-induced changes in place field stability and firing field location have, in turn, been shown to influence navigation behavior (e.g., Lenck-Santini et al., 2002, 2001; O'Keefe and Speakman, 1987).

As described previously, one means by which navigation can be performed in the absence of external cues is through an idiothetic cue-dependent computational process known as path integration, in which position is estimated through the continuous integration of linear and angular motion feedback (Mittelstaedt and Mittelstaedt, 1980; Etienne, 1992; McNaughton et al., 2006). While the rotation of visual cues is a simple and effective means of assessing the influence of allothetic cues in navigation, removing the animal from the environment prior to changing the cue configuration effectively resets the path integrator system and precludes investigation of the influence of ongoing self-motion feedback. In contrast to the cue rotation manipulation, several studies have instead assessed the differential contribution of idiothetic and allothetic cues by directly manipulated an animals' idiothetic feedback. This has been achieved by varying angular vestibular feedback through the use of a rotating a running platform (Sharp et al., 1995), or varying running distance by shifting a rat's starting position on a linear track (Gothard et al., 1996; Redish et al., 2000; Rosenzweig et al., 2003). In both of these conditions, the manipulation does not require the animal to be removed

from the apparatus and, therefore, does not introduce an interruption to ongoing path integration operations. In a study conducted by (Sharp et al., 1995) the rotation of a rat's running platform resulted in a similar rotation of CA1 place cell firing fields so long as the speed of rotation was detectable (i.e., above some presumed vestibular sensory-perceptual threshold). Similarly, varying relative running distance by shifting a rat's starting position on a linear track from trial to trial was also found alter CA1 firing fields (Gothard et al., 1996; Redish et al., 2000; Rosenzweig et al., 2003). Under this condition, when data was collapsed across trials, CA1 place fields at the start of the track were found to be more strongly aligned to the idiothetic cues (i.e., starting position) while those toward the end of the track were more strongly aligned to the allothetic cues (i.e., unaltered room cues).

Finally, a number of studies have investigated the influence of allothetic cues on spatial representation alignment through altering the availability of visual cues by simply turning the recording room lights on or off. In this paradigm, the baseline spatial orientation of firing fields is first assessed as rats navigate an environment when room lights are on and cues are illuminated. In these studies, the recording room typically contains several symmetry breaking distal visual cues distributed over 360° in the horizontal. Next, room lights are extinguished and firing field orientation is again assessed as the animal continues whatever behavior they are engaged in. In the absence of visual landmarks the spatial tuning

of cortical and thalamic head direction cells (Mizumori and Williams, 1993; Chen et al., 1994; Knierim et al., 1998; Zugaro et al., 2003), and CA3 place cells (Knierim et al., 1998) has been shown to undergo a radial drift that is thought to reflect accumulation of error in the ongoing path integration operation. Lights are then turned back on and directional tuning is again assessed to establish if firing fields realigned to the unchanged visual cues. Under this condition, head direction cells of both the anterior thalamic nucleus (Knierim et al., 1998) and anterodorsal thalamic nucleus (Zugaro et al., 2003) have been shown to realign with the visual cues on at least a subset of trials. A related approach, which does not rely on the intrinsic drift in spatial tuning, is to rotate cues while the room lights are off (Chen et al., 1994). Using this manipulation, head direction cells of the posterior parietal cortex realigned with the rotated cues on some trials but more often failed to realign (Chen et al., 1994). Using either of these experimental approaches exposes animals to an abrupt mismatch in allothetic and idiothetic feedback when illumination is restored without requiring the experimenter to physically interact with the animals at the time of the manipulation. There is, however, notable inconsistency between studies utilizing this technique in terms of the reported reliability with which realignment occurs. For instance, Chen and colleagues (1994) found that very few posterior parietal cortical head direction cells realigned to the cues after a single polarizing cue card was rotated by either 90° or 180° while lights were turned off. Furthermore, for the studies that

assessed realignment based on intrinsic field drift, head direction cells often displayed no change in alignment following the reintroduction of visual cues, but instead either maintained their current direction turning or changed in unpredictable ways (Knierim et al., 1998; Zugaro et al., 2003). One explanation for these incongruities is the differing geometric information provided by behavioral apparatuses and enclosures used in each of these studies, which can influence behavioral strategy (Cheng, 1986; Gallistel, 1990; Hermer and Spelke, 1994) as well as the tuning characteristics of various spatially modulated cell types (Lever et al., 2002; Barry et al., 2007; Krupic et al., 2015). Alternatively, the extent of control allothetic cues exert on spatial tuning may depend on the degree of mismatch between allothetic and idiothetic feedback (Knierim et al., 1998). Consistent with this argument, Knierim and colleagues (1998) observed that greater field drift, presumably reflecting greater accumulated idiothetic error, was found to lead to diminished realignment of directional tuning. A number of studies utilizing physical cue rotation have also reported place field remapping (Knierim et al., 1998; Yoganarasimha and Knierim, 2004; Yoganarasimha et al., 2006), but in studies in which external cues were rotated in an otherwise symmetrical environment by $\leq 90^\circ$, this remapping was infrequent and the majority of place cells showed reliable rotation with visual cues (Muller and Kubie, 1987; Knierim and Rao, 2003).

3.1.2. Stability of spatial representations

While spatial representations in CA3 are stable within the first

exposure to a novel environment and remain fairly consistent, those of CA1 show subtle changes over time (Lever et al., 2002; Leutgeb et al., 2004; Mankin et al., 2012; Ziv et al., 2013). Similarly, a number of studies have reported that CA1 fields are typically broader and more irregular in novel than in familiar environments (Wilson and McNaughton, 1993; Frank et al., 2004; Leutgeb et al., 2004; Brun et al., 2008). Even within a single episode of exposure to an environment, the precise spatial distribution and overall number of spikes emitted during consecutive passes through a place cells preferred firing field tends to vary from one traversal of the field to the next (Fenton et al., 1998, 2010; Olypher et al., 2002; Wikenheiser and Redish, 2011). This phenomena, referred to as *overdispersion*, suggests that a place cells positional code can vary on a trial-by-trial or even moment-by-moment basis. This overdispersion is thought to arise due to the implementation of different independent representations that are informed by additional ongoing space-independent cognitive operations. More recently, it has been found that a subset of both CA1 and CA3 principle cells, referred to as *time cell*, display explicit temporal modulation (Pastalkova et al., 2008; Itskov et al., 2011; Eichenbaum, 2014; Salz et al., 2016). Time cells selectively fire at distinct sequential moments such that, as an ensemble, the population can encode the relative time elapsed following some event such as the start of a delay period (MacDonald et al., 2011). These cells are found in the same neuronal population as place cells and the same cell can encode both

spatial and temporal information. Taken together, these findings suggest that the inclusion of inter-trial delays have the potential to confound the interpretation of pre- and post-manipulation differences in place cell firing following due to the effects of overdispersion and temporal modulation.

There is also evidence that representational stability depends on the perceived reliability and utility of the available spatial cues. In order to induce consistent reinstatement of an environment-specific representation, the orienting allothetic cues in an environment must be perceived as reliable and invariant indicators of an animal's absolute position and orientation within that environment. For instance, in a study in which rats witnessed polarizing cues being rotated, these cues eventually ceased to influence CA1 place field orientation (Jeffery and O'Keefe, 1999). This loss of cue control over firing field orientation persisted over multiple successive trials, suggesting rats learned to perceive these cues as unreliable landmarks. Interestingly, disorienting rats prior to exposure to an environment containing polarizing cues has been shown to impair visual cue-based navigation (Cheng, 1986; Margules and Gallistel, 1988; Biegler and Morris, 1993) and weaken the influence cues exert over place cell and head direction cell firing orientation (Knierim et al., 1995). These results were initially considered counterintuitive because early studies incorporated the use of disorientation with the express intention of disrupting an animal's ongoing heading signal in order to force them to rely on the orienting information provided by external environmental

landmarks. Knierim et al (1995) suggested that disorientation may have the opposite effect, in that rats begin perceiving the orienting visual cues in the environment as unstable and unreliable landmarks specifically because the orientation of these cues conflicts with the animals initial idiothetic estimate of orientation. Consequently, cue orientation may be perceived as varying from one trial to the next due to the mismatch in in the expected and perceived cue orientation. This interpretation was also supported by later modeling work investigating the effect of disorientation using attractor-based representational networks (Zhang, 1996; Redish, 1999). Within the context of these models, during learning external orienting cues (i.e., allothetic; e.g., cue card) are associated with the internal orienting cues (i.e., idiothetic; e.g., head direction representation) and not the other way around. As a consequence, the head direction signal has primacy over the activity of the network, particularly during the early moments of re-exposure to the environment when the various representational networks must be brought into a similar alignment. Under conditions in which the animal is disoriented and the head direction signal is perceived as being out of alignment with the room cues, the network will be biased to settle to the orientation relayed by the head direction network. There is also evidence that cues exert greater control over spatial representation networks under conditions in which the cues are necessary for successful performance of some related behavioral task. For instance, when assessing the stability of CA1 place field firing in mice

within a single episode of experience, Kentros et al. (2004) found that firing fields remained stable over longer intervals of time during conditions in which spatial cues were required for successful task performance as compared to conditions in which mice foraged for randomly scattered food reward. These findings suggest that representation stability depends on the significance of contextual information and, likely, the degree to which animals attend to the environmental cues. Based on these observations, experimental approaches that incorporate behaviorally relevant environmental cues may enable more reliable time- and trial-invariant assessments of allothetic cue control over spatial representation networks.

3.1.3. The time-course of spatial representation updating

The instantiation and maintenance of spatial representations is a dynamic process that requires ongoing and continuous integration of self-motion and sensory-perceptual signals. As previously described, when rats traverse a linear track over successive trials in which the start box (i.e., the rats' starting position) is moved forward incrementally, CA1 place fields show a tendency to transition from being box-aligned to being room-aligned as rats run further along the track. To determine if the point at which the hippocampal map realigned to the allocentric reference frame was better predicted by the time elapsed from when the rat leaves the start box or, alternatively, the rat's position on the track, Redish et al. (2000) investigated the time-course of realignment by assessing the population level CA1 spatial firing activity on a moment-by-moment basis.

Using this approach, they were able to demonstrate that the transition in alignment is better predicted by time than any of the position metrics assessed and, consequently, more likely a function of time and not position. Due to limitations inherent in this experimental approach, however, it was not possible to determine the precise time-course with which the representation updated.

In general, approaches that require manual manipulation of experimental conditions are not optimal for characterizing the time-course over which network updating occurs in response to the manipulation, as there is no discrete event that network changes can be time-locked to. This is an important consideration given the small time scales over which spatial representations can update in response to a sudden change in sensory feedback. For instance, by relying on intrinsic directional drift when room lights were off, Zugaro and colleagues (2003) assessed the time-course of directional realignment of anterodorsal thalamic nucleus head direction cells and found that these cells could realign to the room cues as rapidly as ~80 ms following cue illumination. Similarly, Jezek and colleagues (2011) showed that when contextual lighting cues are instantaneously switched to those associated with a different environment, the CA3 place cell ensemble representation rapidly 'flickers' between the two competing environment representations during the first half of the theta cycle, settling into a stable representation for the new environment by the last half of the theta cycle. This suggests that CA3 place cells can

rapidly and coherently transition between different spatial representations within a time-window of one theta cycle (i.e., ~125 ms).

As previously described, even in the absence of cue manipulation, different place cell representations are rapidly instantiated at compressed time scales within individual theta cycles (see **Chapter 2.3.2**). These *theta sweeps* can trace out multiple options prior to the animal selecting a path and have been shown to co-occur with decision related behaviors, suggesting the activation of transient representations likely plays a meaningful role in real time action selection (Johnson and Redish, 2007). In one of the first studies examining the theta sweep phenomenon, Gupta et al. (2012) found that the majority of sequence representations occurring during theta sweep events tended to correspond to segments of the environment that were bounded by physical landmarks. Similarly, Wikenheiser et al. (2015a) found that theta sequences tended to represent the space between the animal's current position and one of three possible reward locations on a circular track. In addition, the distance these sequences projected ahead of an animal was predictive of the animal's ultimate goal destination. While theta sequences have yet to be assessed under experimental conditions that explicitly vary allothetic or idiothetic feedback, these findings suggest that environmental landmarks may serve to segment the environment and discretize the available sequence representations into the most behaviorally salient set of possible goal-related trajectories (Wikenheiser and Redish, 2015b).

3.1.4. Assessing navigation in virtual reality environments

One relatively recent and important development in the field of navigation research is the introduction of a number of custom and commercially available virtual-reality instruments that enable full experimenter control of the visual landscape during simulated spatial navigation. These tools have been used to study navigation behavior and neural activity in a wide range of animal models (Hölscher et al., 2005; Harvey et al., 2009; Seelig and Jayaraman, 2015). (Hölscher et al., 2005). Prior to its adoption for non-human animal model research, virtual-reality had already been successfully used for human behavioral and imaging investigations of navigation (Gillner and Mallot, 1998; Maguire et al., 1998). Adaptation of virtual reality systems for use in various animal models has allowed for the incorporation of techniques such as intracellular recording (Harvey et al., 2009) and cellular-resolution optical imaging (Rickgauer et al., 2014). This has enabled more detailed and comprehensive investigations of spatially-modulated neural activity, some of which would otherwise be impossible in freely behaving animals. One important limitation of virtual reality, however, is that human subjects are typically stationary while non-human subjects are often head-fixed, which diminishes the presence of vestibular feedback. The resulting attenuation of vestibular information is likely not a trivial consideration given the role vestibular feedback plays in spatial processing (Stackman et al., 2002; Shinder and Taube, 2011). Consistent with this, studies comparing the

activity of place cells in virtual reality and real-world (i.e., non-virtual) conditions, both of which incorporated a similar configuration of distal visual cues, reported diminished spatial selectivity in the virtual reality compared to real-world place fields (Ravassard et al., 2013; Aghajan et al., 2015). Alternatively, virtual reality 3D headsets have also been adapted for use during real-world navigation, allowing the experimenter to precisely control external visual cues while preserving naturalistic self-motion (i.e., idiothetic) feedback (Tcheang et al., 2011). At present, however, these systems are only designed for use with human participants, limiting their application to behavioral research and non-invasive recording techniques.

3.1.5. Aims and design principles

The purpose of the present study was to assess a novel behavioral apparatus, the Instantaneous Cue Rotation (ICR) arena, which was designed to enable manipulation of real-world environmental cues in a repeatable, rapid and precisely timed manner as rats traverse a circular track. Using this system, an animal's allothetic feedback can be varied while idiothetic feedback is held constant, allowing these two spatial signals to be put in direct and immediate conflict while preserving all other navigation-related sensory input. This is achieved by utilizing projected visual cues to provide all symmetry breaking visual information in the environment. As a consequence, the orienting cues in the environment can be rotated remotely and instantaneously during real-world running

behavior, precluding any interruption to ongoing path integration operations while also preserving angular and vestibular feedback. In addition, the absence of delays between pre- and post-manipulation testing diminishes the potential for unintended effects from overdispersion or temporally modulated changes in unit firing. Furthermore, with the ability to alter cues remotely and without any direct experimenter intervention, behavioral changes driven by experimenter interaction with the animal or unintended alterations in spatial context can be avoided. Finally, because the manipulation of visual feedback is immediate, event-related changes in running behavior and neural activity can be assessed with a high degree of temporal precision.

The ICR apparatus also incorporates a goal navigation task that requires animals to utilize the projected visual cues to navigate to a designated visual cue-aligned reward location. Importantly, identification of the goal location cannot be achieved using local cues proximal to the goal location but instead requires rats to use the full 360° panorama of cues. The inclusion of the goal navigation task allows for real-time and ongoing assessment of allothetic cue-based navigation accuracy. This approach also ensures that cues provide behaviorally relevant information, which reinforces attending to the allothetic cues in order to successfully navigate to the correct goal location. Importantly, comparison of goal navigation performance before and after cues are rotated enables allocentric realignment to be quantified in the behavioral domain. This metric can in

turn be used to contextualize neurophysiological changes with respect to an animal's behavioral output. The data presented here were collected as part of two separate exploratory behavioral studies that were performed to assess the feasibility of either *fixed feeder* or *mobile feeder* reward delivery systems, which are described in detail in the next section. The present chapter presents the data from both of these studies in the context of the single larger study assessing the overall behavioral component of the ICR task.

3.2. Materials and methods

3.2.1. Subjects

A total of 18 9- to 26-month-old male F344 rats participated in the study. Of these 9 (9- to 26-month-old) and 9 (13- to 25-month-old) rats were included in the fixed feeder and mobile feeder experiments, respectively. Due to the visual demands of the task, rats unable to perform the visual portion of the Morris watermaze were excluded from participation in the study. All experimental procedures were in accordance with National Institutes of Health guidelines. Both fixed feeder and mobile feeder experiments included an old and young cohort. For all findings reported in this chapter, however, no age comparisons were performed and data was averaged across age groups. For results and discussion from the age comparison see Chapter 4.

3.2.2. *Instantaneous Cue Rotation apparatus design*

The apparatus consists of an arena designed to allow rats to traverse a circular track in the clockwise direction and to stop at a learned goal location defined exclusively by a panorama of visual cues projected onto the surrounding walls. The circular track is 1.4 m in diameter and is enclosed by 68 cm tall cylindrical walls made up of four panels of FlexGlass[®] designed for rear projection (Screen Innovations). The track is 10 cm wide and includes a 7 cm tall inner wall. The track base and inner wall are made of acrylic plastic with an electrostatic dissipative coating making it compatible with electrophysiological recording. We refer to these components of the apparatus as the *arena* throughout. The entire assembly is suspended from U-Channel tracks in the ceiling of a 4 m x 4 m x 2.5 m room. The structural framing is built from 80/20[®] t-slotted extruded aluminum while the main body of the apparatus is built from custom fabricated components composed predominantly of acrylic and Sintra[®] PVC foam board. The 360-degree panorama of visual cues is produced by four BenQ MW621ST short throw projectors that are mounted at fixed intervals around the outside of the apparatus (**Figure 3.1**).

Position coordinates for the rat and mobile feeder are collected online using a Neuralynx Digital Lynx SX Cheetah Data Acquisition System (Neuralynx) that acquires video tracking data through a video camera mounted above the apparatus (**Figure 3.1**). For the purpose of

tracking, a battery-powered red LED with a diffuser lens is clipped to the fur of the rats upper back. The Digital Lynx SX is also used to store synchronous timestamps for various operations. Reward events are triggered by an Arduino® Due microcontroller (referred to from here on as *AD1*) connected to the Digital Lynx SX TTL input panel to store the corresponding timestamps. To acquire precise timestamps corresponding to changes in the projected image (i.e., when the rotated version of the image is displayed), a small yellow circle is briefly projected onto phototransistors mounted next to each wall quadrant, which triggers a 5V TTL pulse that is also sent to the Digital Lynx SX.

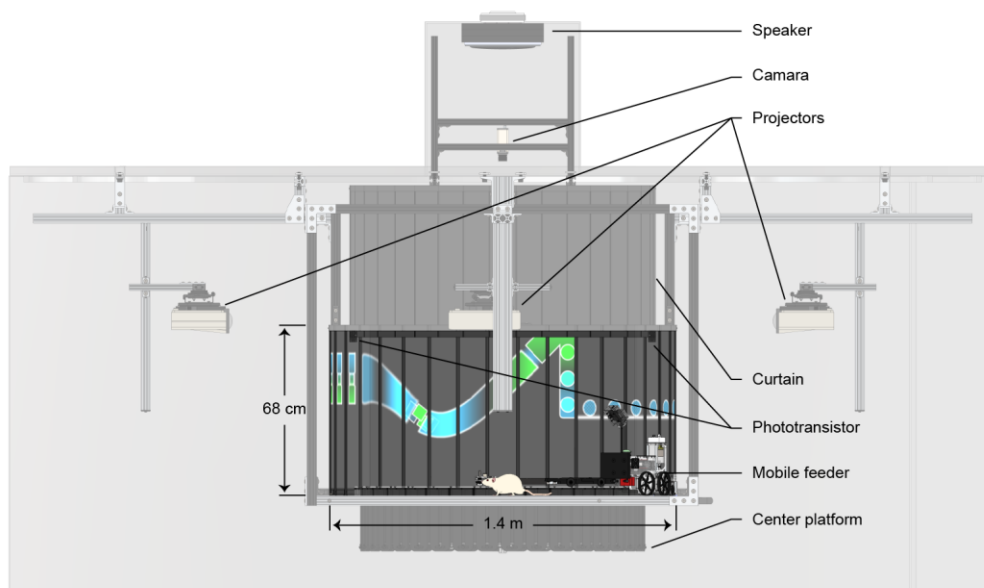


Figure 3.1: Schematic of the Instantaneous Cue Rotation apparatus.

Side view of the apparatus with a cross-sectional view of the interior of the arena. The apparatus is suspended from U-Channels in the ceiling of the recording room. The arena is made up of a 1.4 m diameter circular track with a 68 cm tall outer wall and 7 cm tall inner track wall. A speaker and camera are mounted in a recess of the ceiling above. Three of the four projectors are shown as is a partial interior view of the projected wall image. Phototransistors mounted to the arena walls detect when a new image is displayed and send a signal to the Digital Lynx SX that stores a corresponding timestamp. A curtain above the arena, and platform below, occlude the visibility of features outside the arena. The mobile feeder is also shown in the position it maintains relative to the rat when actively tracking the rat's movement.

Considerable effort has been devoted to limiting any orienting cues other than those provided by the projectors. All structural components within the apparatus are identical every 10 degrees such that they provide no symmetry breaking spatial information. In order to mask orienting auditory cues, white noise was played continuously through a speaker mounted above the track. A number of steps were also taken to diminish the influence of food reward related olfactory cues as well as potential scent cues from rat excretions, which are discussed in the following sections.

3.2.3. Fixed feeder reward system

For the fixed feeder version of the task, a liquid food reward is dispensed from one of 36 identical black polyethylene feeder dishes that are evenly spaced along the outer perimeter of the track. Only two of the dishes provide a liquid food reward while the rest act as sham feeders. The two active feeders are connected to a reservoir of vanilla Ensure[®] that is dispensed into the dish using hydraulic solenoid valves controlled by the AD1 microcontroller. For each reward event the AD1 microcontroller also sends a 5V TTL pulse to the Digital Lynx SX, which in turn stores a corresponding timestamp.

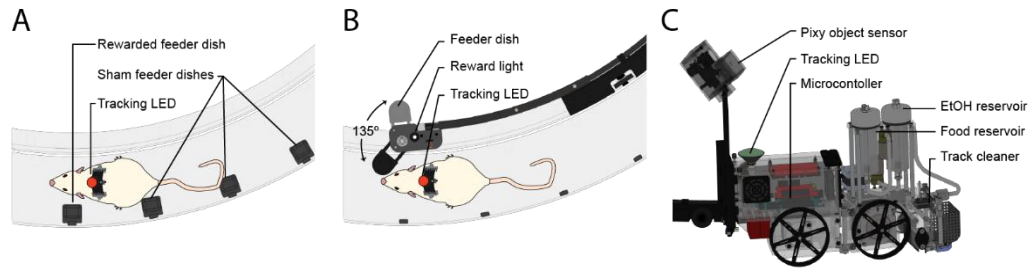


Figure 3.2: Reward delivery systems for the fixed and mobile feeder versions of the Instantaneous Cue Rotation task.

(A) Top view of the track illustrating the feeder dish placement for the fixed feeder version of the task. For each traversal, only one feeder dish is rewarded while the rest act as shams. A red LED is clipped to the fur of the rat's upper back for the purpose of position tracking. At the time of reward delivery, a tone is sounded and the liquid food reward dispensed into the dish from a reservoir of liquid food reward housed outside the arena **(B)** Top view of the mobile feeder dish used for the mobile feeder version of the task. At the time of reward delivery, the feeder dish is extended within reach of the rat, liquid food reward is released into the dish from the food reservoir and a reward light is lit. **(C)** Side view of the mobile feeder cart showing the Pixy object sensor that is used, in addition to the overhead camera, to track the rat's position on the track. A tracking LED is also mounted to the mobile feeder to continually track the position of the mobile feeder using the overhead camera. As the mobile feeder pursues the rat, the track cleaner removes waste from the track and wipes the surface clean.

3.2.4. Mobile feeder reward system

For the mobile feeder version of the task, liquid food reward is delivered from a single dish that moves in concert with the rat. The advantage of a moving reward delivery system is that it limits the presence of stationary odor cues that could become associated with a given position on the track. The mobile feeder is composed of a two-wheeled stepper motor driven cart with a raised arm that rides along the inner track wall **(Figure 3.2B and 3.2C)**. The arm extends 60 cm ahead of the cart and terminates with a feeder dish from which vanilla Ensure[®] is dispensed. The mobile feeder has been designed to unobtrusively match the rats pace, maintaining a fixed distance from the rat such that the feeder dish is always to the immediate right of the rat's head. Control of the stepper

drivers and all peripheral components and onboard computations is performed by a second Arduino® Due microcontroller (referred to from here on as *AD2*) housed in the body of the mobile feeder cart (**Figure 3.2C**). The mobile feeder is designed to be completely wireless, which eliminates both the need for a commutator as well as the additional visual cues caused by cable lines. Commands are relayed to and from the mobile feeder through the use of XBee-PRO® Series 1 radio frequency modules and all power is provided by a Venom® 30C 3S 7500mAh 11.1V LiPo Battery.

The robot smoothly tracks the rat's position and velocity using real-time positional tracking data from two separate sources. The first is a video camera mounted above the apparatus (**Figure 3.1**) and the second is a Pixy (CMUcam5) object sensor mounted above the front of the mobile feeder (**Figure 3.2C**). In order to attain a more accurate estimate of the rat's position and velocity an extended Kalman filter is employed using the position measurements from both the overhead camera and Pixy (CMUcam5) vision sensor.

Reward events are initiated directly from the mobile feeder using the rat's tracking data. In its default retracted state the feeder dish is positioned out of the rat's reach. At the time of reward delivery, the robot comes to a complete stop and the feeder dish pivots to a position easily accessible by the rat. Concurrently with the arm extension, a reward light next to the dish is illuminated and reward is dispensed into the dish using

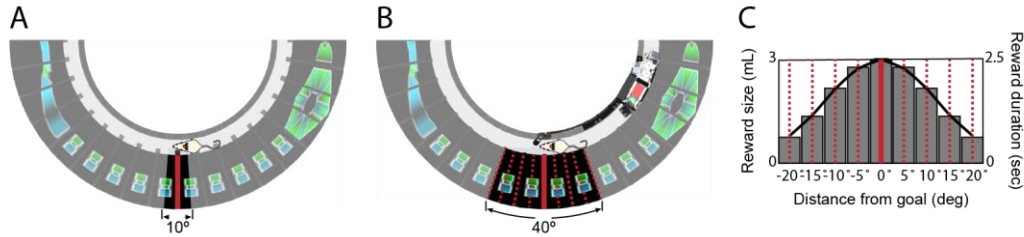


Figure 3.3: Reward schedule for the fixed and mobile feeder versions of the Instantaneous Cue Rotation task.

(A, B) Top view of the ICR arena showing the location of one of the two goal locations with respect to the projected cues, as well as the goal bounds that the rat is required to stop within in order to receive food reward for the (A) fixed feeder and (B) mobile feeder version of the task. For the fixed feeder version of the task rats must stop within $\pm 5^\circ$ of the goal bounds to trigger reward. (C) For the mobile feeder version of the task the bounds are widened to $\pm 20^\circ$ and the size of the food reward, as well as the duration of the reward light and tone, are varied as a function of the animal's distance from the goal and follow a normal distribution (bottom).

a hydraulic solenoid valve connected to a reservoir of the liquid food reward (Figure 3.2C). Once 15 seconds has elapsed or the rat has moved passed the feeder dish, the feeder dish retracts and the robot resumes following the rat. Timestamps for reward events, as well as other operations performed by the mobile feeder, are synchronized using an IR sensor on the top of the cart body in conjunction with an IR emitter array mounted above the ICR arena. Every 60 seconds the AD1 microcontroller pulses the emitter array and stores a timestamp using the Digital Lynx SX TTL input panel. Concurrently with each pulse a local timestamp is saved by the mobile feeder and written to an onboard SD card. The log of events and timestamps are streamed to the primary PC at the end of each session to be synchronized with other events offline.

In order to further limit any contamination of the environment with unintended visual or odor cues the mobile feeder is equipped with a system for continuously cleaning the surface of the track. At the rear most

end of the mobile feeder cart is a perforated PVC plastic receptacle that scoops waste from the track with the assistance of a rotating neoprene rubber flap connected to the main drive train of the mobile feeder (**Figure 3.2C**). A strip of high-absorbency polyurethane foam clipped to the underside of the receptacle wipes liquid waste from the track and is periodically saturated with 75% ethanol from a hydraulic solenoid valve connected to an ethanol reservoir suspended above. The entire assembly can then be easily removed from the mobile feeder cart for cleaning at the end of each session.

3.2.5. Software

For both the fixed feeder and mobile feeder system, a custom Matlab[®] script is used as the basis of the front end user interface. This script is also responsible for processing tracking data collected through the Neuralynx Digital Lynx SX Cheetah Data Acquisition System (Neuralynx). Control of the projectors, white noise and reward tone is performed by a second custom Matlab[®] script running on a separate computer. A custom Matlab script was used to pre-process the projected images using a coordinate transformation to match the optics of the projector and the curved wall surface. A custom C⁺⁺/C script running on the AD1 microcontroller is used for processing signals from the wall mounted phototransistors during image changes as well as to trigger the reward tone during reward events via an optical AC relay.

The mobile feeder system requires a number of additional

programs. Because of performance limitations of the Matlab[®] interpreted language, a custom C# script running on the same computer was used for all wireless communications with the mobile feeder including streaming real time position data and relaying commands from the Matlab[®] user interface. The AD2 microcontroller is loaded with a custom C++/C script that handles the wireless communication, processing of tracking data, stepper motor control, control of the liquid food reward and EtOH solenoids, feeder dish positioning, triggering of the reward cue light, as well as a number of auxiliary operations.

3.2.6. Instantaneous Cue Rotation experiment

The Instantaneous Cue Rotation (ICR) task was designed to assess the timing and degree to which rats utilized external orienting visual cues to navigate to a goal location. At the start of training, animals were food restricted until they reached 85–90% of their free feeding weight based on their motivation to run for liquid food reward.

We describe two different versions of the ICR task that utilize the two different reward delivery systems described above. For both versions of the task rats are trained to traverse the circular track and stop at the goal location for a fixed period of time in order to receive food reward. At the start of the experiment, each rat is pseudo-randomly assigned one of two possible goal locations that are at opposite sides of the arena. The goal location for each rat is preserved for the duration of training and testing. The projected cues adjacent to each of the two possible goal

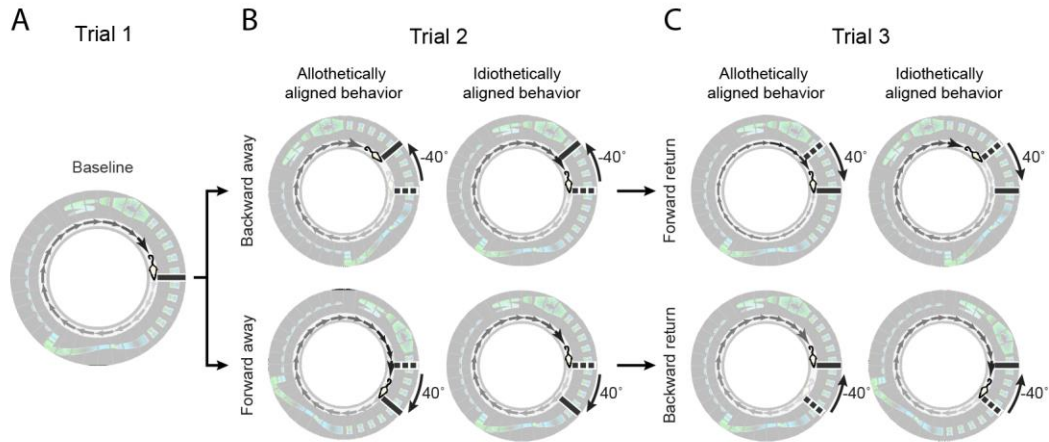


Figure 3.4: Instantaneous Cue Rotation (ICR) task overview.

Schematics shows a top-down view of the ICR arena illustrating the possible combinations of projected cue configurations and expected running behaviors over three consecutive trials within a single day of testing on the ICR task. The example shown here applies to both the fixed feeder and mobile feeder versions of the task. For each example, gray lines denote the current goal location (solid line) and, where applicable, the previous (i.e., non-current) goal location (dashed line). Small arrows on the track denote the rat's running distance from the non-current goal to the current goal location, going from light gray to black based on the rat's proximity to the new goal location. **(A)** Each session begins with a *baseline* trial in which rats must stop at their learned goal location over consecutive laps to receive food reward (solid line). Note, while each rat is trained to stop at one of two possible goal locations, each of which is embedded in a repeating pattern within the panorama of projected cues at opposite sides of the arena, only one of the baseline goals is shown for this example. **(B)** Once rats have completed 5-15 baseline laps, the projected cues and goal location are rotated away from their baseline configuration either backward (*backward away*; top panels) or forward (*forward away*; bottom panels). At this time rats are no longer rewarded if they stop at the non-current goal location (dashed line) but must instead stop at the new goal location (solid line). If rats are primarily utilizing allothetic cues (i.e., the projected image) to navigate to the goal, they should stop at the new goal location (left panels). Alternatively, if rats are instead relying on idiothetic cues (e.g., running distance) they should continue to stop at the non-current goal location (right panels). **(C)** After rats have completed 5-15 laps with the cues in their rotated configuration, the cues are then rotated either forward (*forward return*; top panels) or backward (*backward return*; bottom panels) returning them back to their baseline configuration. Once again, the expected navigation behavior is shown for situations in which rats utilize either allothetic cues (left panels) or idiothetic cues (right panels) to navigate to the goal.

locations are identical for 50 degrees to either side (**Figure 3.3**). This is done to eliminate any local visual cue information in the projected image, requiring the rats to use the full panorama of visual cues for accurate navigation to the goal location.

3.2.7. Training on the Instantaneous Cue Rotation task

The training protocol for both versions of the task is divided into three stages: 1) *task acclimation*, in which rats are acquainted with running on a circular track and eating from the food dish; 2) *goal learning*, in which rats learn a specific rewarded goal location; 3) *delayed reward*, in which rats learn to stop for successively longer intervals within the goal bounds prior to receiving reward.

For both versions of the task, reward delivery is always accompanied by a 2500 Hz ~50 dB tone, although the duration of the tone varies based on several factors (See below). For the mobile feeder version of the task, a light next to the feeder dish is also flashed when rewards are delivered (**Figure 3.2B**). For the fixed feeder version of the task, rats are required to stop for either 0.5, 1 or 1.5 seconds within $\pm 5^\circ$ (i.e., $\pm \sim 6$ cm) of the goal location in order to receive food reward (**Figure 3.3A**). For the mobile feeder version of the task, rats are required to stop for either 1, 2 or 3 seconds within the goal bounds and the goal boundary is widened to $\pm 20^\circ$ (i.e., $\pm \sim 24$ cm; **Figure 3.3B**). In addition, the reward size, as well as tone and reward light duration, is varied as a function of the animal's distance from the reward target and follows a normal distribution (**Figure 3.3B**). For instance, stopping within $\pm 2.5^\circ$ of the goal location results in the largest reward (3 ml) and longest tone and reward light (2.5 sec), whereas stopping at the furthest bounds of the goal location (i.e., -20° or $+20^\circ$ from the goal, **Figure 3.3B**) results in the

smallest reward (0.8 ml) and the shortest tone and reward light (0.5 sec). The purpose of this reward structure is to provide animals more detailed feedback on their performance as well as to sustain the animal's motivation even when accuracy is not at the highest levels.

For the fixed feeder version of the task, the *task acclimation* stage of training requires rats to learn to traverse a smaller 94 cm diameter enclosed circular track housed in a different room from the ICR apparatus. This track includes only one feeder dish. Directly above the dish is a flashing 5 cm by 5 cm white square. After each traversal, rats are automatically rewarded from the feeder dish and a tone is sounded for 1.5 seconds. In the event that a rat attempts to run in the incorrect direction (i.e., counter-clockwise) they are physically blocked by the experimenter using a hand held barrier. At the same time, a 4000 Hz ~50 dB beeping tone is sounded to indicate incorrect behavior. Rats performing the fixed feeder version of the task are transitioned to the next stage of training once they are able to complete 20 laps within 20 minutes. For the mobile feeder version of the task, the *task acclimation* stage does not require the second circular track. Instead, rats are immediately introduced to the ICR arena. The mobile feeder is manually moved by the experimenter as the rat ambulates along the track and reward is delivered anytime the rat approached the dish. Rats performing the mobile feeder version of the task are transitioned to the next stage of training once they are consistently moving toward, and eating from, the dish.

For the fixed feeder version of the task, during the *goal learning* stage of training rats are transitioned to the ICR arena and taught to stop at their designated goal location using a projected flashing white square similar to that used in the separate task acclimation environment. Rats are automatically rewarded at their respective goal location following each clockwise traversal of the track and a tone is sounded for 1.5 seconds. In the event that rats run in the incorrect direction an aversive beeping tone is sounded, similar to that used in the task acclimation environment, and the rat is physically corrected by the experimenter only if they fail to self-correct after 30 seconds. For the mobile feeder version of the task, during the *goal learning* stage rats are actively tracked by the mobile feeder. Instead of using a flashing cue to indicate the rat's goal location, the mobile feeder automatically stops and dispenses reward within the bounds of the goal location. For both versions of the task, rats are transitioned to the next training stage once they are able to complete a minimum of 20 laps within 20 minutes.

For the fixed feeder version of the task, the *delayed reward* stage of training requires rats to stop within $\pm 5^\circ$ of the goal location on their own for a minimum of 0.5 seconds to receive food reward (**Figure 3.3A**). The latency of reward delivery is then incrementally increased over successive training days to 1.5 seconds, forcing the animals to pause for longer intervals to trigger reward delivery. For the mobile feeder version of the task, during the *delayed reward* stage rats must stop within $\pm 20^\circ$ of the

goal and the latency until reward delivery is incrementally increased from 1 to 3 seconds over successive training days. As previously described, for the mobile feeder version of the task the reward size, as well as tone and reward light duration, varies as a function of the animal's distance from the reward target (**Figure 3.3B**). For both versions of the task, training is completed once rats are able to run 20 laps within 20 minutes and trigger a reward at the maximum delay on at least 80% of the traversals.

3.2.8. Testing on the Instantaneous Cue Rotation task

Testing on the ICR task is similar for both the fixed and mobile feeder versions of the task. Testing begins once the rat is able to trigger a reward at the maximum delay period on 80% of traversals. Each testing session begins with a *baseline* phase in which rats are allowed to run between 5 and 15 laps in order to collect a baseline of their navigation accuracy for that day (**Figure 3.4A**). Following the baseline phase of testing rats experience either a *forward rotation* or *backwards rotation* in which all projected cues are rotated either 40° clockwise or counterclockwise, respectively (**Figure 3.4B**). Each rotation event occurs when the animal is either 90°, 180° or 270° from the goal location, which is determined based on random sampling without replacement. Following rotation, the rewarded goal location, or dish in the case of the fixed feeder version of the task, is changed such that the relative position of the goal is maintained with respect to the projected image. Rats are allowed to run an additional 5 – 15 laps with the cues in their rotated configuration, at which

point cues once again undergo either a forward or backward rotation to bring them back to their original configuration (**Figure 3.4C**). Rats are then required to stop at the original goal location in order to receive a reward. This procedure is performed 1 – 3 times for each day of testing.

3.2.9. Data analysis

All post-processing and data analyses are performed using Matlab® 2017a. All video tracking data are converted from Cartesian to polar coordinates and only radial (rad) values are used in order to reduce the tracking data to a single dimension (i.e., the rats position on the circular track in radians). Position data collected while rats are consuming reward are excluded. Unless otherwise specified, data are organized hierarchically by *lap* (i.e., a single traversal of the track), *trial* (i.e., all laps run for a given day when cues are in either their baseline, backward rotated or forward rotated configuration) or *session* (i.e., a given day of running on the Instantaneous Cue Rotation Task).

Instantaneous velocity is also computed separately for each lap from the smoothed rad and timestamp time-series values by taking the difference of adjacent rad values divided by the difference of the adjacent timestamps values. These values are then used to compute the velocity at each position on the track by binning the data using 1° ($\pi/180$) bins and computing the average velocity within each bin for each lap.

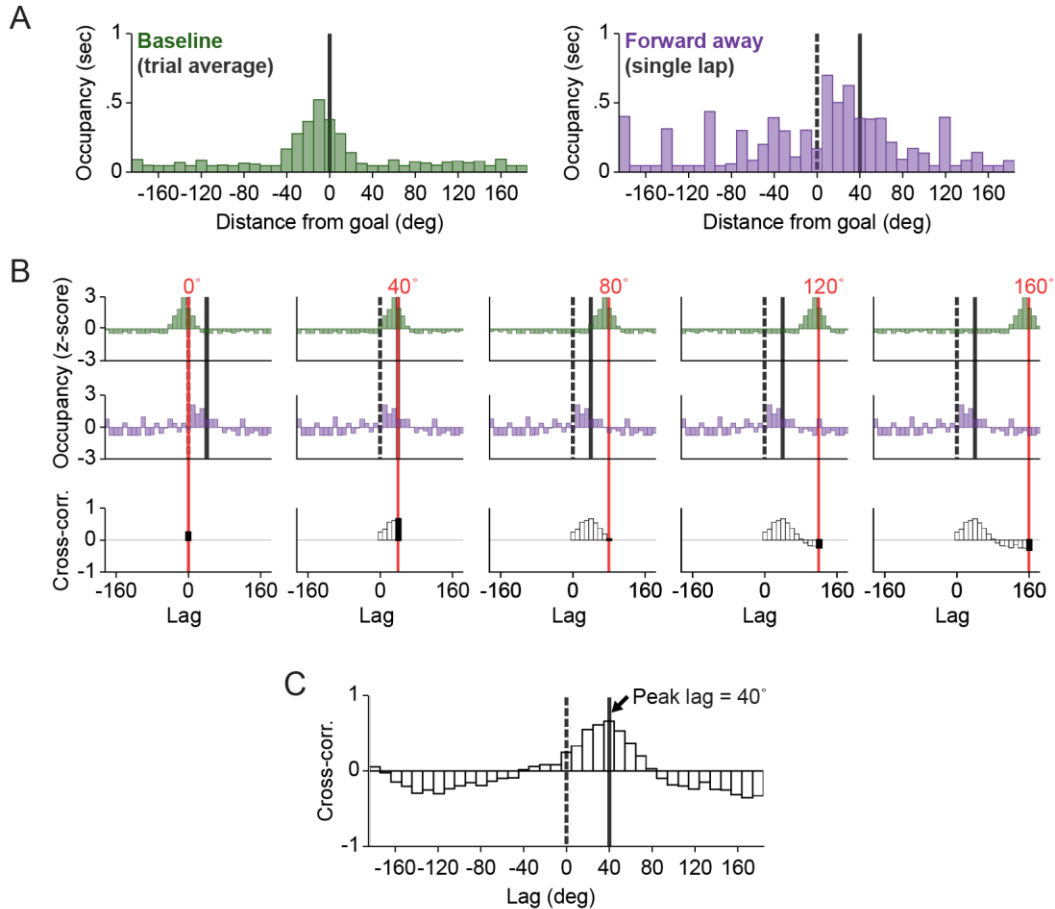


Figure 3.5: Procedure for quantifying behavioral realignment.

Illustration of the procedure used to compute overall behavioral realignment following cue rotation. Gray vertical lines denote the current (solid) and non-current goal location (dashed). **(A)** Simulated data representing a typical occupancy vector averaged across all laps within a single baseline trial (green) and simulated occupancy data from a single lap following forward away cue rotation (purple). Note that occupancy data is shown using 10° bins for the purposes of illustration. **(B)** For each rotation trial, the z-scored occupancy vector from the preceding trial (top row of panels) is lagged (i.e., shifted) bin-by-bin and correlated with the z-scored occupancy vector for a given post-rotation lap (middle row of panels) resulting in a single correlation value for each lag (bottom row of panels). Several example lags between 0° and 160° are highlighted. Note that correlating the shifted baseline occupancy vector (top panels) and un-shifted post-rotation occupancy vector (middle panels) results in a different correlation value (bottom panels; solid black bar) for each lag. **(C)** This procedure is used to construct the cross-correlogram, which includes the correlation between the pre- and post-rotation running behavior for all possible lags. Identifying the lag at which the maximal correlation is found (i.e., *peak lag*) provides a lap-by-lap scalar metric of behavioral realignment that quantifies the degree to which an animal's running behavior rotated with the cues.

Occupancy histograms were computed separately for each lap from rad values using 1° ($\pi/180$) bins divided by the time spent within each bin.

Occupancy cross-correlations are computed using the occupancy

histogram values (**Figure 3.5**). The occupancy vector for each lap is detrended by subtracting the mean and dividing by the standard deviation (i.e., z-scored). Each occupancy vector is then normalized so that the autocorrelation at 0° lag is equal to 1. Occupancy is then averaged across laps within each rotation trial for each daily session. Cross-correlograms are then constructed between the occupancy data for each lap following rotation and the mean occupancy data from the previous trial, using a lag range of -180° to 180° incremented by 1°. This results in a cross-correlation vector for each lap following a backward or forward rotation lap, providing a measure of the similarity between the post-rotation occupancy vector and the mean occupancy vector prior to each cue rotation at lags from -180° to 180°. The cross-correlation can therefore be used to determine the degree to which an animal's running behavior rotated with the projected cues following a cue rotation event by assessing the correlation value for each lag. For instance, if the cross-correlogram for a given lap shows a single peak centered at the 40° lag following a 40° cue rotation, this would indicate that the animal's running behavior for that lap rotated by exactly the same amount as the projected cues.

3.2.10. Statistical analysis

Statistical analyses are performed using Matlab® version 2017a. All results are reported as mean ± S.E.M. and are considered significant for p values < 0.05 (two-tailed). Statistical significance is indicated as p < 0.05 (*), p < 0.01 (**), and p < 0.001 (***). ANOVA is used for statistical analysis

in which the predictor variables are categorical. Post-hoc tests are applied when necessary using two sample Student's t-tests and Bonferroni-Holm corrections are performed to adjust for familywise error. Unpaired t-tests were used for any post-hoc comparison between fixed feeder and mobile feeder versions of the task, otherwise paired t-tests were used. Simple linear regression was used for statistical analysis in which the predictor variable was continuous.

3.3. Results

3.3.1. Training on the Instantaneous Cue Rotation task

While both the fixed feeder and mobile feeder experiments included an old and young cohort, age differences were not assessed for the findings reported in this chapter and both old and young rats were grouped together. Findings from the age comparison will be reported and discussed in the following chapter (see **Chapter 4**). The total number of days required to reach criterion for all three training stages was 45 ± 25 days for the fixed feeder version of the task and 31 ± 9 days for the mobile feeder version of the task. Repeated measures 2-way ANOVA revealed a significant feeder version \times training stage interaction (ANOVA: $F_{2,18} = 3.95$, $p < 0.05$) and post-hoc comparison showed that rats participating in the fixed feeder version of the task required significantly more days to reach criterion for the task acclimation stage than did rats participating in the mobile feeder version of the task (fixed feeder: 29 ± 17 days; mobile

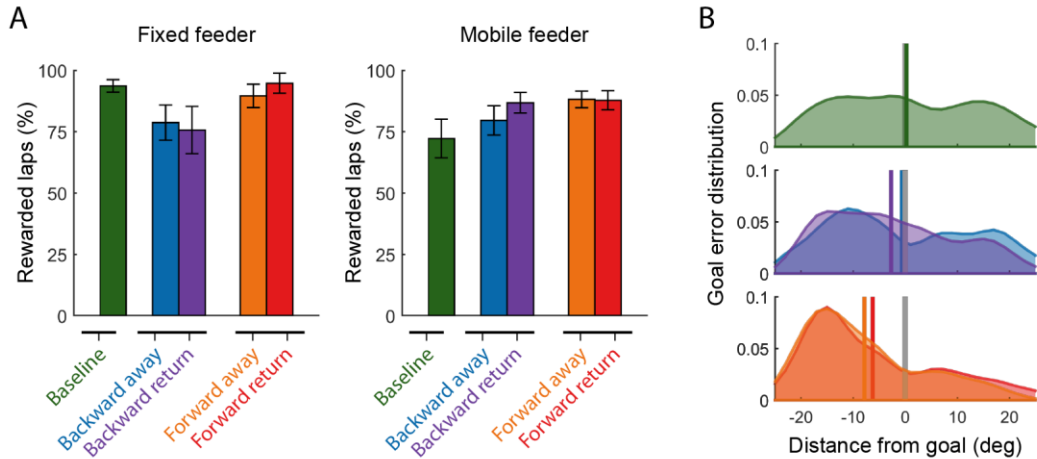


Figure 3.6: Goal navigation performance and accuracy on the Instantaneous Cue Rotation task.

(A) Mean percentage of laps rewarded \pm S.E.M for baseline trials as well as each of the four rotation conditions from rats participating in the fixed feeder (left) and mobile feeder (right) versions of the task. (B) For the mobile feeder version of the task, rats were able to trigger reward delivery by stopping anywhere within $\pm 20^\circ$ of the designated current goal location. The distributions show the goal error (i.e., position at the time of reward minus the goal position in degrees) for each of the rotation conditions for the rats participating in the mobile feeder version of the task. Black vertical lines denote the current goal location and colored vertical lines denote the distribution mean. Vertical colored lines denote the mean goal error for each cue condition. Note that following forward rotations rats showed a significant negative mean goal error indicating that rats were more likely to stop ahead of the goal.

feeder: 3 ± 1 days; t-test: $t_{13} = 3.69$, $p < 0.05$). This result was expected because of the greater difficulty of the fixed feeder version of the task acquisition training stage. There was no significant difference between rats participating in the fixed and mobile feeder versions of the tasks in the number of days required to reach criterion for either the goal learning (fixed feeder: 11 ± 7 days; mobile feeder: 13 ± 5 days; t-test: $t_{12} = -0.53$, $p = 1.82$) or delayed reward (fixed feeder: 6 ± 14 days; mobile feeder: 6 ± 10 days; t-test: $t_{15} = -0.03$, $p = 1.27$) stages of training.

3.3.2. Goal navigation performance on the Instantaneous Cue Rotation task

Once testing began, rats participating in both versions of the task underwent an equivalent number of rotation sessions (4 ± 2 days). For all analysis described in this section data were segregated for each cue condition (**Figure 3.4**). These include *baseline* trials as well as trials in which cues were rotated $\pm 40^\circ$ away from or back to their baseline configuration in either counter-clockwise direction (i.e., *backward away*, *backward return*) or clockwise direction (i.e., *forward away*, *forward return*). First, the percentage of rewarded laps was computed for each cue condition to assess overall goal navigation performance both before and after cue rotation (**Figure 3.6A**). Rats trained on the fixed feeder and mobile feeder version of the task performed equivalently with respect to the percentage of laps rewarded averaged across all cue conditions (fixed feeder: $85.91\% \pm 12.44\%$; mobile feeder: $78.09\% \pm 18.35\%$; t-test: $t_{17} = 1.48$, $p = 0.16$). 2-way ANOVA was used to assess if the percentage of rewarded laps differed between the two versions of the task as a function of cue condition. While 2-way ANOVA did not reveal a significant feeder version \times cue condition interaction (ANOVA: $F_{4,74} = 1.73$, $p = 0.15$), it is worth noting that the mobile feeder group did show a significantly lower percentage of laps rewarded for baseline trials than did the fixed feeder group when pairwise comparisons were performed separately for each cue condition (fixed feeder: $93.62\% \pm 8.12\%$; mobile feeder: $72.24\% \pm$

25.09%; t-test: $t_{16} = 2.43$, $p < 0.05$). No pairwise differences were found between the two groups for any of the cue rotation conditions. These results suggest that rats participating in the mobile feeder version of the task performed worse during baseline trials but that, following cue rotation, rats from both groups performed equivalently. When the percentage of laps rewarded was assessed separately for each feeder condition, no significant effect of rotation condition was found for either the fixed feeder (ANOVA: $F_{4,40} = 1.79$, $p = 0.15$) or mobile feeder (ANOVA: $F_{4,40} = 1.49$, $p = 0.22$) version of the task, suggesting that rats from both versions of the task were able to correctly navigate to the goal location even after cues were rotated. As described above, because rats participating in the mobile feeder version of the task were able to trigger reward delivery by stopping anywhere within $\pm 20^\circ$ of the goal, there was a broader range of possible positions at which an animal might trigger a reward. Consequently, it was possible to assess goal navigation accuracy for the mobile feeder experiment by quantifying the *goal error* for each reward event based on the rat's distance from the designated goal when a reward was triggered (**Figure 3.6B**). 1-way ANOVA were used to assess if goal errors differed between cue conditions and revealed a significant main effect of cue condition (ANOVA: $F_{4,40} = 2.75$, $p < 0.05$). Post-hoc comparisons, however, did not reveal any significant differences between baseline goal errors and those during any of the rotation conditions after correcting for familywise error. Goal errors were also assessed separately for each

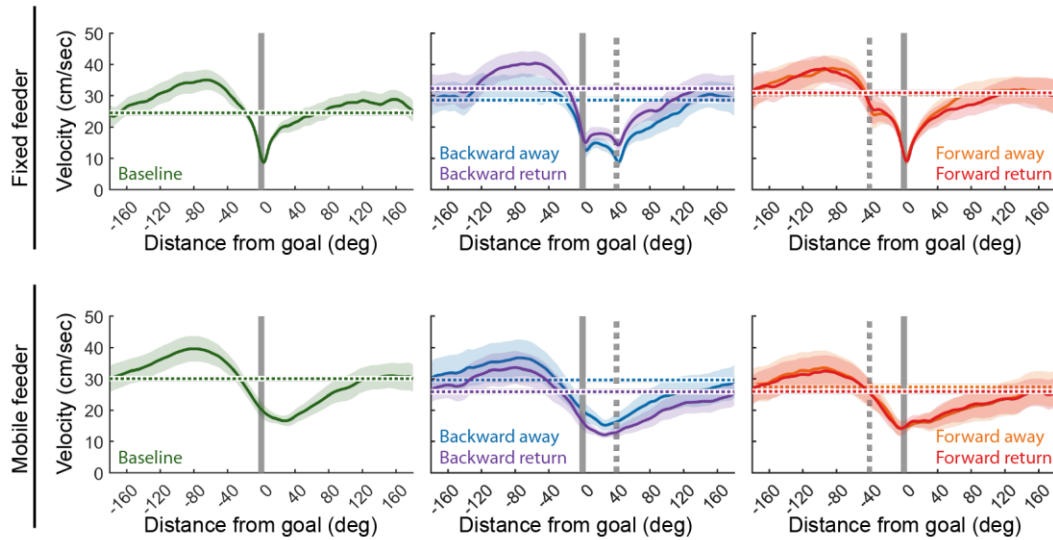


Figure 3.7: Comparison of running velocity at all positions along the track between the two versions of the task.

Mean running velocity \pm S.E.M across the full extent of the track for baseline trials as well as each of the four rotation conditions from rats performing the fixed feeder (top) and mobile feeder (bottom) version of the task. Horizontal dashed colored lines denote the mean running speed for each condition. Vertical gray lines denote the current (solid) and, where applicable, non-current (i.e., pre-rotation goal; dashed) goal locations. Position data is centered at the current goal location (0°). Rats performing the fixed feeder version of the task tended to show a more marked reduction in running speed preceding arriving to the current goal location (0°) but also tended slow down at the non-current goal location ($\pm 40^\circ$) following cue rotation.

rotation condition using one-sample t-tests, which revealed that goal

errors were significantly different from 0 for both forward away trials (-

$7.91^\circ \pm 5.83^\circ$; t-test: $t_8 = -4.07$, $p < 0.01$) and forward return trials (-

$6.53^\circ \pm 6.63^\circ$; t-test: $t_8 = -2.96$, $p < 0.05$). In both instances, goal errors

were shifted backward relative to the goal indicating that rats were biased

to stop before reaching the goal following forward cue rotations.

The percentage of laps rewarded provides only a binary measure of

goal navigation performance and goal error could only be characterized

for rats participating in the mobile feeder version of the task. To assess

the degree to which the cues influenced animals' running behavior

preceding their arrival to the goal, instantaneous velocity was first

computed for each position along the track (**Figure 3.7**). Average running speed across all positions along the track was similar for both versions of the task (fixed feeder: 28.71 ± 10.06 cm/sec; mobile feeder: 26.33 ± 10.85 cm/sec; t-test: $t_{17} = 0.49$, $p = 0.63$). To assess changes in *pre-goal velocity*, instantaneous velocity was then averaged within 10° bins over the range of -40° to 0° with respect to the designated goal and a simple linear regression was calculated for each cue condition (**Figure 3.8A**). Within the context of this analysis, significant negative regression slopes (i.e., β coefficients) indicate that rats significantly reduced their running velocity prior to arriving at a given goal location. For both versions of the task, rats showed a significant decrease in speed preceding their arrival to the goal during baseline trials as well as during all cue rotation trials (i.e., backward away, backward return, forward away or forward return). For the fixed feeder version of the task, for every 10° of travel, the predicted change in pre-goal velocity was -4.9 cm/sec during baseline trials ($\beta = -0.49$, $F_{1,44} = 52.34$, $p < 0.001$, $R^2 = 0.55$). During cue rotation trials for the fixed feeder group, the predicted change was -3.8 cm/sec following backward away rotation ($\beta = -0.38$, $F_{1,44} = 15.35$, $p < 0.001$, $R^2 = 0.26$), -5.1 cm/sec following backward return rotation ($\beta = -0.51$, $F_{1,44} = 20.07$, $p < 0.001$, $R^2 = 0.32$), -3 cm/sec following forward away rotation ($\beta = -0.30$, $F_{1,44} = 8.24$, $p < 0.01$, $R^2 = 0.16$) and -3.6 cm/sec following forward return rotation ($\beta = -0.36$, $F_{1,44} = 10.78$, $p < 0.01$, $R^2 = 0.20$). For the mobile feeder version of the task, for every 10° of travel, the predicted change in

pre-goal velocity was -3.7 cm/sec during baseline trials ($\beta = -0.37$, $F_{1,44} = 16.85$, $p < 0.001$, $R^2 = 0.28$), -3.1 cm/sec following backward away rotation ($\beta = -0.31$, $F_{1,44} = 4.87$, $p < 0.05$, $R^2 = 0.10$), -3.2 cm/sec following backward return rotation ($\beta = -0.32$, $F_{1,44} = 5.75$, $p < 0.05$, $R^2 = 0.12$), -2.9 cm/sec following forward away rotation ($\beta = -0.29$, $F_{1,44} = 7.11$, $p < 0.05$, $R^2 = 0.14$) and -2.8 cm/sec following forward return rotation ($\beta = -0.28$, $F_{1,44} = 8.47$, $p < 0.01$, $R^2 = 0.16$). These findings suggest that rats were able to use the visual cues, both in their pre- and post-rotated configurations, to identify the current goal location and began slowing well in advance of their arrival to the goal.

Although rats were only rewarded at the goal location designated by the current cue configuration (*current goal*), it was evident that rats performing the fixed feeder version of the task also tended to decelerate at the previously rewarded goal (*non-current goal*) following both backward and forward cue rotation (**Figure 3.7 and 3.8A**). Simple linear regression was also performed for the velocities leading up to the non-current goal location and the pre-goal velocity regression slopes (i.e., β coefficients) for the current and non-current goal were compared. One-tailed t-tests were performed to determine if the pre-goal velocity slope preceding the current goal was more negative than that preceding the non-current goal, which would indicate that slowed down more preceding their arrival at the current goal than they did at the non-current goal (**Figure 3.8B**). For the fixed feeder task, the pre-goal velocity slope was significantly more negative at

the current goal location than at the non-current goal during both backward away (current goal: -0.38 ± 0.16 ; non-current goal: -0.12 ± 0.16 ; t-test: $t_8 = -3.00$, $p < 0.01$) and backward return trials (current goal: -0.51 ± 0.13 ; non-current goal: -0.05 ± 0.20 ; t-test: $t_8 = -5.26$, $p < 0.001$) but not during forward away (current goal: -0.30 ± 0.30 ; non-current goal: -0.29 ± 0.18 ; t-test: $t_8 = -0.10$, $p = 0.46$) or forward return trials (current goal: -0.36 ± 0.31 ; non-current goal: -0.25 ± 0.09 ; t-test: $t_8 = -0.93$, $p = 0.19$). For the mobile feeder group, slopes were also significantly more negative for the current goal than non-current goal for both backward away trials (current goal: -0.31 ± 0.25 ; non-current goal: -0.10 ± 0.21 ; t-test: $t_8 = -2.15$, $p < 0.05$) and backward return trials (current goal: -0.32 ± 0.23 ; non-current goal: -0.08 ± 0.18 ; t-test: $t_8 = -2.30$, $p < 0.05$). Similar to the fixed feeder group, the mobile feeder group also did not show significantly more negative slopes for the current than non-current goal for either forward rotation trials, although there was a trend for both forward away (current goal: -0.29 ± 0.28 ; non-current goal: -0.17 ± 0.17 ; t-test: $t_8 = -1.61$, $p = 0.073$) and forward return trials (current goal: -0.28 ± 0.23 ; non-current goal: -0.16 ± 0.18 ; t-test: $t_8 = -1.87$, $p = 0.052$). These findings suggest that, at least following backward rotations, rats from both versions of the task decreased their running speed to a greater extent at the current (i.e., cue-aligned) goal location than they did at the non-current goal.

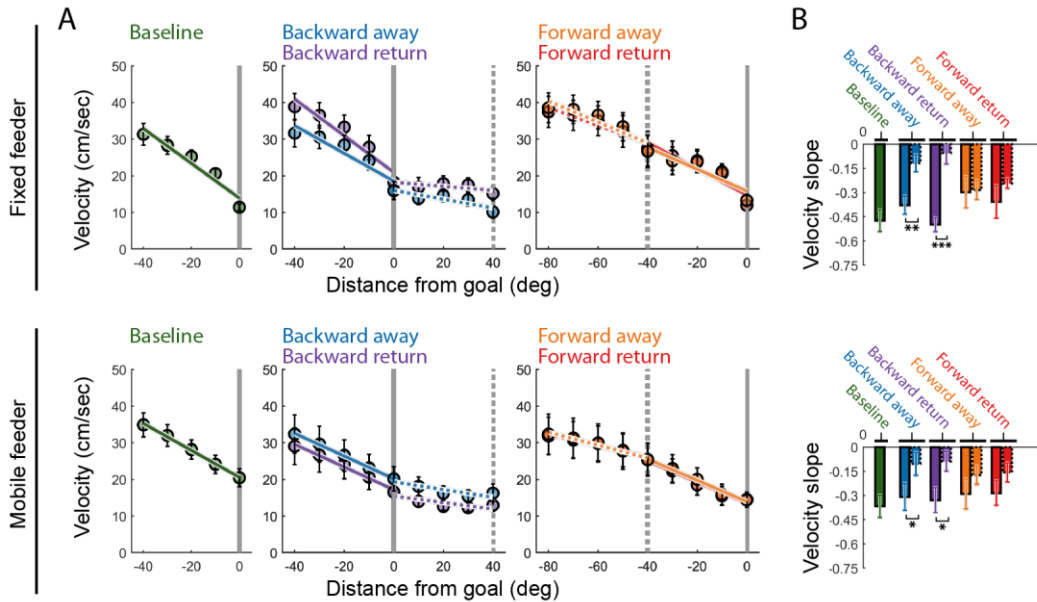


Figure 3.8: Effects of cue rotation on running velocity preceding goal arrival.

Data from rats performing the fixed feeder (top) and mobile feeder (bottom), segregated for baseline trials as well as each of the four rotation conditions. Vertical lines denote the current (solid) and, where applicable, non-current (i.e., pre-rotation goal; dashed) goal locations. **(A)** Mean running velocity \pm S.E.M preceding arrival to the goal (i.e., pre-goal velocity) averaged within 10° bins. Position is centered at the current goal location (0°). Velocity data is also shown for the approach to the non-current goal location (dashed vertical line) during each of the four rotation conditions. Lines are shown representing the linear fit from regressions performed on the group mean velocities preceding arrival to the current (solid) and non-current goal (dashed) locations. Note, for both versions of the task, rats showed a significant decrease in pre-goal velocity as a function of distance from current goal for baseline trials as well as all rotation conditions. **(B)** Mean regression slopes \pm S.E.M computed using the data shown in (A). Regression slopes from velocities preceding the current goal are shown for each condition (solid color) along with regression slopes for the velocities preceding arrival to the non-current goal for each rotation condition (dashed color). Asterisks denote significant pairwise comparisons between current and non-current goal slopes for each rotation condition. Statistical significance is indicated as $p < 0.05$ (*), $p < 0.01$ (**), $p < 0.001$ (***). Note the rats from both groups show significantly more negative slopes for the current goal during both backward away and backward return trials, indicating a greater reduction in speed at the new current cue-aligned goal than at the non-current goal. For both forward away and forward return rotation trials, the slope corresponding to the current goal do not show as strong of a difference from the non-current goal.

3.3.3. Influence of visual cue rotation on overall running behavior

In order to quantify how strongly the projected cues influenced running behavior over the complete extent of the track, and not just in proximity to the goal location, occupancy time was computed for each

position on the track, and the cross-correlogram was then calculated between occupancy data from each lap with that from the preceding trial (**Figure 3.5 and 3.9A**). The resulting cross-correlation provides a means of dissociating the influence of allothetic and idiothetic feedback on overall running behavior following cue rotation. For instance, if both before and after cues are rotated, rats consistently spend more or less time at the same locations on the track relative to the cues, this will be revealed in the cross-correlogram by a larger value at either the -40° or 40° lag depending on the direction of rotation. This would, in turn, indicate that the rats' running behavior is strongly anchored to the allothetic cues. Alternatively, if the running behavior remains constant with respect to the distance traveled along the track, this will be revealed in the cross-correlogram by a larger value at the 0° lag, indicating that the running behavior is more strongly anchored to the idiothetic cues. To assess the degree to which running behavior was anchored to either the allothetic cues, idiothetic cues or a combination of the two, cross-correlation values were averaged within 20° bins for lags between -40° to 40° for the two rotation conditions (**Figure 3.9B**). 2-way ANOVA revealed a significant lag \times rotation condition interaction both for the fixed feeder (ANOVA: $F_{12,160} = 3.23$, $p < 0.001$) and mobile feeder (ANOVA: $F_{12,160} = 17.07$, $p < 0.001$) version of the task, suggesting that the running behavior of both groups differed depending on the direction of cue rotation. Next, for each rotation condition the correlations from all lags between -40° and 40° were

assessed with respect to the mean correlation to identify which lags were significantly greater than the average. For rats performing the fixed feeder version of the task, only the 0° lag correlation was significantly greater than the average for backward away trials (0° lag: 0.053 ± 0.032 ; mean: 0.020 ± 0.011 ; t-test: $t_8 = 3.61$, $p < 0.05$), backward return trials (0° lag: 0.061 ± 0.032 ; mean: 0.021 ± 0.011 ; t-test: $t_8 = 4.90$, $p < 0.01$), forward away trials (0° lag: 0.062 ± 0.043 ; mean: 0.023 ± 0.014 ; t-test: $t_8 = 3.55$, $p < 0.05$) and forward return trials (0° lag: 0.074 ± 0.063 ; mean: 0.026 ± 0.018 ; t-test: $t_8 = 3.04$, $p < 0.05$). These results suggest that the fixed feeder group did not show a significant realignment of their running behavior in response to cue rotation. For the mobile feeder version of the task, in contrast, the 0° lag correlation was not significantly greater than the average for any of the rotation conditions. Instead, mobile feeder rats showed correlations at the -40° lag that were significantly greater than the mean for both backward away (-40° lag: 0.052 ± 0.020 ; mean: 0.023 ± 0.013 ; t-test: $t_8 = 5.50$, $p < 0.01$) and backward return (-40° lag: 0.046 ± 0.021 ; mean: 0.022 ± 0.015 ; t-test: $t_8 = 6.14$, $p < 0.001$) trials. Similarly, the 40° correlations were significantly greater than the mean for forward away (40° lag: 0.054 ± 0.025 ; mean: 0.026 ± 0.015 ; t-test: $t_8 = 4.09$, $p < 0.01$) and forward return (40° lag: 0.053 ± 0.020 ; mean: 0.024 ± 0.011 ; t-test: $t_8 = 5.64$, $p < 0.01$) trials. These findings suggest that rats performing the mobile feeder version of the task were most likely to behaviorally rotate with allothetic cues, while those performing the fixed feeder version

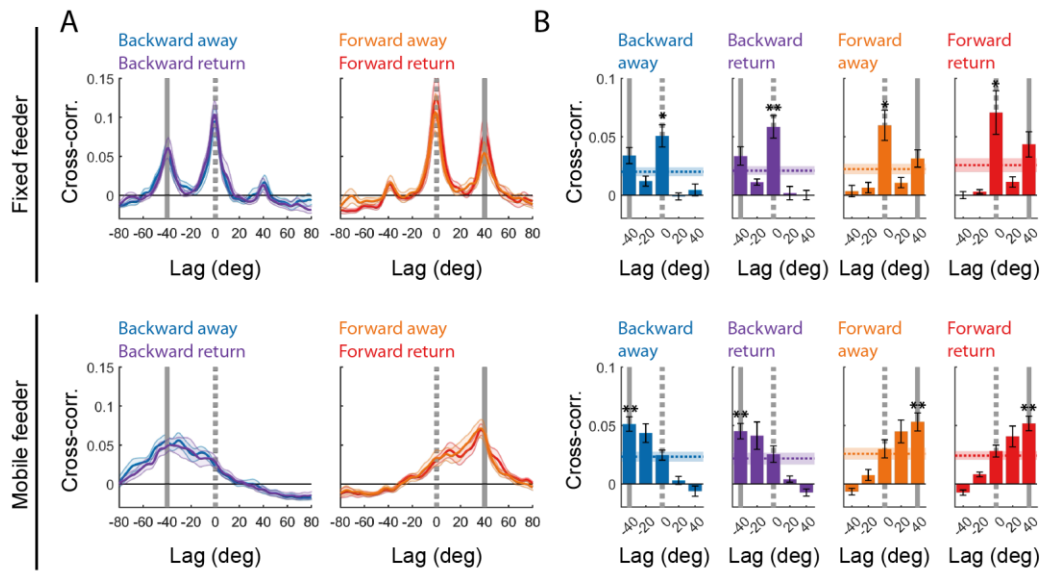


Figure 3.9: Comparison of behavioral realignment following cue rotation for the two versions of the task.

Data are shown for both the fixed feeder (top panels) and mobile feeder (bottom panels) groups for each of the four rotation conditions. Vertical gray lines denote the 0° lag (dashed) as well as lags corresponding to degree of cue rotation (solid) for backward (-40°) and forward (40°) cue rotation. **(A)** The mean occupancy cross-correlogram \pm S.E.M. Fixed feeder rats show narrower cross-correlogram peaks than do the mobile feeder rats, suggesting that the fixed feeder rats' behavior realigned more precisely with the rotated cues. The fixed feeder rats, however, also show pronounced peaks in the cross-correlogram not only at the lags corresponding with the cue rotation (i.e., -40° or 40° lag), but also at the 0° lag for all rotation conditions. **(B)** Cross-correlation values averaged within 20° bins for lags between -40° and 40° . The mean of the -40° to 40° lag correlations is also shown (dashed horizontal line). Those lags that showed statistically significant differences from the mean are indicated as $p < 0.05$ (*), $p < 0.01$ (**), $p < 0.001$ (***)). For all rotation conditions, only the 0° lag correlations are significantly larger than the mean for the fixed feeder rats, while mobile feeder rats show significantly greater correlations at lags corresponding to the rotated cue. Additionally, the mobile feeder group, but not fixed feeder group, show correlations at the $\pm 40^\circ$ lag are significantly greater than those at the 0° lag for all rotation conditions.

were more likely to remain anchored to the idiothetic cues.

In order to more precisely assess the degree of behavioral realignment following cue rotation, the *peak correlation* (i.e., maximum value in the cross-correlogram) and *peak lag* (i.e., the corresponding lag value in degrees) were identified for each lap within each cue rotation condition (**Figure 3.5 and 3.10B**). Differences in mean peak lag were assessed using a 2-way ANOVA, which revealed a significant feeder

version \times rotation condition interaction (ANOVA: $F_{3,64} = 17.81$, $p < 0.001$). Post-hoc comparison showed that the average peak lag of rats performing the fixed feeder version of the task was significantly different from that of the rats performing the mobile feeder version of the task for backward away trials (fixed feeder: $-1.04^\circ \pm 15.57^\circ$; mobile feeder: $-30.63^\circ \pm 14.62^\circ$; t-test: $t_{16} = 4.16$, $p < 0.01$), backward return trials (fixed feeder: $-6.87^\circ \pm 15.56^\circ$; mobile feeder: $-34.22^\circ \pm 13.54^\circ$; t-test: $t_{16} = 3.98$, $p < 0.01$), forward away trials (fixed feeder: $9.76^\circ \pm 16.86^\circ$; mobile feeder: $29.98^\circ \pm 10.69^\circ$; t-test: $t_{16} = -3.04$, $p < 0.01$) and forward return trials (fixed feeder: $10.47^\circ \pm 17.81^\circ$; mobile feeder: $32.19^\circ \pm 7.19^\circ$; t-test: $t_{16} = -3.39$, $p < 0.01$). In all cases, the average peak lags were closer to 0° in the fixed feeder group and closer to $\pm 40^\circ$ in the mobile feeder group, again suggesting that the mobile feeder rats' behavior was more strongly anchored to the allothetic cues. When the peak lag was assessed separately for each feeder version and rotation condition using one-sample t-tests, rats performing the fixed feeder version of the task did not show peak lags significantly different from 0 for any of the rotation conditions, including backward away: ($-1.04^\circ \pm 15.57^\circ$, t-test: $t_8 = -0.20$, $p = 0.85$), backward return ($-6.87^\circ \pm 15.56^\circ$, t-test: $t_8 = -1.32$, $p = 0.22$), forward way ($9.76^\circ \pm 16.86^\circ$, t-test: $t_8 = 1.74$, $p = 0.12$) or forward return ($10.47^\circ \pm 17.81^\circ$, t-test: $t_8 = 1.76$, $p = 0.12$) trials. For rats performing the mobile feeder version of the task, in contrast, the peak lag was significantly different from 0° for all rotation conditions, including backward

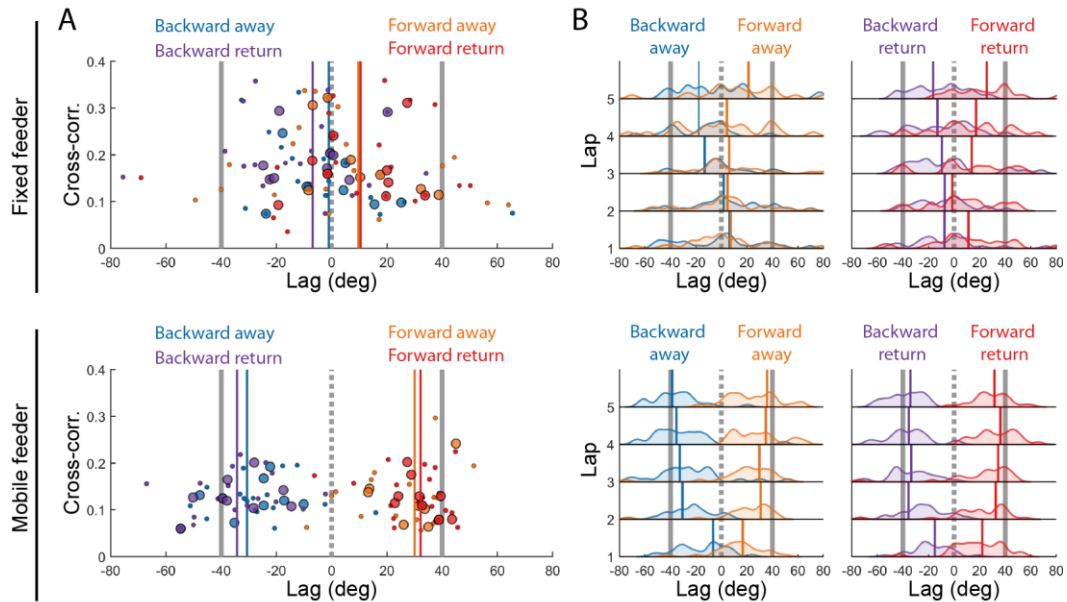


Figure 3.10: Time-course of behavioral realignment following cue rotation.

Data are shown for both the fixed feeder (top panels) and mobile feeder (bottom panels) groups for each of the four rotation conditions. Vertical gray lines denote the 0° lag (dashed) as well as lags corresponding to degree of cue rotation (solid) for backward (-40°) and forward (40°) cue rotation. **(A)** Cross-correlogram peak correlation values are plotted as a function of the peak lag. Vertical colored lines denote the mean peak lags in the cross-correlogram for each rotation condition. Rat means are denoted by large circles and session means are denoted as small circles. Note that, for all rotation conditions, the mean peak lags (vertical colored lines) for the fixed feeder group tended to be closer to the 0° lag than the ±40° lag while those of the mobile feeder group tended to be closer to the ±40° lag. Overall, the fixed feeder rats show a less clear delineation between the two rotation conditions. **(B)** Distribution of peak lags from each session for the first five laps following cue rotation for away (left) and return (right) cue rotation trials. The mean of the distribution for each lap is denoted by vertical colored lines. Note that the peak lags of the rats participating in the mobile feeder version of the tasks become progressively more strongly aligned to the rotated allothetic cues over successive laps for all rotation conditions. For the fixed feeder group, on the other hand, peak lags predominantly remain aligned to 0° lag suggesting minimal cue control of their running behavior.

away ($-30.63^\circ \pm 14.62^\circ$; t-test: $t_8 = -6.28$, $p < 0.001$), backward return (-

$34.22^\circ \pm 13.54^\circ$; t-test: $t_8 = -7.59$, $p < 0.001$), forward away ($29.98^\circ \pm$

10.69° ; t-test: $t_8 = 8.41$, $p < 0.001$) and forward return ($32.19^\circ \pm 7.19^\circ$; t-

test: $t_8 = 13.44$, $p < 0.001$) trials. These results provide further evidence

that rats performing the mobile feeder version of the task reliably realigned

their running behavior in response to both backward and forward cue

rotation.

Finally, to assess the time-course over which rats realigned their behavior to the rotated allothetic cues, the peak lags were assessed over successive laps following cue rotation (**Figure 3.10B**). Analysis was restricted to the first five laps following cue rotation and post-hoc comparisons were performed using one-sample t-tests to identify laps in which the peak lag was significantly different from 0°. 2-way ANOVA revealed a significant lap × rotation condition interaction for both the fixed feeder (ANOVA: $F_{4,32} = 4.69$, $p < 0.01$) and mobile feeder (ANOVA: $F_{4,40} = 5.04$, $p < 0.01$) version of the task. For the fixed feeder task, however, the peak lags were not significantly different than 0° for any lap after correcting for familywise error. For the mobile feeder task, the peak lag was significantly different than 0° by the second lap of backward away trials ($-30.57^\circ \pm 13.44^\circ$; t-test: $t_8 = -7.29$, $p < 0.001$), the first lap of backward return trials ($-15.07^\circ \pm 12.67^\circ$; t-test: $t_8 = -3.57$, $p < 0.01$), the first lap of forward away trials ($16.69^\circ \pm 21.56^\circ$; t-test: $t_8 = 2.32$, $p < 0.05$) and the first lap of forward return trials ($22.06^\circ \pm 17.26^\circ$; t-test: $t_8 = 3.83$, $p < 0.01$). Taken together, these findings suggest that, while rats participating in the fixed feeder version of the task were able to use the projected cues to navigate to the current goal location, their overall running behavior indicates that they were less strongly influenced by cue rotation. On the other hand, for rats participating in the mobile feeder version of the task, both the goal-related and overall running behavior analysis indicate that these rats consistently realigned their behavior to the

allothetic cues within one to two laps following cue rotation.

3.4. Discussion

3.4.1. Summary of salient results

The Instantaneous Cue Rotation (ICR) apparatus utilizes an augmented reality system to allow for repeatable and precisely timed manipulation of real-world environmental cues during ongoing behavior. Two versions of the apparatus were compared, each of which incorporated a different method to enable reward delivery at a goal location that could be rotated concurrently, and by the same degree, as the projected cues. During the task, cues were rotated $\pm 40^\circ$ in the backward (i.e., counter-clockwise) or forward (i.e., clockwise) direction, either away from (i.e., backward/forward away) or back to (i.e., backward/forward return) their baseline configuration. In both the fixed feeder and mobile feeder versions of the task, rats were able to utilize the projected cues to navigate to a learned goal location and trigger reward delivery even when the cues and goal were rotated during active navigation. To the best of our knowledge, this is the first demonstration that allothetic cue-based goal navigation behavior can be rapidly recalibrated in response to an immediate alteration of real-world environmental cues during ongoing navigation.

Rats participating in the mobile feeder version of the task showed robust behavioral realignment following both backward and forward cue

rotation when cues were rotated either away from or back to their baseline configuration. This was the case for all metrics evaluated, including percentage of laps rewarded, change in running speed preceding goal arrival and overall track-wide behavioral realignment as assessed through the cross-correlation analysis. The results from the fixed feeder version of the task were less definitive. While these rats showed equivalent performance across rotation conditions with respect to the percentage of laps rewarded and change in running speed preceding goal arrival, the cross-correlation analysis indicated that they did not demonstrate a consistent change in overall track-wide running behavior in response to cue rotation.

One possible explanation for the differences observed between the two versions of the task is that the inclusion of the fixed feeder may have created a stationary olfactory cue that reduced the influence of the visual cues. Overall, these results do indicate that rats can rapidly update their navigation behavior in response to sudden alterations in allothetic feedback. Furthermore, these findings provide behavioral evidence in support of models of path integration in which allothetic cues are utilized to continuously correct for accumulated error (e.g., Etienne et al., 1996; Loomis et al., 1993; McNaughton et al., 1996; Mittelstaedt and Mittelstaedt, 1980; Redish, 1999; Samsonovich and McNaughton, 1997).

3.4.2. *Design considerations*

A number of studies have investigated the role of allothetic cue-based navigation by altering physical symmetry-breaking features of the environment. As previously described, many of these studies have historically relied on experimental manipulations that require the subject to be removed from the environment before cues can be altered (Suzuki et al., 1980; Muller and Kubie, 1987; O'Keefe and Speakman, 1987; McGauran et al., 2004), which prevent any assessment of ongoing self-motion feedback. Alternatively, some of the paradigms discussed circumvent this issues by manipulating either idiothetic (Sharp et al., 1995; Gothard et al., 1996; Redish et al., 2000; Rosenzweig et al., 2003) or allothetic (Cheng, 1986; Knierim et al., 1998; Yoganarasimha and Knierim, 2004; Yoganarasimha et al., 2006) spatial feedback with the animal left in place. While these approaches do not interrupt path integration operations they do necessitate blocking an animal's perceptual access to spatial cues while the manipulation is performed (Jeffery and O'Keefe, 1999). Importantly, a number of studies have shown that altering spatial contextual information over successive exposure to the same space (i.e., recording room) alters the spatial tuning of CA1 and CA3 place cells (Muller and Kubie, 1987; Lever et al., 2002; Jeffery and Anderson, 2003; Leutgeb et al., 2004; Vazdarjanova and Guzowski, 2004). Consequently, altering access to visual features of the room by extinguishing all lighting or occluding and animal's view of the surrounding environment using

some physical barrier also creates temporary contextual changes that could have unintended effects on representational network activity. Finally, any manual manipulation requires some delay between pre- and post-manipulation testing that can introduce space-independent variability in neural activity due to overdispersion and other forms of temporally mediated firing (Fenton et al., 1998, 2010; Olypher et al., 2002; MacDonald et al., 2011; Wikenheiser and Redish, 2011). Virtual-reality systems, in contrast, enable full and immediate experimenter control of the complete visual landscape during simulated spatial navigation (Gillner and Mallot, 1998; Maguire et al., 1998; Hölscher et al., 2005; Harvey et al., 2009, 2009; Ravassard et al., 2013; Rickgauer et al., 2014; Aghajan et al., 2015; Seelig and Jayaraman, 2015). One limitation of virtual reality, however, is that it typically requires the subject to be physically stationary. This can greatly diminish vestibular feedback, which plays an important role in the instantiation and maintenance of stable spatial representations (Stackman and Taube, 1997; Stackman et al., 2002; Muir et al., 2009; Ravassard et al., 2013). Additionally, studies directly comparing place field activity in similar virtual reality and real-world conditions have shown diminished spatial selectivity in virtual reality environments (Ravassard et al., 2013; Aghajan et al., 2015).

The ICR apparatus was designed to allow for control of visual cues during uninterrupted real-world navigation in order to preserve all navigation-related sensory input. By utilizing projected, as opposed to

physical, visual cues, allothetic cue manipulation can be performed during naturalistic non-virtual running behavior in the presence of ongoing path integration operations and unaltered angular and vestibular feedback. The manipulation is performed remotely and without any direct physical interaction with the animal. As a consequence, unintended effects arising from inter-experimenter differences in operation and handling as well as unnecessary contextual changes, such as may occur when occluding or blocking and animals sensory/perceptual access to the environment, can be avoided. The goal navigation task was designed to require animals to localize a goal location using the global panorama of projected cues by minimizing the unique spatial information carried by features proximal to the goal location. The mobile feeder version of the task provides a non-binary measure of navigation accuracy in the form of a *goal error* metric. For electrophysiological applications, this metric could be used to generate a more detailed characterization of the relationship between representational and behavioral realignment with respect to both degree and timing.

It is worth noting that several options exist that could simplify some features of the system without significantly compromising its function. One of the benefits of using an annular design of the arena is that cues can be rotated by any increment the study requires. It also allows for the inclusion of a circular track and removes the geometric cues implicit in a square enclosure. If this is not necessary, however, a square enclosure could be

used, simplifying both construction and the technical difficulties involved in calibrating the projector positioning and performing the coordinate transformation required when projecting onto a curved wall surface (Ravassard et al., 2013). Another option for generating a projected panorama is to use a dome shaped enclosure and using a hemispherical mirror at its center off of which a single projected image can be reflected onto the full interior surface of the enclosure (Jayakumar et al., 2016). This design approach requires only a single projector to create an image that covers 360° of the horizontal and 180° of the vertical enclosure surface while also allowing for a continuous rotation of cues.

The mobile feeder system could also be simplified depending on experiment specific requirements. For instance, the primary utility of the overhead tracking in the mobile feeder version of the apparatus is to provide real time positional tracking of the mobile feeder. The overhead tracking was initially introduced in the fixed feeder version of the system and was incorporated into the mobile feeder version of the apparatus in part because the constituent hardware and software was already in place and it provided a robust and reliable means of tracking both the mobile feeder and rat position. While the inclusion of multiple independent position measurements allows for a more robust estimate of the rat's position, if a closed-loop system were employed for driving the stepper motors (i.e., some form of position encoder) the robots position could be estimated without video tracking. This would preclude the need for the

Digital Lynx SX for behavioral applications, requiring only the Pixy (CMUcam5) vision sensor to track the rat's position.

Finally, it is worth noting that the decision to use a fairly conservative rotation magnitude of $\pm 40^\circ$ was intentional and was based on several considerations. Cue rotation has been shown, in some contexts, to result in place field remapping (Knierim et al., 1998; Yoganarasimha and Knierim, 2004; Yoganarasimha et al., 2006). However, in studies in which rats were not disoriented prior to recording, and external cues were rotated in an otherwise symmetrical environment by $\leq 90^\circ$, this remapping was infrequent and the majority of place cells showed reliable rotation with visual cues (Muller and Kubie, 1987; Knierim and Rao, 2003). One explanation for this is that when two competing spatial reference frames are put in great enough conflict, place cells will settle on producing an entirely new representation (Knierim and Rao, 2003). The use of remotely controlled cues, however, does not require the experimenter to remove the animal from the environment and interrupt the ongoing path integration operation. It remains to be determined how large a dissociation between allothetic and idiothetic cues would be required to induce global remapping in a behavioral paradigm in which idiothetic feedback is uninterrupted. Therefore, in order to limit the likelihood of inducing a complete change in the animal's spatial representation (i.e., global remapping) the cue rotation was intentionally kept small.

3.4.3. Performance differences on the fixed feeder and mobile feeder versions of the Instantaneous Cue Rotation task

In the present study, two versions of the Instantaneous Cue Rotation (ICR) apparatus were tested and compared. In the fixed feeder version of the task, rats were rewarded from one of 36 evenly spaced feeders that were fixed to the outer wall of the track, while in the mobile feeder version of the task reward was delivered from a single dish that moved with the rat. Rats from both the fixed feeder and mobile feeder versions of the task were able to navigate to, and stop within, the goal bounds and trigger reward delivery. No statistical difference between these versions of the task was identified in the proportion of rewarded laps for any of the cue rotation trials (**Figure 3.6A**). Rats performing the mobile feeder version of the task did, however, show significantly poorer performance during baseline trials than rats performing the fixed feeder version of the task. One possible explanation for this difference in baseline performance is that the 36 feeder dishes collectively provide some form of additional spatial information. For instance, while the arrangement of the feeder dishes does not, in itself, provide any symmetry breaking cues that the rat could draw upon to localize the goal location, the incremental spacing of the dishes does reduce the number of potential stopping positions to a discrete number of possibilities (i.e., 36). As a consequence, the two versions of the task may not be equivalent with respect to overall difficulty. Alternatively, in addition to the projected cues, rats may have

been using olfactory cues from residual food in the rewarded dish to identify the goal feeder (see below). Goal error was also examined for the mobile feeder version of the task as a means of assessing navigation accuracy (**Figure 3.6B**). Rats tended to trigger rewards earlier after cues were rotated forward when cues were rotated both away from and back to their baseline configuration. The tendency for rats to stop ahead of the forward rotated goal suggests they may have been stopping at a position that was intermediate to the current (i.e., rotated, cue-aligned) and non-current (i.e., preceding trial) goal location. Alternatively, rats may have been adopting a more cautious strategy when approaching the goal due to uncertainty arising from the conflict between allothetic and idiothetic spatial cues following cue rotation. Because the goal error metric only accounts for laps in which rats were successful in triggering reward delivery, the bias to stop early within the reward bounds following cue rotation could reveal an advantageous strategy. Furthermore, in conditions in which there is greater uncertainty, it may be advantageous to settle for a smaller reward by triggering reward delivery early in order to decrease the likelihood of overshooting the goal bounds entirely.

Rats from both versions of the task showed a monotonic slowing in their running velocity starting from 40° (~33 cm) before the goal, suggesting that rats anticipated reaching the goal well in advance of their arrival (**Figure 3.8A**). This was true both for baseline trials as well as all cue rotation conditions, indicating that rats were able to update their

internal representation based on the global panorama of cues and not just the local cues proximal to the goal location. Rats performing the fixed feeder version of the task, however, displayed a pronounced tendency to slow not just at the current goal location but also at the non-current goal location following cue rotation (**Figure 3.7 and 3.8**). When the regression slopes were compared between current and non-current goal velocities, both groups showed a significantly greater reduction in speed for the current goal for both away and return backward rotation conditions. In contrast, no significant difference was identified for either the fixed or mobile feeder version of the task during away and return forward rotation trials, indicating that rats slowed to an equivalent degree at both the current and non-current goals following forward cue rotation (**Figure 3.8B**). It is important to note, however, that this analysis has some limitations. When comparing current and non-current goal velocities any change in running speed at the first goal reached (e.g., the current or non-current goal) will have a direct effect on the velocities leading up to the second goal location. On average, rats tended to show a decrease in running speed well in advance of the goal (**Figure 3.7**). Due to the fact that the non-current goal precedes the current goal following forward rotation, if rats begin decelerating before either goal is reached this will result in a similar decrease in velocity at both the non-current and current goal even if the rat does not intend to stop at the old goal location.

Cross-correlations were computed between pre- and post-rotation

occupancies as an alternative means of quantifying behavioral realignment that can detect changes in running behavior over the full extent of the track and not just in proximity to the goal. In the context of this analysis, the more strongly running behavior realigns with the backward or forward rotated cue the closer the peaks in the cross-correlogram will be to either the -40° or 40° lag, respectively. The cross-correlograms from both versions of the task show a pronounced peak at the lag corresponding to the current goal location (i.e., $\pm 40^\circ$; **Figure 3.9A**), again confirming that the running behavior of rats performing either version of the task was influenced by cue rotation in either direction. The cross-correlogram of the fixed feeder group, however, exhibited a distinctly bimodal shape with a second, even larger, pronounced peak at the 0° lag for all rotation conditions. This suggests that there was a large subset of laps in which rats from the fixed feeder group did not behaviorally realign with the rotated cues. When comparing the cross-correlation values for lags between -40° to 40° to the average within that range, only the 0° lags of fixed feeder groups were significantly greater than the mean (**Figure 3.9B**). These observations suggest that rats from the fixed feeder group may have failed to realign with the rotated cues more often than not. Consistent with this interpretation, when peak lags were identified and averaged for each rotation condition (**Figure 3.10A**), the mean peak lags were closer to 0° for all rotation conditions in the fixed feeder group (backward away: -1° ; backward return: -7° ; forward away:

10°; forward return: 10°), while those of the mobile feeder group were closer to $\pm 40^\circ$ (backward away: -31° ; backward return: 34° ; forward away: 30° ; forward return: 32°). This suggests that, the fixed feeder group were more likely to maintain the same profile of running behavior both before and after cue rotation. By contrast, the mobile feeder group showed significantly larger cross-correlation values for lags corresponding to the cue rotation for all rotation conditions, suggesting that these rats robustly realigned with the rotated cues. One possible explanation for why the average peak lags were closer to 0° than to the expected -40° or 40° for the fixed feeder version of the task is that the fixed feeder rats may have rotated with the cues only some of the time. This would also reconcile why the cross-correlation results suggest a weak influence of the visual cues on the fixed feeder rats' running behavior despite the fact that these rats were able to decelerate and trigger reward delivery at the current goal location following cue rotation in either direction.

Based on observations of rats engaged in the task as well as several ancillary tests (see **Chapter 3.5**), the most likely explanation for the observed difference between the two versions of the task is that the static feeder dishes developed an odor cue over subsequent visits to the rewarded dish. If this is the case, the odor may have become associated with a given position and this association may have induced rats to continue stopping at the non-current goal location. By contrast, the mobile feeder system ensures that the feeder dish and any corresponding food-

related olfactory cues are in constant motion, diminishing the potential for these cues to influence goal selection. The observation that the fixed feeder group did not show a tendency to rapidly decelerate at both current and non-current goal location following cue rotation is consistent with this interpretation (**Figure 3.7**). Even if rats from the fixed feeder group were using the cues to navigate, they may have been biased to stop at the old feeder location once they were near the feeder dish and the smell of the reward food was detectable. This possibility is also consistent with anecdotal observations that the fixed feeder rats often tended to stop at both the current or non-current goal locations on a single track traversal. Rats performing the mobile feeder version of the task also differed from fixed feeder rats with respect to how precisely their running behavior aligned to one or the other forms of spatial feedback as evidenced by the occupancy cross-correlograms. In contrast to the narrow peaks seen in the fixed feeder groups cross-correlograms, those of the mobile feeder group had wider and more asymmetric peaks, which were strongly skewed toward lags corresponding to the degree of cue rotation (i.e., $\pm 40^\circ$; **Figure 3.9A**). This indicates that while the mobile feeder rats realigned more strongly with the allothetic cues than they did with the idiothetic cues, there was a greater degree of variability in their running behavior. In addition, the fact that the mean peak lags fell between 0° and $\pm 40^\circ$ (i.e., -32° and 31°) suggests that the mobile feeder rats' behavior may have reflected the combined influence of both allothetic

and idiothetic feedback. It is important to note that in order to assess overall running behavior independently of goal stopping behavior, occupancy data following reward delivery was excluded for the cross-correlation analysis. In spite of this, it is likely that the prevalence of peak lags at both $0^\circ \pm 40^\circ$ in the fixed feeder group is largely a consequence of the tendency to stop at both the current and non-current goals. When mean peak lags were assessed on a lap-by-lap basis following cue rotation, the mobile feeder group showed a clear transition in their running behavior, which became progressively more strongly aligned with the allothetic cues over successive laps while no such pattern was identified for the fixed feeder group (**Figure 3.10B**). For the mobile feeder group, this transition typically occurred within one or two laps following cue rotation. One interpretation of this observation is that, from the time cues are rotated there is a progressive accumulation of path integration error that must be continually corrected using the environmental cues in their new configuration. As a consequence, over a sufficient interval of time, the process of error correction continues until the spatial signals are brought into agreement. Based on the results described, the spatial or temporal interval required to reconcile the conflicting spatial signals and alter behavior may be as short a single lap or less. Taken together, these findings are consistent with several studies characterizing the progressive realignment of place field firing in response to allothetic and idiothetic cue mismatch (Gothard et al., 1996; Redish et al., 2000; Rosenzweig et al.,

2003). In these studies, the distribution of hippocampal CA1 place fields was assessed as rats traversed a linear track over successive trials in which the rats' starting position was moved forward incrementally. Under this condition, fields at the start of the track were found to be more strongly aligned to the egocentric reference frame (i.e., starting position) while those toward the end of the track were more strongly aligned to the allocentric reference frame (i.e., allothetic cues; unaltered room cues). Similarly, it was observed that rats from the mobile feeder group did not fully realign with the rotated cues immediately after cue rotation, but instead showed a progressive shift in behavioral realignment to the rotated cues over the first several laps. Future electrophysiology experiments utilizing the ICR arena will have to be performed to investigate the relationship between this behavioral realignment and the time-course of spatial representation updating.

3.5. Conquering confounding odor cues

The primary purpose of the ICR task was to require rats to learn to navigate to a specific goal location utilizing only the pattern of wall images. To this end, all structural features of the ICR arena were made to be identical every 10 degrees including the 36 feeders, and the goal feeder was positioned within a repeating pattern of cues so that the rewarded feeder dish could be identified only by its spatial relationship with the panorama of projected cues. It was discovered, however, that after

subsequent visits to the rewarded feeder rats were able to locate the feeder based on odor cues alone. This was assessed by allowing the rats to perform several laps as they normally would, eating from the dish after triggering reward delivery. When lights were then turned off and all projected cues were extinguished, it was found that, in most instances, rats continued to run directly to the rewarded feeder dish even in the presumed absence of any visual cues. In an attempt to mask and/or eliminate the odor cue, while still retaining the fixed feeder design, several solutions were developed and tested.

Solution 1: Pre-dosing the active and sham feeders

During the conception of the ICR apparatus, it was anticipated that the active feeder dishes would likely give off some amount of odor that would have to be controlled for. It was believed, in retrospect naively, that pre-dosing all 36 feeder dishes with a small amount of the liquid reward prior to the start of each session would be sufficient to mask any potential odor cues. This was the control used for the majority of sessions that were included in the fixed feeder component of the present study. While this did diminish the influence of the food odor to a degree, the effect was attenuated over the course of the session as the pre-dosed feeders dried and the active feeder accumulated progressively more odor over subsequent reward deliveries.

Solution 2: Continually pumping food odor through the active and sham feeders

The second solution tested was to mask the odor at the active feeder by continuously pumping the liquid reward odor through each of the 36 feeders over the full course of each session. This required a fairly elaborate modification to the setup. A 35W commercial air pump fed a continuous flow of air to a large reservoir containing the liquid food reward. The food reward was aerosolized by having the air enter the reservoir through an air diffuser (i.e., aquarium bubbler) that breaks up the air stream generating bubbles in the liquid food. The outlet of the reservoir was connected to ports on each of the 36 feeders via a series of daisy-chained sections of vinyl tubing. The pump was mounted directly above the arena in the same recess as the camera and speaker to prevent rats using the noise of the pump as an orienting cue. This solution, however, also did not prove reliable in preventing rats from identifying the active feeder in the dark run tests.

Solution 3: Vacuum residual food in conjunction with Solution 2

For the third solution, the setup was further modified to enable any excess liquid reward to be vacuumed from the feeder after each reward delivery. For these test, the aerosolizer setup (i.e., Solution 2) was retained and a second air pump was incorporated and modified to generate a vacuum. The inlet of the vacuum was connected to the rewarded feeder dish through the same line that carried the liquid food.

Following each reward event, after a 15 second delay, the vacuum was powered on through an optical AC relay via the Arduino® Due microcontroller (i.e., AD1; see **Chapter 3.2.2**) and residual liquid reward was collected in a reservoir connected in line with the vacuum and dish. This solution, however, was no more effective than the others tested.

Solution 4: Periodically pump low levels of ozone through the active and sham feeders in conjunction with Solution 3

For the fourth and final fixed feeder modification tested, the vacuum was retained but the original aerosolizer system was modified to periodically pump a low level of ozone through each of the 36 feeders following each reward event. The rationale behind this approach is that ozone (i.e., O³) is commonly used to reduce odor through its affinity to bind and oxidize odorant molecules and, consequently, neutralize them. An ozone generator was connected in line with the air pump and was powered on via an optical AC relay via the AD1 microcontroller at the start of each session. It is also important to note that prolonged exposure to ozone can result in various respiratory complications (for review, see Boeniger, 1995). In order to minimize ozone exposure while maintaining a stable level of ozone immediately around feeders, low levels of ozone were periodically released from the each of the 36 feeders by periodically activating a solenoid valve via the AD1 microcontroller connected between the pump and ozone generator. This solution, however, proved even less effective than the others tested.

Solution 5: Making the feeder mobile

It was ultimately concluded that, while some of these approaches diminished the rat's ability to use olfactory cues to localize the reward site, none of them eliminated the cue entirely. Having exhausted every means of masking the olfactory cues generated by the active feeder, a non-stationary feeder system was opted for as the only evident means of ensuring the reward food would not provide a stationary orienting cue. Instead of 36 feeders fixed to the walls of the arena, the mobile feeder was designed to move along the inner perimeter of the track at the same pace as the rat by smoothly and rapidly tracking the animal's movements. Finally, to preempt any further potential odor-related confounds in the study, the mobile feeder was equipped with a system that continually cleans the track, capturing stray feces and sponging the track surface with a strip of polyurethane foam, which is periodically soaked with ethanol from an onboard reservoir (see **Chapter 3.2.4** and **Figure 3.2**).

CHAPTER 4: ASSESSING OLD AND YOUNG RATS ON THE INSTANTANEOUS CUE ROTATION TASK

4.1. Introduction

As previously described, aged humans and animals are impaired in a number of spatial learning tasks. Of particular interest, is the observation that advanced age preferentially impairs navigation performance when an allocentric navigation strategy is required (Barnes et al., 1980; Rosenzweig et al., 2003). Similarly, aged animals show a bias towards using an egocentric over an allocentric strategy for task in which either option is available (Barnes et al., 1980; Nicolle et al., 2003). One related, but still poorly understood, physiological change that could shed some light on this behavioral bias is the observation that place fields of aged rats tend to be less strongly influenced by external cues under a number of different conditions (Tanila et al., 1997b; Rosenzweig et al., 2003; Wilson et al., 2003). In a study conducted by Rosenzweig and colleagues (2003), the spatial distribution of hippocampal CA1 place fields was assessed in old and young rats as they traversed a linear track over successive trials in which the start box (i.e., the rats' starting position) was moved forward incrementally (**Figure 4.1**). Under this condition, the place fields of both groups were anchored to the egocentric reference frame (i.e., start box) at the start of the track but the fields became more strongly aligned to the allocentric reference frame (i.e., unaltered room cues) toward the end of the track (**Figure 4.1A**). When young and old rats were

compared with respect to the position at which their firing fields realigned with the room cues (i.e., map realignment position), the place fields of aged rats were found to realign further down the track than did those of the young rats (**Figure 4.1C**). These results suggest that place cells of aged rats are subject to some form of delay in their hippocampal map realignment.

While the physiological basis of these observed age-related realignment delays is still unclear, Rosenzweig and colleagues (2003) propose possible neurophysiological sources that could account for the observed aged differences. For instance, the deficits could result from sensory-perceptual impairments related to the speed or accuracy with which sensory signals are processed. Given that the allothetic cues constituting the room reference frame are visual, it follows that age-related vision impairments would be a likely candidate for place field realignment delays, and could result in degraded visuospatial sensory information reaching the hippocampus (for review, see Owsley, 2011). On the other hand, age is also associated with impaired self-motion perception (Warren Jr et al., 1989; Kavcic et al., 2011; Roditi and Crane, 2012; Lich and Bremmer, 2014) suggesting the deficits could be idiothetic in nature. It is also possible that widespread alterations in plasticity mechanisms accompanying normal aging could contribute to delayed realignment (see **Chapter 2.2**). Within this framework, deficits in LTP may impair aged rats' ability to associate sensory-perceptual cues with track position, as

suggested by existing computational models (Redish, 1999; see **Chapter 2.3.1**). Beyond just age-related alterations in LTP, the reported realignment delays may arise from a number of circuit disruptions due to various functional and anatomical changes within the aged hippocampal processing pathway (**Figure 2.1**). Both altered sensory-perceptual input and changes in interregional processing could have the effect of slowing external cue processing or weakening the ability of these cues to influence firing field alignment, which could in turn result in the delayed realignment observed in aged rats.

Due to limitations inherent to the design of the task used by Rosenzweig et al. (2003), it remains unclear at present if the age-related realignment deficits they report are temporal or spatial in nature. Specifically, the point at which the alignment of the hippocampal map transitions from the egocentric (i.e., box) to allocentric (i.e., room) reference frame may depend on the amount of time the rat has been exposed to the mismatched spatial cues or it may depend on the rat's proximity to the room-aligned barrier at the end of the track (Redish et al., 2000). Because the time elapsed from when the rat leaves the start box is strongly correlated with the rat's position on the track, it is difficult to determine which variable is more important for predicting when the place cell population will realign. An earlier non-aging study conducted by Redish et al. (2000) utilized the same experimental manipulation to investigate the time-course of realignment by assessing the population

level CA1 spatial firing activity on a moment-by-moment basis. Using this approach, they observed the same age-independent delayed realignment as Rosenzweig et al. (2003), and were able to demonstrate that the transition in alignment is better predicted by time than any of the position metrics assessed. Consequently, they concluded that the delayed realignment observed in their young rats was more likely a function of time and not position. These findings are what would be expected for dynamical systems models of spatial network function, such as those that model the transition of network states using attractor-based neural networks (see below). Within this framework, the network is gradually pulled into a new stable representation state following some period of exposure to a change in environmental inputs. One important implication of these findings is that the age-related realignment impairments reported by Rosenzweig et al. (2003) are likely temporal in nature and therefore properly characterized as a delay in network updating.

Rosenzweig et al. (2003) also assessed allothetic cue-based goal navigation performance by rewarding rats with medial forebrain bundle stimulation when they successfully stopped at an unmarked goal location that was always at the same position relative to the room reference frame (**Figure 4.1C**). Consequently, successful goal navigation required animals to learn and subsequently identify the location of the goal zone based on the available allothetic cues. When goal navigation accuracy was assessed with respect to changes in velocity near the goal location, aged

rats were significantly impaired compared to young rats. These age-related performance differences did not, however, significantly correlate with the degree to which place field representations realigned with the allothetic (i.e., room) cues. When data was collapsed across age groups, however, an age-independent correlation between goal navigation performance and place field realignment was identified, suggesting that delays in hippocampal map realignment may have a meaningful influence on behavioral output.

The purpose of the present study was to assess and compare the performance of old and young rats on the behavioral component of the Instantaneous Cue Rotation (ICR) task. Similar to the task used by Rosenzweig et al. (2003), the ICR apparatus also incorporates a goal navigation task that requires animals to use projected visual cues to navigate to a reward location that is always aligned to the allocentric (i.e., visual cue) reference frame. The data reported in this chapter was included in results described previously in which age-related differences were not investigated (see **Chapter 3**). Findings will be shared for old and young animals that were trained and assessed using two versions of the ICR task that utilized either a fixed feeder or mobile feeder reward delivery system (see **Chapter 3.2**).

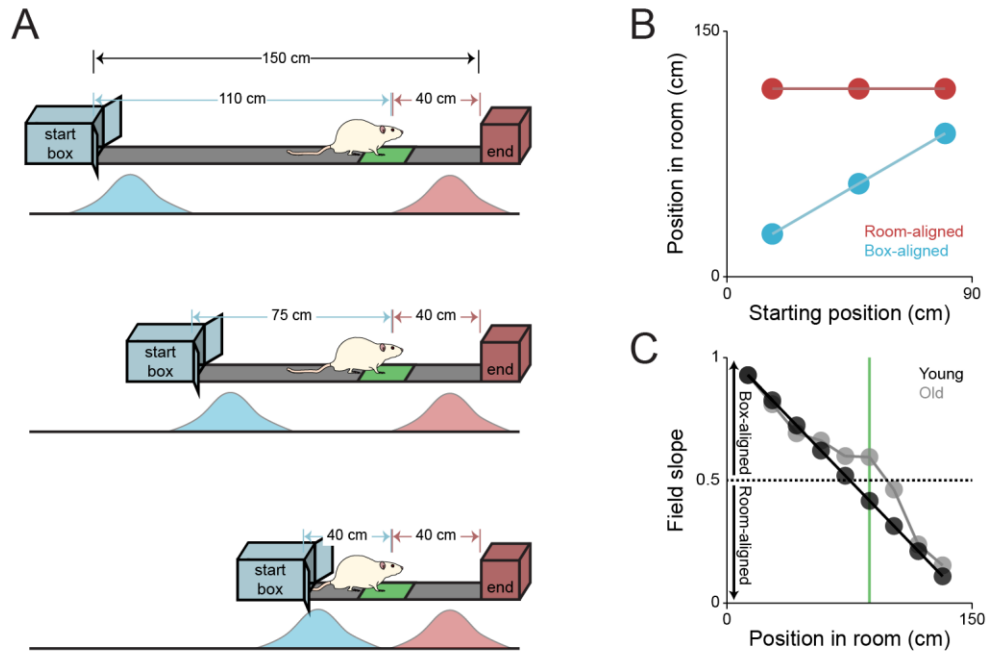


Figure 4.1: Delayed realignment of aged place fields in response to allothetic and idiothetic mismatch.

(A) Illustration of the moving start box task used by Redish et al. (2000) and Rosenzweig et al. (2003). Rats began from the start box and were required to slow at a designated goal zone (green patch), which was always at the same position with respect room-aligned barrier at the end of the track (red block). The box and track were then moved forward over successive trials. Importantly, during the period that the track was moved, the doors of the box were closed with the rat inside in order to prevent them from witnessing the movement. Illustrations of example box aligned field (blue) and room-aligned (red) field are shown for 3 possible start box positions. **(B)** Graph illustrating the expected firing field position of box-aligned (blue) and room-aligned (red) place fields. Lines represent the linear fit (i.e., regression β coefficients). Note that room-aligned fields always maintain the same firing position with respect to the room cues regardless of the start box position. The resulting regression slopes were used to assess the degree to which each place field position varies as a function of the start box position (i.e., slope > 0). **(C)** Characterization of the results from Rosenzweig and colleagues (2003), showing the mean field slopes as a function of the animal's position on the track for both young and old rats. The transition point between box- and room-aligned slope values is shown (horizontal dashed line) as is the goal zone position (green vertical line). Note that the graph shown is only an approximation of the results published by Rosenzweig et al. (2003), highlighting the age-related differences they observed. The place fields of both age groups gradually transitioned from being box-aligned to being room-aligned as rats ran further along the track, but for aged rats this transition tended to occur later.

In addition to the behavioral findings collected from old and young rats performing the Instantaneous Cue Rotation (ICR) task, results are also presented from a computational model that utilizes a continuous attractor neural network to assess spatial network activity in the presence

of a sudden rotation of visual cue input. Attractor networks have been used extensively to model the spatiotemporal dynamics of spatially modulated neural networks and provide an accessible and biologically plausible means of simulating various nonlinear dynamical features of representation updating. Continuous attractor neural networks represent a specific class of attractor network that are composed of synaptically coupled units or nodes, each of which represent a distinct sub-population of functionally related neurons. Units are reciprocally connected to one another through differentially weighted connections. The specific profile of connection weights results in a *continuous attractor*, characterized by a stable pattern of ensemble activity that can coherently shift between any number of transiently stable states (Hebb, 1949; Wilson and Cowan, 1973; Amari, 1977; Droulez and Berthoz, 1991; Tsodyks and Sejnowski, 1995; McNaughton et al., 2006). To achieve stability, local-excitation must typically be paired with some form of inhibitory feedback (Wilson and Cowan, 1972; Amari, 1977; Kishimoto and Amari, 1979; Kohonen, 1982; Skaggs et al., 1995; Redish et al., 1996; Zhang, 1996; Redish, 1999). This can be achieved by incorporating an additional population of inhibitory units or by including a single inhibitory unit that supplies a changing level of global inhibitory feedback based on the overall level of excitation in network. A number of early models of spatial networks utilized a particular type of one-dimensional continuous attractor neural network termed *ring attractors* (Wilson and Cowan, 1973; Amari, 1977; Droulez and Berthoz,

1991; Skaggs et al., 1995; Redish et al., 1996; Zhang, 1996; Redish, 1999). Within this framework, the topology of network connections organizes the constituent units into a ring, such that the synaptic strength between units decreases as a function of their relative distance from one and other on the ring (**Figure 4.2A**). This topology creates a similar tuning for adjacent units resulting in a stable bump of activity when the network is subjected to some form of initial excitatory drive. An important feature of these networks is that the activity bump will persist even after external drive is removed. If some form of external excitatory drive is introduced to units neighboring the currently active set, the orientation of the bump can be made to smoothly shift its position and settle to a new stable orientation on the ring. Conceptually related attractor models have also been used to simulate place and grid cell like activity in one spatial dimension, such as would occur when an animal traverses a linear or circular track (Tsodyks and Sejnowski, 1995; Battaglia and Treves, 1998; Tsodyks, 1999; Blair et al., 2008). Similarly, models that expand the network to include a second dimension have also been used to simulate both place and grid cell networks in the context of two-dimensional spatial exploration (Samsonovich and McNaughton, 1997; Battaglia and Treves, 1998; Fuhs and Touretzky, 2006; McNaughton et al., 2006; Guanella et al., 2007; Bonnevie et al., 2013).

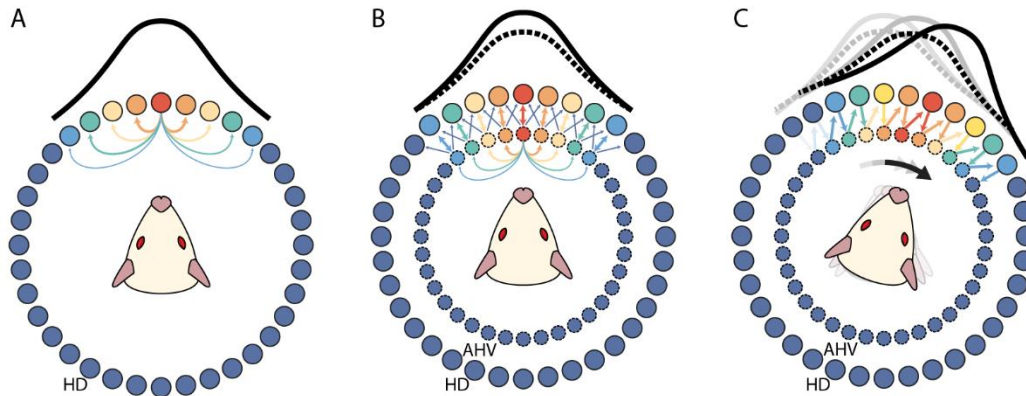


Figure 4.2: Ring attractor model of head direction encoding.

(A) Conceptual illustration of a one-dimensional continuous attractor neural network with a ring topology. The example depicts a specific type of ring attractor that can be used to model various features of head direction (HD) cell networks. In this framework, units (colored circles) are organized around the ring based on their relative directional preference. The strength of excitatory connections between adjacent units decreases with distance as indicated for the north most unit (red circle). This enables a stable pattern of local activity in a subset of units that gradually tapers off with distance (warm to cool colors). The resulting activity bump (black curve) allows for a representation of head direction that is centered at the animals current heading. Additionally, some type of uniform global inhibitory feedback is also typically required to maintain an equilibrium in overall network activity, which is not shown. **(B)** In the model originally proposed by Redish et al. (1996), a second network (dashed circles) tuned to angular head velocity (AHV) enables the directional representation in the HD network to be continuously updated based on changes in angular head velocity. The intrinsic connections of the AHV network have the same profile of local excitation and global inhibition as the HD network, while *matching* connections reciprocally connect units in HD and AHV with the same preferred direction (double sided arrows). Additionally, the AHV network also sends projections to units in the HD network that are *offset* in the clockwise or counterclockwise direction. When the animals head is stationary, units with a common preferred direction reciprocally drive one and other, maintaining a stationary bump of activity in HD (solid curve) and AHV (dashed curve) that is centered at the current heading. **(C)** During head rotation (e.g., in the clockwise direction; black arrow) vestibular angular velocity inputs transiently increase the relative strength of the AHV→HD clockwise offset connection. The resulting increase in synaptic drive to offset units in HD moves the HD activity bump in the direction of head rotation. Concurrently, HD→AHV feedback pulls the activity bump of AHV in the same direction. This maintains a common directional alignment in both networks, although the activity bump of the AHV network will always trail that of the HD network to some degree. Through this process the direction representations of both networks are able to dynamically track changes in heading.

Attractor network models have been used extensively to investigate how head direction representations might utilize movement-related self-motion signals and environmental cues to generate coherent and reliable spatial representations that can be continuously updated as an animal moves through the environment. The conceptual model originally

proposed by McNaughton et al. (1991) posited that head direction cells could utilize self-motion information carried by incoming angular vestibular signals to continuously update their directional tuning. This idea was subsequently implemented in a number of different ring attractor models (Skaggs et al., 1995; Blair and Sharp, 1996; Redish et al., 1996; Zhang, 1996; Redish, 1999). For instance, Redish et al. (1996) incorporated an additional intermediate angular head velocity (AHV) network to update the main head direction (HD) network based on changes in vestibular input. In this particular model, the AHV network provides asymmetric inputs to units in the HD network, which enables the AHV network to bias the HD activity bump to move in one or the other direction around the ring (**Figure 4.2B**). Both the direction and speed with which the HD activity bump transitions through states in the network (i.e., positions in the ring) depends on the level of AHV executive drive relaying angular movement in either the clockwise or counterclockwise direction (**Figure 4.2C**). Because angular head velocity is integrated over time, the updating of directional representations relies on incremental changes in self-motion in a manner akin to a path integration operation. Furthermore, this can be achieved without relying on any explicit information about directional orientation in absolute space, such as that provided by external environmental cues. While vestibular signals provide an effective means of driving the moment-by-moment displacement of the network activity bump, a number of models include some form of external cue-related input to anchor the

relative orientation of directional representations within the environment (i.e., allocentric) frame of reference (Sharp, 1991; Hetherington and Shapiro, 1993; Skaggs et al., 1995; Redish et al., 1996; Zhang, 1996; Redish, 1999; Hahnloser, 2003; Degris et al., 2004; Boucheny et al., 2005; Huang, 2010). One means of modeling allothetic input is to include a separate network whose units code for the orientation of one or more landmarks in the environment. Alternatively, visual cue input can be modeled explicitly as an abstract excitatory input. This is often modeled as a Gaussian-shaped pattern representing the relative orientation of the visual scene (Degris et al., 2004; Boucheny et al., 2005; Wiener and Taube, 2005; Huang, 2010).

The purpose of the model presented in this chapter was to simulate how a sudden mismatch in allothetic (e.g., visual) and idiothetic (e.g., vestibular) feedback might be resolved by attractor-based directional networks and how network function may be altered in the context of known age-related processing impairments. Similar to the model proposed by Redish et al. (1996), the present model is composed of two ring attractor networks. These include a head direction (HD) cell network that has a matching-plus-offset pattern of connections to a second angular head velocity (AHV) network. For the simulations, AHV receives ongoing angular velocity vestibular input that modulates the synaptic drive of AHV→HD offset connections. The HD network also receives visual cue input, which is modeled as a Gaussian distributed pattern that carries

information about the orientation of the animal in the allocentric reference frame (**Figure 4.3**). Within the framework of the model, self-motion and external cue inputs work collectively to update the alignment and temporal trajectory of the directional representations in the AHV and HD networks. Using this approach, the conditions created by the ICR manipulation are simulated by introducing a sudden rotation of the visual cue input and assessing the how the network responds to the conflicting self-motion and visual cue inputs. In addition, the model was also tested with varying levels of accumulating idiothetic (angular velocity) error, representing known age-related path integration deficits, which will be discussed in the context of findings from the behavioral experiment.

4.2. Methods

4.2.1. Age comparison of behavioral performance on the Instantaneous Cue Rotation task

A total of 18 9- to 26-month-old male F344 rats participated in the ICR task experiment. Of these, 5 young (9 – 13-month-old) and 4 aged (23 - 25-month-old) animals were tested using the fixed feeder version of the arena, while five young (9 – 15-month-old) and four aged (23 - 30-month-old) animals were tested in the mobile feeder version of the arena.

As described in detail previously (see **Chapter 3.4**), it was determined that

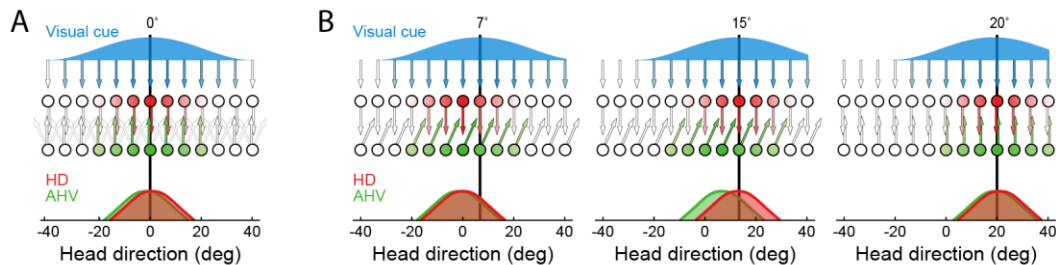


Figure 4.3: Overview of the head direction cell model.

(A) The model includes two separate networks, corresponding to the head direction (HD) and angular head velocity (AHV) networks described above (**Figure 4.2**). Each network is composed of 360 units (small circles) corresponding to one unit per degree, however, fewer units are depicted in the illustration. HD units receive a visual cue input (blue curve), which is always aligned to the current heading (black vertical lines). HD units also receive connections from the AHV network, which follow the matching-plus-offset pattern already described. Briefly, AHV→HD connections include reciprocal matching projections as well as offset projections. The relative strength of these connections varies based on the speed and direction of angular velocity provided by vestibular signals (not shown). For all illustrations, lighter to darker coloring indicates the relative activity of each unit (colored circles) as well as synaptic drive (colored arrows) between different components of the model. In the absence of any head movement, visual cue and reciprocal AHV-HD connections keep both activity bumps aligned at the current heading (e.g., 0° in the example). **(B)** A change in heading (e.g. rotation of the head in the clockwise direction), causes a comparable change in visual cue inputs. At the same time, angular velocity inputs upregulate the AHV→HD offset connections (green arrows). Consequently, both the visual cue and AHV inputs to HD collectively drive the HD activity bump in the direction of head movement (e.g., clockwise; left panel). As the head continues to rotate, the combined visual and self-motion inputs drive the HD network to continue rotating, while HD→AHV feedback connections induce a comparable rotation in the AHV network (middle panel). Once movement ceases, all representations once again reach equilibrium with both the HD and AHV activity bumps stabilized to the new heading (e.g., 20°; right panel).

odor cue contamination likely confounded the interpretation of data collected from rats performing the fixed feeder version of the ICR task. Because of this, the following sections primarily focus on results from the mobile feeder version of the task, although the results of the fixed feeder version of the task will be presented and discussed as well. Detailed descriptions of the ICR apparatus and task as well as the data and statistical analysis performed were described previously (see **Chapter 3.2**). The statistical analysis procedures performed here are identical to those presented in Chapter 3 with one exception. Due to the relatively small number of subjects in the young and aged cohorts, non-significant statistical trends (i.e., $p < 0.1$) will also be reported and discussed.

4.2.2. Attractor network-based model of the Instantaneous Cue Rotation task

All modeling was performed using the Matlab[®] scripting environment. Networks representing head direction (HD) and angular head velocity (AHV) cell populations were modeled as two separate one-dimensional continuous ring attractor networks. Both networks consisted of a pool of 360 units in which each unit was assigned a preferred position on the attractor ring, corresponding to the units preferred direction ϕ_i in the heading space ($0^\circ \leq \phi \leq 360^\circ$). Units produced nonlinear and continuous-valued outputs (0, 1) corresponding to their activity level at each at time t . Because each unit in the network represents a subpopulation of neurons, the output of each unit can be thought of as representing an individual

neuron or a subpopulation of neurons with a similar firing preference. The profile of excitatory connections between units within each network was dictated by the profile of connection weights, which decreased as a function of the unit-to-unit distance on the ring (**Figure 4.2A**). Specifically, excitatory weights w_{ij} from unit i to unit j are expressed as a Gaussian function of their distance (i.e., difference in position) on the ring (Pinto et al., 1996; Redish, 1999; Goodridge and Touretzky, 2000; Zeidman and Bullinaria, 2008). For N units on a ring, a Gaussian weighting function can be used that is independent of the number of units:

$$w_{ij} = \exp(-n_{ij}^2/2\sigma^2), \quad n_{ij} = d_{ij}/(N/2), \quad d_{ij} = \Phi_i - \Phi_j$$

where n_{ij} is the normalized version of the distance d_{ij} of unit i and unit j based on their preferred firing position Φ in one-dimensional space. The standard deviation σ controls the width of the Gaussian and, as a consequence, indirectly determines the width of the attractor bump. The excitatory output of the i th unit can be thought of as the firing rate or probability of spiking at time t . The equations and corresponding numerical algorithms used for computing the output of each unit in the network are based on those of Wiener and Taube (2005), which can be referred to for a description of the derivation of the following equations:

$$z_i(t + \Delta t) = z_i(t) + \left(-z_i(t) + \left[\gamma_E + w_{EE} \sum w_{ij} z_j(t) + w_{EI} u(t) + \text{inp}_i(t) \right]_+ \right) \cdot \frac{\Delta t}{\tau_E}$$

$$u(t + \Delta t) = u(t) + \left(-u(t) + \left[\gamma_I + w_{IE} \sum z_i(t) + w_{II} u(t) \right]_+ \right) \cdot \frac{\Delta t}{\tau_I}$$

Parameter			Parameter		
Parameter		Value	Parameter		Value
Number of HD and AHV units	N	360	Standard deviation for weights	σ	0.3
Integration time step, ms	Δt	0.01	E \rightarrow E coupling strength	w_{EE}	0.13
Excitatory unit time constant, ms	τ_E	0.1	E \rightarrow I coupling strength	w_{EI}	-6
Inhibitory unit time constant, ms	τ_I	0.03	I \rightarrow E coupling strength	w_{IE}	0.17
Excitatory unit tonic inhibition	γ_E	-1.5	I \rightarrow I coupling strength	w_{II}	-1
Inhibitory unit tonic inhibition	γ_I	-7.5	HD \rightarrow AHV coupling strength	$w_{HD \rightarrow AHV}$	0.75
			AHV \rightarrow HD coupling strength	$w_{AHV \rightarrow HD}$	1

Table 4.1: Parameters used for simulations

where $z_i(t)$ defines the output of unit i at time t based on the linear combination of synaptic drive received, which is updated over consecutive time steps Δt . These inputs include a single inhibitory interneuron whose output $u(t)$ is modulated by the net excitatory unit activity at time t . Both equations rely on a semilinear threshold function $[x]_+$ to determine the activation state of each unit – i.e., when $x > 0$ the function will output x , otherwise it will output 0. The coupling constants w_{EE} and w_{EI} govern the ratio of excitatory and inhibitory drive of the excitatory units, while w_{IE} and w_{II} serve the same role for the inhibitory unit. Additionally, the excitatory and inhibitory components of the network each have a corresponding tonic inhibition γ_E and γ_I as well as differing time constants τ_E and τ_I that and govern how rapidly the state of the network changes. Similarly, each component also includes some level of the tonic inhibition specified by γ_E and γ_I as well as associated time constants τ_E and τ_I that govern how rapidly the state of the network changes. Table 4.1 shows the values used for these parameters during all the simulations discussed.

The HD and AHV networks are subjected to different external inputs denoted in the above equation by $inp_i(t)$, which describes the

specific external synaptic inputs received by each unit i at time t . For the AHV network, the only external input is the matching connections from HD:

$$inp_i^{AHV}(t) = w_{HD \rightarrow AHV} \cdot HD_i(t)$$

where HD_i is the synaptic input from the HD network that is scaled by $w_{HD \rightarrow AHV}$, which dictates relative strength of HD→AHV connections. For the HD network inputs are described by:

$$inp_i^{HD}(t) = N(h(t) + \theta^{cue}, \sigma^2) + w_{AHV \rightarrow HD} \cdot AHV_i(t)$$

where N is a normal (i.e., Gaussian) distributed pattern representing the visual cue input with standard deviation σ and a mean equal to the current heading $h(t)$ plus the cue rotation $\theta^{cue} \in \{0^\circ, 40^\circ\}$. Collectively, these terms determine the width and central position of the visual cue input. AHV_i denotes the input from both the matching and offset connections the i th AHV unit to the i th HD unit at time t , scaled by the overall connection strength parameter $w_{AHV \rightarrow HD}$. The strength of the offset connections to HP is also determined by the empirically defined function $\xi(v)$ used by Redish et al. (1996), which dictates the drive of the offset connections as a function of current angular velocity $v(t)$. For the present model, angular velocity inputs were modified to simulate an accumulated self-motion error:

$$v'(t + \Delta t) = v(t) + E(0, \varepsilon)$$

where $v(t)$ represents the actual angular velocity relayed from the vestibular system at time t and $v'(t)$ is the angular velocity with an added error E . The error term E is a random variable following the normal distribution with

standard deviation ε . Consequently, ε dictates the possible level of *idiothetic error* added to the vestibular input at each time step Δt , which can be thought of as representing the level of error in ongoing self-motion-based path integration operations. For the simulations, the vestibular angular velocity $v(t)$ input was based on the current heading $h(t)$, which was modeled as a sinusoidal directional profile (van der Meer et al., 2007) that covered 180° the directional range (0°, 180°) with a maximum angular velocity of 200 degrees per second.

4.3. Results

4.3.1. Age-related differences in goal navigation performance

For all analysis described in this section, data were segregated for each cue condition, which include *baseline* trials as well as cue rotation trials characterized as *backward away*, *backward return*, *forward away* or

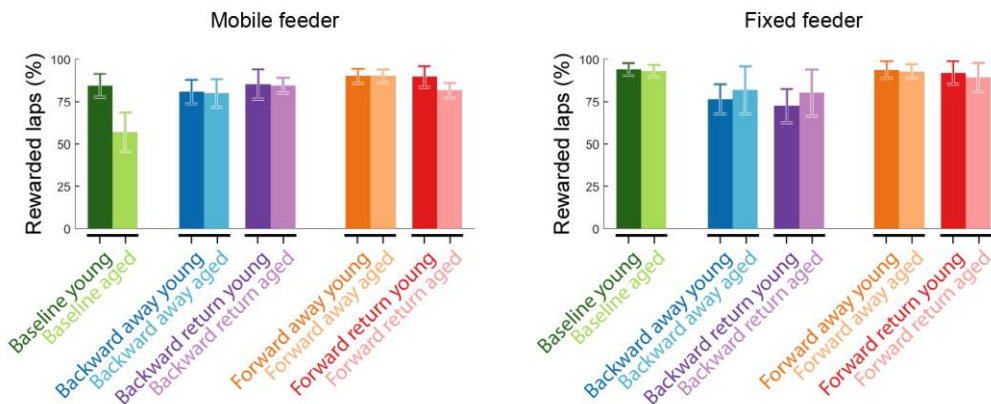


Figure 4.4: Goal navigation performance in old and young rats.

Mean percentage of laps rewarded \pm S.E.M during each cue condition. Data are segregated for old and young rats participating in the mobile feeder (left) and fixed feeder (right) versions of the Instantaneous Cue Rotation task. Note that the mean percentage of rewarded laps for the mobile feeder group during baseline trials is notably smaller for aged rats as compared to young rats, although the difference was not statistically significant.

forward return (see **Chapter 3.2** and **Figure 3.4A**). First, overall goal navigation performance was assessed for old and young rats with respect to the percentage of rewarded laps for each cue condition (**Figure 4.4**). For animals participating in the mobile feeder version of the task, old rats displayed a noticeably lower percentage of rewarded laps during baseline trials than did young rats, however, this difference was not statistically significant (young: 84.47% \pm 17.20%; old: 56.96% \pm 26.91%; t-test: $t_7 = 1.87$, $p = 0.10$). Following cue rotation, young and aged rats displayed an equivalent percentage of rewarded laps for all rotation conditions, including backward away (young: 80.72% \pm 17.46%; old: 79.86% \pm 19.30%; t-test: $t_7 = 0.07$, $p = 0.95$), backward return (young: 85.29% \pm 22.08%; old: 84.46% \pm 10.58%; t-test: $t_7 = 0.07$, $p = 0.95$), forward away (young: 90.06% \pm 10.85%; old: 90.01% \pm 8.92%; t-test: $t_7 = 0.01$, $p = 0.99$) and forward return (young: 89.66% \pm 15.45%; old: 81.55% \pm 10.39%; t-test: $t_7 = 0.89$, $p = 0.40$) trials. This suggests that, while there was some indication of an age-related performance difference for baseline trials, following cue rotation young and aged rats performed equivalently with respect to the percentage of laps rewarded. Similarly, no age-related differences in percentage of rewarded laps was detected for rats participating in the fixed feeder version of the task for baseline (young: 94.05% \pm 8.92%; old: 93.08% \pm 8.31%; t-test: $t_7 = 0.17$, $p = 0.87$), backward away (young: 76.43% \pm 21.87%; old: 81.77% \pm 32.43%; t-test: $t_7 = -0.30$, $p = 0.78$), backward return (young: 72.42% \pm 25.30%; old:

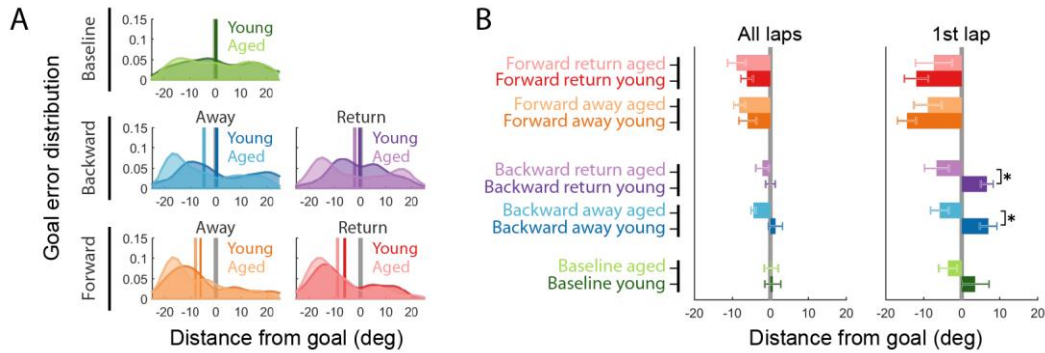


Figure 4.5: Goal navigation accuracy in old and young rats.

(A) The distribution of goal errors, which were computed by taking the difference in rats' position at the time of reward minus the goal position in degrees. Distributions are shown for old and young rats for each cue condition. Vertical gray lines denote the current goal location. Vertical colored lines indicate the distribution mean. (B) Mean goal error \pm S.E.M within each age group and cue condition are shown averaged across all laps (left) as well as for first lap of each trial (right). Statistics are shown for pairwise comparisons between age groups for each condition. Note that a significant difference in goal error was detected between old and young rats for the first lap following both backward away and backward return rotations. Significance is indicated as $p < 0.05$ (*), $p < 0.01$ (**), $p < 0.001$ (***)).

80.12% \pm 31.77%; t-test: $t_7 = -0.41$, $p = 0.70$), forward away (young:

93.69% \pm 12.69%; old: 92.75% \pm 9.50%; t-test: $t_7 = 0.12$, $p = 0.91$) or

forward return (young: 92.04% \pm 16.81%; old: 89.12% \pm 19.48%; t-test: t_7

= 0.24, $p = 0.82$) trials. Collectively, these results indicate that old and

young rats from both the mobile feeder and fixed feeder versions of the

task where able to navigate to the goal and trigger reward delivery even

after cue rotation.

Goal navigation accuracy was also assessed for the mobile feeder

group by quantifying the *goal error* for each reward event based on the

rat's distance from the designated goal when reward was triggered

(Figure 4.5). No significant difference in goal error was identified between

old and young rats for overall baseline (young: 0.62° \pm 5.21°; old: 0.24° \pm

4.25°; t-test: $t_7 = 0.09$, $p = 0.93$), backward away (young: 1.35° \pm 7.57°;

Mobile feeder										
	Baseline		Backward away		Backward return		Forward away		Forward return	
	mean ± SD	P-value†	mean ± SD	P-value†	mean ± SD	P-value†	mean ± SD	P-value†	mean ± SD	P-value†
Young	-0.033 ± 0.009	p < 0.001	-0.037 ± 0.010	p < 0.001	-0.030 ± 0.008	p < 0.001	-0.032 ± 0.013	p < 0.001	-0.035 ± 0.010	p < 0.01
Aged	-0.025 ± 0.013	p < 0.001	-0.022 ± 0.013	p < 0.05	-0.015 ± 0.012	p < 0.01	-0.016 ± 0.024	p < 0.05	-0.013 ± 0.021	p < 0.05
P-value‡	p = 0.31		p = 0.091		p = 0.064		p = 0.14		p = 0.11	

Fixed feeder										
	Baseline		Backward away		Backward return		Forward away		Forward return	
	mean ± SD	P-value†	mean ± SD	P-value†	mean ± SD	P-value†	mean ± SD	P-value†	mean ± SD	P-value†
Young	-0.053 ± 0.012	p < 0.001	-0.041 ± 0.016	p < 0.001	-0.042 ± 0.008	p < 0.001	-0.031 ± 0.023	p < 0.001	-0.033 ± 0.020	p < 0.001
Aged	-0.047 ± 0.013	p < 0.001	-0.026 ± 0.030	p < 0.001	-0.024 ± 0.026	p < 0.01	-0.044 ± 0.018	p < 0.05	-0.043 ± 0.024	p < 0.01
P-value‡	p = 0.55		p = 0.82		p = 0.97		p = 0.79		p = 0.58	

Table 4.2: Comparison of running velocities preceding arrival to the goal location.

Pre-goal velocities slope values ± SD are shown for old and young rats. Data is segregated by feeder version, age group, and cue condition. † P-values from linear regressions performed on the pre-goal velocities for each age group. ‡ P-values from pairwise comparisons of pre-goal velocity slopes between young and aged rats.

old: $-4.48^\circ \pm 2.38^\circ$; t-test: $t_7 = 1.10$, $p = 0.31$), backward return (young: $0.008^\circ \pm 5.26^\circ$; old: $-2.111^\circ \pm 6.49^\circ$; t-test: $t_7 = 0.41$, $p = 0.70$), forward away (young: $-5.98^\circ \pm 5.70^\circ$; old: $-8.15^\circ \pm 3.41^\circ$; t-test: $t_7 = 0.50$, $p = 0.63$) or forward return (young: $-6.19^\circ \pm 3.97^\circ$; old: $-8.91^\circ \pm 5.52^\circ$; t-test: $t_7 = 0.65$, $p = 0.54$) trials. When analysis was restricted to the first lap following cue rotation, however, a significant difference in goal error was identified between young and old rats for both backward away (young: $7.00^\circ \pm 6.65^\circ$; old: $-5.79^\circ \pm 6.32^\circ$; t-test: $t_7 = 2.46$, $p < 0.05$) and backward return (young: $6.34^\circ \pm 4.66^\circ$; old: $-6.62^\circ \pm 8.50^\circ$; t-test: $t_7 = 2.36$, $p < 0.05$) trials. These results indicate that, immediately following backward cue rotation, young rats tended to stop past the current goal location while old rats tended to stop before the current goal location.

Goal navigation behavior was also assessed for old and young rats by first computing the instantaneous velocity at each position on the track. While old rats performing the mobile feeder version of the task tended to show lower average running velocities than the young cohort, this difference was not statistically significant (young: 30.25 ± 11.86 cm/sec; old: 23.17 ± 10.66 cm/sec; ANOVA: $F_{1,7} = 0.86$, $p = 0.38$). Similarly, no age-related difference in overall running velocity was identified for the fixed feeder group (young: 30.14 ± 12.32 cm/sec; old: 26.97 ± 9.66 cm/sec; ANOVA: $F_{1,7} = 0.20$, $p = 0.67$). To assess changes in running velocity preceding animals' arrival to a given goal location (i.e., *pre-goal velocity*), instantaneous velocity was averaged within 10° bins over the

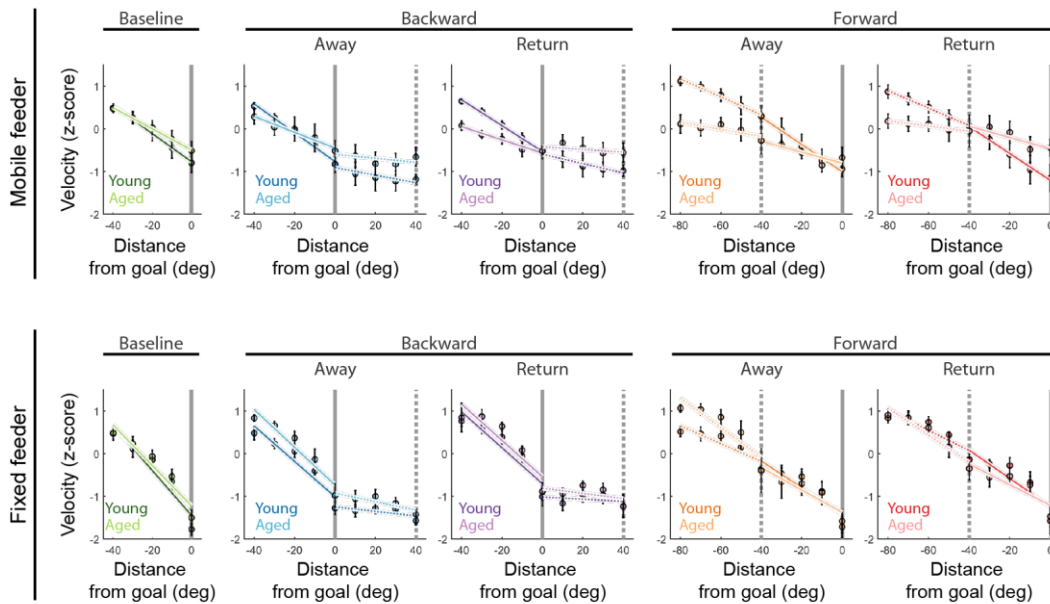


Figure 4.6: Age-related differences in goal-related running velocity.

Data are shown for old and young rats participating in the mobile feeder (top) and fixed feeder (bottom) version of the task and are segregated by age group and cue condition. Position is centered at the current cue-aligned goal location (0°). Vertical gray lines denote the current (solid) and, where applicable, the non-current goal (dashed) location. Mean z-scored running velocity \pm S.E.M (circles) preceding arrival to the current and non-current goals averaged within 10° bins. Lines are shown representing the linear fit for pre-goal velocities for the current (solid) and non-current goal (dashed) locations.

range of -40° to 0° with respect to the designated goal for each cue condition (**Figure 4.6**). In order to correct for individual differences in average running speed, all analysis was performed using z-scored velocity values. Simple linear regressions were then performed to determine if regression slopes (i.e., β coefficients) were statistically significant and negative, which would indicate that animals reliably decreased their running velocity preceding goal arrival. Changes in pre-goal velocity were first assessed separately for old and young rats. Table 4.2 shows the p values from linear regressions performed for each task version, age group and cue condition. Both young and old rats from the mobile feeder task showed a significant decrease in velocity preceding arrival to the current goal location for all cue conditions. This was also true for old and young rats participating in the fixed feeder version of the task. This suggest that young and old rats from both version of the task were able to identify the current goal location for all cue conditions and began slowing in advance of their arrival to the goal. When pre-goal velocity slopes (i.e., β coefficients) were compared between old and young rats for each feeder group, no significant difference was detected for any of the rotation conditions (**Table 4.2**). For the mobile feeder group, however, there was a trend for an age difference for both backward away and backward return trials, suggesting that young rats in the mobile feeder version of the task may have tended to decelerate more preceding arrival to the backward rotated goal than did old rats.

4.3.2. Age-related differences in visual cue control of overall running behavior

In order to quantify cue driven changes in running behavior over the complete extent of the track, and not just in proximity to the goal location, occupancy time was computed for each position on the track and cross-correlations were then calculated between occupancy data from each lap

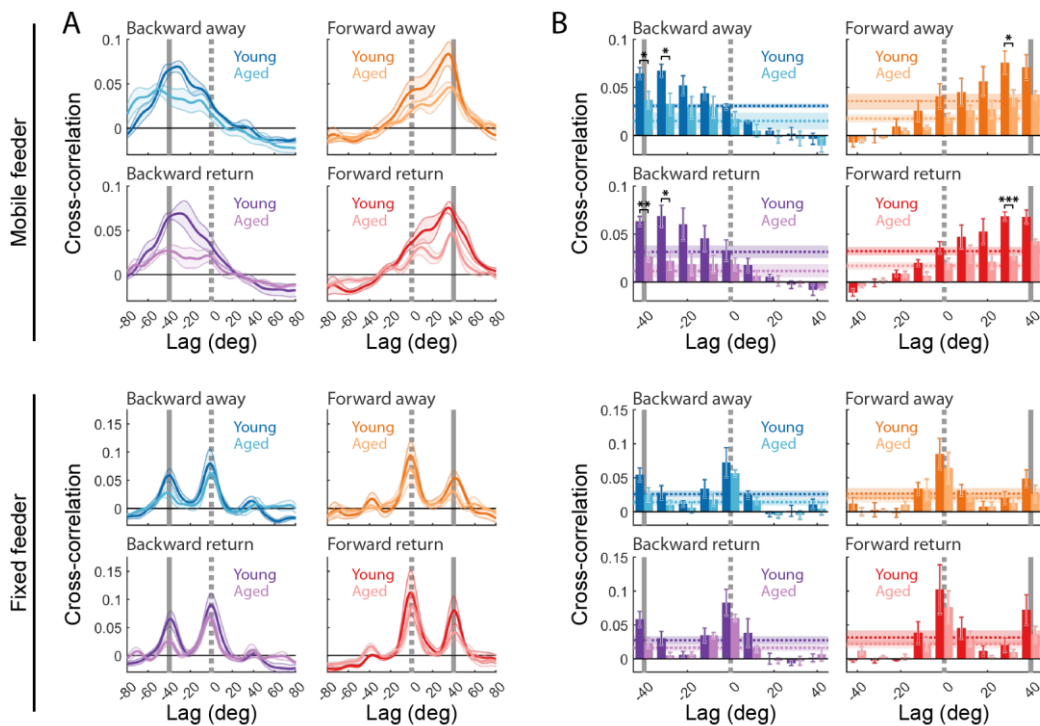


Figure 4.7: Age-related differences in behavioral realignment following cue rotation.

Data are shown for old and young rats participating in the mobile feeder (top) and fixed feeder (bottom) versions of the task, segregated for each rotation condition. Gray vertical lines denote lags corresponding the current (solid) and non-current 0° (dashed) goal location. **(A)** Mean occupancy cross-correlogram \pm S.E.M calculated between occupancy data from each post-rotation lap with that from the preceding trial. Peaks in the occupancy cross-correlogram indicate the degree to which an animal's running behavior realigned with the projected cues following cue rotation. **(B)** Cross-correlation values averaged within 10° bins for lags between -40° and 40° . The across-bins mean (colored dashed lines) and S.E.M (colored shaded regions) is shown. Note that, for the mobile feeder group, young rats showed notably larger cross-correlation values at than aged rats and that the difference tended to be most pronounced at the $\pm 30^\circ$ lags, corresponding to a slightly lesser degree of rotation than the cues would dictate (i.e., $\pm 40^\circ$). Asterisks denote significant pairwise comparisons between old and young rats. Significance indicated as $p < 0.05$ (*), $p < 0.01$ (**), $p < 0.001$ (***)

with that from the preceding trial (for a graphical overview of the cross-correlation procedure, see **Figure 3.5**). Because old and young rats varied in their average running speed, and by extension average occupancy time at each position on the track, occupancy data was z-scored prior to computing the cross-correlations. Within the context of the cross-correlation analysis, the more strongly overall running behavior realigns with the backward or forward rotated cue, the closer the peaks in the cross-correlogram will be to either the -40° or 40° lag, respectively. In order to perform statistical comparisons, cross-correlation values were averaged within 10° bins for lags between -40° to 40° for each rotation condition (**Figure 4.7B**). First, 3-way ANOVAs were performed separately for each feeder group to assess for significant age \times rotation condition \times lag interactions, which would indicate that young and old rats differed in the degree to which their running behavior realigned in response to the different cue rotation conditions. 3-way ANOVA revealed a significant age \times rotation condition \times lag interaction for the mobile feeder group (ANOVA: $F_{12,140} = 1.90$, $p < 0.05$) but not the fixed feeder group (ANOVA: $F_{12,140} = 0.62$, $p = 0.82$). 2-Way ANOVAs were then performed for the mobile feeder group to identify which rotation conditions showed significant age \times lag interactions. 2-Way ANOVA revealed a significant age \times lag interaction for backward return trials (ANOVA: $F_{8,63} = 2.46$, $p < 0.05$) and the same trend was detected for backward away ($F_{8,63} = 1.99$, $p = 0.073$), forward away ($F_{8,63} = 2.22$, $p < 0.058$) and forward return ($F_{8,63} = 1.88$, $p =$

0.092) trials. Table 4.3 shows p values for subsequent pairwise comparisons between young and aged rats for cross-correlation values at each lag (i.e., 0° to $\pm 40^\circ$). Post-hoc comparisons showed a significant difference in correlation values at the -40° bin for young and aged rats for both away and return backward rotations. Similarly, for both away and return forward rotations, there was a trend for larger correlation values at the 40° lag for young as compared to aged rats (**Table 4.3**). This suggests that for all rotation conditions, young rats tended to show larger correlations at the lags corresponding to the rotated cues (i.e., $\pm 40^\circ$). Interestingly, for all rotation conditions, young rats also showed significantly larger correlations at the $\pm 30^\circ$ than did old rats (**Table 4.3; Figure 4.7B**). No comparable age differences were detected for rats participating in the fixed feeder version of the task (**Table 4.3**). These results suggest that, irrespective of rotation direction, for animals participating in the mobile feeder version of the task, young rats showed a greater tendency to realign with the cues than did aged rats, however, young rats may have been biased to rotate to a slightly lesser degree than the cues.

Mobile feeder						
Lag	Backward away			Backward retrun		
	Young	Aged	<i>P-value</i>	Young	Aged	<i>P-value</i>
0°	0.030 ± 0.008	0.017 ± 0.015	<i>p</i> = 0.14	0.034 ± 0.028	0.020 ± 0.015	<i>p</i> = 0.41
-10°	0.045 ± 0.016	0.032 ± 0.028	<i>p</i> = 0.40	0.045 ± 0.034	0.018 ± 0.020	<i>p</i> = 0.20
-20°	0.051 ± 0.027	0.028 ± 0.025	<i>p</i> = 0.25	0.061 ± 0.045	0.019 ± 0.027	<i>p</i> = 0.15
-30°	0.070 ± 0.017	0.033 ± 0.027	<i>p</i> < 0.05	0.069 ± 0.029	0.022 ± 0.022	<i>p</i> < 0.05
-40°	0.066 ± 0.016	0.037 ± 0.021	<i>p</i> < 0.05	0.065 ± 0.013	0.027 ± 0.012	<i>p</i> < 0.01
Lag	Forward away			Forward return		
	Young	Aged	<i>P-value</i>	Young	Aged	<i>P-value</i>
0°	0.042 ± 0.034	0.019 ± 0.013	<i>p</i> = 0.25	0.036 ± 0.016	0.020 ± 0.012	<i>p</i> = 0.14
10°	0.044 ± 0.035	0.027 ± 0.011	<i>p</i> = 0.38	0.048 ± 0.031	0.031 ± 0.022	<i>p</i> = 0.39
20°	0.056 ± 0.040	0.027 ± 0.022	<i>p</i> = 0.23	0.051 ± 0.035	0.020 ± 0.018	<i>p</i> = 0.15
30°	0.076 ± 0.028	0.039 ± 0.021	<i>p</i> < 0.05	0.069 ± 0.010	0.025 ± 0.009	<i>p</i> < 0.001
40°	0.075 ± 0.037	0.044 ± 0.007	<i>p</i> = 0.089	0.070 ± 0.020	0.048 ± 0.007	<i>p</i> = 0.072
Fixed feeder						
Lag	Backward away			Backward retrun		
	Young	Aged	<i>P-value</i>	Young	Aged	<i>P-value</i>
0°	0.083 ± 0.065	0.067 ± 0.015	<i>p</i> = 0.64	0.094 ± 0.056	0.028 ± 0.021	<i>p</i> = 0.43
-10°	0.030 ± 0.032	0.014 ± 0.024	<i>p</i> = 0.45	0.031 ± 0.025	0.001 ± 0.012	<i>p</i> = 0.91
-20°	0.010 ± 0.011	0.005 ± 0.019	<i>p</i> = 0.65	0.003 ± 0.013	0.006 ± 0.010	<i>p</i> = 0.72
-30°	0.025 ± 0.026	0.008 ± 0.017	<i>p</i> = 0.28	0.028 ± 0.026	0.033 ± 0.010	<i>p</i> = 0.12
-40°	0.061 ± 0.029	0.029 ± 0.029	<i>p</i> = 0.14	0.066 ± 0.032	0.070 ± 0.017	<i>p</i> = 0.10
Lag	Forward away			Forward return		
	Young	Aged	<i>P-value</i>	Young	Aged	<i>P-value</i>
0°	0.098 ± 0.066	0.075 ± 0.061	<i>p</i> = 0.61	0.117 ± 0.101	0.090 ± 0.062	<i>p</i> = 0.66
10°	0.027 ± 0.017	0.016 ± 0.010	<i>p</i> = 0.30	0.041 ± 0.035	0.022 ± 0.020	<i>p</i> = 0.38
20°	0.006 ± 0.020	0.007 ± 0.014	<i>p</i> = 0.97	0.011 ± 0.021	0.002 ± 0.005	<i>p</i> = 0.42
30°	0.018 ± 0.024	0.011 ± 0.018	<i>p</i> = 0.65	0.014 ± 0.021	0.007 ± 0.010	<i>p</i> = 0.59
40°	0.053 ± 0.040	0.033 ± 0.034	<i>p</i> = 0.43	0.084 ± 0.069	0.042 ± 0.031	<i>p</i> = 0.30

Table 4.3: Comparison of the occupancy cross-correlations between young and aged rats.

Cross-correlation values are shown for lags between 0° and ±40°. Data is segregated by feeder version, age group, and cue condition. P-values are shown for pairwise comparisons between young and aged rats' cross-correlation values at each lag (i.e., 0° to ±40°).

In order to reduce the results from the cross-correlation calculation to a single meaningful value, *peak correlation* (i.e., maximum value in the cross-correlogram) and *peak lag* (i.e., the corresponding lag value in degrees) were identified for each lap and averaged within each cue rotation condition (**Figure 4.8A**). The peak lag values were then used as a

means of further assessing *behavioral realignment* in terms of the degree to which young and aged animals' running behavior rotated with the cues (**Figure 4.8B**). Peak lags were first assessed for old and young rats participating in the mobile feeder version of the task. One-way ANOVA revealed a significant main effect of rotation condition for both young (ANOVA: $F_{3,16} = 70.87$, $p < 0.001$) and aged rats (ANOVA: $F_{3,12} = 39.38$, $p < 0.001$). One-sample t-tests that were calculated separately for each age group and rotation condition revealed that both age groups showed mean peak lags that were significantly different than 0° for all cue rotation conditions (**Table 4.4**), suggesting that both age groups underwent some degree of behavioral rotation following cue rotation. Additionally, one-sample t-tests were performed to assess if peak lags were also significantly different than $\pm 40^\circ$, which would reveal if there was a tendency of either age group to consistently under-rotate relative to the cues. Interestingly, one-sample t-tests revealed that the mean peak lags of young, but not aged, rats were significantly different from the $\pm 40^\circ$ for forward away, forward return and backward return trials, while the same trend was identified for backward away trials (**Table 4.4; Figure 4.8B**). Taken together, these results suggest that, while both young and aged rats rotated with the cues by some degree, young rats showed a tendency to under-rotate relative to the cues. In contrast to the results from the mobile feeder group, the peak lags of young and old rats participating in the fixed feeder version of the task did not show any clear evidence of

Mobile feeder						
	Backward away			Backward return		
	Peak lag	P-value† (≠ 0)	P-value†† (≠ -40)	Peak lag	P-value† (≠ 0)	P-value†† (≠ -40)
Young	-31.11° ± 9.02°	p < 0.01	p = 0.082	-29.11° ± 10.47°	p < 0.01	p < 0.05
Aged	-34.73° ± 16.43°	p < 0.05	p = 0.57	-34.70° ± 17.42°	p < 0.05	p = 0.59
P-value‡	p = 0.68			p = 0.57		
	Forward away			Forward return		
	Peak lag	P-value† (≠ 0)	P-value†† (≠ -40)	Peak lag	P-value† (≠ 0)	P-value†† (≠ -40)
Young	28.13° ± 10.05°	p < 0.01	p < 0.05	29.15° ± 5.73°	p < 0.001	p < 0.05
Aged	33.49° ± 8.30°	p < 0.01	p = 0.21	36.43° ± 3.97°	p < 0.001	p = 0.17
P-value‡	p = 0.42			p = 0.069		

Fixed feeder						
	Backward away			Backward return		
	Peak lag	P-value† (≠ 0)	P-value†† (≠ -40)	Peak lag	P-value† (≠ 0)	P-value†† (≠ -40)
Young	-6.18° ± 13.83°	p = 0.37	p < 0.01	-9.58° ± 13.63°	p = 0.19	p < 0.01
Aged	0.88° ± 19.86°	p = 0.93	p < 0.05	-3.49° ± 21.39°	p = 0.77	p < 0.05
P-value‡	p = 0.55			p = 0.62		
	Forward away			Forward return		
	Peak lag	P-value† (≠ 0)	P-value†† (≠ -40)	Peak lag	P-value† (≠ 0)	P-value†† (≠ -40)
Young	12.90° ± 20.53°	p = 0.23	p < 0.05	11.79° ± 17.80°	p = 0.21	p < 0.05
Aged	10.76° ± 13.68°	p = 0.21	p < 0.05	9.61° ± 14.30°	p = 0.27	p < 0.05
P-value‡	p = 0.86			p = 0.85		

Table 4.4: Comparison of peak lag values between old and young rats

‡ Pairwise comparisons between young and aged rats

† One-sample t tests assessing if mean peak lags were different from 0

†† One-sample t tests assessing if mean peak lags were different from ±40

behavioral realignment. For this group, one-way ANOVA revealed a significant main effect of rotation condition for young (ANOVA: $F_{3,16} = 3.21$, $p < 0.05$) but not aged rats (ANOVA: $F_{3,12} = 0.61$, $p = 0.62$). One-sample t-tests, however, did not reveal any instances where mean peak lags were significantly different from 0° for either age group. Rather, both age groups showed peak lags that were significantly different from ±40° for all rotation conditions (**Table 4.4; Figure 4.8B**). These results suggest that young and aged rats participating in the fixed feeder version of the task showed a consistent and comparable absence of behavioral realignment following cue rotation.

Peak lags were then separated for the first three laps following cue rotation in order to assess the time-course over which young and aged rats realigned their behavior with the rotated cues (**Figure 4.8C**). First, repeated measures 3-way ANOVAs were performed to detect if peak lags differed between young and old rats as a function of rotation condition and lap. No significant 3-way interaction was found for either the mobile feeder (ANOVA: $F_{6,56} = 0.28$, $p = 0.95$) or fixed feeder (ANOVA: $F_{6,54} = 1.32$, $p = 0.27$) task, suggesting that there was not a detectable age difference in

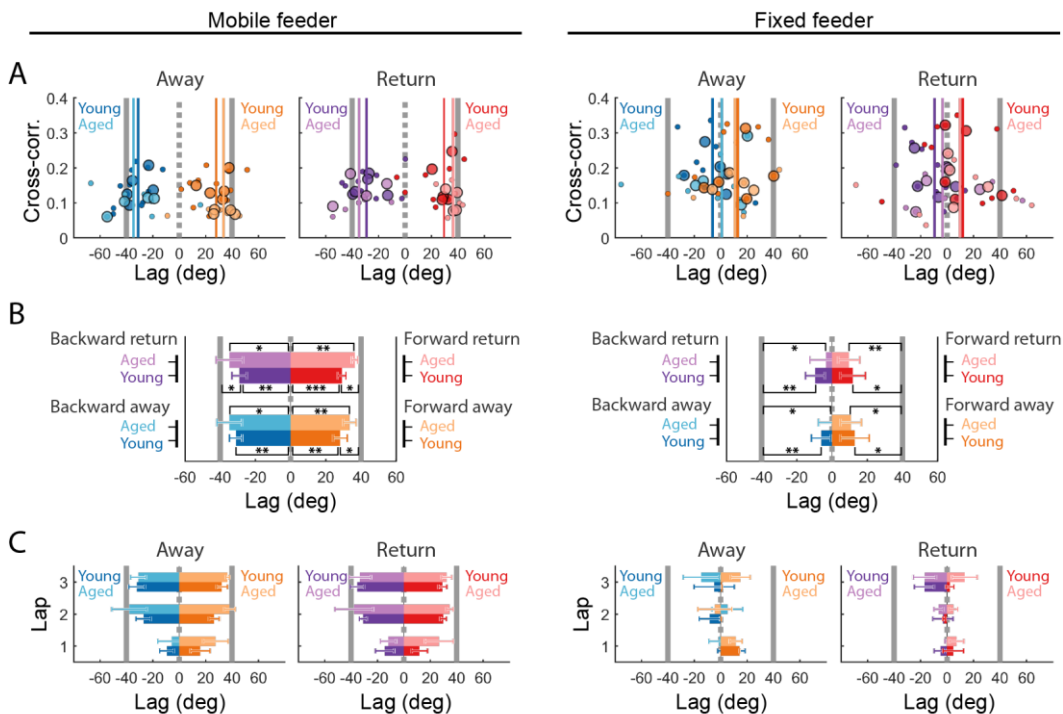


Figure 4.8: Magnitude and time-course of behavioral realignment in young and aged rats.

Data are shown for rats participating in the mobile feeder (left) and fixed feeder (right) versions of the task, segregated by age group and rotation condition. Gray vertical lines denote lags corresponding the current (solid) and non-current 0° (dashed) goal location. **(A)** Peak correlation values from the cross-correlograms are plotted as a function of the peak lag. Rat means are denoted by large circles and session means are denoted by small circles. **(B)** Mean peak lags \pm S.E.M for each age group and rotation condition. Asterisks denote statistics for one-sample t-tests of mean peak lags that were significantly different from 0° as well as those that were significantly different from $\pm 40^\circ$. **(C)** The same data as in B segregated for the first three laps following cue rotation. Significance indicated as $p < 0.05$ (*), $p < 0.01$ (**), $p < 0.001$ (***)

overall lap-by-lap realignment between old and young rats based on rotation direction. For the mobile feeder group, 2-way ANOVA did reveal a significant lap \times rotation condition interaction for young rats (ANOVA: $F_{6,32} = 6.43$, $p < 0.001$), while for old rats this was only a statistical trend (ANOVA: $F_{6,24} = 2.05$, $p = 0.098$). For the fixed feeder group, no lap \times rotation condition interaction was identified for either young (ANOVA: $F_{6,20} = 0.39$, $p = 0.88$) or aged (ANOVA: $F_{6,24} = 1.37$, $p = 0.26$) rats. These results suggest that both old and young rats in the mobile feeder group showed some tendency for a change in their lap-by-lap behavioral alignment in response to cue rotation, while no such change was evident in the fixed feeder group (**Figure 4.8C**). For the mobile feeder group, post-hoc comparisons were then performed separately for each age cohort and rotation condition in order to identify the first lap at which peak lags were significantly different than 0° . For young rats, peak lags were significantly different than 0° by the second lap for all rotation conditions (backward away: $-27.35^\circ \pm 12.05^\circ$, t-test: $t_4 = -5.07$, $p < 0.01$; backward return: $-30.72^\circ \pm 6.34^\circ$, t-test: $t_4 = -10.83$, $p < 0.001$; forward away: $25.73^\circ \pm 9.24^\circ$, t-test: $t_4 = 6.23$, $p < 0.01$; forward return: $29.73^\circ \pm 5.15$, t-test: $t_4 = 12.90$, $p < 0.001$). The same pattern was also found for aged rats, in that, for all rotation conditions their peak lags significantly differed from 0° by the second lap (backward away: $-37.88^\circ \pm 26.40^\circ$, t-test: $t_3 = -5.31$, $p < 0.05$; backward return: $-37.75^\circ \pm 28.70^\circ$, t-test: $t_3 = -4.03$, $p < 0.05$; forward away: $38.13^\circ \pm 8.17^\circ$, t-test: $t_3 = 9.33$, $p < 0.01$; forward return: $34.75^\circ \pm$

5.19°, t-test: $t_3 = 13.40$, $p < 0.001$). These results suggest that, at least within the context of the mobile feeder task, both old and young rats undergo a realignment of their behavioral output within the first two laps following cue rotation.

4.3.3. Model of directional representation updating during simulated instantaneous cue rotation

An attractor-based model of head direction (HD) and angular head velocity (AHV) networks was created that incorporated two forms of spatial input. The first input consisted of a vestibular (i.e., idiothetic) signal relaying current angular velocity, which was used to modulate the profile of AHV→HD synaptic drive. The second input relayed current heading with respect to visual (i.e., allothetic) cues in the environment, which was modeled as a Gaussian-shaped pattern of inputs (**Figure 4.3**). The width of the visual cue Gaussian was 90°, corresponding to the four sets of polarizing cues used in the ICR apparatus, which each span approximately 90° of the wall. Heading was modeled as a sinusoidal directional profile, which can be thought of as simulating a continuous scanning of the environment. Modeling heading in this manner allowed for an equal sampling of a wide range of headings ($0^\circ \leq h \leq 180^\circ$) and angular velocities ($0 \frac{\text{deg}}{\text{sec}} \leq v \leq 200 \frac{\text{deg}}{\text{sec}}$) during the course of each simulation. Except during cue rotation, the relative orientation of visual cue input was always aligned to the current simulated heading. The same heading signal was also used to compute the vestibular angular velocity inputs.

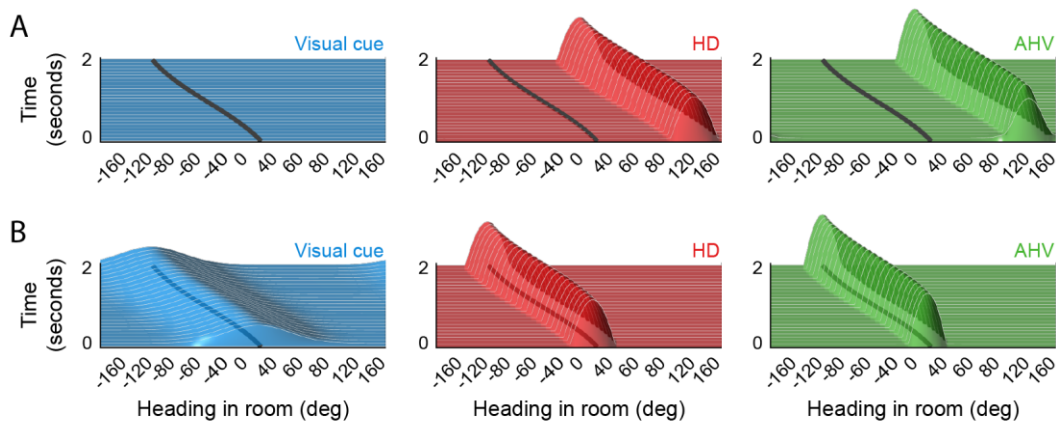


Figure 4.9: Influence of allothetic and idiothetic input on directional updating in the head direction network model.

Simulations showing the spatiotemporal trajectory of the head direction (HD; red) and angular head velocity (AHV; green) activity bumps during 2 seconds of simulated head movement. Data are depicted with respect to head direction in absolute space (i.e., room reference frame). **(A)** Results from a simulation that did not include the visual cue input (blue). The orientation of the simulated rat heading is denoted in each graph by a black trace. During the course of the simulation the rat's head orientation gradually moved in the counterclockwise direction. Note that, in the absence of visual cue input, the HD and AHV activity bumps stabilized to a starting orientation (i.e., 130°) that was out of alignment with the rat's initial heading (i.e., 35° ; black line). Subsequently, vestibular input alone was sufficient for both the HD and AHV representations (i.e., activity bumps) to track the movement of the rat's head but not its actual head direction/orientation in the room reference frame; i.e., the trajectory of the HD and AHV activity bumps mirrored the rat's head movement but its actual alignment in the room. **(B)** Results from a simulation that included visual cue input. Note that this simulation was performed using the same pattern of head movement as in A (black trace). The inclusion of visual cue input anchored the HD-AHV representations to the rat's heading (i.e., black trace) in the room reference frame, such that the HD-AHV representations were able to accurately track both head movement and head direction.

The HD and AHV networks were first tuned by adjusting the model parameters until both networks produced a stable bump of activity characteristic of continuous attractor networks (**Figure 4.2**). In addition, the model parameters dictating the relative influence of vestibular and visual cue inputs were adjusted so that either input alone was sufficient to modulate the directional tuning of HD-AHV representations. This was done to ensure that the default alignment and trajectory of the HD and AHV representations depended on both self-motion and external cue inputs (**Figure 4.3**). Importantly, while vestibular input alone was sufficient

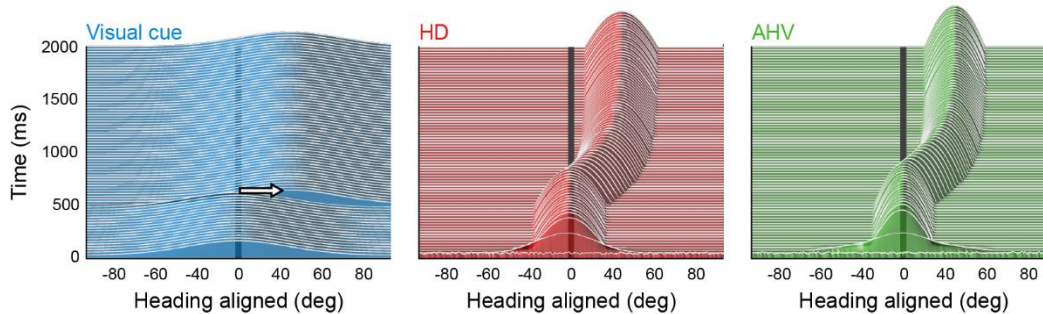


Figure 4.10: Time-course of realignment in the head direction network model following visual cue rotation.

Simulations showing the spatiotemporal trajectory of the head direction (HD; red) and angular head velocity (AHV; green) activity bumps following rotation of the visual cue input (blue). All simulations were performed in the presence of continuous head movement. For clarity, head movement has been omitted from the graphs by centering all data to the current simulated head direction (i.e., 0°; black line). After the first 500 milliseconds of the simulation the visual cue input pattern was rotated 40° (white arrow). Note that, following cue rotation, both the HD and AHV activity bumps gradually realigned with the rotated visual cue input and maintained this new alignment for the duration of the simulation.

for HD and AHV networks to track relative changes in heading (**Figure 4.90A**), visual cue input was required to align the network representations to the actual head direction of the simulated rat (**Figure 4.90B**). Following this initial tuning, the resulting parameters were held constant for all subsequent simulations discussed (**Table 4.1**).

The model was then assessed during simulated cue rotation in order to mimic conditions present in the ICR task. Because none of the parameters or computations used in the model differentiated the effects of rotation direction (i.e., clockwise versus counterclockwise), the direction that visual cues were rotated was not a meaningful factor in how the model behaved. For all simulations discussed, rotation events were arbitrarily modeled as occurring in the clockwise direction. The simulation was run for a total of 2000 milliseconds. After 500 milliseconds, the HD network was subjected to an immediate 40° rotation of the visual cue input

(Figure 4.10). Following cue rotation, both HD and AHV networks showed a coherent and gradual transition in which the directional representation (i.e., activity bump) of both networks realigned to an orientation that was consistent with the new visual cue orientation (i.e., 40°). This transition typically took approximately 500 milliseconds, after which time both networks maintained the new alignment for the duration of the simulation.

In order to assess how cumulative error in the self-motion signal may influence the time-course and reliability with which the HD network realigns following visual cue rotation, simulations were run with differing levels of error in the angular velocity input. This was modeled by adding an *idiothetic error* to the angular velocity input at each time step, which can be thought of as representing the accumulated errors implicit in path integration operations. Idiothetic error was controlled by a single parameter ε , which specified the standard deviation of the random normal distribution used to generate the errors. Consequently, ε dictated the amount of variance in the time-course of idiothetic error for each simulation. Three different idiothetic error conditions were evaluated, corresponding to a value of ε equal to 1.0°, 1.25° or 1.5°. A total of 50 simulations were performed for each error condition. Steps were taken to ensure that only the relative magnitude of idiothetic error differed between each error conditions. For each condition, the same seed value was used for the random number generator to allow for a similar spatiotemporal pattern of errors between error conditions, but with different degrees of

variance. In addition, head direction was initialized to the same orientation across error conditions for each simulation in order to minimize unintended differences in cue realignment due to differences in the particular speed or direction of head movement occurring at the time of cue rotation.

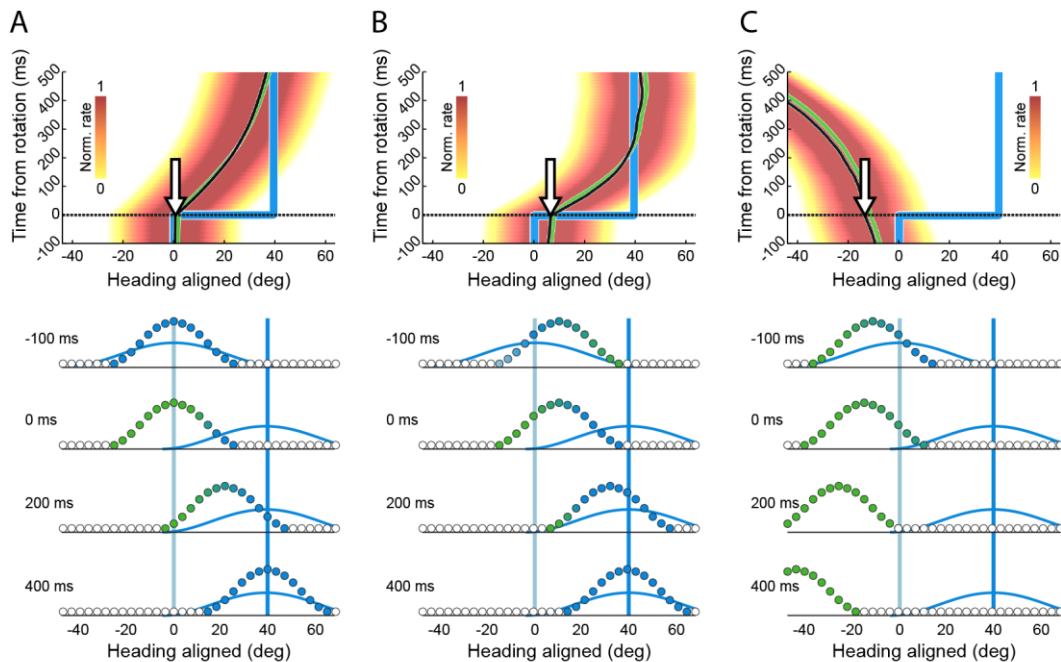


Figure 4.11: Effects of combined idiothetic error and allothetic rotation in the head direction network model.

Results from three example simulations showing different realignment outcomes in the presence of idiothetic error (top panels), accompanied by illustrations depicting the models behavior in each scenario (bottom panels). All simulations were performed in the presence of continuous head movement. For clarity, head movement has been omitted from the graphs by centering all data to the current simulated head direction (i.e., 0°). **(A)** Shows the spatial and temporal trajectory of network activity during the periods preceding and following visual cue rotation (top panel). Heat maps show the normalized firing rate of the HD network. The peak position of the activity bump is also denoted for both HD (black trace) and AHV (green trace) networks. Blue lines denote the centroid of the visual cue Gaussian. White arrows indicate the position/orientation of the HD activity bump at the time of cue rotation (i.e., 0 ms), which, in this case, was near 0° . Subsequent to the rotation event, the networks underwent a gradual realignment to the new allothetic bearing over approximately 500 milliseconds. Illustration depicts changes that the network underwent at successive periods in the simulation (bottom panel). Vertical blue lines denote the visual cue position both prior to (light) and following (dark) forward rotation. The activity of the HD population (circles) is color coded to indicate the relative drive from visual (blue) and idiothetic (green) inputs. Because the HD network was aligned near the visual cue input (i.e., 0°) at the time of cue rotation (i.e., 0 ms), at the moment cues were rotated there was sufficient overlap between the active units (i.e., activity bump) and the rotated visual cue input for the network to be gradually pulled into the new orientation (i.e., 40°). **(B)** Example of a simulation that showed more rapid realignment of the HD network when idiothetic error was present. During this simulation, idiothetic error caused the network to drift to an orientation (i.e., 8°) where the active units had greater overlap with the rotated visual cue input at the time of rotation (i.e., 0 ms), resulting in a more powerful drive from of the rotated visual cue inputs and a more rapid transition of the network. **(C)** Example of a simulation in which idiothetic error caused visual cues to lose all control over the network following cue rotation. During this simulation, idiothetic error pulled the network in the opposite direction from the direction of cue rotation (i.e., -15°). As a consequence, the activity bump was out of the range of influence of the rotated visual cue input at the time of cue rotation. Subsequently, the trajectory of the activity bump became solely controlled by the idiothetic input and the network become unanchored from the allothetic (i.e., visual) cues. The resulting loss of visual cue control lasted for the remainder of the simulation.

The model was first assessed for periods preceding visual cue rotation. Under all conditions, HD and AHV network representations remained strongly coupled, however, larger idiothetic errors introduced more overall variability in how faithfully the trajectory of HD-AHV representations tracked head movement. Similarly, larger errors tended to cause the HD-AHV representations to periodically drift out of alignment with the visual cue input, although visual cue input always maintained some degree of control when in its default (i.e., baseline) orientation. Following visual cue rotation, the spatial-temporal trajectory of the HD-AHV representation became less predictable. For some simulations, the cumulative idiothetic error had little impact on the overall spatiotemporal trajectory of the HD-AHV network representations. Under these conditions, HD-AHV representations remained closely aligned with the visual cue input and typically underwent a smooth but gradual transition to the rotated visual cue coordinates (**Figure 4.11A**), in a manner similar to that observed for simulations that did not include any idiothetic error component. Alternatively, when idiothetic error caused the trajectory of the HD-AHV networks to drift out of alignment with the visual cue input, a general pattern was observed in that the degree and direction of drift in HD-AHV representations had a notable impact on the speed and reliability with which the network realigned when the visual cue input was rotated. For simulations in which idiothetic error biased the HD-AHV representations to drift to a position somewhere between the pre- and

post-rotated position of the visual cue input, HD-AHV realigned to the rotated visual cue coordinates at a more rapid rate. Under these conditions, idiothetic errors had already skewed the HD-AHV representations in the direction of cue rotation resulting in greater overlap of the HD representation and the rotated visual cue inputs immediately following the cue rotation. Consequently, visual cue inputs exerted a stronger asymmetric drive to the active units of the HD network, resulting in a more rapid transition of the network to the new position (**Figure 4.11B**). A complimentary but opposite pattern was observed for simulation in which idiothetic error biased HD-AHV representations in a direction opposite to that of visual cue rotation. Under these conditions, the rotated visual cues had less spatial overlap with the HD representation and, therefore, exerted weaker control over HD and AHV activity. For simulations where the HD-AHV representations ended up outside the effective range of influence of the rotated visual cue input, the HD-AHV networks became unanchored from the visual cue input (**Figure 4.11C**). As a consequence, the HD-AHV networks became solely controlled by the error-prone idiothetic input and ceased to accurately track head direction. This loss of visual cue control occurred more frequently for sessions with larger idiothetic errors (**Figure 4.12A**). The same simulations were also performed using identical inputs but without any visual cue rotation (**Figure 4.12B**). Under these conditions, the networks continued to show some degree of variability in how closely their trajectory tracked the visual

cue input. In the absence of cue rotation, however, visual cues never failed to maintain some degree of control over the HD-AHV networks, even under the largest error condition (i.e., $\varepsilon = 1.5^\circ$). When the trajectory of HD-AHV network representations were compared across all visual cue rotation simulations and error conditions a clear pattern emerged (**Figure 4.12C**). Overall, HD-AHV networks showed a progressively more rapid transition to the new cue orientation the closer the directional representation was to the new visual cue input at the time of rotation. Conversely, greater drift of HD-AHV networks away from the direction of cue rotation resulted in a progressively slower time-course of realignment or a complete loss of visual cue control if the directional representation was sufficiently displaced from the rotated visual cue input.

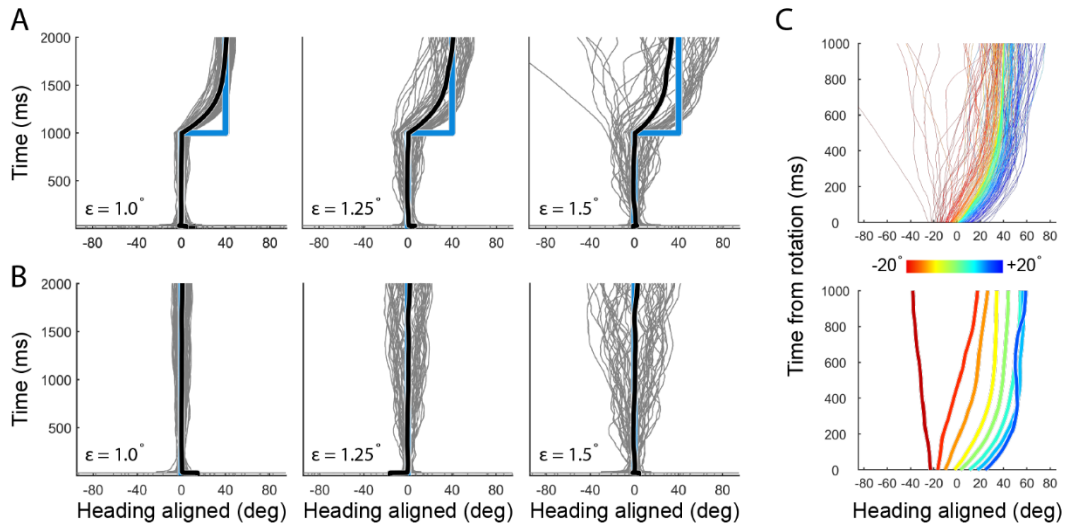


Figure 4.12: Comparison of attractor network realignment with varying levels of idiothetic error.

The spatiotemporal trajectory of the HD network during visual cue rotation for simulations with different levels of idiothetic error. Data are shown for three different levels of angular velocity error. A total of 50 simulations were performed for each idiothetic error condition ($\epsilon = 1.0^\circ$, $\epsilon = 1.25^\circ$, $\epsilon = 1.5^\circ$). All data are shown centered to the current simulated rat heading (i.e., 0°). **(A)** Graphs show the trajectory of the HD activity bump for each simulation (thin gray traces) as well as averaged across simulations (thick black trace) for each idiothetic error condition. Blue lines denote the position of the visual cue input, which was rotated 1000 ms into the simulation. Note that simulations with greater idiothetic errors showed more session-by-session variability in the trajectory of HD activity after cue rotation (gray traces). Furthermore, with respect to across-simulation averages (black traces), the HD network displayed a slower average time-course of realignment when larger idiothetic errors were used. This slower average realignment may be accounted for by the fact that, in a subset of the simulations run for the largest error condition ($\epsilon = 1.5^\circ$), visual cues lost all control over the directional representation. **(B)** Results from simulations that used identical inputs as in A, but without any visual cue rotation. Note that the HD activity bump still showed some deviation from visual cue input when larger idiothetic error was used. In the absence of cue rotation, however, visual cues never lost control over the network. **(C)** All data from A color coded based on the distance of the HD activity bump and the visual cue input (i.e., 0°) at the time of rotation (i.e., 0 ms). The top graph shows the color coded data for each session. The bottom graph shows averages within several ranges of distances between -20° and 20° . Note that the speed and reliability with which the HD network realigned with the rotated visual cues largely depended on the proximity of the HD activity bump (colored traces) and the visual cue input at the moment cues were rotated (i.e., 0 ms). Additionally, the HD network showed a greater tendency to break free of visual cue control for sessions in which idiothetic error had pulled the network in a direction (i.e., counterclockwise; red traces) that was opposite to the direction cues were rotated (i.e., clockwise).

4.4. Discussion

4.4.1. Summary of salient results

The present behavioral experiment assessed how real-time rotation of allothetic cues influenced the goal navigation and overall running behavior of young and aged rats as they performed the Instantaneous Cue Rotation (ICR) task. The purpose of the present study was to expand on existing findings showing that aging is accompanied by various alterations in the relative control environmental (i.e., allothetic) and self-motion (i.e., idiothetic) feedback exert over spatial representation networks and navigation behavior (see **Chapter 4.1**). In the present study, spatial signals were put in direct and immediate conflict by rotating all orienting visual cues in the environment while preserving ongoing self-motion feedback. Two separate groups of rats were assessed, each of which participated in either the mobile feeder or fixed feeder version of the ICR task. Each version of the task included both a young ($n = 5$) and an old ($n = 4$) cohort. Behavioral data from the mobile feeder version of the task suggest that both young and old rats were able to utilize visuospatial cues to navigate to the cue-aligned goal, even when cues were suddenly rotated during ongoing behavior. The results from the aged mobile feeder cohort, however, suggest that allothetic cues exerted less pronounced control over the behavior of aged rats as compared to that of the young rats. Interestingly, while the behavior of the young cohort was more reliably influenced by allothetic cue rotation, they also had a tendency to

slightly under-rotate relative to the cues. One interpretation of these findings is that when exposed to mismatched allothetic and idiothetic feedback, young rats may settle on a navigation strategy that combines the two conflicting sources of spatial information.

The results from young and old cohorts in the fixed feeder version of the task were less conclusive. With respect to goal navigation performance and goal-related changes in running speed, both age groups displayed clear, and largely equivalent, cue-rotation induced changes in running behavior. Results from analyses looking at changes in track-wide running behavior, in contrast, did not indicate a consistent realignment of running behavior in either age group following cue rotation. As previously described, the use of stationary feeder dishes introduced olfactory cues at the rewarded feeder (see **Chapter 3.5**). Consequently, this may have allowed both young and aged rats from the fixed feeder version of the task to identify the cue-aligned goal feeder based on odor, masking the age-related differences that were identified for rats participating in the mobile feeder version of the task.

In addition to the behavioral experiment, a computational model was created to assess how a sudden rotation of visual (i.e., allothetic) cue input may affect head direction representation networks and how the behavior of these networks may be altered in the presence of error-prone self-motion feedback (i.e., idiothetic error). In the absence of any idiothetic error, network representations underwent a gradual but reliable

realignment of their directional firing following a sudden forward rotation of visual cue input (**Figure 4.10**). In contrast, the introduction of idiothetic errors had a complex effect on the control that visual cues exert on the network activity. The results suggest that idiothetic errors could either amplify or diminish the control visual cues exerted over directional representations depending on the degree and direction of drift these errors induced in the network (**Figure 4.12**). In the most extreme circumstances, network activity could become completely dissociated from the visual cue input following cue rotation. The results from the model have interesting implications for the present behavioral findings when considered in the context of known age-related deficits in self-motion perception and path integration, which will be discussed in detail below (see **Chapter 4.3.3**).

4.4.2. Age-related differences in the Instantaneous Cue Rotation task

Rats were assessed during baseline trials as well as trials following Instantaneous Cue Rotation (ICR) in which visual cues were rotated $\pm 40^\circ$ away from or back to their baseline configuration. Comparison of goal navigation performance between young and aged rats did not reveal any significant age-related difference for either version of the task with respect to the percentage of laps that were rewarded for each cue condition.

There was, however, a trend of poorer performance for aged rats during baseline trials for the mobile feeder version of the task (**Figure 4.4**). The fact that aged rats' performance improved to match that of young rats for all subsequent cue rotation trials indicates that the deficit was only evident

during the early (i.e., baseline) period of the session. One interpretation of these results is that aged rats may have had difficulty retaining some element of the task from one session to the next, resulting in poorer performance until they reacquired this knowledge. For instance, although each animals' designated goal location did not vary between session, there is evidence that aged individuals are less efficient in using place-based knowledge to navigate to already learned locations in the environment (Iaria et al., 2009; Bohbot et al., 2012; Harris and Wolbers, 2014). Consequently, aged animals may have been impaired in retaining a memory of the goal location between sessions, which would also be consistent with the observed LTP maintenance deficits that have been shown to occur with age (Barnes, 1979; Barnes and McNaughton, 1980b, 1985; Dieguez and Barea-Rodriguez, 2004). It could also be the case that all rats required some period of time to relearn the goal location irrespective of age, but that this reacquisition took longer for aged rats. Consistent with this possibility, a number of aging rodent and human studies have reported slower acquisition for tasks that require navigating to a specific learned location in the environment, such as a hidden escape tunnel or platform (Barnes, 1979; Barnes et al., 1980, 1997; Barnes and McNaughton, 1985; Rapp et al., 1987; Aitken and Meaney, 1989; Burwell and Gallagher, 1993; Lindner, 1997; Gallagher et al., 2015; Daugherty et al., 2016). Similarly, aged humans have been shown to require longer acquisition periods to reduce their search path length in a virtual Morris

watermaze task (Daugherty et al., 2016). Consequently, it may be that aged rats showed selective performance impairments early in the session (i.e., baseline trials) because they required an extended period of time to relearn the location of the goal.

Differences in the navigation strategy used by the young and old rats during the ICR task may also account for the observed baseline performance impairments as well as additional age-related differences that were identified in the present study. Aging is associated with well-established biases for egocentric over allocentric navigation strategies as well as more severe performance deficits for tasks which rely on allocentric navigation (Barnes et al., 1980; Nicolle et al., 2003; Rosenzweig et al., 2003; Moffat et al., 2007; Iaria et al., 2009; Head and Isom, 2010; Bohbot et al., 2012; Rodgers et al., 2012; Wiener et al., 2013). Consequently, while the ICR task favors an allocentric strategy to successfully navigate to the allothetic cue-aligned goal, aged rats may have been biased toward perseveration in using an egocentric strategy. Because animals began each session in a different starting location, any estimate of position based on self-motion feedback is uninformative with respect to the location of the goal. In theory, an animal that did not utilize the cues at all might still trigger reward delivery if they eventually stopped within the goal bounds by chance (i.e., $\pm 20^\circ$) and could, in principle, rely on path integration-based estimates of distance traveled to localize the goal on subsequent traversals. While such a scenario could account for

the poorer performance during baseline trials, it is unlikely that the strategy bias was this severe, as a complete failure to utilize allothetic cues would likely result in markedly worse performance following cue rotation than what was observed. For both versions of the task and all cue rotation conditions, young and aged rats had a comparable percentage of rewarded laps (**Figure 4.4**) and both young and aged rats showed a reliable decrease in running speed preceding goal arrival even after cues were rotated (**Figure 4.6**).

While these results may suggest that both young and aged animals were able to successfully adopt an allocentric strategy to navigate to the visual cue-aligned goal, the implications of the results from fixed feeder version of the task are confounded both the potential to use odor cues in this version of the task. In the presence of these unintended olfactory cues, rats could have been identifying the goal location based on odor cues, visual cues, or some combination of the two. As a consequence, with respect to the goal navigation results collected from rats using the fixed feeder system, it is difficult to determine to what degree visual or olfactory cues may have accounted for the observed changes in either age-group's goal-related running following cue rotation. For both age groups, results from the cross-correlation analysis suggest that, more often than not, these rats tended to maintain the same profile of running behavior both before and after cue rotation (**Figure 4.7 and Figure 4.8**). Collectively the results from the fixed feeder version of the task suggest

that the presence of olfactory cues at the current and previously rewarded feeder tended to bias rats from both the young and aged cohort to slow down at whichever feeder had the greatest accumulation of odor, irrespective of the spatial information relayed by the current visual cue configuration. By contrast, the mobile feeder system was designed to ensure that food-related olfactory cues were in constant motion, diminishing the potential for these cues to influence goal selection. Consequently, the results from the mobile feeder version of the task, showing that both age cohorts were able to navigate to the goal even following cue rotation, suggests both young and aged rats were able to recalibrate their behavior based on the change in allothetic feedback. These findings are also supported by results from the occupancy cross-correlation peak lag analysis, which show that both aged groups underwent some degree of realignment of their overall running behavior in response to cue rotation (**Figure 4.8B**).

Although both age cohorts from the mobile feeder task showed evidence of a realignment in running behavior in response to visual cue rotation, suggesting some propensity for relying on an allocentric navigation strategy, notable differences were evident in the degree of control visual cues exerted over young and aged rats. For the mobile feeder group, comparison of pre-goal running speed following cue rotation indicated that young rats tended to decelerate more than aged rats in anticipation of goal arrival (**Figure 4.6**), suggesting allothetic cues tended

to have a weaker influence on the aged rats goal navigation behavior as compared to young rats. These results are consistent with the age-related goal navigation deficits observed by Rosenzweig et al. (2003) following allocentric-egocentric mismatch, in which aged rats were found to perform significantly worse than young rats when required to decelerate at a learned goal location that was fixed with respect to the allothetic cues in the environment. Similar differences were also identified in analyses that assessed running behavior over the full extent of the track and not just in proximity to the goal. For the mobile feeder version of the task, the mean cross-correlogram of young rats displayed a distinct asymmetric peak that was centered near the lag corresponding to the rotated cue (i.e., $\pm 40^\circ$) for all rotation conditions (**Figure 4.7A**). Conversely, the mean cross-correlograms of the aged mobile feeder cohort tended to be smaller in overall magnitude for all rotation conditions. Age-comparisons of the correlation values for lags over the range of -40° to 40° revealed that young rats tended to have larger correlation values at the $\pm 40^\circ$ (i.e., the lag corresponding to the magnitude of cue rotation) than aged rats for all rotation conditions in the mobile feeder version of the task, suggesting that young rats in this group realigned with the cues more reliably than did aged rats (**Figure 4.7B**).

Interestingly, while young rats in the mobile feeder group showed more reliable realignment in response to cue rotation than their aged counterparts, there was evidence that young rats tended to only partially

realign with the cues. For instance, although no significant difference in peak lags was identified when direct comparisons were performed between old and young rats (**Table 4.4**), the mean peak lags of aged rats tended to be in closer agreement with the rotated cues than were those of young rats (i.e., backward away: young: -31° , old: -35° ; backward return: young: -29° , old: -34° ; forward away: young: 29° , old: 33° ; forward return: young: 29° ; old: 35° ; **Figure 4.8B**). Consistent with these observations, for all cue rotation conditions, young rats showed correlation values at the $\pm 30^\circ$ lag that were significantly greater than those of aged rats (**Figure 4.7B**). This suggests that the running behavior of young rats may have tended to reflect some combination of the mismatched allothetic and idiothetic feedback. For both age cohorts in the mobile feeder group, it was found that running behavior became more strongly aligned with the allothetic cues over successive laps (**Figure 4.8C**), which parallels the progressive realignment observed in place cell firing fields under similar conditions of allocentric-egocentric mismatch (Gothard et al., 1996; Redish et al., 2000; Rosenzweig et al., 2003). The pattern of progressive realignment observed in the present behavioral findings, as well as that reported for CA1 place cells, may reflect the gradual correction of path integration estimates in response to a mismatch of allothetic and idiothetic (i.e., self-motion) signals (Mittelstaedt and Mittelstaedt, 1980; Gallistel, 1990; Benhamou, 1997; Redish, 1999). Interestingly, while the results of the peak lag analysis suggest that both age groups showed an equivalent

lap-by-lap realignment that typically occurred within the first two laps following cue rotation, the goal errors of young rats were significantly different than those of aged rats during the first lap following backward away and return cue rotation (**Figure 4.5B**). Immediately following backward rotations, young rats tended to overshoot the current goal and stop at a position on the track that was intermediate to the allothetically-aligned (i.e., current) and ideothetically-aligned (i.e., non-current) goal locations. Collectively these results could be explained by a bias of young rats to settle on a behavioral strategy that takes both allothetic and idiothetic feedback into account. Given the limited sample sizes in the present study, as well as the fact that some of the results highlighted are based on analyses performed separately for each of the age groups, these findings should be considered preliminary.

Despite these caveats, it is worth noting that the under-rotation bias of young rats suggested by the results discussed is consistent with anecdotal observations of these rats as they engaged in the ICR task. While the pattern was not consistent, on a number of occasions following cue rotation, young rats were observed to come to a sudden stop at some intermediate location between the current and non-current goal location (e.g., -20° or 20°). This pattern of behavior was rarely observed in aged rats. In the context of natural day-to-day navigation, organisms must adapt to variable environmental and behavioral conditions in which allothetic and idiothetic feedback may be vulnerable to differing levels of sensory-

perceptual error. For instance, unstable terrain can result in erratic motor feedback that is periodically dissociated from actual distance traveled, while visual obstructions and certain weather conditions can result in inconsistent landmark visibility. In most scenarios, some level of noise will be present in both domains, which may vary from moment-to-moment such the highest fidelity representation of one's actual position is constantly changing. It follows, therefore, that dynamically calibrating behavioral output on the basis of both forms of sensory feedback should, on average, result in the most robust and circumstance-invariant estimates of position and orientation. A similar principle is commonly applied in signal processing applications in which signals carrying redundant information can be blended in such a way that the unshared noise is identified and rejected. Based on this reasoning, the partial rotation observed in the young cohort may reflect an optimal default navigation strategy under ecologically typical conditions in which both allothetic and idiothetic signals will likely carry some degree of noise.

4.4.3. Implications of the behavioral findings within the context of the proposed computation model and existing electrophysiological findings

A continuous attractor-based model was created to assess the differential influence of allothetic and idiothetic input during simulated Instantaneous Cue Rotation (ICR). The model was composed of a head direction (HD) network that received visual cue inputs as well as vestibular signals that were relayed by a second angular head velocity (AHV)

network (**Figure 4.3**). Over the course of each simulation, the HD and AHV network representations (i.e., activity bumps) remained closely coupled and underwent a gradual but reliable realignment of their directional firing following a sudden 40° forward rotation of the visual cue input (**Figure 4.10**). During this time, the directional representations of both networks gradually and coherently transitioned into alignment with the visual cue input and maintained the new alignment for the remainder of the simulation.

The model was also assessed under conditions in which different degrees of error were present in the vestibular input. There is extensive evidence that disrupting vestibular signals can result in significant navigation and spatial memory performance deficits in rodents (Potegal et al., 1977; Miller et al., 1983; Matthews et al., 1989; Semenov and Bures, 1989; Chapuis et al., 1992; Stackman and Herbert, 2002; Wallace et al., 2002), while similar findings have also been reported in humans with impaired vestibular function (Brandt et al., 2005). Consistent with its role in navigation and spatial mnemonic performance, vestibular feedback is also crucial for establishing and updating the directional tuning of head direction cells (Stackman and Taube, 1997; Muir et al., 2009; Shinder and Taube, 2011) as well as for maintaining precise and stable place cell firing fields (Stackman et al., 2002; Ravassard et al., 2013; Aghajani et al., 2015). Aging has been associated with declines in vestibular function based on various anatomical, physiological and behavioral metrics (for

review, see Anson and Jeka, 2015). Given that vestibular signals convey information about ongoing linear and angular movement, age-related changes in vestibular functioning may lead to less accurate self-motion-based estimates of position and orientation (i.e., path integration). Consistent with this possibility, aged humans show reliable impairments for task relying on path integration. For instance, aged individuals tend to underestimate travelled distances and turns after moving about in an environment (Allen et al., 2004; Mahmood et al., 2009; Adamo et al., 2012; Harris and Wolbers, 2012) and make significantly greater errors in perceived heading direction (Warren Jr et al., 1989). In order to simulate these reported age-related deficits in self-motion-based updating (i.e., path integration), the model was evaluated under conditions in which *idiothetic error* was incrementally added to the vestibular input over consecutive time steps. In general, the activity bump of the HD network displayed a more variable spatiotemporal trajectory when the network was subjected to greater levels of idiothetic error. For some simulations, greater idiothetic error resulted in a more rapid realignment of the HD network in response to cue rotation (**Figure 4.11B**), while in other instances, idiothetic errors resulted in slower realignment or, in more severe cases, a complete loss of visual cue control following cue rotation (**Figure 4.11C**). A pattern was identified suggesting that the degree of control visual cues exerted over the network following cue rotation largely depended on the amount and direction of drift idiothetic errors had

induced in the network during the period leading up to the cue rotation event (**Figure 4.12**). Specifically, when idiothetic errors happened to move the network closer to where the visual cues were going to be (i.e., the visual cues rotated orientation/position), the rotated visual cue input exerted greater control over the network than it normally would, resulting in a more rapid realignment. On the other hand, when idiothetic error caused the network to drift away from where the visual cues were going to be (i.e., in the opposite direction of cue rotation), the influence of the rotated visual cue input was weaker. Under these conditions, the network realigned more slowly or, in the more extreme cases, broke free of the visual cue's influence entirely. Importantly, this loss of visual cue control was not observed during otherwise identical simulations performed without visual cue rotation (**Figure 4.12B**). This indicates that errors in self-motion (i.e., idiothetic) feedback alone was not sufficient to cause the HD network to become unanchored from the allothetic inputs. Rather, the results suggest that visual cues were able to continually correct for errors in the self-motion signal so long as the cues remained stable with respect to the room reference frame. At the moment visual cues were rotated, however, the HD network became subject to whatever errors had accumulated in the self-motion signal.

The modeling results described have interesting potential implications for the findings from the behavioral component of the study. Comparisons of young and aged rats performing the ICR task revealed

that the aged cohort underwent a less pronounced and robust behavioral realignment in response to cue-rotation as compared to the young cohort. Based on results from the model, these age-related realignment deficits could arise due to greater error in signals relaying self-motion-related information. Within this framework, greater levels of cumulative self-motion error will result in a diminished ability of aged spatial networks to reliably reorient with the rotated visual cues. In the present model, self-motion errors were carried by the angular velocity input, which represented signals arising from upstream vestibular systems. Given the established age-related decline in vestibular function described previously, vestibular signals are a likely source of erroneous self-motion information in aged animals. With respect to a possible anatomical locus of such errors, one candidate is the vestibular nucleus, which shows a number abnormal structural changes with age (Johnson and Miquel, 1974) as well as alterations in glutamate levels that suggest reduced excitatory afferent drive (Liu et al., 2010). It is worth noting, however, that aging is associated with multifactorial changes in vestibular processing across wide-ranging systems, including peripheral organs, brain stem, cerebellum and cerebral cortex (for review, see Arshad and Seemungal, 2016).

Results from the behavioral study also indicated that the young cohort tended to slightly under-rotate relative to the cues, while the same pattern was not observed in the aged cohort. One interpretation of these findings is that young rats may resolve conflicting idiothetic-allothetic

feedback by averaging or blending the mismatched signals, while aged rats may be more likely to resolve such mismatch by preferentially aligning their behavioral output to one or the other spatial reference frames. Consistent with this interpretation, introducing idiothetic error in the model resulted in a tendency for the network to either rapidly snap to the new visual cue orientation or break free of visual cue input entirely (**Figure 4.12**). An analogous pattern to this was observed in the goal navigation behavior of young and aged rats immediately following cue rotation, in that old rats were more frequently observed stopping near either the current (i.e., allothetically aligned) or the non-current (i.e., idiothetically aligned) goal locations, whereas young rats more often stopped somewhere midway between the two. If the running behavior observed in the present study reflects the pattern of network realignment observed in the model, it would be expected that, following sudden visual cue rotation, the directional representations of young animals will tend to settle to an orientation representing some combination of allothetic and idiothetic cues, whereas those of aged animals will tend to fall under the control of one or the other conflicting spatial cues depending on what errors have accumulated in the aged animal's path integrator at the time visual cues are rotated.

While there are currently no electrophysiological studies investigating how aged head direction networks resolve conflicting spatial information, evidence suggest that place cell networks of aged rats tend to

be less strongly influenced by changes in environmental cues (Tanila et al., 1997b; Wilson et al., 2003) and display a bias for relying on idiothetic over allothetic cues when a mismatch is present (Rosenzweig et al., 2003). As previously discussed, Rosenzweig et al. (2003) exposed old and young rats to conflicting allothetic and idiothetic feedback by varying the rat's starting location on a linear track (**Figure 4.1**). Under these conditions, it was observed that CA1 place fields tended to realign to the allothetic (i.e., room) cues further along the track in the aged rats as compared to the young rats, suggesting a delayed realignment of the aged place cell networks. Importantly, the findings of Rosenzweig et al. (2003) were based on analysis of the spatial distribution of concurrently recorded place fields averaged across all track traversals (i.e., trials) and therefore did not assess realignment on trial-by-trial basis. Results from the present model showed that the time-course of HD realignment could vary greatly from one simulation to the next when idiothetic error was present and that this realignment could be either more or less rapid than what was observed when no idiothetic error was included. Similar to the place cell findings of Rosenzweig et al. (2003), however, when averaged across all simulations performed for a given idiothetic error condition, the average realignment of the HD network was slower for the larger idiothetic error conditions (**Figure 4.12A**). This overall slower average realignment was largely due to the loss of visual cue control that occurred during some simulations, which, as discussed, was dictated by a several factors that

varied from one simulation to the next (**Figure 4.12C**). It may, therefore, be that aged spatial networks will show delayed allothetic realignment when assessed based on across- cell and trial averages, but that this delay may reflect trial-by-trial differences in the relative control exerted by allothetic and idiothetic feedback. Furthermore, there is evidence that CA1 networks can show differential allothetic-idiothetic control even on a cell-by-cell basis. For instance, previous non-aging electrophysiological studies have reported that allothetic and idiothetic mismatch can result in CA1 place fields that fire in the context of both spatial reference frames (Zinyuk et al., 2000). Similarly, when local and distal visual cues are rotated in conflicting directions, simultaneously recorded CA1 place cells can align with one or the other cue types (Shapiro et al., 1997; Lee et al., 2004b; Yoganarasimha et al., 2006). Under these same conditions, CA3 place cells coherently rotate as an ensemble with local cues (Yoganarasimha et al., 2006), while anterior thalamic head direction cells collectively follow the distal visual cues only (Lee et al., 2004b). Assuming that thalamic head direction cells inform the directional tuning in MEC populations (Taube, 2007; Knierim and Hamilton, 2011), these studies suggest that CA1 may, under some conditions, be subject to incongruous spatial signals from CA3 and MEC during conditions of cue mismatch. If the partial behavioral rotation observed in young rats is the consequence of improved integration, the magnitude of behavioral rotation should be correlated with the average magnitude of realignment in the CA1 place

cell population. Additionally, if the premises of the model are correct, the time-course of realignment of aged CA1 network representations (i.e., the activity bump of the place cell population) should be slower when averaged across cue rotation trials, similar to the findings of Rosenzweig (2003), but more variable when assessed on a trial-by-trial basis. Finally, the model suggests that both the time-course and degree of place cell realignment will depend on the degree of error present in self-motion signals, such as may originate from MEC networks responsible for path integrator operations.

CHAPTER 5: ONGOING WORK AND FUTURE DIRECTIONS FOR INVESTIGATING AGE-RELATED CHANGES IN ENTORHINAL-HIPOCAMPAL SPATIAL UPDATING

Since O'Keefe and Dostrovsky's seminal discovery of place cells in the hippocampus almost half a century ago (O'Keefe and Dostrovsky, 1971), the cognitive map has been broadened to include a number of functionally distinct spatial networks, and a great deal of progress has been made characterizing the particular spatial and mnemonic computations they subserve. A majority of the single-unit investigations of hippocampal spatial networks have focused on the CA1 region. This is due in part to both practical and theoretical considerations related to the relative ease of performing large ensemble recordings in CA1 as well as the evident role CA1 plays as a source of hippocampal output to other brain regions (Witter and Amaral, 2004). The past two decades, however, have seen a notable increase in single-unit investigations of other hippocampal subregions, including dentate gyrus (DG) and CA3, which have provided experimental support for early theoretical models suggesting unique computational roles that are subregion specific (e.g., Marr, 1971; McNaughton and Morris, 1987; Treves and Rolls, 1994). This period has also seen a surge of interest in extrahippocampal neocortical areas implicated in spatial processing, particularly those of the entorhinal cortex. This renewed interest in entorhinal systems has, in part, been inspired by the discovery of grid cells in medial entorhinal cortex (MEC) and the subsequent discovery of a number of other types of spatially

modulated cells in the MEC (Hafting et al., 2005; Sargolini et al., 2006; Kropff et al., 2015). Additionally, while the investigations of lateral entorhinal cortex (LEC) are limited and suggest weak spatial tuning in these networks (Hargreaves, 2005), a subset of LEC cells have been found to display changes in positional firing based on the spatial arrangement of objects in the environment (Deshmukh and Knierim, 2011; Tsao et al., 2013). Collectively, the experimental and theoretical work that has been done over the past several decades has greatly expanded the conceptual framework within which spatial processing is understood, while also highlighting the importance of characterizing how different forms of spatial information are presented to, and processed by, various representational systems across the entorhinal-hippocampal system.

As previously discussed, it has been proposed that CA1 may act as a comparator of the spatial information relayed by CA3 and MEC (Hasselmo et al., 1995; Vinogradova, 2001; Hasselmo, 2005b), which is coordinated by various slow and fast oscillations that allow for segregation of neuronal information processing in the temporal domain (Skaggs et al., 1996; Hasselmo et al., 2002; Dragoi and Buzsáki, 2006; Diba and Buzsáki, 2008; Sirota et al., 2008; Mizuseki et al., 2009; Bieri et al., 2014). In this capacity, CA1 provides an ongoing readout of hippocampal processed information to other brain regions involved in hippocampus-dependent spatial and mnemonic operations. Under conditions of mismatched spatial feedback, CA1 populations often show a split in their

place field firing orientation (Shapiro et al., 1997; Zinyuk et al., 2000; Lee et al., 2004b), suggesting that that CA1 output can form a split representation that mimics the divergent spatial inputs it receives. Likely due in part to the autoassociative nature of the CA3 network, the population activity of CA3 place cells show coherent control by visual cues (Lee et al., 2004b, 2004a), which can occur at very short time scales (Jezek et al., 2011). When exposed to a change in environmental cues, such as occurs during Instantaneous Cue Rotation (ICR), pattern completion could allow for rapid updating and stabilization of the CA3 network representation immediately following cue rotation, while input from object selective cells of LEC may help anchor CA3 to the new visual cue orientation (Neunuebel et al., 2013; Knierim and Neunuebel, 2016). On the other hand, several lines of evidence suggest that MEC spatial networks may preferentially relay information related to self-motion-based path integration operations (Redish and Touretzky, 1997; Redish, 1999; McNaughton et al., 2006; Sargolini et al., 2006; Kropff et al., 2015; Jacob et al., 2017b). For instance, the real-time speed and heading signals carried by MEC spatially modulated cells are ideally suited for path integration computations (Sargolini et al., 2006; Kropff et al., 2015) and lesioning of MEC, but not hippocampus, results in impaired estimations of linear distance (Jacob et al., 2017a). Within the context of the ICR manipulation, CA3 place cell networks would be well suited to provide rapidly updated allothetic information about the current configuration of

environmental cues. MEC networks on the other hand, may continue to preferentially relay idiothetic estimates of orientation and position based on ongoing path integration operations. If this is the case, CA1 will have to reconcile the sudden change in allothetic cue orientation relayed by CA3 with the idiothetic feedback signaled by MEC networks. With respect to the ICR, there are at least two dimensions over which allothetic visual cue-driven changes in spatial activity can be assessed. First, realignment can be assessed with respect to the degree to which spatially tuned cells realign following cue rotation. Second, because cue-rotation induced changes in spatial firing can be time-locked to the precise instant cues are rotated, the time-course of allothetic realignment can be characterized with respect to event-related as well as theta phase-related single unit activity (Redish et al., 2000; Zugaro et al., 2003; Jezek et al., 2011).

When confronted with a mismatch in allothetic and idiothetic feedback, CA1 place cell representations of both young and aged rats show a delay in realigning to the allocentric spatial cues, however, the delay is greater for aged rats (Gothard et al., 1996; Redish et al., 2000; Rosenzweig et al., 2003). This suggests not only that the aged hippocampal networks are more biased toward relying on idiothetic feedback, such as may be relayed by MEC networks, but that these biases may reflect altered spatial processing in the temporal domain. It still remains to be determined, however, what the physiological basis of the observed age-related realignment delays may be. Due to limitations

related to task design and the analysis performed, it also remains unclear if the age-related realignment deficits reported by Rosenzweig et al. (2003) are temporal or spatial in nature (Redish et al., 2000). Investigating the time-course of updating in hippocampal and MEC networks simultaneously should enable a more complete characterization of the mechanisms that underlie reported age-related and age-independent realignment delays (Gothard et al., 1996; Redish et al., 2000; Rosenzweig et al., 2003) as well as the broader age-related differences in allothetic/idiothetic processing (Tanila et al., 1997a, 1997b; Rosenzweig et al., 2003; Wilson et al., 2003) and navigation (Barnes et al., 1980; Nicolle et al., 2003; Rosenzweig et al., 2003).

By identifying where in the processing hierarchy the realignment deficit first manifests itself, it may then be possible to determine if the realignment delays that accompany advanced age arise from alterations within entorhinal-hippocampal processing pathways or, alternatively, are simply a byproduct of sensory-perceptual deficits upstream of the hippocampus. As previously discussed, projections from entorhinal cortex provide the majority of all neocortical input to the hippocampus, however, it is important to note that the input/output distinction between these two structures does not completely capture the actual processing hierarchy. The deep layers of the MEC also receive return projections from CA1 (Kloosterman et al., 2003; van Haeften et al., 2003), and it has been shown that excitatory drive from CA1 is required to maintain the spatial

tuning of grid fields (Bonnievie et al., 2013). These observations suggest that information flow within the greater entorhinal-hippocampal network is not purely unidirectional. There is, however, evidence that information transfer between MEC and hippocampal sub-fields occurs in a sequential manner (Mizuseki et al., 2009), suggesting some degree of hierarchical processing in the temporal domain. By investigating spatial processing at both the input (i.e., MEC) and output (i.e., CA1) level, it should be possible to narrow down the source of the age-related spatial processing deficits discussed. If both the MEC and downstream hippocampus of aged rats are subject to degraded sensory-perceptual information, the spatially modulated cells of both MEC and CA1 would be expected to display equivalent realignment impairments following cue rotation. If, on the other hand, realignment impairments are a byproduct of altered intrahippocampal processing, aged animals should show greater disparity in CA1 and MEC realignment as compared to young rats. This outcome would indicate that the age-related changes in allothetic/idiothetic processing are not purely sensory-perceptual in nature, but rather may originate from dysfunctional processing within the entorhinal-hippocampal circuit.

The precise nature of such entorhinal-hippocampal dysfunction may, in turn, be tied to altered interregional communication through the direct and indirect pathways between MEC and CA1. While there is no evidence of age-related synaptic alterations in the direct entorhinal-CA1

synapses, various functional and anatomical changes have been identified in the indirect pathways between entorhinal cortex and CA1, including those of the entorhinal-DG perforant path and CA3-CA1 Shaffer collateral synapses (see **Chapter 2.2; Figure 2.1**). As a consequence, aged CA1 spatial networks may be more strongly biased by inputs carried by the direct MEC-CA1 pathway compared to those that arrive from CA3. Assuming MEC networks preferentially relay spatial information computed from idiothetic-based path integration, this could in turn account for the general pattern in existing aging CA1 investigations suggesting diminished control by environmental (i.e., allothetic) cues and, conversely, greater control by idiothetic cues (Tanila et al., 1997b; Rosenzweig et al., 2003; Wilson et al., 2003). Furthermore, results from the behavioral study and associated computational model presented in Chapter 4 further suggest that impaired integration of allothetic and idiothetic signals could account for the delayed realignment observed in CA1 networks. Within this framework, the delayed realignment reported by Rosenzweig (2003) may reflect more complex trial-by-trial variability in how aged CA1 networks resolve conflicting spatial feedback such that both the time-course and degree of realignment in CA1 will depend on the particular level of error present in MEC idiothetic-based signals. By simultaneously recording single unit activity in both MEC and CA1 from young and old rats performing the ICR task (**Figure 3.4**), it should be possible to characterize not only where in the processing hierarchy the age-related realignment

deficits manifest, but also how young and old rats differ with respect to the timing, magnitude and reliability with which MEC and CA1 spatial networks realign.

5.1. Pilot MEC and CA1 recordings assessing realignment following manual rotation of visual cues.

The primary purpose of the present study was to assess CA1 and MEC spatial networks while animals were exposed to an abrupt rotation of visual cues in order to validate several key intended functions of the Instantaneous Cue Rotation (ICR) apparatus prior to its final design and construction (see **Chapter 3**). The test apparatus incorporated several important features that would later be refined and implemented in the design of the ICR apparatus. These features include: 1) a method for altering the orienting visual cues in the environment that will be perceived by rats as a sudden and discrete change in visual cue orientation; 2) a means of performing this manipulation that does not require interfering with the rat's ongoing behavior; 3) the incorporation of symmetry breaking visual-cues that are pronounced and ubiquitous enough to be visibly accessible regardless of the rat's current position or heading within the environment.

As previously described, manual rotation of a single polarizing cue has been shown to induce a proportional rotation in the spatial firing orientation of CA1 place cells (e.g., O'Keefe & Conway, 1978) as well as

MEC grid, head direction and border cells (Hafting et al., 2005; Solstad et al., 2008). Under conditions in which rats were allowed to witness the cues being moved, however, it was found that these cues eventually ceased to control the alignment of CA1 place cells (Jeffery and O'Keefe, 1999). Furthermore, this loss of visual cue control persisted over multiple trials, suggesting rats learned to perceive these cues as unreliable landmarks. More typically, animals are removed from the environment when cues are changed and spatial tuning is re-assessed after animals are reintroduced to the environment (e.g., O'Keefe and Conway, 1978; Muller and Kubie, 1987). While this approach necessitates interrupting ongoing path integration operations, an alternative method is to leave the animal in place and simply turn the recording room lights off while the cues are moved. Using this approach, posterior parietal cortical head direction cells were shown to realigned with the rotated cues when room lights were turned back on for at least a subset of trials (Chen et al., 1994). A similar approach has also been used in which cues are left unchanged during the lights off period. In the absence of visual feedback, a number of different functional cell types have been found to undergo a radial drift in their firing field orientation (Mizumori and Williams, 1993; Knierim et al., 1998; Zugaro et al., 2003), which is thought to reflect accumulation of error in the ongoing path integration operation. Exploiting this naturally occurring drift, head direction cells recorded from the anterior thalamic nucleus (Knierim et al., 1998) and anterodorsal thalamic nucleus (Zugaro et al., 2003) were

sometimes found to rotate back into alignment with the unchanged visual cues after the room lights were turned back on. Importantly, using either of these lights on/off experimental manipulations exposes animals to an abrupt mismatch in allothetic and idiothetic feedback when illumination is restored. There are, however, some notable inconsistencies between these studies in the reported reliability with which this realignment occurs, which will be discussed within the context of the present findings (see **Chapter 5.1.3**).

In the present study, CA1 place cells and MEC grid, head direction and border cells were assessed while rats experienced an abrupt rotation of all orienting visual cues in the environment. Using an experimental manipulation similar to that of Chen and colleagues (1994), spatial tuning was assessed before and after visual cues were manually rotated while the room lights were off. This approach was chosen because it provides a simple means of assessing firing field realignment in response to a perceived abrupt rotation of visual cues, which is presumed to result in a perceptually similar experience to that of the ICR manipulation. Additionally, this approach does not require the animal to be removed from the apparatus and, therefore, does not introduce any interruption to ongoing path integration operations.

5.1.1. Material and methods

Behavioral apparatus

A greatly simplified proof of concept version of the Instantaneous

Cue Rotation (ICR) manipulation was performed using a square enclosure that was 50 cm on each side and 30 cm tall. The inner face of each wall of the enclosure was laminated with a distinct pattern of visual features that covered a large portion of the wall surface (**Figure 5.2A**). The enclosure had no attached floor but instead rested on a raised platform in the center of the recording room, which allowed for the walls of the enclosure to be rotated without interfering with the rats ongoing running behavior. All distal visual cues outside of the enclosure were occluded by a black curtain connected to an annular track suspended from the ceiling of the recording room. A commutator mounted above the enclosure was used to relay signals from the recording headstage to a Neuralynx Digital Lynx SX Cheetah Data Acquisition System (Neuralynx) and video tracking data was simultaneously acquired through a video camera that was also mounted above the enclosure.

Subjects and microdrive implantation surgeries

Surgery was conducted according to National Institutes of Health guidelines for rodents and approved Institutional Animal Care and Use Committee protocols. All surgeries were performed under 1.5 – 3.5 % isoflurane anesthesia (JD Medical Distribution Company, Phoenix, AZ). A total of three rats were implanted with a twelve tetrode hyperdrive positioned over the medial entorhinal cortex (MEC) of the right hemisphere (ML: 4.5 mm, 0.3 mm anterior to the transverse sinus). Only one of the MEC implanted rats was included as part of the present pilot

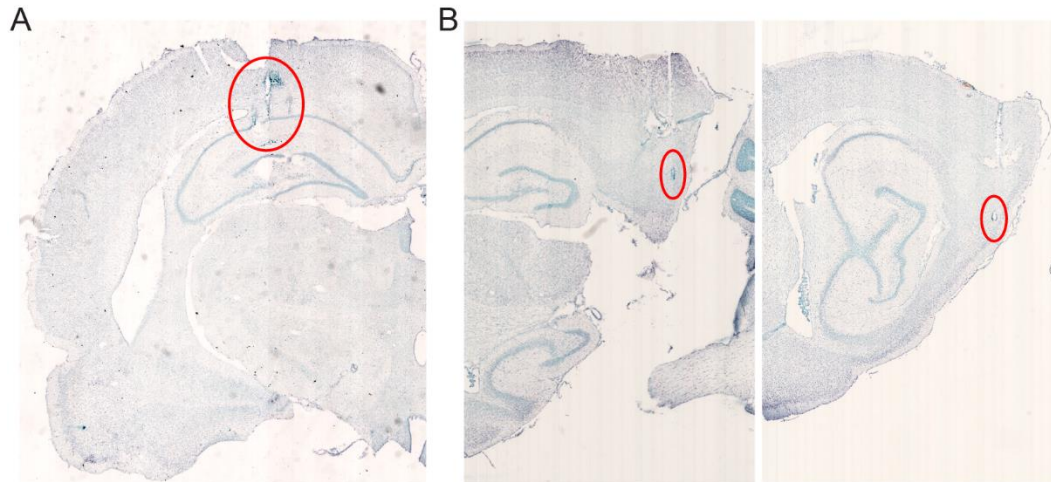


Figure 5.1: Histology from CA1 and MEC implanted rats.

(A) Coronal section from the CA1 implanted rat (~3.6 mm posterior to Bregma). Lesion sites are outlined in red. **(B)** Two sagittal sections from the MEC implanted rat (~3.9 mm and ~4.6 mm lateral to Bregma, respectively).

study because no spatially modulated cells were identified in the other two MEC implanted rats. The hyperdrive was modified for use with a custom designed 3D printable bundle collar that held the tetrodes at a 10° angle in the anterior direction (see **Chapter 5.2; Figure 5.5A**). A single additional rat was implanted with a standard hyperdrive over the intermediate region of hippocampus on the right hemisphere and tetrodes were lowered to the pyramidal cell layer of CA1 (ML: 2 mm, AP: -3.5 mm, DV: 2.5 mm from brain surface). Tetrodes were constructed of four polyimide-coated nichrome wires (13 μm in diameter) that were twisted together. For both the CA1 and MEC implanted rat, tetrode locations were confirmed post-mortem based on lesion sites using standard histologic procedures with Nissl and Prussian blue staining (**Figure 5.1**).

Data acquisition, preprocessing and analysis

Video data were obtained via LEDs mounted on the headstage.

Video tracking was recorded with a sampling frequency of 60 Hz, and converted to Cartesian coordinates online. Spike signals were amplified (500–5000 V/V), bandpass filtered (600 Hz to 6 kHz.), and digitized (32 kHz) using the Neuralynx Digital Lynx SX Cheetah Data Acquisition System (Neuralynx). Events that reached a custom-set threshold (typically 5–20 V) above the level of baseline noise were recorded for a 1-ms duration. Spikes were sorted offline by first using the automated spike-sorting algorithm KlustaKwik (K. D. Harris, University College, London, United Kingdom) to isolate units and separate them from noise. The resulting clusters were then refined manually using cluster cutting software (MClust 3.2; A. D. Redish, University of Minnesota, Minneapolis, MN, with customizations by P. Lipa, University of Arizona, Tucson, S.L. Cowen, University of Arizona, Tucson, AZ and D. Euston, University of Lethbridge, Canada). All functional classification of cell types was performed based on visual inspection of spatial or directional selectivity of the units using graphs of spike by position, firing rate by position, 2D spatial autocorrelograms and head direction tuning.

5.1.2. Results

For the CA1 implanted rat, recordings were conducted over the course of 2 weeks. Tetrodes were lowered over the first 7 days following microdrive implantation and were targeted to the CA1 pyramidal cell layer (~2 mm from brain surface; **Figure 5.1A**). Three rats were implanted with microdrives in MEC but only one rat was included in the present study. In

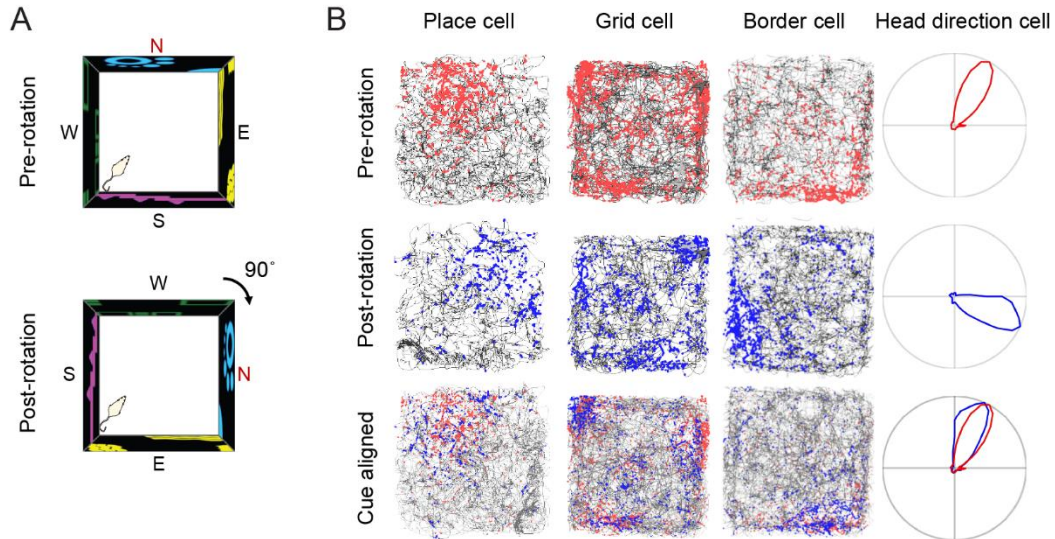


Figure 5.2: Example visual cue rotation-induced firing field realignment following rotation of the running enclosure.

(A) Schematic of the 50 x 50 cm enclosure used for the lights on/off rotation procedure showing a top-down view of the visual wall cues both before and after the enclosure is manually rotated 90° in the clockwise direction. **(B)** Recordings were collected from two separate rats with microdrives implanted in either CA1 or MEC. Example spike by positions graphs for hippocampal and MEC spatially-modulated cells recorded during period before (red; top row of panels) and after (blue; middle row of panels) visual cues were rotated. For comparison, bottom panels show overlaid graphs of the spike by position for both the pre- and post-rotation period with data aligned to the pre-rotation orientation denoted as 'cue-aligned'.

all three rats, some proportion of tetrodes were localized to MEC based on a sudden increase in theta power and theta modulated cell firing, however, spatially modulated cells were identified in only one of the rats. For this rat, recordings were collected over approximately 2 mm of the dorsal ventral range and over the course of 3 weeks (**Figure 5.1B**). Tetrodes were lowered over the first 10 days following implantation and power in the theta band of the local field potential was used to identify when tetrodes had reached MEC.

Prior to testing on the enclosure rotation component of the study, both the CA1 and MEC implanted rat were trained to randomly forage in

the enclosure for fruit flavored rice cereal that was distributed over the floor of the track by the experimenter. Training continued until rats were consistently traversing a sufficient enough area of the enclosure to enable two-dimensional positional firing to be assessed. Testing began once rats demonstrated consistent foraging behavior and at least some proportion of the recorded cells were displaying spatial selectivity. For each day of testing, single unit activity was recorded as rats foraged for randomly scattered food reward while the enclosure wall cues were in their default orientation. Rats continued to forage until the complete area of the enclosure had been traversed at least once. At this time, the room lights were extinguished and the experimenter manually rotated the enclosure 90° in the clockwise direction. The duration of time the lights were off was typically no more than 30 to 60 seconds. Lights were then turned back on and the animal was allowed to resume foraging until all positions in the enclosure had been traversed a second time (**Figure 5.2A**).

The CA1 implanted rat underwent a total of 5 days of enclosure rotation while the MEC implanted rat underwent a total of 6 days. For each day of testing the enclosure was rotated only once. Spatial firing was assessed during periods before and after enclosure rotation for CA1 place cells (n=6) as well as MEC grid cells (n=7), border cells (n=13) and head direction cells (n=9). The firing rate by position graphs from each of the recorded CA1 place cells were assessed to determine if their firing fields underwent some degree of realignment after the enclosure was rotated.

Following rotation of the enclosure, the majority of the CA1 place cells showed a clear rotation in their firing fields (**Figure 5.2B**). Because the place cell firing fields often covered a large area of the enclosure, however, it was not always readily apparent how much the fields rotated following enclosure rotation, particularly when the firing fields were close to the center of the enclosure. Nonetheless, the rotation observed in the place fields assessed tended to be comparable to the rotation of the enclosure cues (i.e., 90°), suggesting the CA1 place fields remained strongly anchored to the visual cues of the enclosure walls even after the enclosure was rotated.

For the MEC implanted rat, the spatial tuning of all MEC cell types assessed showed some evidence of realignment in response to enclosure rotation (**Figure 5.2B**). The majority of the grid cells showed a clear rotation with the enclosure based on both the firing rate by position graphs as well as the 2D spatial autocorrelograms. Due to the small size of the enclosure, however, for grid cells with larger grid field scales (i.e., wider spacing between respective firing fields) it was often difficult both to identify the grid structure and to establish if grid fields had rotated. Furthermore, because of the 6-fold symmetry of the grid fields, it was not always possible to discern if and to what degree fields rotated, particularly for trials in which the rats' spatial coverage was poor. With respect to the MEC border and head direction cells, firing rate by position graphs of most border cells also displayed a clear realignment with the cues as did the

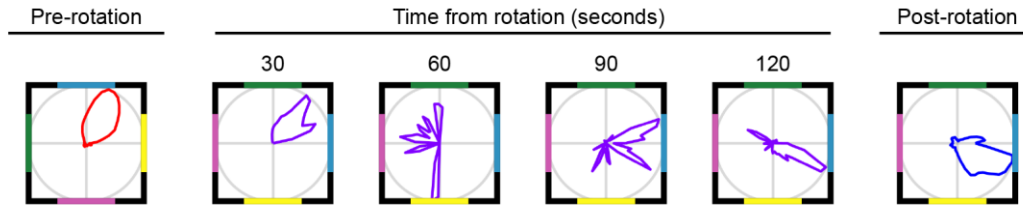


Figure 5.3: Example of delayed realignment of MEC head direction cells following cue rotation.

An example MEC head direction cell that was delayed in realigning with the visual cues of the enclosure after the enclosure was rotated 90° in the clockwise direction. Directional tuning curves are shown for the pre-rotation (red) and post-rotation (blue) periods as well as for the first 2 minutes following rotation, which is broken down into 30 second intervals (purple). The enclosure wall cues are also illustrated for each graph in order to indicate the orientation of the visual cues during each time period.

directional tuning curves of the head direction cells. Additionally, for each head direction cell identified, data collected during the first 2 minutes following cue rotation was divided into 30 second intervals. The tuning curves generated for each interval were then compared to assess the time-course over which each cell's directional tuning realigned in response to cue rotation. In a number of instances, head direction cells were found to initially maintain their old directional tuning immediately after the enclosure was rotated and the lights were turned back on. Subsequently, these cells typically rotated by approximately 90° over course of several tens of seconds to minutes (**Figure 5.3**). These results suggest that visual cue control was delayed in at least a subset of the MEC head direction cells.

5.1.3. Discussion

CA1 place cells and MEC grid, head direction and border cells, were assessed while rats experienced an abrupt rotation of all orienting visual cues during uninterrupted foraging. The preliminary findings from

the present study suggest that each of the CA1 and MEC cell types assessed were capable of updating their firing position/orientation even when cues were altered during ongoing running behavior. Due to the fact that only one rat was assessed for each of the implant sites and only a small sample of spatially modulated cells was identified within each functional class, no attempt was made to quantify these observations. Nonetheless the influence of visual cue rotation was evident in many cases based on visual inspection alone (**Figure 5.2B**). With respect to the place cell recordings from the CA1 implanted rat, the reliable realignment observed in place field firing following enclosure rotation is consistent with a number of existing studies reporting robust realignment of CA1 place fields in response to visual cue rotation (O'Keefe and Conway, 1980; Muller and Kubie, 1987; O'Keefe and Speakman, 1987; Bostock et al., 1991; Knierim et al., 1998; Knierim and Rao, 2003; Yoganarasimha and Knierim, 2004; Yoganarasimha et al., 2006). Visual cue rotation has, however, also been found to occasionally result in CA1 place cell remapping (Bostock et al., 1991; Knierim et al., 1998; Yoganarasimha and Knierim, 2004; Yoganarasimha et al., 2006). While no attempt was made to quantitatively check for remapping in the present study, visual inspection did not reveal any clear instances of remapping in the place cells identified. Given the limited sample of place cells assessed, the absence of observed remapping events does not necessarily indicate that such events did not occur. Rather, it may be that remapping events

occurred too infrequently to be detected with the limited sample size. Consistent with this possibility, occasional but infrequent remapping has been reported for other studies when visual cues were rotated by a similar degree (i.e., $\leq 90^\circ$) as the present study (Muller and Kubie, 1987; Knierim and Rao, 2003). The environmental geometry of the square enclosure may also have supported place field stability and realignment as geometric cues have been shown to help establish and maintain place cell spatial tuning (O'Keefe and Burgess, 1996; Lever et al., 2002).

Each of the MEC cell types assessed in the present study also showed fairly consistent realignment with the rotated enclosure, suggesting overall robust visual cue control of MEC spatial networks. These results are consistent with existing studies reporting that visual cue rotation induces a proportional rotation in MEC grid, head direction and border cells (Hafting et al., 2005; Solstad et al., 2008). One important distinction, however, is that these studies assessed the influence of visual cues by rotating a single polarizing cue between successive exposures to an environment. Because the approach used in the present study did not require animals to be removed from the environment during cue rotation, self-motion feedback was preserved. Consequently, spatial networks had to resolve the conflicting information carried by the rotated allothetic cues and the uninterrupted idiothetic feedback. To the best of the authors knowledge, there are currently no other studies which have investigated MEC networks under similar conditions. As discussed previously,

however, several studies have investigated other head direction cell networks using a similar 'lights on/off' manipulation in order to create a sudden mismatch in allothetic-idiothetic feedback. Although the approach used by Chen et al. (1994) was very similar to that used in the present study, they found that posterior parietal cortex head direction cells typically failed to realign with the rotated cues when the room lights were turned back on. A similarly inconsistent pattern of visual cue realignment has also been reported for studies that assessed thalamic head direction cells based on the directional drift these networks undergo in the absence of visual input (Mizumori and Williams, 1993; Knierim et al., 1998; Zugaro et al., 2003). Under these conditions, head direction cells often either maintained their current 'drifted' directional tuning when lights were turned back on or changed in unpredictable ways (Knierim et al., 1998; Zugaro et al., 2003). For instance, Knierim et al. (1998) observed that greater drift in directional tuning, presumably reflecting greater accumulated idiothetic error, typically resulted in less reliable visual cue realignment when lights were turned back on. In light of these observations, Knierim et al. (1998) concluded that the extent of control allothetic cues exert over directional tuning may depend on the degree of mismatch between allothetic and idiothetic feedback. In contrast, all MEC cell types assessed in the present study, including head direction cells, showed fairly reliable visual cue control in the presence of allothetic-idiothetic mismatch.

Although the MEC spatial networks showed consistent realignment

following enclosure rotation in the present study, there was evidence that the control visual cues exerted over the MEC spatial networks was not immediate. It was observed that, in some instances, head direction cells required some minimal period of time to realign their directional firing with the rotated visual cues, suggesting that visual cue control of these cells was delayed (**Figure 5.3**). In addition to the 'directional drift' experiment already discussed, Knierim et al. (1998) also assessed the time-course of anterior thalamic head direction cell realignment after slowly rotating the behavioral enclosure, including the enclosure walls and floor, while recording room lights were off. It was found that when the speed of rotation was sufficiently fast and abrupt, the head direction cells typically tracked the enclosure movement even when lights were off; presumably based on vestibular angular velocity signals. When the speed of rotation fell below some presumed vestibular threshold, however, the head direction network was unable to track the movement. Under such conditions, Knierim et al. (1998) found that, after turning the lights back on and revealing the new orientation of the enclosure wall cues, head direction cells initially maintained their old (i.e., 'lights off') directional tuning, but then realigned with the wall cues over several tens of seconds to minutes. In light of the delayed visual cue control observed in these head direction networks, Knierim et al. (1998) concluded that idiothetic cues are likely the primary source of information relied upon by these cells for updating their directional tuning, whereas static environmental cues

may provide a secondary corrective influence. Similarly, the delayed realignment observed in MEC head direction cells in the present study could be explained by a preferential reliance on idiothetic cues for real-time updating (i.e., path integration), while allothetic cues are relied on to gradually correct for any mismatch in allothetic-idiothetic feedback (Mittelstaedt and Mittelstaedt, 1980; Gallistel, 1990; Benhamou, 1997; Redish, 1999).

It was not possible to assess the time-course of realignment for place, grid and border cells in the same manner as was done for the head direction cells; because characterizing their positional tuning necessitates that animals sample a sufficient area of the environment, which limits the temporal resolution of the subsequent tuning analysis. Interestingly, however, some of the MEC cells that displayed conjunctive border and head direction tuning also showed delayed realignment in their directional tuning, suggesting these delays may be a more general feature of MEC spatial networks. Although the various cell types of MEC code for different forms of spatial information, they are organized into discrete modules such that cells of the same module show a coherent change in directional alignment from one environment to the next (Sargolini et al., 2006; Barry et al., 2007; Stensola et al., 2012; Krupic et al., 2015). Consequently, while the different functional classes code for different information, it stands to reason that they will share a coherent collective directional representation. It therefore follows that the delayed directional realignment

observed in the present study may be a more general property of MEC networks. Furthermore, these delays could reflect prolonged idiothetic control over the spatial turning of MEC networks, consistent with the idea that MEC may preferentially support path integration operations (Redish and Touretzky, 1997; Redish, 1999; McNaughton et al., 2006).

Taken together, the findings from the present pilot study allow for some general predictions with respect to how MEC and CA1 networks may behave in the context of the Instantaneous Cue Rotation (ICR). While both MEC and CA1 spatial modulated cells can be expected to eventually undergo some degree of realignment with the rotated visual cues, immediately following cue rotation, the various constituent cell types of MEC should persist in displaying a profile of spatial activity consistent with current path integration-based estimates of position and direction. Although the present study was largely restricted to within cell-type comparisons that were based on qualitative analysis of a limited number of cells collected from two separate CA1 and MEC implanted rats, an additional purpose of this study was to develop procedures for single-region CA1 and MEC microdrive implantation and recording prior to the design and development of a dual-region microdrive. The following section details subsequent work that has been conducted developing technologies for simultaneous high-density single unit recordings from both MEC and CA1.

5.2. Developing technologies for simultaneous hippocampal and MEC recording

The initial discovery of MEC grid cells generated a great deal of excitement in the neuroscience community due, in part, to their potential role in the network level mechanisms that might support hippocampal place field generation and maintenance. Based on anatomical connectivity, neurophysiological findings and theoretical modeling, it has been suggested that the geometrically arranged firing fields of medial entorhinal cortex (MEC) grid cells may provide a more general, environment-invariant, metric of space that informs the location specific firing fields of hippocampal place cells (McNaughton et al., 2006; Solstad et al., 2006; Moser and Moser, 2008; Savelli and Knierim, 2010). More recently, the discovery of MEC speed cells (Kropff et al., 2015) filled several critical gaps in prominent models of place field generation and path integration (e.g., Burgess et al., 2007; McNaughton et al., 2006). Furthermore, it has been found that the hippocampus receives projections not just from grid cells, but also border cells and head direction cells (Zhang et al., 2013), opening up the possibility that grid cells are not the only contributor to place cell firing. To date, however, investigations comparing simultaneously recorded single unit activity in both MEC and hippocampus are limited (Mizuseki et al., 2009; O'Neill et al., 2010; Igarashi et al., 2014). Furthermore, to the best of the author's knowledge, no studies yet exist assessing the impact of conflicting allothetic and

idiothetic feedback on concurrently recorded MEC and hippocampal spatially-modulated cell populations. In order to generate a more complete understanding of the differential role allothetic and idiothetic information plays in entorhinal-hippocampal spatial processing and how this information is processed at differing stages in the entorhinal-hippocampal network, it is important that the diverse cell types that constitute the greater cognitive map be assessed in the same animal and behavioral/environmental conditions concurrently. The following section outlines the development and testing of a number of microdrive technologies for the purpose of performing dual-region single unit recordings. While the prospect of investigating and comparing simultaneously recorded spatially-modulated cells from both MEC and hippocampus has exciting potential within the context of existing theory, there were a number of practical obstacles that had to be overcome on the path to a viable solution.

One difficulty inherent in performing cross-regional entorhinal-hippocampal comparisons at the single unit level is that a sufficient number of functionally classifiable units must be detected and recorded concurrently from both regions to make quantitative comparisons possible. While tetrode recordings (i.e., four-channel electrodes; See **Chapter 5.1.1**) can provide a high yield of active CA1 place cells during a given recording session (Wilson and McNaughton, 1993), the typical reported yield of grid, border and head direction cells from MEC is substantially less

(Sargolini et al., 2006). In order to improve overall cell yield, it is necessary to be able to consistently localize recording electrodes to the region or regions of interest. The anatomical positioning of the septal portion of the CA1 subfield makes this region notoriously amenable to electrophysiological investigation. In contrast, the proximity of MEC to the sinus, as well as the oblique and non-uniform angle of its lamina, make the MEC a very challenging region to reliably target electrodes to, even in single-region recording applications (**Figure 5.4A**). In addition, because the largest proportion of spatially-modulated MEC cells is found in layers II and III (Sargolini et al., 2006), tetrodes should ideally be targeted to superficial layers of MEC if cell yield is a concern. The laboratory this research was conducted in has almost three decades of experience performing high-density single-unit recordings utilizing chronically implanted microdrives (Wilson and McNaughton, 1993). These drives carry multiple tetrodes that can be independently adjusted to a specified depth. The tetrodes are housed in a one or more guide cannula bundles that provide support as tetrodes are lowered into the brain. In order to improve the accuracy and precision with which tetrodes could be targeted to the superficial layers of MEC (i.e., layers II and III) for the present study, an instrument was developed to construct cannula bundles with more precise spatial geometry (**Figure 5.4B and 5.4C**). With this tool, bundles can be configured such that the distribution of tetrodes is optimized to target the specific region of interest. A custom 3D printable bundle collar

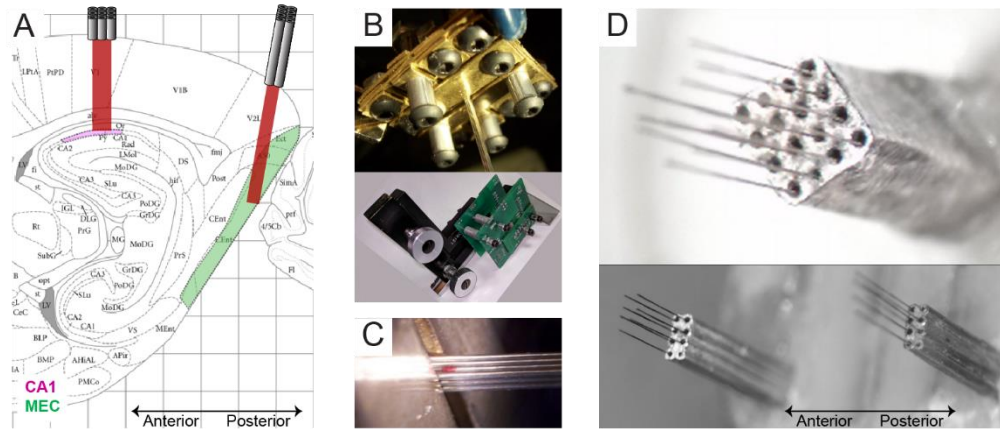


Figure 5.4: Optimizing tetrode configurations for the target regions of interest.

(A) Sagittal rat atlas image highlighting the of pyramidal cell layer of proximal CA1 as well as superficial layers of MEC (adapted from Paxinos & Watson, 2013). Example cannula bundle configurations are shown as are and the expected trajectory of tetrodes (red bars). Note that the dorsal surface of the CA1 implant site is notably more shallow than CA1. **(B)** Pictures showing the first (top) and second (middle) iteration of the square bundle builder. The second version is constructed using salvaged stereotax manual actuators, which greatly simplifies the loading and removal of cannula. **(C)** Close up view of a 4x4 cannula bundle sandwiched in the bundle builder. **(D)** Close up of a fully assembled 4x4 bundle used in a single bundle drive (left) and two 2x4 bundles used in a dual-bundle drive (right) both with tetrodes extended.

was also developed in-house for use with the existing microdrive (i.e., the *hyperdrive*) that could hold a single 4x4 bundle of tetrodes at a 10° angle in the anterior direction (**Figure 5.5A**). Together, these tools enable tetrodes to travel at an angle parallel with the MEC lamina, increasing the distance over which MEC layer II/III cells could be recorded. This modified drive design was used to successfully record a number of MEC grid, head direction and border cells in the cue rotation pilot study rat (see **Chapter 5.1**).

The next step was to develop a means of recording from both MEC and CA1 simultaneously in the same animal. To achieve this, several drive designs were pursued to allow for tetrodes to be split and targeted to these two regions within a single dual-bundle drive. One of the most

difficult obstacles identified in the course of developing and testing different version of the dual-bundle drive was the inter-regional and intra-animal differences in anatomical position between MEC and CA1. For instance, the depths of the dorsal cortical surface typically differs between MEC and CA1 by 1 to 1.5 mm (**Figure 5.4A**). At the time of surgery, bundle tips must be placed as close to the cortical surface as possible in order to minimize any potential for the craniotomy sealant to block the bundle tip. As a consequence, the difference in the dorsal-ventral spacing of the two implant sites must be precisely accounted for during drive construction. In addition, while hippocampal implant coordinates are typically specified with respect to bregma, which is the standard origin used in anatomical atlases (Paxinos and Watson, 2013), the predominant anterior-posterior anatomical reference used for MEC implants is the transverse sinus (Hafting et al., 2005). The transverse sinus actually represents the posterior limit of where one can feasibly implant. Over the course of several dual-bundle implant surgeries, it was observed that the differing origin coordinates introduced notable inter-animal variability in terms of the optimal anterior-posterior bundle spacing. This is assumed to be due to greater variability in the sinus position, which is presumably a much less reliable anatomical landmark than the bone sutures (e.g., bregma and lambda). Similar, although less pronounced, inter-animal variability was also observed with respect to dorsal-ventral cortical surface depths. Collectively, this variability made it difficult to establish a standard

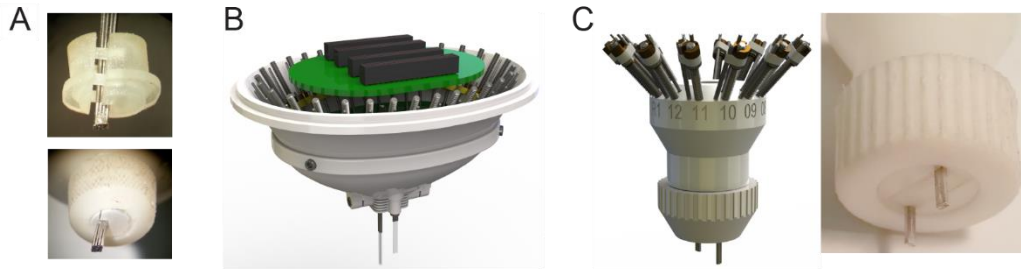


Figure 5.5: Initial designs for a dual-bundle drive.

(A) Pictures showing the first square bundle collar used to collect single region recordings from MEC during the lights off rotation pilot study (see **Chapter 5.1**). **(B)** Rendering of the 28-channel dual bundle drive. **(C)** Rendering of the modified primate hyperdrive (left) and a picture showing a close up view of the modified dual-bundle collar and collet nut made of 3D printed ABS plastic (right).

bundle configuration that would allow for accurate and repeatable targeting of both regions across animals.

A series of solutions were pursued and tested to enable more precise control over the MEC and CA1 bundle spacing in order to minimize the issues related to intra-animal anatomical variability. The initial approach was to develop a wholly new drive design that was specifically tailored to the needs of the experiment (**Figure 5.5B**). The drive included a total of 28 independently adjustable tetrode shuttles in order to increase potential cell yield. The design also incorporated a 3D printable bundle collar to hold the two bundles in the desired configuration. Despite the drive requiring a larger overall footprint to accommodate the increased channel capacity, manufacturing the drive using 3D printing enabled a lighter design than what would have been possible using standard high-density plastics and traditional machining fabrication. A pilot implant of the drive, however, revealed that, while the rat appeared to tolerate the weight of the drive (~32 grams), the collective size and weight impaired normal running too much for it to be considered a feasible option

to pursue.

The next approach considered was to modify the existing 14 shuttle hyperdrive to accommodate two bundles, however, in order to accommodate required anterior-posterior spacing between the two bundles (~5 mm), it was necessary to use a larger version of the hyperdrive that was originally intended for primate recording (**Figure 5.5C**). While this option did not provide an optimal channel capacity for dual-region recording, the weight was less than that of the 28 shuttle drive (~24 grams). Furthermore, the only modification to the base design that was required was a 3D printable bundle collar and collet nut to hold the bundles in the desired configuration. Based on a single pilot implant, the combined weight of the drive and tethers used to transmit the signal to the acquisition system proved too much of an impediment to the pilot rats' normal running behavior. In spite of these caveats, there has been some limited success using this drive, with the modifications described, for dual ACC and CA1 implants by others in the lab. The current version of the dual-bundle drive is the result of a significant period of iterative design and testing. The drive body and tetrode shuttles are adapted from the commercially available Neuralynx Halo-18 microdrive. The remaining components have all been redesigned or developed in-house for the purposes of the present application (**Figure 5.6**). The drive supports 18 independently movable shuttles and is primarily composed of 3D printed components allowing for a total weight of approximately 24 grams. As

described above, the optimal anterior-posterior distance between CA1 and MEC implant sites varies noticeably between rats, as does the dorsal cortical surface depth to which the bundle tips are lowered during surgery. To accommodate the variability in both the anterior-posterior (y-axis) and dorsal-ventral (z-axis) spacing, the base design of the drive was altered to allow the CA1 and MEC bundles to be repositioned as needed along the z-axis and y-axis, respectively, at the time of surgery. (**Figure 5.6D**). This is achieved by securing the bundles in two separate 3D printed collars that can be moved within the bundle housing using adjustment screws.

In parallel with the development and testing of the modified Neuralynx Halo-18 microdrive, testing was also performed to assess the feasibility of a wireless telemetric headstage (i.e., NeuraLynx Cube2-64). Extracellular recording systems historically have relied on high channel capacity tethers to relay voltage potentials from a miniature preamplifier (i.e., headstage), which is attached to an interface board on the drive during recording sessions. Tethered recording of freely behaving animals typically requires a commutator and some form of boom arm to partially support the additional weight of the cables and help prevent the tethers from interfering with the animal's movements. A number of tests were performed to ensure that the quality of recordings and overall performance of the system was adequate for the needs of the experiment. The single unit waveform features and frequency distribution of LFPs collected simultaneously from the same recording channels on both the wireless

and tethered systems were found to be virtually identical. While the use of a wireless headstage enables more freedom of movement than what is possible with traditional tethered recording, it does require rats to support the combined weight of the Cube2 system (~25 grams) and drive (~24 grams). In order to acclimate rats to the weight of the Cube2 headstage, a detachable housing was developed in-house to which 3.2 gram washers could be added incrementally over consecutive days post-surgery (**Figure 5.6A and 5.6C**). While testing the Cube2's operation as rats engaged in the ICR task, it was found that the headstage tended to get knocked against various features on the track and would frequently detach from the drive. This issue was resolved by designing a 3D printable cover that secures the Cube2 headstage to the drive body at the time of recording while still allowing the cover and Cube2 headstage to be easily attached and detached as needed. The cover also incorporates two colored LEDs and utilizes diffuser lenses to improve position tracking. The results of a recent pilot implant of the current drive design indicate that the combined dual-bundle drive and Cube2 headstage are within a tolerable weight range for rats to engage in the ICR task. Single unit activity from both MEC and CA1 bundles has been recorded using the Cube2 headstage along with two-position video tracking while the rat actively engaged in the Instantaneous Cue Rotation (ICR) task training (see **Chapter 3** for details about the task). While no spatially-modulated cells have been identified at this time, single unit waveforms have been detected from tetrodes in both

bundles and recorded using the wireless headstage while the rat actively engaged in the Instantaneous Cue Rotation (ICR) task training (see **Chapter 3** for details about the task). More recently, single unit activity has also been successfully recorded from a second animal, participating in a separate study, which was also implanted with the CA1-MEC dual bundle drive. Although additional piloting is still required before any definitive conclusions can be drawn, these initial successes strongly suggest that the current drive design is a viable solution for performing dual-region recording.

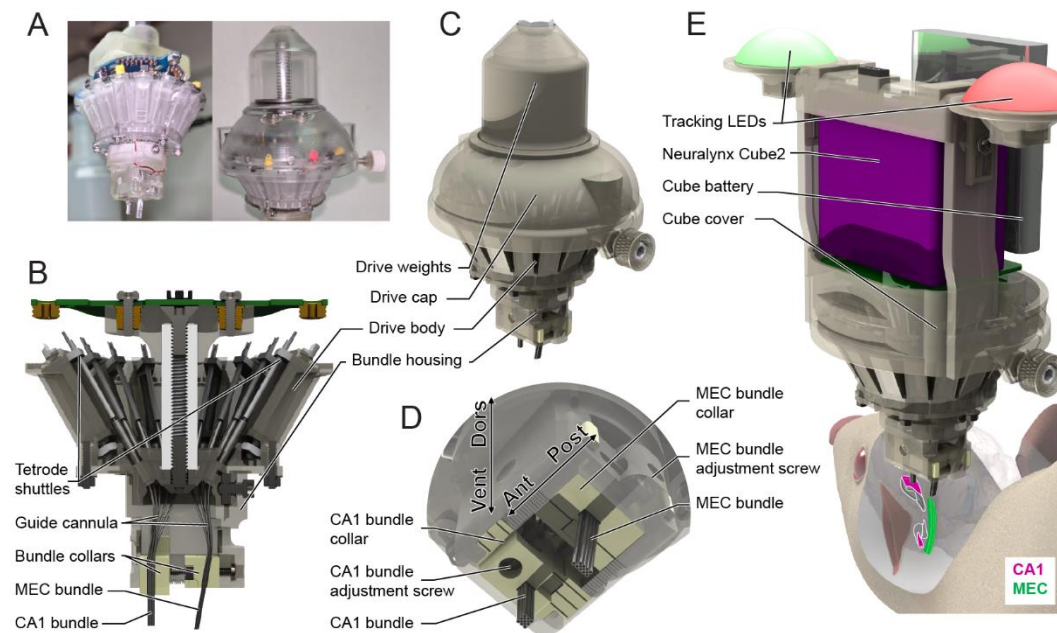


Figure 5.6: Modified Neuralynx Halo-18 microdrive and Cube2 wireless recording system.

(A) Picture of the modified Neuralynx Halo-18 Microdrive fully assembled. **(B)** Schematic of the drive showing an internal view of the tetraode shuttles, drive body, bundle housing and bundle collars that hold the CA1 and MEC bundles. **(C)** Rendering of the outside of the drive including the drive cap and weight attachment. **(D)** Rendering showing an enlarged view of the exit tip. Adjustment screws allow the MEC bundle and CA1 bundle to be moved along the anterior-posterior axis and dorsal-ventral axis, respectively. Note that, with the exception of the drive body and tetraode shuttles, all the components highlighted were developed or substantially redesigned for the current study. **(E)** Rendering of the complete recording system including the Neuralynx Cube2 wireless headstage and custom designed headstage cover. Rat and target brain regions are also shown to scale.

CHAPTER 6: SUMMARY AND CONCLUSIONS

6.1. Summary of the thesis

This thesis was conceived to address several important gaps in the current understanding of how environmental (allothetic) and self-motion (idiothetic) sensory-perceptual information inform ongoing spatial processing, with a particular focus on how the use of these differing forms of information changes with age. The questions that motivated this work can be broadly summarized as follows: 1) how do allothetic and idiothetic cues differentially influence navigation-related processing; 2) what is the time-course of cue-based neural and behavioral updating with respect to very short time-scales of tens of milliseconds as well as longer, behaviorally observable time intervals of seconds to minutes; 3) how is spatial information processed hierarchically in the greater entorhinal-hippocampal network; 4) to what extent if any are the above factors impacted during normal aging and what are the implications within the context of known age-related changes in idiothetic-allothetic processing and navigation. The following is a summary of the salient results as well as the primary contributions of the thesis both in terms of methodology and theory:

1. Much of the existing research investigating visual-cue control of navigation behavior and spatial representation systems is based on experimental approaches that interrupt ongoing navigation behavior

during cue manipulation (e.g., McGauran et al., 2004; Muller & Kubie, 1987; O'Keefe & Speakman, 1987; Suzuki et al., 1980) or, as is the case with more recent virtual-reality approaches, diminish the presence of vestibular idiothetic feedback (e.g., Chen et al., 2013; Seelig & Jayaraman, 2015). As a consequence, it is difficult to compare the relative influence of allothetic and idiothetic feedback using such approaches. With these considerations in mind, the ICR arena was designed to enable manipulation of real-world environmental cues in a rapid and precisely timed manner such that allothetic and idiothetic based spatial signals can be put in direct and immediate conflict while preserving all other navigation-related sensory input (**Chapter 3**).

2. The ICR also incorporates a goal navigation task that assesses the influence that competing allothetic and idiothetic feedback have on an animals' navigation strategy (**Chapter 3.2**). The ICR task assesses allothetic navigation performance by requiring animals to stop at a visual cue-aligned goal location in order to receive reward. Varying the magnitude of reward based on the animal's distance from the goal location allows for a continuous (i.e., non-discrete) metric of navigation accuracy. In support of the utility of this metric, 'goal error' proved informative for identifying age and rotation direction-dependent behavioral changes that were not revealed using the other behavioral measures assessed (**Chapter 3.4.3; Chapter 4.4.2**). The reward

structure also ensures that animals will receive some amount of food reward even if navigation accuracy is poor, which can both facilitate goal-related learning as well as decrease the likelihood of animals becoming non-compliant due to lack of reinforcement to run.

3. The mobile feeder is a critical component of the ICR system because it enables place-based reinforcement using food reward without introducing localizable olfactory cues (**Chapter 3.2.4**). The mobile feeder smoothly tracks the position and velocity of rats as they perform the ICR task and delivers food reward when rats successfully stop at the designated goal location, while also continually removing olfactory and visual cues created by the rat. This design ensures that confounding spatial cues from food reward and other unintended olfactory contaminants are minimized to the greatest extent possible. While medial forebrain bundle stimulation is an alternative option for reinforcing place-based learning without introducing unintended spatial cues (e.g., Redish et al., 2000; Rosenzweig et al., 2003), the fibers of this pathway target wide-spread cerebral and brainstem structures that may also be activated when current is injected into this pathway (Nieuwenhuys et al., 1982). The present approach allows for 'natural' food-based reward that does not require any surgical implantation or artificial stimulation of reinforcement pathways. Having tested and validated the mobile feeder system, the same design principles can be utilized for future studies requiring place-based reinforcement.

4. Behavioral results from the mobile feeder version of the ICR task showed that rats robustly altered their goal-related and overall running behavior in response to cue rotation, suggesting that allothetic cues continued to anchor running behavior even when these cues were put in sudden conflict with ongoing self-motion (i.e., idiothetic) feedback (**Chapter 3**). Importantly, however, the control allothetic cues exerted over the behavior of these animals was not absolute. Rather, running behavior underwent a gradual realignment over the first several laps following visual cue rotation, suggesting that allothetic cues gained progressively more control relative to the mismatched idiothetic cues. These findings provide behavioral evidence in support of models of path integration in which allothetic cues are utilized to continuously correct for accumulated error in idiothetic-based estimates of position (e.g., Etienne et al., 1996; Loomis et al., 1993; McNaughton et al., 1996; Mittelstaedt and Mittelstaedt, 1980; Redish, 1999; Samsonovich and McNaughton, 1997).

5. Consistent with existing rodent and human aging studies reporting age-related impairments for tasks that require an allocentric navigation strategy (Barnes et al., 1980; Rosenzweig et al., 2003; Moffat et al., 2007; Iaria et al., 2009; Head and Isom, 2010), the navigation behavior of old rats was less reliably anchored by the allothetic cues during the ICR task (**Chapter 4**). The overall pattern for young rats, in contrast, suggested a reliable although incomplete control by allothetic cues,

which may reflect a greater tendency for young animals to resolve conflicting allothetic-idiothetic feedback by integrating information from both. Consistent with this idea, the attractor-based head direction network model showed more variable realignment to the rotated visual cue input when accumulating self-motion errors were also present. Considered in the context of known age-related deficits in self-motion perception and path integration (Warren Jr et al., 1989; Allen et al., 2004; Mahmood et al., 2009; Adamo et al., 2012; Harris and Wolbers, 2012), the findings from the computational model suggest a plausible mechanism that could contribute impaired integration of conflicting spatial signals in aged spatial networks.

6. While spatially-modulated cells have yet to be investigated in the ICR, recordings were collected from one CA1 and one MEC implanted rat in a simplified proof of concept experiment that mimicked conditions in the ICR arena (**Chapter 5.1**). Using an experimental paradigm similar to that of Chen et al. (1994), visual cues were rotated while room lights were off, which resulted in an abrupt perceived rotation of cues after the lights were turned back on. When the firing orientation of CA1 and MEC spatial networks was assessed before and after cue rotation, it was found that the majority of all place, grid, head direction and border cells displayed a pronounced realignment with the wall cues in the period following cue rotation. The preliminary findings of this study suggest that visual cue rotation can exert strong control over the

spatial tuning of CA1 and MEC networks, even when self-motion feedback is preserved and the rotation is perceived as sudden. Additionally, the time-course of realignment observed in the directional tuning of MEC populations indicated that visual cue control was often delayed, which parallels the delays observed in thalamic head direction cell populations under conditions of allothetic-idiothetic mismatch (Knierim et al., 1998). This pattern suggests that MEC networks may continue to preferentially rely on idiothetic signals immediately after exposure to mismatch spatial signals, which lends further experimental support for theoretical and computational models implicating MEC networks in path integration operations (e.g., Redish and Touretzky, 1997; Redish, 1999; McNaughton et al., 2006; Moser et al., 2008; Giocomo et al., 2011).

7. Several technologies were developed to support reliable dual-region CA1 and MEC single unit recordings (**Chapter 5.2**). While there are a number of theories suggesting some form of interdependence of MEC and hippocampal spatial processing, particularly with respect their constituent classes of functionally specialized cells (e.g., Guanella et al., 2007; McNaughton et al., 2006; Moser & Moser, 2008; Savelli & Knierim, 2010; Solstad et al., 2006), there is limited research directly assessing simultaneously recorded spatially modulated unit activity from both MEC and hippocampus. One of the aims of the thesis was to develop a dual-region microdrive in order to directly investigate the

inter-regional coordination of MEC and CA1 neural activity in the context of the ICR task. Technologies were tested and developed to optimize the accuracy and precision with which tetrodes can be targeted to the specific regions and cell layers of interest as well as to accommodate intra-animal variability in anatomical spacing between CA1 and MEC by incorporating a means of adjusting bundle spacing at the time of surgery. In addition, several custom ancillary components were developed to support reliable wireless recording and position tracking during active engagement in the ICR task. At present, two rats have been successfully implanted with the current version of the CA1-MEC dual-bundle, one of which is part of a separate study. For each of these pilot implants, single units have been successfully recorded from both bundle sites during active behavior. Although testing is still underway, the results of these tests provide encouraging support for the viability of the current dual-region recording system.

6.2. Conclusions

When I first began this dissertation, I was operating from the belief that the ideal approach for any investigation is to identify the simplest and most parsimonious solutions available to comprehensively address the questions that motivate the work. Spatial navigation, however, is a particularly complex behavior as it requires integrating different types of spatial information, selecting and switching between optimal navigation

strategies and, in many circumstances, coordinating multiple ongoing behavioral sub-tasks or processes. Given this complexity, formulating an experimental approach that could more fully characterize the precise nature of the age-related 'egocentric-over-allothetic' pattern of behavior, which persistently shows up in the aging literature, required accounting for various factors; not least of which was how young and aged animals may differentially utilize body-based and environmental spatial cues. The development of the ICR system was, therefore, motivated by the fact that no existing experimental paradigms provided a means to independently manipulate allothetic and idiothetic cues such that their relative and respective influence on ongoing navigation can be assessed. The development of the ICR arena included a fairly exhaustive accounting of, and correction for, any potential confounding auditory, visual and olfactory cues which might be present. While there were a number of hurdles to overcome over this period, the formidableness of the reward odor contamination issue proved much more of an obstacle than I had anticipated. While the final solution required implementing and testing a number of increasingly elaborate solutions, and ultimately a complete reconceptualization of the reward deliver system, the end product of this work and the cumulative efforts that went into the ICR system, was a thoroughly considered experimental apparatus that, unbelievably, represented the simplest feasible option to perform the experiment I originally set out to do. Findings from the behavioral studies validate the

ICR system as a viable tool for assessing both the degree and time-course with which navigation behavior is recalibrated in response to dynamically changing allothetic feedback. The results from these studies showed that running behavior was strongly anchored by the allothetic cues and showed a pronounced, although gradual, realignment in response to visual cue rotation, suggesting running behavior underwent a progressive correction as conflicting egocentric and allocentric reference frames were brought into agreement. To the best of my knowledge, this is the first evidence of a behavioral change that parallels the progressive realignment of place field firing observed under similar conflicting spatial cue conditions (Gothard et al., 1996; Redish et al., 2000; Rosenzweig et al., 2003).

Age comparisons of ICR task behavior reported in Chapter 4 also yielded interesting, and somewhat surprising, results that suggest visual cues exerted more robust but incomplete control over the young cohort. Based on these findings and the accompanying computational model, my current hypothesis is that the partial realignment observed in the running behavior of young rats reflects more effective integration of allothetic and idiothetic information streams. Similar to the signal processing techniques that detect the shared underlying information from two noisy signals, the behavior of young animals may reflect more optimal spatial processing under normal real-world conditions where allothetic and idiothetic feedback is subject to variable levels of signal-to-noise due to changing

environmental conditions. The attractor network model presented in Chapter 4 suggests one plausible mechanism that could lead to impaired allothetic-idiothetic integration in aged spatial networks based on established deficits in self-motion-based processing. Importantly, however, successful navigation is contingent on the quality of various forms of sensory-perceptual information that collectively inform downstream spatial representational systems. Given that aging is associated with widespread impairments across multiple sensory domains, it may be the case that the age-related impairments observed in the ICR task, as well as those reported for other tasks requiring allocentric navigation (e.g., Rosenzweig et al., 2003), are attributable to the degraded nature of the sensory-perceptual signals that inform entorhinal-hippocampal spatial networks. The ability to assess how mismatched allothetic-idiothetic feedback is resolved at different stages within the entorhinal-hippocampal circuit could help to narrow down if the age-related changes in allothetic/idiothetic processing are primarily a byproduct of upstream sensory-perceptual deficits or altered spatial processing within entorhinal-hippocampal spatial networks.

Chapter 5 details efforts, to date, developing and refining technologies for simultaneous MEC and CA1 single unit recording from rats engaged in the ICR task. Although the technical challenges encountered over the course of this endeavor have been substantial, I believe the tools developed through this undertaking, applied within the

context of the ICR system, have significant potential for advancing our understanding of how aging impacts the inter-regional and temporal coordination of information processing across the greater entorhinal-hippocampal network. My ideas regarding how these networks may resolve the sudden conflict in spatial feedback introduced in ICR have evolved since the original conception of my dissertation. In light of the behavioral and modeling findings, as well as preliminary observations from the pilot CA1 and MEC recordings, I have a series of predictions. First, immediately following cue rotation, CA1 place cells of both young and aged rats are expected to be delayed in realigning to the new cue orientation—consistent with the age-independent timing delay suggested by Redish et al. (2000)—and will subsequently undergo a progressive realignment with the cues as the mismatch in path-integration based estimates are gradually corrected (Mittelstaedt and Mittelstaedt, 1980; Gallistel, 1990; Benhamou, 1997; Redish, 1999). Second, given the tendency for CA1 to generate split representations under various conditions of spatial cue mismatch (Shapiro et al., 1997; Zinyuk et al., 2000; Lee et al., 2004b), the particular time-course and degree of realignment may differ across simultaneously recorded CA1 place cells. Based on preliminary recordings from the proof of concept ICR experiment presented in Chapter 5, I predict that the constituent spatial networks of MEC will show a coherent age-independent realignment delay, consistent with MEC's presumed role in idiothetic-based path integration operations

(Redish and Touretzky, 1997; Redish, 1999; McNaughton et al., 2006; Moser et al., 2008; Giocomo et al., 2011). If this is case, and assuming that the longer age-related delays reported by Rosenzweig et al. (2003) are temporal in nature and result from greater idiothetic control over aged CA1 networks, the third prediction is that aged rats should show a slower average time-course of CA1 realignment proportional to that of the idiothetic-biased MEC networks. This would be constant with the hypothesis that there is a stronger influence of the direct and unaltered layer III MEC inputs in older animals. Importantly, the overall longer age-related realignment delay would be with respect to across- cell and trial averages. If the premises of the model presented in Chapter 4 are correct, CA1 place cell realignment in aged rats should also be more variable when assessed on a trial-by-trial basis such that both the time-course and degree of place cell realignment will depend on the degree of idiothetic-based error in aged MEC networks. While these ideas remain to be validated experimentally in the ICR task, they represent a coherent framework and also provide some testable predictions.

In retrospect, the scope of this project may have been... ambitious. Nonetheless, the work performed to date support the tractability of the methods developed and their feasibility to bear valuable fruit in the electrophysiological investigations already underway. I still believe that valuing quality and thoroughness over quantity and expediency can prove the faster route to reaching robust and tractable theoretical outcomes.

Avoiding shortcuts during the conception and implementation of an experiment limits the subsequent potential for overfitting or overstating the implications of the data gleaned, which ensures the integrity of the conceptual framework within which we all operate. These are particularly salient considerations for systems neuroscience, where reported findings are often based on analysis that represent a high degree of abstraction from the underlying data. Although the hurdles encountered in the course of my dissertation work have been legion, I believe that our understanding the neural systems that subserve navigation and spatial cognition can be greatly advanced by access to tools that enable precise control of the sensory-perceptual inputs that inform these systems, while also providing behavioral metrics in which to contextualize neurophysiological findings. In his book *Rhythms of the Brain* (2009), György Buzsáki repurposes a well-known quote by Theodosius Dobzhansky, stating that “nothing in the brain makes sense except in the light of behavior”. While this may be intentionally hyperbolic, the logic of it is simple and intuitively appealing: the entirety of the brain’s utility to an organism comes down to the behavioral output it is responsible for generating. An equivalently simple and universal truism is that the brain’s only input is the sensory-spatial environment in which the organism is embedded. The overarching ambition of systems neuroscience is, as I see it, to fully map out the tangled, branching and complex pathways that take sensory input to behavioral output. It is my sincere hope that the time, effort and resources

invested over the course of this dissertation work has brought us closer to the point where, being able to precisely control the sensory 'input' and quantify the behavioral 'output', we can better trace what path is being traversed in the steps between.

REFERENCES

- Adamo DE, Briceño EM, Sindone JA, Alexander NB, Moffat S (2012) Age differences in virtual environment and real world path integration. *Frontiers in aging neuroscience* 4:26.
- Adams SV, Winterer J, Müller W (2004) Muscarinic signaling is required for spike-pairing induction of long-term potentiation at rat Schaffer collateral-CA1 synapses. *Hippocampus* 14:413–416.
- Aghajan ZM, Acharya L, Moore JJ, Cushman JD, Vuong C, Mehta MR (2015) Impaired spatial selectivity and intact phase precession in two-dimensional virtual reality. *Nature neuroscience* 18:121.
- Aitken DH, Meaney MJ (1989) Temporally graded, age-related impairments in spatial memory in the rat. *Neurobiology of aging* 10:273–276.
- Alexander GE, Chen K, Aschenbrenner M, Merkley TL, Santerre-Lemmon LE, Shamy JL, Skaggs WE, Buonocore MH, Rapp PR, Barnes CA (2008) Age-related regional network of magnetic resonance imaging gray matter in the rhesus macaque. *Journal of Neuroscience* 28:2710–2718.
- Allen GL, Kirasic KC, Rashotte MA, Haun DB (2004) Aging and path integration skill: Kinesthetic and vestibular contributions to wayfinding. *Perception & Psychophysics* 66:170–179.
- Amari S (1977) Dynamics of pattern formation in lateral-inhibition type neural fields. *Biological cybernetics* 27:77–87.
- Amemiya S, Noji T, Kubota N, Nishijima T, Kita I (2014) Noradrenergic modulation of vicarious trial-and-error behavior during a spatial decision-making task in rats. *Neuroscience* 265:291–301.
- Amemiya S, Redish AD (2016) Manipulating Decisiveness in Decision Making: Effects of Clonidine on Hippocampal Search Strategies. *J Neurosci* 36:814–827.
- Amemiya S, Redish AD (2018) Hippocampal Theta-Gamma Coupling Reflects State-Dependent Information Processing in Decision Making. *Cell reports* 22:3328–3338.
- Anson E, Jeka J (2015) Perspectives on aging vestibular function. *Frontiers in neurology* 6.
- Antonova E, Parslow D, Brammer M, Dawson GR, Jackson SHD, Morris

- RG (2009) Age-related neural activity during allocentric spatial memory. *Memory* 17:125–143.
- Applegate MD, Landfield PW (1988) Synaptic vesicle redistribution during hippocampal frequency potentiation and depression in young and aged rats. *J Neurosci* 8:1096–1111.
- Arshad Q, Seemungal BM (2016) Age-Related Vestibular Loss: Current Understanding and Future Research Directions. *Front Neurol* 7.
- Aston-Jones G, Cohen JD (2005) An integrative theory of locus coeruleus-norepinephrine function: adaptive gain and optimal performance. *Annu Rev Neurosci* 28:403–450.
- Bach ME, Barad M, Son H, Zhuo M, Lu YF, Shih R, Mansuy I, Hawkins RD, Kandel ER (1999) Age-related defects in spatial memory are correlated with defects in the late phase of hippocampal long-term potentiation in vitro and are attenuated by drugs that enhance the cAMP signaling pathway. *Proceedings of the national academy of sciences* 96:5280–5285.
- Bai L, Hof PR, Standaert DG, Xing Y, Nelson SE, Young AB, Magnusson KR (2004) Changes in the expression of the NR2B subunit during aging in macaque monkeys. *Neurobiology of aging* 25:201–208.
- Baker S, Vieweg P, Gao F, Gilboa A, Wolbers T, Black SE, Rosenbaum RS (2016) The Human Dentate Gyrus Plays a Necessary Role in Discriminating New Memories. *Current Biology* 26:2629–2634.
- Ban TA, Morey L, Aguglia E, Azzarelli O, Balsano F, Marigliano V, Cagliaris N, Sterlicchio M, Capurso A, Tomasi NA, Crepaldi G, Volpe D, Palmieri G, Ambrosi G, Polli E, Cortellaro M, Zanussi C, Frolidi M (1990) Nimodipine in the treatment of old age dementias. *Progress in Neuro-Psychopharmacology and Biological Psychiatry* 14:525–551.
- Barnes CA (1979) Memory deficits associated with senescence: a neurophysiological and behavioral study in the rat. *Journal of comparative and physiological psychology* 93:74.
- Barnes CA, McNaughton BL (1980a) Physiological compensation for loss of afferent synapses in rat hippocampal granule cells during senescence. *The Journal of Physiology* 309:473–485.
- Barnes CA, McNaughton BL (1980b) Spatial memory and hippocampal synaptic plasticity in senescent and middle-aged rats.
- Barnes CA, McNaughton BL (1985) An age comparison of the rates of

acquisition and forgetting of spatial information in relation to long-term enhancement of hippocampal synapses. *Behavioral neuroscience* 99:1040.

- Barnes CA, Nadel L, Honig WK (1980) Spatial memory deficit in senescent rats. *Canadian Journal of Psychology/Revue canadienne de psychologie* 34:29.
- Barnes CA, Rao G, Foster TC, McNaughton BL (1992) Region-specific age effects on AMPA sensitivity: Electrophysiological evidence for loss of synaptic contacts in hippocampal field CA1. *Hippocampus* 2:457–468.
- Barnes CA, Rao G, Houston FP (2000) LTP induction threshold change in old rats at the perforant path–granule cell synapse. *Neurobiology of aging* 21:613–620.
- Barnes CA, Rao G, McNaughton BL (1996) Functional integrity of NMDA-dependent LTP induction mechanisms across the lifespan of F-344 rats. *Learning & Memory* 3:124–137.
- Barnes CA, Suster MS, Shen J, McNaughton BL (1997) Multistability of cognitive maps in the hippocampus of old rats. *Nature* 388:272–275.
- Barry C, Hayman R, Burgess N, Jeffery KJ (2007) Experience-dependent rescaling of entorhinal grids. *Nature Neuroscience* 10:682–684.
- Bates SL, Wolbers T (2014) How cognitive aging affects multisensory integration of navigational cues. *Neurobiology of Aging* 35:2761–2769.
- Battaglia FP, Treves A (1998) Attractor neural networks storing multiple space representations: a model for hippocampal place fields. *Physical Review E* 58:7738.
- Beas BS, McQuail JA, Bañuelos C, Setlow B, Bizon JL (2016) Prefrontal cortical GABAergic signaling and impaired behavioral flexibility in aged F344 rats. *Neuroscience*.
- Benhamou S (1997) Path integration by swimming rats. *Animal Behaviour* 54:321–327.
- Betts MJ, Acosta-Cabronero J, Cardenas-Blanco A, Nestor PJ, Düzel E (2016) High-resolution characterisation of the aging brain using simultaneous quantitative susceptibility mapping (QSM) and R2* measurements at 7 T. *NeuroImage* 138:43–63.

- Bian Z, Andersen GJ (2013) Aging and the perception of egocentric distance. *Psychology and aging* 28:813.
- Biegler R, Morris RG (1993) Landmark stability is a prerequisite for spatial but not discrimination learning. *Nature*; London 361:631–633.
- Bieri KW, Bobbitt KN, Colgin LL (2014) Slow and Fast Gamma Rhythms Coordinate Different Spatial Coding Modes in Hippocampal Place Cells. *Neuron* 82:670–681.
- Birrell JM, Brown VJ (2000) Medial frontal cortex mediates perceptual attentional set shifting in the rat. *Journal of Neuroscience* 20:4320–4324.
- Bizon JL, LaSarge CL, Montgomery KS, McDermott AN, Setlow B, Griffith WH (2009) Spatial reference and working memory across the lifespan of male Fischer 344 rats. *Neurobiology of Aging* 30:646–655.
- Blair HT, Gupta K, Zhang K (2008) Conversion of a phase- to a rate-coded position signal by a three-stage model of theta cells, grid cells, and place cells. *Hippocampus* 18:1239–1255.
- Blair HT, Sharp PE (1996) Visual and vestibular influences on head-direction cells in the anterior thalamus of the rat. *Behavioral neuroscience* 110:643.
- Bliss TV, Gardner-Medwin AR (1973) Long-lasting potentiation of synaptic transmission in the dentate area of the unanaesthetized rabbit following stimulation of the perforant path. *The Journal of physiology* 232:357–374.
- Bliss TV, Lømo T (1973) Long-lasting potentiation of synaptic transmission in the dentate area of the anaesthetized rabbit following stimulation of the perforant path. *The Journal of physiology* 232:331–356.
- Blum KI, Abbott LF (1996) A Model of Spatial Map Formation in the Hippocampus of the Rat. *Neural Computation* 8:85–93.
- Boccaro CN, Sargolini F, Thoresen VH, Solstad T, Witter MP, Moser EI, Moser M-B (2010) Grid cells in pre- and parasubiculum. *Nature Neuroscience* 13:987–994.
- Boeniger MF (1995) Use of ozone generating devices to improve indoor air quality. *Am Ind Hyg Assoc J* 56:590–598.
- Bohbot VD, McKenzie S, Konishi K, Fouquet C, Kurdi V, Schachar R, Boivin M, Robaey P (2012) Virtual navigation strategies from

childhood to senescence: evidence for changes across the life span. *Frontiers in aging neuroscience* 4:28.

- Bondareff W, Geinisman Y (1976) Loss of synapses in the dentate gyrus of the senescent rat. *American Journal of Anatomy* 145:129–136.
- Bonnevie T, Dunn B, Fyhn M, Hafting T, Derdikman D, Kubie JL, Roudi Y, Moser EI, Moser M-B (2013) Grid cells require excitatory drive from the hippocampus. *Nature Neuroscience*.
- Boric K, Muñoz P, Gallagher M, Kirkwood A (2008) Potential Adaptive Function for Altered Long-Term Potentiation Mechanisms in Aging Hippocampus. *J Neurosci* 28:8034–8039.
- Bostock E, Muller RU, Kubie JL (1991) Experience-dependent modifications of hippocampal place cell firing. *Hippocampus* 1:193–205.
- Boucheny C, Brunel N, Arleo A (2005) A continuous attractor network model without recurrent excitation: maintenance and integration in the head direction cell system. *Journal of computational neuroscience* 18:205–227.
- Braak H, Braak EVA (1995) Staging of Alzheimer's disease-related neurofibrillary changes. *Neurobiology of aging* 16:271–278.
- Brandt T, Schautzer F, Hamilton DA, Brüning R, Markowitsch HJ, Kalla R, Darlington C, Smith P, Strupp M (2005) Vestibular loss causes hippocampal atrophy and impaired spatial memory in humans. *Brain* 128:2732–2741.
- Breton Y-A, Seeland KD, Redish AD (2015) Aging impairs deliberation and behavioral flexibility in inter-temporal choice. *Frontiers in Aging Neuroscience* 7 Available at: http://www.frontiersin.org/Aging_Neuroscience/10.3389/fnagi.2015.00041/abstract [Accessed October 7, 2016].
- Brigman JL, Wright T, Talani G, Prasad-Mulcare S, Jinde S, Seabold GK, Mathur P, Davis MI, Bock R, Gustin RM, Colbran RJ, Alvarez VA, Nakazawa K, Delpire E, Lovinger DM, Holmes A (2010) Loss of GluN2B-Containing NMDA Receptors in CA1 Hippocampus and Cortex Impairs Long-Term Depression, Reduces Dendritic Spine Density, and Disrupts Learning. *J Neurosci* 30:4590–4600.
- Brim BL, Haskell R, Awedikian R, Ellinwood NM, Jin L, Kumar A, Foster TC, Magnusson KR (2013) Memory in aged mice is rescued by enhanced expression of the GluN2B subunit of the NMDA receptor. *Behavioural brain research* 238:211–226.

- Brun VH, Solstad T, Kjelstrup KB, Fyhn M, Witter MP, Moser EI, Moser M-B (2008) Progressive increase in grid scale from dorsal to ventral medial entorhinal cortex. *Hippocampus* 18:1200–1212.
- Burgess N, Barry C, O'Keefe J (2007) An oscillatory interference model of grid cell firing. *Hippocampus* 17:801–812.
- Burke SN, Barnes CA (2006) Neural plasticity in the ageing brain. *Nature Reviews Neuroscience* 7:30–40.
- Burns PC (1999) Navigation and the Mobility of Older Drivers. *J Gerontol B Psychol Sci Soc Sci* 54B:S49–S55.
- Burwell RD, Amaral DG (1998) Perirhinal and postrhinal cortices of the rat: interconnectivity and connections with the entorhinal cortex. *Journal of Comparative Neurology* 391:293–321.
- Burwell RD, Gallagher M (1993) A longitudinal study of reaction time performance in Long-Evans rats. *Neurobiology of aging* 14:57–64.
- Buzsáki G (1996) The hippocampo-neocortical dialogue. *Cerebral Cortex* 6:81–92.
- Buzsaki G (2009) *Rhythms of the Brain*. Oxford University Press, USA.
- Buzsáki G, Eidelberg E (1983) Phase relations of hippocampal projection cells and interneurons to theta activity in the anesthetized rat. *Brain Res* 266:334–339.
- Buzsáki G, Horváth Z, Urioste R, Hetke J, Wise K (1992) High-frequency network oscillation in the hippocampus. *Science* 256:1025–1027.
- Byrne P, Becker S, Burgess N (2007) Remembering the past and imagining the future: a neural model of spatial memory and imagery. *Psychological review* 114:340.
- Caetano MJD, Lord SR, Schoene D, Pelicioni PH, Sturnieks DL, Menant JC (2016) Age-related changes in gait adaptability in response to unpredictable obstacles and stepping targets. *Gait & posture* 46:35–41.
- Caetano MS, Jin LE, Harenberg L, Stachenfeld KL, Arnsten AF, Laubach M (2013) Noradrenergic control of error perseveration in medial prefrontal cortex. *Frontiers in integrative neuroscience* 6:125.
- Campbell DT, Stanley JC (1963) Experimental and quasi-experimental designs for research. *Handbook of research on teaching*:171–246.

- Carpenter HE, Kelly KB, Bizon JL, Frazier CJ (2016) Age-related changes in tonic activation of presynaptic versus extrasynaptic γ -amniobutyric acid type B receptors in rat medial prefrontal cortex. *Neurobiology of aging* 45:88–97.
- Carr MF, Jadhav SP, Frank LM (2011) Hippocampal replay in the awake state: a potential substrate for memory consolidation and retrieval. *Nature neuroscience* 14:147–153.
- Chadwick MJ, Jolly AEJ, Amos DP, Hassabis D, Spiers HJ (2015) A Goal Direction Signal in the Human Entorhinal/Subicular Region. *Current Biology* 25:87–92.
- Chapuis N, Krimm M, de Waele C, Vibert N, Berthoz A (1992) Effect of post-training unilateral labyrinthectomy in a spatial orientation task by guinea pigs. *Behavioural brain research* 51:115–126.
- Chen G, King JA, Burgess N, O'Keefe J (2013) How vision and movement combine in the hippocampal place code. *PNAS* 110:378–383.
- Chen G, Manson D, Cacucci F, Wills TJ (2016) Absence of Visual Input Results in the Disruption of Grid Cell Firing in the Mouse. *Current Biology* 26:2335–2342.
- Chen LL, Lin LH, Barnes CA, McNaughton BL (1994) Head-direction cells in the rat posterior cortex. II. Contributions of visual and ideothetic information to the directional firing. *Experimental brain research* 101:24.
- Cheng K (1986) A purely geometric module in the rat's spatial representation. *Cognition* 23:149–178.
- Chouinard ML, Gallagher M, Yasuda RP, Wolfe BB, McKinney M (1995) Hippocampal muscarinic receptor function in spatial learning-impaired aged rats. *Neurobiology of Aging* 16:955–963.
- Colgin LL, Denninger T, Fyhn M, Hafting T, Bonnevie T, Jensen O, Moser M-B, Moser EI (2009) Frequency of gamma oscillations routes flow of information in the hippocampus. *Nature* 462:353–357.
- Collingridge GL, Kehl SJ, McLennan H (1983) Excitatory amino acids in synaptic transmission in the Schaffer collateral-commissural pathway of the rat hippocampus. *J Physiol* 334:33–46.
- Cowen SL, Gray DT, Wiegand J-PL, Schimanski LA, Barnes CA (2018) Age-associated changes in waking hippocampal sharp-wave ripples. *Hippocampus*.

- Craig M, Wolbers T, Harris MA, Hauff P, Della Sala S, Dewar M (2016) Comparable rest-related promotion of spatial memory consolidation in younger and older adults. *Neurobiology of aging* 48:143–152.
- Cui Y, Jin J, Zhang X, Xu H, Yang L, Du D, Zeng Q, Tsien JZ, Yu H, Cao X (2011) Forebrain NR2B overexpression facilitating the prefrontal cortex long-term potentiation and enhancing working memory function in mice. *PloS one* 6:e20312.
- Dalley JW, Cardinal RN, Robbins TW (2004) Prefrontal executive and cognitive functions in rodents: neural and neurochemical substrates. *Neuroscience & Biobehavioral Reviews* 28:771–784.
- Daugherty AM, Bender AR, Yuan P, Raz N (2016) Changes in Search Path Complexity and Length During Learning of a Virtual Water Maze: Age Differences and Differential Associations with Hippocampal Subfield Volumes. *Cereb Cortex* 26:2391–2401.
- Degrís T, Sigaud O, Wiener SI, Arleo A (2004) Rapid response of head direction cells to reorienting visual cues: a computational model. *Neurocomputing* 58:675–682.
- Derdikman D, Whitlock JR, Tsao A, Fyhn M, Hafting T, Moser MB, Moser EI (2009) Fragmentation of grid cell maps in a multicompartiment environment. *Nature neuroscience* 12:1325–1332.
- Deshmukh SS, Knierim JJ (2011) Representation of Non-Spatial and Spatial Information in the Lateral Entorhinal Cortex. *Frontiers in Behavioral Neuroscience* 5 Available at: http://www.frontiersin.org/Behavioral_Neuroscience/10.3389/fnbeh.2011.00069/abstract [Accessed November 21, 2012].
- Deupree DL, Bradley J, Turner DA (1993) Age-related alterations in potentiation in the CA1 region in F344 rats. *Neurobiology of Aging* 14:249–258.
- Diana G, Domenici MR, Loizzo A, de Carolis AS, Sagratella S (1994) Age and strain differences in rat place learning and hippocampal dentate gyrus frequency-potentiation. *Neuroscience Letters* 171:113–116.
- Dias R, Robbins TW, Roberts AC (1996) Dissociation in prefrontal cortex of affective and attentional shifts. , Published online: 07 March 1996; | doi:101038/380069a0 380:69–72.
- Diba K, Buzsáki G (2008) Hippocampal Network Dynamics Constrain the Time Lag between Pyramidal Cells across Modified Environments. *J Neurosci* 28:13448–13456.

- Dieguez D, Barea-Rodriguez EJ (2004) Aging impairs the late phase of long-term potentiation at the medial perforant path-CA3 synapse in awake rats. *Synapse* 52:53–61.
- Doeller CF, Barry C, Burgess N (2010) Evidence for grid cells in a human memory network. *Nature* 463:657–661.
- Dowiasch S, Marx S, Einhäuser W, Bremmer F (2015) Effects of aging on eye movements in the real world. *Frontiers in human neuroscience* 9:46.
- Dragoi G, Buzsáki G (2006) Temporal encoding of place sequences by hippocampal cell assemblies. *Neuron* 50:145–158.
- Droulez J, Berthoz A (1991) A neural network model of sensoritopic maps with predictive short-term memory properties. *Proceedings of the National Academy of Sciences* 88:9653–9657.
- Dupret D, O’Neill J, Pleydell-Bouverie B, Csicsvari J (2010) The reorganization and reactivation of hippocampal maps predict spatial memory performance. *Nature Neuroscience* 13:995–1002.
- Dyall SC, Michael GJ, Whelpton R, Scott AG, Michael-Titus AT (2007) Dietary enrichment with omega-3 polyunsaturated fatty acids reverses age-related decreases in the GluR2 and NR2B glutamate receptor subunits in rat forebrain. *Neurobiology of Aging* 28:424–439.
- Ego-Stengel V, Wilson MA (2010) Disruption of ripple-associated hippocampal activity during rest impairs spatial learning in the rat. *Hippocampus* 20:1–10.
- Eichenbaum H (2014) Time cells in the hippocampus: a new dimension for mapping memories. *Nature Reviews Neuroscience* 15:732.
- Ekstrom AD, Arnold AEGF, Iaria G (2014) A critical review of the allocentric spatial representation and its neural underpinnings: toward a network-based perspective. *Front Hum Neurosci* 8.
- Ekstrom AD, Kahana MJ, Caplan JB, Fields TA, Isham EA, Newman EL, Fried I (2003) Cellular networks underlying human spatial navigation. *Nature* 425:184–188.
- Ekstrom AD, Meltzer J, McNaughton BL, Barnes CA (2001) NMDA receptor antagonism blocks experience-dependent expansion of hippocampal “place fields.” *Neuron* 31:631–638.
- Etchamendy N, Konishi K, Pike GB, Marighetto A, Bohbot VD (2012)

- Evidence for a virtual human analog of a rodent relational memory task: a study of aging and fMRI in young adults. *Hippocampus* 22:869–880.
- Etienne AS (1992) Navigation of a Small Mammal by Dead Reckoning and Local Cues. *Current Directions in Psychological Science* 1:48–52.
- Etienne AS, Maurer R, Séguinot V (1996) Path integration in mammals and its interaction with visual landmarks. *Journal of Experimental Biology* 199:201–209.
- Feigenbaum JD, Rolls ET (1991) Allocentric and egocentric spatial information processing in the hippocampal formation of the behaving primate. *Psychobiology* 19:21–40.
- Fenton AA, Lytton WW, Barry JM, Lenck-Santini P-P, Zinyuk LE, Kubík Š, Bureš J, Poucet B, Muller RU, Olypher AV (2010) Attention-like modulation of hippocampus place cell discharge. *Journal of Neuroscience* 30:4613–4625.
- Fenton AA, Wesierska M, Kaminsky Y, Bures J (1998) Both here and there: simultaneous expression of autonomous spatial memories in rats. *Proceedings of the National Academy of Sciences* 95:11493–11498.
- Floresco SB, Seamans JK, Phillips AG (1997) Selective roles for hippocampal, prefrontal cortical, and ventral striatal circuits in radial-arm maze tasks with or without a delay. *Journal of Neuroscience* 17:1880–1890.
- Foster TC, Kumar A (2007) Susceptibility to induction of long-term depression is associated with impaired memory in aged Fischer 344 rats. *Neurobiology of Learning and Memory* 87:522–535.
- Foster TC, Norris CM (1997) Age-associated changes in Ca²⁺-dependent processes: Relation to hippocampal synaptic plasticity. *Hippocampus* 7:602–612.
- Frank LM, Stanley GB, Brown EN (2004) Hippocampal Plasticity across Multiple Days of Exposure to Novel Environments. *J Neurosci* 24:7681–7689.
- Frick KM, Baxter MG, Markowska AL, Olton DS, Price DL (1995) Age-related spatial reference and working memory deficits assessed in the water maze. *Neurobiology of aging* 16:149–160.
- Fu H, Rodriguez GA, Herman M, Emrani S, Nahmani E, Barrett G, Figueroa HY, Goldberg E, Hussaini SA, Duff KE (2017) Tau

Pathology Induces Excitatory Neuron Loss, Grid Cell Dysfunction, and Spatial Memory Deficits Reminiscent of Early Alzheimer's Disease. *Neuron* 93:533-541.e5.

Fuhs MC, Touretzky DS (2006) A Spin Glass Model of Path Integration in Rat Medial Entorhinal Cortex. *J Neurosci* 26:4266–4276.

Fyhn M, Hafting T, Treves A, Moser M-B, Moser EI (2007) Hippocampal remapping and grid realignment in entorhinal cortex. *Nature* 446:190–194.

Fyhn M, Molden S, Witter MP, Moser EI, Moser M (2004) Spatial Representation in the Entorhinal Cortex. *Science* 305:1258–1264.

Gage FH, Dunnett SB, Björklund A (1984) Spatial learning and motor deficits in aged rats. *Neurobiology of aging* 5:43–48.

Gallagher M, Burwell RD, Burchinal M (2015) Severity of Spatial Learning Impairment in Aging: Development of a Learning Index for Performance in the Morris Water Maze. *Behav Neurosci* 129:540–548.

Gallistel CR (1990) *The organization of learning*. The MIT Press.

Gazzaley AH, Siegel SJ, Kordower JH, Mufson EJ, Morrison JH (1996) Circuit-specific alterations of N-methyl-D-aspartate receptor subunit 1 in the dentate gyrus of aged monkeys. *Proc Natl Acad Sci USA* 93:3121–3125.

Geinisman Y, Bondareff W, Dodge JT (1977) Partial deafferentation of neurons in the dentate gyrus of the senescent rat. *Brain research* 134:541.

Geinisman Y, De Toledo-Morrell L, Morrell F (1986) Loss of perforated synapses in the dentate gyrus: morphological substrate of memory deficit in aged rats. *Proceedings of the National Academy of Sciences* 83:3027–3031.

Geinisman Y, de Toledo-Morrell L, Morrell F, Persina IS, Rossi M (1992) Age-related loss of axospinous synapses formed by two afferent systems in the rat dentate gyrus as revealed by the unbiased stereological dissector technique. *Hippocampus* 2:437–444.

Geinisman Y, Ganeshina O, Yoshida R, Berry RW, Disterhoft JF, Gallagher M (2004) Aging, spatial learning, and total synapse number in the rat CA1 stratum radiatum. *Neurobiology of Aging* 25:407–416.

- Gerrard JL, Burke SN, McNaughton BL, Barnes CA (2008) Sequence Reactivation in the Hippocampus Is Impaired in Aged Rats. *J Neurosci* 28:7883–7890.
- Gerrard JL, Kudrimoti H, McNaughton BL, Barnes CA (2001) Reactivation of hippocampal ensemble activity patterns in the aging rat. *Behavioral Neuroscience* 115:1180–1192.
- Gillner S, Mallot HA (1998) Navigation and acquisition of spatial knowledge in a virtual maze. *Journal of Cognitive Neuroscience* 10:445–463.
- Giocomo LM, Moser M-B, Moser EI (2011) Computational Models of Grid Cells. *Neuron* 71:589–603.
- Girardeau G, Benchenane K, Wiener SI, Buzsáki G, Zugaro MB (2009) Selective suppression of hippocampal ripples impairs spatial memory. *Nat Neurosci* 12:1222–1223.
- Goodrich-Hunsaker NJ, Livingstone SA, Skelton RW, Hopkins RO (2010) Spatial deficits in a virtual water maze in amnesic participants with hippocampal damage. *Hippocampus* 20:481–491.
- Goodridge JP, Touretzky DS (2000) Modeling attractor deformation in the rodent head-direction system. *Journal of neurophysiology* 83:3402–3410.
- Gorny JH, Gorny B, Wallace DG, Wishaw IQ (2002) Fimbria-Fornix Lesions Disrupt the Dead Reckoning (Homing) Component of Exploratory Behavior in Mice. *Learn Mem* 9:387–394.
- Gothard KM, Skaggs WE, McNaughton BL (1996) Dynamics of mismatch correction in the hippocampal ensemble code for space: interaction between path integration and environmental cues. *The Journal of neuroscience* 16:8027–8040.
- Gozlan H, Daval G, Verge D, Spampinato U, Fattaccini CM, Gallissot MC, El Mestikawy S, Hamon M (1990) Aging associated changes in serotonergic and dopaminergic pre- and postsynaptic neurochemical markers in the rat brain. *Neurobiology of Aging* 11:437–449.
- Gray DT, Smith AC, Burke SN, Gazzaley A, Barnes CA (2017) Attentional updating and monitoring and affective shifting are impacted independently by aging in macaque monkeys. *Behavioural brain research* 322:329–338.
- Grön G, Brandenburg I, Wunderlich AP, Riepe MW (2006) Inhibition of

hippocampal function in mild cognitive impairment: targeting the cholinergic hypothesis. *Neurobiology of aging* 27:78–87.

- Grudzien A, Shaw P, Weintraub S, Bigio E, Mash DC, Mesulam MM (2007) Locus coeruleus neurofibrillary degeneration in aging, mild cognitive impairment and early Alzheimer's disease. *Neurobiology of aging* 28:327–335.
- Guanella A, Kiper D, Verschure P (2007) A model of grid cells based on a twisted torus topology. *International journal of neural systems* 17:231–240.
- Gupta AS, Van Der Meer MA, Touretzky DS, Redish AD (2012) Segmentation of spatial experience by hippocampal theta sequences. *Nature neuroscience* 15:1032.
- Gupta AS, van der Meer MAA, Touretzky DS, Redish AD (2010) Hippocampal Replay Is Not a Simple Function of Experience. *Neuron* 65:695–705.
- Guzowski JF, Knierim JJ, Moser EI (2004) Ensemble dynamics of hippocampal regions CA3 and CA1. *Neuron* 44:581–584.
- Hafting T, Fyhn M, Molden S, Moser M-B, Moser EI (2005) Microstructure of a spatial map in the entorhinal cortex. *Nature* 436:801–806.
- Hahnloser RHR (2003) Emergence of neural integration in the head-direction system by visual supervision. *Neuroscience* 120:877–891.
- Hamlin AS, Windels F, Boskovic Z, Sah P, Coulson EJ (2013) Lesions of the Basal Forebrain Cholinergic System in Mice Disrupt Idiopathic Navigation. *PLoS ONE* 8:e53472.
- Hargreaves EL (2005) Major Dissociation Between Medial and Lateral Entorhinal Input to Dorsal Hippocampus. *Science* 308:1792–1794.
- Harris MA, Wiener JM, Wolbers T (2012) Aging specifically impairs switching to an allocentric navigational strategy. *Front Ag Neurosci* 4:29.
- Harris MA, Wolbers T (2012) Ageing effects on path integration and landmark navigation. *Hippocampus* 22:1770–1780.
- Harris MA, Wolbers T (2014) How age-related strategy switching deficits affect wayfinding in complex environments. *Neurobiology of Aging* 35:1095–1102.
- Hartley T, Maguire EA, Spiers HJ, Burgess N (2003) The well-worn route

and the path less traveled: distinct neural bases of route following and wayfinding in humans. *Neuron* 37:877–888.

Harvey CD, Collman F, Dombeck DA, Tank DW (2009) Intracellular dynamics of hippocampal place cells during virtual navigation. *Nature* 461:941–946.

Hasselmo ME (2005a) What is the function of hippocampal theta rhythm?—Linking behavioral data to phasic properties of field potential and unit recording data. *Hippocampus* 15:936–949.

Hasselmo ME (2005b) The role of hippocampal regions CA3 and CA1 in matching entorhinal input with retrieval of associations between objects and context: theoretical comment on Lee et al.(2005).

Hasselmo ME (2006) The role of acetylcholine in learning and memory. *Current opinion in neurobiology* 16:710–715.

Hasselmo ME, Bodelón C, Wyble BP (2002) A proposed function for hippocampal theta rhythm: separate phases of encoding and retrieval enhance reversal of prior learning. *Neural computation* 14:793–817.

Hasselmo ME, Schnell E, Barkai E (1995) Dynamics of learning and recall at excitatory recurrent synapses and cholinergic modulation in rat hippocampal region CA3. *The Journal of neuroscience* 15:5249–5262.

Head D, Isom M (2010) Age effects on wayfinding and route learning skills. *Behavioural Brain Research* 209:49–58.

Head E, Mehta R, Hartley J, Kameka M, Cummings BJ, Cotman CW, Ruehl WW, Milgram NW (1995) Spatial learning and memory as a function of age in the dog. *Behavioral Neuroscience* 109:851–858.

Hebb DO (1949) *The organization of behavior*. Wiley, New York.

Hermer L, Spelke ES (1994) A geometric process for spatial reorientation in young children. *Nature* 370:57.

Hersi AI, Rowe W, Gaudreau P, Quirion R (1995) Dopamine D1, receptor ligands modulate cognitive performance and hippocampal acetylcholine release in memory-impaired aged rats. *Neuroscience* 69:1067–1074.

Hetherington PA, Shapiro ML (1993) A simple network model simulates hippocampal place fields: II Computing goal-directed trajectories and memory fields. *Behavioral Neuroscience* 107:434–443.

- Hok V, Chah E, Reilly RB, O'Mara SM (2012) Hippocampal Dynamics Predict Interindividual Cognitive Differences in Rats. *J Neurosci* 32:3540–3551.
- Hölscher C, Schnee A, Dahmen H, Setia L, Mallot HA (2005) Rats are able to navigate in virtual environments. *Journal of Experimental Biology* 208:561–569.
- Hort J, Andel R, Mokrisova I, Gazova I, Amlerova J, Valis M, Coulson EJ, Harrison J, Windisch M, Laczó J (2014) Effect of donepezil in Alzheimer disease can be measured by a computerized human analog of the Morris water maze. *Neurodegenerative Diseases* 13:192–196.
- Hötting K, Holzschneider K, Stenzel A, Wolbers T, Röder B (2013) Effects of a cognitive training on spatial learning and associated functional brain activations. *BMC neuroscience* 14:73.
- Huang Y-CS (2010) Exploring how spatial learning can affect the firing of place cells and head direction cells: the influence of changes in landmark configuration and the development of goal-directed spatial behaviour.
- Huentelman MJ, Stephan DA, Talboom J, Corneveaux JJ, Reiman DM, Gerber JD, Barnes CA, Alexander GE, Reiman EM, Bimonte-Nelson HA (2009) Peripheral delivery of a ROCK inhibitor improves learning and working memory. *Behavioral Neuroscience* 123:218–223.
- Huerta PT, Lisman JE (1995) Bidirectional synaptic plasticity induced by a single burst during cholinergic theta oscillation in CA1 in vitro. *Neuron* 15:1053–1063.
- Huguet F, Tarrade T (1992) α 2-Adrenoceptor Changes During Cerebral Ageing. The Effect of Ginkgo biloba Extract. *Journal of Pharmacy and Pharmacology* 44:24–27.
- Iaria G, Palermo L, Committeri G, Barton JJS (2009) Age differences in the formation and use of cognitive maps. *Behavioural Brain Research* 196:187–191.
- Iaria G, Petrides M, Dagher A, Pike B, Bohbot VD (2003) Cognitive Strategies Dependent on the Hippocampus and Caudate Nucleus in Human Navigation: Variability and Change with Practice. *J Neurosci* 23:5945–5952.
- Igarashi KM, Lu L, Colgin LL, Moser M-B, Moser EI (2014) Coordination of entorhinal-hippocampal ensemble activity during associative

- learning. *Nature* 510:143–147.
- Ingram DK (1988) Complex maze learning in rodents as a model of age-related memory impairment. *Neurobiology of Aging* 9:475–485.
- Ingram DK, Joseph JA, Spangler EL, Roberts D, Hengemihle J, Fanelli RJ (1994) Chronic nimodipine treatment in aged rats: Analysis of motor and cognitive effects and muscarinic-induced striatal dopamine release. *Neurobiology of Aging* 15:55–61.
- Insausti R, Herrero MT, Witter MP (1997) Entorhinal cortex of the rat: cytoarchitectonic subdivisions and the origin and distribution of cortical efferents. *Hippocampus* 7:146–183.
- Itskov V, Curto C, Pastalkova E, Buzsáki G (2011) Cell Assembly Sequences Arising from Spike Threshold Adaptation Keep Track of Time in the Hippocampus. *J Neurosci* 31:2828–2834.
- Jacob P-Y, Gordillo-Salas M, Facchini J, Poucet B, Save E, Sargolini F (2017a) Medial entorhinal cortex and medial septum contribute to self-motion-based linear distance estimation. *Brain Structure and Function* 222:2727–2742.
- Jacob P-Y, Gordillo-Salas M, Facchini J, Poucet B, Save E, Sargolini F (2017b) Medial entorhinal cortex and medial septum contribute to self-motion-based linear distance estimation. *Brain Struct Funct* 222:2727–2742.
- Jacobs J, Weidemann CT, Miller JF, Solway A, Burke JF, Wei X-X, Suthana N, Sperling MR, Sharan AD, Fried I, Kahana MJ (2013) Direct recordings of grid-like neuronal activity in human spatial navigation. *Nat Neurosci* advance online publication.
- Jadhav SP, Kemere C, German PW, Frank LM (2012) Awake Hippocampal Sharp-Wave Ripples Support Spatial Memory. *Science* 336:1454–1458.
- Jayakumar RP, Madhav MS, Savelli F, Breault M, Blair HT, Knierim JJ, Cowan NJ (2016) Extreme control of CA1 spatial maps by coherently moving virtual reality landmarks. In: *Society for Neuroscience*.
- Jeewajee A, Barry C, Douchamps V, Manson D, Lever C, Burgess N (2014) Theta phase precession of grid and place cell firing in open environments. *Philosophical Transactions of the Royal Society of London B: Biological Sciences* 369:20120532.
- Jeffery KJ, Anderson MI (2003) Dissociation of the geometric and

- contextual influences on place cells. *Hippocampus* 13:868–872.
- Jeffery KJ, O'Keefe J (1999) Learned interaction of visual and idiothetic cues in the control of place field orientation. *Experimental Brain Research* 127:151–161.
- Jezek K, Henriksen EJ, Treves A, Moser EI, Moser M-B (2011) Theta-paced flickering between place-cell maps in the hippocampus. *Nature* 478:246–249.
- Johnson A, Redish AD (2007) Neural Ensembles in CA3 Transiently Encode Paths Forward of the Animal at a Decision Point. *J Neurosci* 27:12176–12189.
- Johnson JE, Miquel J (1974) Fine structural changes in the lateral vestibular nucleus of aging rats. *Mechanisms of Ageing and Development* 3:203–224.
- Jones MW, Wilson MA (2005) Theta Rhythms Coordinate Hippocampal–Prefrontal Interactions in a Spatial Memory Task Morris R, ed. *PLoS Biology* 3:e402.
- Kanak DJ, Rose GM, Zaveri HP, Patrylo PR (2013) Altered Network Timing in the CA3-CA1 Circuit of Hippocampal Slices from Aged Mice. *PLoS ONE* 8:e61364.
- Karlsson MP, Frank LM (2009) Awake replay of remote experiences in the hippocampus. *Nat Neurosci* 12:913–918.
- Kavcic V, Vaughn W, Duffy CJ (2011) Distinct visual motion processing impairments in aging and Alzheimer's disease. *Vision research* 51:386–395.
- Kentros CG, Agnihotri NT, Streater S, Hawkins RD, Kandel ER (2004) Increased Attention to Spatial Context Increases Both Place Field Stability and Spatial Memory. *Neuron* 42:283–295.
- Kishimoto K, Amari S (1979) Existence and stability of local excitations in homogeneous neural fields. *Journal of Mathematical Biology* 7:303–318.
- Kloosterman F, Van Haeften T, Witter MP, Da Siiva FHL (2003) Electrophysiological characterization of interlaminar entorhinal connections: an essential link for re-entrance in the hippocampal–entorhinal system. *European Journal of Neuroscience* 18:3037–3052.
- Knierim JJ, Hamilton DA (2011) Framing spatial cognition: neural

representations of proximal and distal frames of reference and their roles in navigation. *Physiological Reviews* 91:1245–1279.

Knierim JJ, Kudrimoti HS, McNaughton BL (1995) Place cells, head direction cells, and the learning of landmark stability. *The Journal of Neuroscience* 15:1648–1659.

Knierim JJ, Kudrimoti HS, McNaughton BL (1998) Interactions between idiothetic cues and external landmarks in the control of place cells and head direction cells. *Journal of Neurophysiology* 80:425–446.

Knierim JJ, Neunuebel JP (2016) Tracking the flow of hippocampal computation: Pattern separation, pattern completion, and attractor dynamics. *Neurobiology of learning and memory* 129:38–49.

Knierim JJ, Rao G (2003) Distal landmarks and hippocampal place cells: effects of relative translation versus rotation. *Hippocampus* 13:604–617.

Kohonen T (1982) Self-organized formation of topologically correct feature maps. *Biological cybernetics* 43:59–69.

Kolarik BS, Shahlaie K, Hassan A, Borders AA, Kaufman KC, Gurkoff G, Yonelinas AP, Ekstrom AD (2016) Impairments in precision, rather than spatial strategy, characterize performance on the virtual Morris Water Maze: A case study. *Neuropsychologia* 80:90–101.

Konishi K, Bhat V, Banner H, Poirier J, Joobar R, Bohbot VD (2016) APOE2 Is Associated with Spatial Navigational Strategies and Increased Gray Matter in the Hippocampus. *Front Hum Neurosci* 10 Available at: <https://www.frontiersin.org/articles/10.3389/fnhum.2016.00349/full> [Accessed December 22, 2018].

Konishi K, Bohbot VD (2013) Spatial navigational strategies correlate with gray matter in the hippocampus of healthy older adults tested in a virtual maze. *Frontiers in aging neuroscience* 5:1.

Konishi K, Etchamendy N, Roy S, Marighetto A, Rajah N, Bohbot VD (2013) Decreased functional magnetic resonance imaging activity in the hippocampus in favor of the caudate nucleus in older adults tested in a virtual navigation task. *Hippocampus* 23:1005–1014.

Kropff E, Carmichael JE, Moser M-B, Moser EI (2015) Speed cells in the medial entorhinal cortex. *Nature* 523:419–424.

Krupic J, Bauza M, Burton S, Barry C, O'Keefe J (2015) Grid cell symmetry is shaped by environmental geometry. *Nature* 518:232–

235.

- Kumar A, Foster TC (2005) Intracellular calcium stores contribute to increased susceptibility to LTD induction during aging. *Brain Research* 1031:125–128.
- Kumar A, Foster TC (2007) Shift in Induction Mechanisms Underlies an Age-Dependent Increase in DHPG-Induced Synaptic Depression at CA3–CA1 Synapses. *Journal of Neurophysiology* 98:2729–2736.
- Kunz L, Schröder TN, Lee H, Montag C, Lachmann B, Sariyska R, Reuter M, Stirnberg R, Stöcker T, Messing-Floeter PC (2015) Reduced grid-cell-like representations in adults at genetic risk for Alzheimer's disease. *Science* 350:430–433.
- Laczó J, Andel R, Vyhnalek M, Matoska V, Kaplan V, Nedelska Z, Lerch O, Gazova I, Moffat SD, Hort J (2015) The effect of TOMM40 on spatial navigation in amnesic mild cognitive impairment. *Neurobiology of Aging* 36:2024–2033.
- Laczo J, Andel R, Vyhnalek M, Vlcek K, Magerova H, Varjassyova A, Tolar M, Hort J (2010) Human analogue of the morris water maze for testing subjects at risk of Alzheimer's disease. *Neurodegenerative Diseases* 7:148–152.
- Lalonde-Parsi M-J, Lamontagne A (2015) Perception of self-motion and regulation of walking speed in young-old adults. *Motor control* 19:191–206.
- Landfield PW, Lynch G (1977) Impaired Monosynaptic Potentiation in in Vitro Hippocampal Slices From Aged, Memory-deficient Rats. *J Gerontol* 32:523–533.
- Landfield PW, McGaugh JL, Lynch G (1978) Impaired synaptic potentiation processes in the hippocampus of aged, memory-deficient rats. *Brain research* 150:85–101.
- Landfield PW, Pitler TA, Applegate MD (1986) The effects of high Mg²⁺-to-Ca²⁺ ratios on frequency potentiation in hippocampal slices of young and aged rats. *Journal of Neurophysiology* 56:797–811.
- Lee I, Rao G, Knierim JJ (2004a) A double dissociation between hippocampal subfields: differential time course of CA3 and CA1 place cells for processing changed environments. *Neuron* 42:803–815.
- Lee I, Yoganarasimha D, Rao G, Knierim JJ (2004b) Comparison of population coherence of place cells in hippocampal subfields CA1

and CA3. *Nature* 430:456–459.

- Lenck-Santini PP, Muller RU, Save E, Poucet B (2002) Relationships between place cell firing fields and navigational decisions by rats. *The Journal of neuroscience* 22:9035–9047.
- Lenck-Santini P-P, Save E, Poucet B (2001) Evidence for a relationship between place-cell spatial firing and spatial memory performance. *Hippocampus* 11:377–390.
- Leutgeb S, Leutgeb JK, Treves A, Moser M-B, Moser EI (2004) Distinct Ensemble Codes in Hippocampal Areas CA3 and CA1. *Science* 305:1295–1298.
- Lever C, Burton S, Jeewajee A, O’Keefe J, Burgess N (2009) Boundary vector cells in the subiculum of the hippocampal formation. *The Journal of Neuroscience* 29:9771–9777.
- Lever C, Wills T, Cacucci F, Burgess N, O’Keefe J (2002) Long-term plasticity in hippocampal place-cell representation of environmental geometry. *Nature* 416:90–94.
- Levere TE, Walker A (1992) Old age and cognition: Enhancement of recent memory in aged rats by the calcium channel blocker nimodipine. *Neurobiology of Aging* 13:63–66.
- Levy WB, Steward O (1979) Synapses as associative memory elements in the hippocampal formation. *Brain Research* 175:233–245.
- Liang Z, Yang Y, Li G, Zhang J, Wang Y, Zhou Y, Leventhal AG (2010) Aging affects the direction selectivity of MT cells in rhesus monkeys. *Neurobiology of Aging* 31:863–873.
- Lich M, Bremmer F (2014) Self-motion perception in the elderly. *Frontiers in human neuroscience* 8:681.
- Lindner MD (1997) Reliability, Distribution, and Validity of Age-Related Cognitive Deficits in the Morris Water Maze. *Neurobiology of Learning and Memory* 68:203–220.
- Lipman PD (1991) Age and exposure differences in acquisition of route information. *Psychology and aging* 6:128.
- Lippa AS, Loullis CC, Rotrosen J, Cordasco DM, Critchett DJ, Joseph JA (1985) Conformational changes in muscarinic receptors may produce diminished cholinergic neurotransmission and memory deficits in aged rats. *Neurobiology of Aging* 6:317–323.

- Lister JP, Barnes CA (2009) Neurobiological changes in the hippocampus during normative aging. *Arch Neurol* 66:829–833.
- Liu I, Levy RM, Barton JJ, Iaria G (2011) Age and gender differences in various topographical orientation strategies. *Brain research* 1410:112–119.
- Liu P, Zhang H, Devaraj R, Ganesalingam GS, Smith PF (2010) A multivariate analysis of the effects of aging on glutamate, GABA and arginine metabolites in the rat vestibular nucleus. *Hearing Research* 269:122–133.
- Loomis JM, Klatzky RL, Golledge RG, Cicinelli JG, Pellegrino JW, Fry PA (1993) Nonvisual navigation by blind and sighted: Assessment of path integration ability. *Journal of Experimental Psychology: General* 122:73–91.
- Lövdén M, Schaefer S, Noack H, Bodammer NC, Kühn S, Heinze H-J, Düzel E, Bäckman L, Lindenberger U (2012) Spatial navigation training protects the hippocampus against age-related changes during early and late adulthood. *Neurobiology of aging* 33:620–e9.
- Lynch GS, Dunwiddie T, Gribkoff V (1977) Heterosynaptic depression: a postsynaptic correlate of long-term potentiation. *Nature* 266:737–739.
- MacDonald CJ, Lepage KQ, Eden UT, Eichenbaum H (2011) Hippocampal “Time Cells” Bridge the Gap in Memory for Discontiguous Events. *Neuron* 71:737–749.
- Maguire EA, Frith CD, Burgess N, Donnett JG, O’Keefe J (1998) Knowing where things are: Parahippocampal involvement in encoding object locations in virtual large-scale space. *Journal of cognitive neuroscience* 10:61–76.
- Mahmood O, Adamo D, Briceno E, Moffat SD (2009) Age differences in visual path integration. *Behavioural brain research* 205:88–95.
- Manaye KF, McIntire DD, Mann DM, German DC (1995) Locus coeruleus cell loss in the aging human brain: A non-random process. *Journal of Comparative Neurology* 358:79–87.
- Mankin EA, Sparks FT, Slayyeh B, Sutherland RJ, Leutgeb S, Leutgeb JK (2012) Neuronal code for extended time in the hippocampus. *PNAS* 109:19462–19467.
- Margules J, Gallistel CR (1988) Heading in the rat: Determination by environmental shape. *Animal Learning & Behavior* 16:404–410.

- Marr D (1971) Simple memory: a theory for archicortex. *Philosophical Transactions of the Royal Society of London Series B, Biological Sciences* 262:23–81.
- Martin MM, Horn KL, Kusman KJ, Wallace DG (2007) Medial septum lesions disrupt exploratory trip organization: Evidence for septohippocampal involvement in dead reckoning. *Physiology & Behavior* 90:412–424.
- Matthews BL, Ryu JH, Bockaneck C (1989) Vestibular contribution to spatial orientation. *Acta Oto-Laryngologica* 108:149–154.
- McGauran AMT, Harvey D, Cunningham L, Craig S, Commins S (2004) Retention of cue-based associations in the water maze is time-dependent and sensitive to disruption by rotating the starting position. *Behavioural brain research* 151:255–266.
- McHugh TJ, Blum KI, Tsien JZ, Tonegawa S, Wilson MA (1996) Impaired Hippocampal Representation of Space in CA1-Specific NMDAR1 Knockout Mice. *Cell* 87:1339–1349.
- McNaughton BL, Barnes CA, Gerrard JL, Gothard K, Jung MW, Knierim JJ, Kudrimoti H, Qin Y, Skaggs WE, Suster M, Weaver KL (1996) Deciphering the hippocampal polyglot: the hippocampus as a path integration system. *J Exp Biol* 199:173–185.
- McNaughton BL, Battaglia FP, Jensen O, Moser EI, Moser M-B (2006) Path integration and the neural basis of the “cognitive map.” *Nature Reviews Neuroscience* 7:663–678.
- McNaughton BL, Chen LL, Markus EJ (1991) “Dead reckoning,” landmark learning, and the sense of direction: A neurophysiological and computational hypothesis. *Journal of Cognitive Neuroscience* 3:190–202.
- McNaughton BL, Morris RGM (1987) Hippocampal synaptic enhancement and information storage within a distributed memory system. *Trends in Neurosciences* 10:408–415.
- McQuail JA, Beas BS, Kelly KB, Simpson KL, Frazier CJ, Setlow B, Bizon JL (2016) NR2A-containing NMDARs in the prefrontal cortex are required for working memory and associated with age-related cognitive decline. *Journal of Neuroscience* 36:12537–12548.
- Mehta MR, Quirk MC, Wilson MA (2000) Experience-Dependent Asymmetric Shape of Hippocampal Receptive Fields. *Neuron* 25:707–715.

- Meilinger T, Strickrodt M, Bühlhoff HH (2016) Qualitative differences in memory for vista and environmental spaces are caused by opaque borders, not movement or successive presentation. *Cognition* 155:77–95.
- Ménard C, Quirion R (2012a) Successful cognitive aging in rats: a role for mGluR5 glutamate receptors, homer 1 proteins and downstream signaling pathways. *PLoS One* 7:e28666.
- Ménard C, Quirion R (2012b) Successful Cognitive Aging in Rats: A Role for mGluR5 Glutamate Receptors, Homer 1 Proteins and Downstream Signaling Pathways Mattson MP, ed. *PLoS ONE* 7:e28666.
- Merrill DA, Chiba AA, Tuszynski MH (2001) Conservation of neuronal number and size in the entorhinal cortex of behaviorally characterized aged rats. *J Comp Neurol* 438:445–456.
- Meulenbroek O, Petersson KM, Voermans N, Weber B, Fernández G (2004) Age differences in neural correlates of route encoding and route recognition. *NeuroImage* 22:1503–1514.
- Miller S, Potegal M, Abraham L (1983) Vestibular involvement in a passive transport and return task. *Physiological Psychology* 11:1–10.
- Mitchell SJ, Ranck Jr JB (1980) Generation of theta rhythm in medial entorhinal cortex of freely moving rats. Available at: <http://deepblue.lib.umich.edu/handle/2027.42/23244> [Accessed December 6, 2012].
- Mitolo M, Borella E, Meneghetti C, Carbone E, Pazzaglia F (2017) How to enhance route learning and visuo-spatial working memory in aging: a training for residential care home residents. *Aging & mental health* 21:562–570.
- Mittelstaedt M-L, Mittelstaedt H (1980) Homing by path integration in a mammal. *Naturwissenschaften* 67:566–567.
- Mizumori SJ, Williams JD (1993) Directionally selective mnemonic properties of neurons in the lateral dorsal nucleus of the thalamus of rats. *The Journal of neuroscience* 13:4015–4028.
- Mizuseki K, Sirota A, Pastalkova E, Buzsáki G (2009) Theta Oscillations Provide Temporal Windows for Local Circuit Computation in the Entorhinal-Hippocampal Loop. *Neuron* 64:267–280.
- Moffat SD (2009) Aging and Spatial Navigation: What Do We Know and Where Do We Go? *Neuropsychol Rev* 19:478–489.

- Moffat SD, Elkins W, Resnick SM (2006) Age differences in the neural systems supporting human allocentric spatial navigation. *Neurobiology of aging* 27:965–972.
- Moffat SD, Kennedy KM, Rodrigue KM, Raz N (2007) Extrahippocampal Contributions to Age Differences in Human Spatial Navigation. *Cereb Cortex* 17:1274–1282.
- Moffat SD, Resnick SM (2002) Effects of age on virtual environment place navigation and allocentric cognitive mapping. *Behavioral Neuroscience* 116:851–859.
- Moffat SD, Zonderman AB, Resnick SM (2001) Age differences in spatial memory in a virtual environment navigation task. *Neurobiol Aging* 22:787–796.
- Mokrisova I, Laczó J, Andel R, Gazova I, Vyhnalek M, Nedelska Z, Levcik D, Cerman J, Vlcek K, Hort J (2016) Real-space path integration is impaired in Alzheimer's disease and mild cognitive impairment. *Behavioural brain research* 307:150–158.
- Moore CI, Browning MD, Rose GM (1993) Hippocampal plasticity induced by primed burst, but not long-term potentiation, stimulation is impaired in area CA1 of aged fischer 344 rats. *Hippocampus* 3:57–66.
- Morris RGM, Garrud P, Rawlins JNP, O'Keefe J (1982) Place navigation impaired in rats with hippocampal lesions. *Nature* 297:681–683.
- Moser EI, Kropff E, Moser M-B (2008) Place Cells, Grid Cells, and the Brain's Spatial Representation System. *Annual Review of Neuroscience* 31:69–89.
- Moser EI, Moser M-B (2008) A metric for space. *Hippocampus* 18:1142–1156.
- Muir GM, Brown JE, Carey JP, Hirvonen TP, Della Santina CC, Minor LB, Taube JS (2009) Disruption of the head direction cell signal after occlusion of the semicircular canals in the freely moving chinchilla. *J Neurosci* 29:14521–14533.
- Müller G, Pilzecker A (1900) Experimental contributions to the theory of memory. *Z Psychol Z Angew Psychol* 1:1–288.
- Muller RU, Kubie JL (1987) The effects of changes in the environment on the spatial firing of hippocampal complex-spike cells. *The Journal of neuroscience* 7:1951–1968.

- Neunuebel JP, Yoganarasimha D, Rao G, Knierim JJ (2013) Conflicts between Local and Global Spatial Frameworks Dissociate Neural Representations of the Lateral and Medial Entorhinal Cortex. *J Neurosci* 33:9246–9258.
- Nicholson DA, Yoshida R, Berry RW, Gallagher M, Geinisman Y (2004) Reduction in Size of Perforated Postsynaptic Densities in Hippocampal Axospinous Synapses and Age-Related Spatial Learning Impairments. *J Neurosci* 24:7648–7653.
- Nicolle MM, Prescott S, Bizon JL (2003) Emergence of a Cue Strategy Preference on the Water Maze Task in Aged C57B6 × SJL F1 Hybrid Mice. *Learn Mem* 10:520–524.
- Nieuwenhuys R, Geeraedts LMG, Veening JG (1982) The medial forebrain bundle of the rat. I. General introduction. *Journal of Comparative Neurology* 206:49–81.
- Noack H, Lövdén M, Schmiedek F (2014) On the validity and generality of transfer effects in cognitive training research. *Psychological research* 78:773–789.
- Norman JF, Adkins OC, Pedersen LE, Reyes CM, Wulff RA, Tungate A (2015) The visual perception of exocentric distance in outdoor settings. *Vision research* 117:100–104.
- Norman JF, Crabtree CE, Bartholomew AN, Ferrell EL (2009) Aging and the perception of slant from optical texture, motion parallax, and binocular disparity. *Perception & Psychophysics* 71:116–130.
- Norris CM, Korol DL, Foster TC (1996) Increased susceptibility to induction of long-term depression and long-term potentiation reversal during aging. *The journal of neuroscience* 16:5382–5392.
- Nyakas C, Oosterink BJ, Keijsers J, Felszeghy K, de Jong GI, Korf J, Luiten PGM (1997) Selective decline of 5-HT_{1A} receptor binding sites in rat cortex, hippocampus and cholinergic basal forebrain nuclei during aging. *Journal of Chemical Neuroanatomy* 13:53–61.
- O'Keefe J, Burgess N (1996) Geometric determinants of the place fields of hippocampal neurons. *Nature* 381:425.
- O'Keefe J, Burgess N (2005a) Dual phase and rate coding in hippocampal place cells: theoretical significance and relationship to entorhinal grid cells. *Hippocampus* 15:853–866.
- O'Keefe J, Burgess N (2005b) Dual phase and rate coding in hippocampal place cells: theoretical significance and relationship to entorhinal

- grid cells. *Hippocampus* 15:853–866.
- O'Keefe J, Conway DH (1978) Hippocampal place units in the freely moving rat: why they fire where they fire. *Experimental Brain Research* 31:573–590.
- O'Keefe J, Conway DH (1980) On the trail of the hippocampal engram. *Psychobiology* 8:229–238.
- O'Keefe J, Dostrovsky J (1971) The hippocampus as a spatial map: Preliminary evidence from unit activity in the freely-moving rat. *Brain research* 34:171–175.
- O'Keefe J, Nadel L (1978) *The hippocampus as a cognitive map*. Oxford: Clarendon Press.
- O'Keefe J, Recce ML (1993) Phase relationship between hippocampal place units and the EEG theta rhythm. *Hippocampus* 3:317–330.
- O'Keefe J, Speakman A (1987) Single unit activity in the rat hippocampus during a spatial memory task. *Experimental Brain Research* 68:1–27.
- Oler JA, Markus EJ (1998) Age-related deficits on the radial maze and in fear conditioning: Hippocampal processing and consolidation. *Hippocampus* 8:402–415.
- Olypher AV, Lánský P, Fenton AA (2002) Properties of the extra-positional signal in hippocampal place cell discharge derived from the overdispersion in location-specific firing. *Neuroscience* 111:553–566.
- O'Neill J, Pleydell-Bouverie B, Dupret D, Csicsvari J (2010) Play it again: reactivation of waking experience and memory. *Trends in Neurosciences* 33:220–229.
- O'Reilly RC, McClelland JL (1994) Hippocampal conjunctive encoding, storage, and recall: avoiding a trade-off. *Hippocampus* 4:661–682.
- Ovsepian SV, Anwyl R, Rowan MJ (2004) Endogenous acetylcholine lowers the threshold for long-term potentiation induction in the CA1 area through muscarinic receptor activation: in vivo study. *European Journal of Neuroscience* 20:1267–1275.
- Owsley C (2011) Aging and vision. *Vision Research* 51:1610–1622.
- Pai M-C, Yang Y-C (2013) Impaired translation of spatial representation in young onset Alzheimer's disease patients. *Current Alzheimer*

Research 10:95–103.

- Pastalkova E, Itskov V, Amarasingham A, Buzsáki G (2008) Internally Generated Cell Assembly Sequences in the Rat Hippocampus. *Science* 321:1322–1327.
- Pavlidis C, Greenstein YJ, Grudman M, Winson J (1988) Long-term potentiation in the dentate gyrus is induced preferentially on the positive phase of Theta-rhythm. *Brain research* 439:383–387.
- Paxinos G, Watson C (2013) *The Rat Brain in Stereotaxic Coordinates*, Seventh Edition. Academic press.
- Pengas G, Hodges JR, Watson P, Nestor PJ (2010) Focal posterior cingulate atrophy in incipient Alzheimer's disease. *Neurobiology of Aging* 31:25–33.
- Pengas G, Williams G, Acosta-Cabronero J, Ash T, Hong Y, Izquierdo-Garcia D, Fryer T, Hodges J, Nestor P (2012) The relationship of topographical memory performance to regional neurodegeneration in Alzheimer's disease. *Frontiers in aging neuroscience* 4:17.
- Pérez-Escobar JA, Kornienko O, Latuske P, Kohler L, Allen K (2016) Visual landmarks sharpen grid cell metric and confer context specificity to neurons of the medial entorhinal cortex. *eLife* 5:e16937.
- Persson K, Bohbot VD, Bogdanovic N, Selbæk G, Bråekhus A, Engedal K (2018) Finding of increased caudate nucleus in patients with Alzheimer's disease. *Acta Neurologica Scandinavica* 137:224–232.
- Pfefferbaum A, Adalsteinsson E, Sullivan EV (2005) Frontal circuitry degradation marks healthy adult aging: evidence from diffusion tensor imaging. *Neuroimage* 26:891–899.
- Pfeiffer BE, Foster DJ (2013) Hippocampal place-cell sequences depict future paths to remembered goals. *Nature* 497:74–79.
- Pinto DJ, Brumberg JC, Simons DJ, Ermentrout GB, Traub R (1996) A quantitative population model of whisker barrels: re-examining the Wilson-Cowan equations. *Journal of computational neuroscience* 3:247–264.
- Pistell PJ, Spangler EL, Kelly-Bell B, Miller MG, de Cabo R, Ingram DK (2012) Age-associated learning and memory deficits in two mouse versions of the Stone T-maze. *Neurobiology of aging* 33:2431–2439.

- Potegal M, Day MJ, Abraham L (1977) Maze orientation, visual and vestibular cues in two-maze spontaneous alternation of rats. *Psychobiology* 5:414–420.
- Powell NJ, Redish AD (2016) Representational changes of latent strategies in rat medial prefrontal cortex precede changes in behaviour. *Nature communications* 7:12830.
- Ranck JB (1985) Head direction cells in the deep cell layer of dorsolateral pre-subiculum in freely moving rats. *Electrical activity of the archicortex*.
- Rapp PR (1990) Visual discrimination and reversal learning in the aged monkey (*Macaca mulatta*). *Behavioral neuroscience* 104:876.
- Rapp PR, Kansky MT, Roberts JA (1997) Impaired spatial information processing in aged monkeys with preserved recognition memory. *Neuroreport* 8:1923–1928.
- Rapp PR, Rosenberg RA, Gallagher M (1987) An evaluation of spatial information processing in aged rats. *Behavioral neuroscience* 101:3.
- Ravassard P, Kees A, Willers B, Ho D, Aharoni D, Cushman J, Aghajian ZM, Mehta MR (2013) Multisensory Control of Hippocampal Spatiotemporal Selectivity. *Science* 340:1342–1346.
- Redish AD (1999) *Beyond the cognitive map: From place cells to episodic memory*. MIT Press.
- Redish AD, Elga AN, Touretzky DS (1996) A coupled attractor model of the rodent head direction system. *Network: Computation in Neural Systems* 7:671–685.
- Redish AD, McNaughton BL, Barnes CA (1998) Reconciling Barnes et al.(1997) and Tanila et al.(1997a, b). *Hippocampus* 8:438–443.
- Redish AD, Rosenzweig ES, Bohanick JD, McNaughton BL, Barnes CA (2000) Dynamics of hippocampal ensemble activity realignment: time versus space. *The Journal of Neuroscience* 20:9298–9309.
- Redish AD, Touretzky DS (1997) Cognitive maps beyond the hippocampus. *Hippocampus* 7:15–35.
- Rich EL, Shapiro M (2009) Rat prefrontal cortical neurons selectively code strategy switches. *Journal of Neuroscience* 29:7208–7219.
- Rickgauer JP, Deisseroth K, Tank DW (2014) Simultaneous cellular-

- resolution optical perturbation and imaging of place cell firing fields. *Nat Neurosci* 17:1816–1824.
- Riekkinen M, Schmidt B, Kuitunen J, Riekkinen Jr P (1997) Effects of combined chronic nimodipine and acute metrifonate treatment on spatial and avoidance behavior. *European Journal of Pharmacology* 322:1–9.
- Robillard JM, Gordon GR, Choi HB, Christie BR, MacVicar BA (2011) Glutathione Restores the Mechanism of Synaptic Plasticity in Aged Mice to That of the Adult. *PLOS ONE* 6:e20676.
- Rodgers MK, Sindone JA, Moffat SD (2012) Effects of age on navigation strategy. *Neurobiology of Aging* 33:202.e15-202.e22.
- Roditi RE, Crane BT (2012) Directional asymmetries and age effects in human self-motion perception. *Journal of the Association for Research in Otolaryngology* 13:381–401.
- Rogalski E, Stebbins GT, Barnes CA, Murphy CM, Stoub TR, George S, Ferrari C, Shah RC, deToledo-Morrell L (2012) Age-related changes in parahippocampal white matter integrity: A diffusion tensor imaging study. *Neuropsychologia* 50:1759–1765.
- Rondi-Reig L, Petit GH, Tobin C, Tonegawa S, Mariani J, Berthoz A (2006) Impaired Sequential Egocentric and Allocentric Memories in Forebrain-Specific–NMDA Receptor Knock-Out Mice during a New Task Dissociating Strategies of Navigation. *J Neurosci* 26:4071–4081.
- Rose GM, Ong VS, Woodruff-Pak DS (2007) Efficacy of MEM 1003, a novel calcium channel blocker, in delay and trace eyeblink conditioning in older rabbits. *Neurobiology of Aging* 28:766–773.
- Rosenzweig ES, Rao G, McNaughton BL, Barnes CA (1997) Role of temporal summation in age-related long-term potentiation–induction deficits. *Hippocampus* 7:549–558.
- Rosenzweig ES, Redish AD, McNaughton BL, Barnes CA (2003) Hippocampal map realignment and spatial learning. *Nature Neuroscience* 6:609–615.
- Salz DM, Tiganj Z, Khasnabish S, Kohley A, Sheehan D, Howard MW, Eichenbaum H (2016) Time Cells in Hippocampal Area CA3. *J Neurosci* 36:7476–7484.
- Samsonovich A, McNaughton BL (1997) Path integration and cognitive mapping in a continuous attractor neural network model. *The*

Journal of Neuroscience 17:5900–5920.

- Sandin M, Jasmin S, Levere TE (1990) Aging and cognition: Facilitation of recent memory in aged nonhuman primates by nimodipine. *Neurobiology of Aging* 11:573–575.
- Sarel A, Finkelstein A, Las L, Ulanovsky N (2017) Vectorial representation of spatial goals in the hippocampus of bats. *Science* 355:176–180.
- Sargolini F, Fyhn M, Hafting T, McNaughton BL, Witter MP, Moser EI (2006) Conjunctive Representation of Position, Direction, and Velocity in Entorhinal Cortex. *Science* 312:758–762.
- Savelli F, Knierim JJ (2010) Hebbian analysis of the transformation of medial entorhinal grid-cell inputs to hippocampal place fields. *Journal of neurophysiology* 103:3167–3183.
- Schimanski LA, Lipa P, Barnes CA (2013) Tracking the Course of Hippocampal Representations during Learning: When Is the Map Required? *J Neurosci* 33:3094–3106.
- Schliebs R, Arendt T (2011) The cholinergic system in aging and neuronal degeneration. *Behavioural Brain Research* 221:555–563.
- Schuck NW, Doeller CF, Schjerve B-MM, Schröder J, Frensch PA, Bertram L, Li S-C (2013) Aging and KIBRA/WWC1 genotype affect spatial memory processes in a virtual navigation task. *Hippocampus* 23:919–930.
- Seelig JD, Jayaraman V (2015) Neural dynamics for landmark orientation and angular path integration. *Nature* 521:186–191.
- Semenov LV, Bures J (1989) Vestibular stimulation disrupts acquisition of place navigation in the Morris water tank task. *Behavioral and neural biology* 51:346–363.
- Serino S, Cipresso P, Morganti F, Riva G (2014) The role of egocentric and allocentric abilities in Alzheimer’s disease: a systematic review. *Ageing research reviews* 16:32–44.
- Serino S, Riva G (2013) Getting lost in Alzheimer’s disease: a break in the mental frame syncing. *Medical hypotheses* 80:416–421.
- Shankar S, Teyler TJ, Robbins N (1998) Aging differentially alters forms of long-term potentiation in rat hippocampal area CA1. *Journal of neurophysiology* 79:334–341.
- Shapiro ML, Tanila H, Eichenbaum H (1997) Cues that hippocampal place

- cells encode: dynamic and hierarchical representation of local and distal stimuli. *Hippocampus* 7:624–642.
- Sharp PE (1991) Computer simulation of hippocampal place cells. *Psychobiology* 19:103–115.
- Sharp PE, Blair HT, Etkin D, Tzanetos DB (1995) Influences of vestibular and visual motion information on the spatial firing patterns of hippocampal place cells. *The Journal of neuroscience* 15:173–189.
- Shen J, Barnes CA (1996) Age-related decrease in cholinergic synaptic transmission in three hippocampal subfields. *Neurobiology of Aging* 17:439–451.
- Shen J, Barnes CA, McNaughton BL, Skaggs WE, Weaver KL (1997) The effect of aging on experience-dependent plasticity of hippocampal place cells. *The Journal of neuroscience* 17:6769–6782.
- Shinder ME, Taube JS (2011) Active and passive movement are encoded equally by head direction cells in the anterodorsal thalamus. *J Neurophysiol* 106:788–800.
- Shine JP, Valdés-Herrera JP, Hegarty M, Wolbers T (2016) The human retrosplenial cortex and thalamus code head direction in a global reference frame. *Journal of Neuroscience* 36:6371–6381.
- Simieli L, Barbieri FA, Orcioli-Silva D, Lirani-Silva E, Stella F, Gobbi LTB (2015) Obstacle crossing with dual tasking is a danger for individuals with Alzheimer's disease and for healthy older people. *Journal of Alzheimer's Disease* 43:435–441.
- Singer AC, Carr MF, Karlsson MP, Frank LM (2013) Hippocampal SWR activity predicts correct decisions during the initial learning of an alternation task. *Neuron* 77:1163–1173.
- Sirota A, Montgomery S, Fujisawa S, Isomura Y, Zugaro M, Buzsáki G (2008) Entrainment of neocortical neurons and gamma oscillations by the hippocampal theta rhythm. *Neuron* 60:683.
- Skaggs WE, Knierim JJ, Kudrimoti HS, McNaughton BL (1995) A model of the neural basis of the rat's sense of direction. In: *Advances in neural information processing systems*, pp 173–180.
- Skaggs WE, McNaughton BL, Wilson MA, Barnes CA (1996) Theta phase precession in hippocampal neuronal populations and the compression of temporal sequences. *Hippocampus* 6:149–172.
- Small SA, Chawla MK, Buonocore M, Rapp PR, Barnes CA (2004)

Imaging correlates of brain function in monkeys and rats isolates a hippocampal subregion differentially vulnerable to aging. *Proceedings of the National Academy of Sciences of the United States of America* 101:7181–7186.

Smith TD, Adams MM, Gallagher M, Morrison JH, Rapp PR (2000) Circuit-specific alterations in hippocampal synaptophysin immunoreactivity predict spatial learning impairment in aged rats. *The Journal of Neuroscience* 20:6587–6593.

Solomon PR, Wood MS, Groccia-Ellison ME, Yang B-Y, Fanelli RJ, Mervis RF (1995) Nimodipine facilitates retention of the classically conditioned nictitating membrane response in aged rabbits over long retention intervals. *Neurobiology of Aging* 16:791–796.

Solstad T, Boccara CN, Kropff E, Moser M-B, Moser EI (2008) Representation of Geometric Borders in the Entorhinal Cortex. *Science* 322:1865–1868.

Solstad T, Moser EI, Einevoll GT (2006) From grid cells to place cells: A mathematical model. *Hippocampus* 16:1026–1031.

Sonntag WE, Bennett SA, Khan AS, Thornton PL, Xu X, Ingram RL, Brunso-Bechtold JK (2000) Age and insulin-like growth factor-1 modulate N-methyl-D-aspartate receptor subtype expression in rats. *Brain research bulletin* 51:331–338.

Spencer RM, Gouw AM, Ivry RB (2007) Age-related decline of sleep-dependent consolidation. *Learning & Memory* 14:480–484.

Stackman RW, Clark AS, Taube JS (2002) Hippocampal spatial representations require vestibular input. *Hippocampus* 12:291–303.

Stackman RW, Herbert AM (2002) Rats with lesions of the vestibular system require a visual landmark for spatial navigation. *Behavioural Brain Research* 128:27–40.

Stackman RW, Taube JS (1997) Firing Properties of Head Direction Cells in the Rat Anterior Thalamic Nucleus: Dependence on Vestibular Input. *J Neurosci* 17:4349–4358.

Stensola H, Stensola T, Solstad T, Frøland K, Moser M-B, Moser EI (2012) The entorhinal grid map is discretized. *Nature* 492:72–78.

Stensola T, Stensola H, Moser M-B, Moser EI (2015) Shearing-induced asymmetry in entorhinal grid cells. *Nature* 518:207–212.

Stone CP (1929) The age factor in animal learning: I. Rats in the problem

box and the maze. *Genetic Psychology Monographs*.

Storsve AB, Fjell AM, Tamnes CK, Westlye LT, Overbye K, Aasland HW, Walhovd KB (2014) Differential longitudinal changes in cortical thickness, surface area and volume across the adult life span: regions of accelerating and decelerating change. *Journal of Neuroscience* 34:8488–8498.

Stranahan AM, Mattson MP, Stranahan AM, Mattson MP (2010) Selective Vulnerability of Neurons in Layer II of the Entorhinal Cortex during Aging and Alzheimer's Disease, Selective Vulnerability of Neurons in Layer II of the Entorhinal Cortex during Aging and Alzheimer's Disease. *Neural Plasticity, Neural Plasticity* 2010, 2010:e108190.

Suzuki S, Augerinos G, Black AH (1980) Stimulus control of spatial behavior on the eight-arm maze in rats. *Learning and Motivation* 11:1–18.

Tait DS, Brown VJ, Farovik A, Theobald DE, Dalley JW, Robbins TW (2007a) Lesions of the dorsal noradrenergic bundle impair attentional set-shifting in the rat. *European Journal of Neuroscience* 25:3719–3724.

Tait DS, Brown VJ, Farovik A, Theobald DE, Dalley JW, Robbins TW (2007b) Lesions of the dorsal noradrenergic bundle impair attentional set-shifting in the rat. *European Journal of Neuroscience* 25:3719–3724.

Tang W, Shin JD, Frank LM, Jadhav SP (2017) Hippocampal-prefrontal reactivation during learning is stronger in awake as compared to sleep states. *Journal of Neuroscience*:2291–17.

Tang Y-P, Shimizu E, Dube GR, Rampon C, Kerchner GA, Zhuo M, Liu G, Tsien JZ (1999) Genetic enhancement of learning and memory in mice. *Nature* 401:63–69.

Tanila H, Shapiro M, Gallagher M, Eichenbaum H (1997a) Brain aging: changes in the nature of information coding by the hippocampus. *The Journal of neuroscience* 17:5155–5166.

Tanila H, Sipilä P, Shapiro M, Eichenbaum H (1997b) Brain aging: impaired coding of novel environmental cues. *The Journal of neuroscience* 17:5167–5174.

Taube JS (2007) The head direction signal: origins and sensory-motor integration. *Annu Rev Neurosci* 30:181–207.

Taube JS, Muller RU, Ranck Jr JB (1990a) Head-direction cells recorded

- from the postsubiculum in freely moving rats. I. Description and quantitative analysis. *The Journal of Neuroscience* 10:420–435.
- Taube JS, Muller RU, Ranck Jr JB (1990b) Head-direction cells recorded from the postsubiculum in freely moving rats. II. Effects of environmental manipulations. *The Journal of Neuroscience* 10:436–447.
- Tcheang L, Bühlhoff HH, Burgess N (2011) Visual influence on path integration in darkness indicates a multimodal representation of large-scale space. *Proceedings of the National Academy of Sciences*:201011843.
- Thibault O, Landfield PW (1996) Increase in Single L-Type Calcium Channels in Hippocampal Neurons During Aging. *Science* 272:1017–1020.
- Thomé A, Gray DT, Erickson CA, Lipa P, Barnes CA (2015) Memory impairment in aged primates is associated with region-specific network dysfunction. *Molecular psychiatry*.
- Topic B, Willuhn I, Palomero-Gallagher N, Zilles K, Huston J p., Hasenöhr R u. (2007) Impaired maze performance in aged rats is accompanied by increased density of NMDA, 5-HT1A, and α -adrenoceptor binding in hippocampus. *Hippocampus* 17:68–77.
- Treves A, Rolls ET (1994) Computational analysis of the role of the hippocampus in memory. *Hippocampus* 4:374–391.
- Trompet S, Westendorp RGJ, Kamper AM, de Craen AJM (2008) Use of calcium antagonists and cognitive decline in old age: The Leiden 85-plus study. *Neurobiology of Aging* 29:306–308.
- Tsao A, Moser M-B, Moser EI (2013) Traces of experience in the lateral entorhinal cortex. *Current Biology* 23:399–405.
- Tsodyks M (1999) Attractor neural network models of spatial maps in hippocampus. *Hippocampus* 9:481–489.
- Tsodyks M, Sejnowski T (1995) Associative memory and hippocampal place cells. *International journal of neural systems* 6:81–86.
- Ulanovsky N, Moss CF (2007) Hippocampal cellular and network activity in freely moving echolocating bats. *Nature Neuroscience* 10:224–233.
- van der Meer MAA, Knierim JJ, Yoganarasimha D, Wood ER, van Rossum MCW (2007) Anticipation in the Rodent Head Direction

System Can Be Explained by an Interaction of Head Movements and Vestibular Firing Properties. *Journal of Neurophysiology* 98:1883–1897.

- van Haeften T, Baks-te-Bulte L, Goede PH, Wouterlood FG, Witter MP (2003) Morphological and numerical analysis of synaptic interactions between neurons in deep and superficial layers of the entorhinal cortex of the rat. *Hippocampus* 13:943–952.
- Van Petten C (2004) Relationship between hippocampal volume and memory ability in healthy individuals across the lifespan: review and meta-analysis. *Neuropsychologia* 42:1394–1413.
- Vanderwolf CH (1969) Hippocampal electrical activity and voluntary movement in the rat. *Electroencephalography and Clinical Neurophysiology* 26:407–418.
- Vazdarjanova A, Guzowski JF (2004) Differences in Hippocampal Neuronal Population Responses to Modifications of an Environmental Context: Evidence for Distinct, Yet Complementary, Functions of CA3 and CA1 Ensembles. *J Neurosci* 24:6489–6496.
- Veng LM, Mesches MH, Browning MD (2003) Age-related working memory impairment is correlated with increases in the L-type calcium channel protein $\alpha 1D$ (Cav1.3) in area CA1 of the hippocampus and both are ameliorated by chronic nimodipine treatment. *Molecular Brain Research* 110:193–202.
- Vieweg P, Stangl M, Howard LR, Wolbers T (2015) Changes in pattern completion—A key mechanism to explain age-related recognition memory deficits? *Cortex* 64:343–351.
- Vinogradova OS (2001) Hippocampus as comparator: role of the two input and two output systems of the hippocampus in selection and registration of information. *Hippocampus* 11:578–598.
- von Engelhardt J, Doganci B, Jensen V, Hvalby Ø, Göngrich C, Taylor A, Barkus C, Sanderson DJ, Rawlins JNP, Seeburg PH, Bannerman DM, Monyer H (2008) Contribution of Hippocampal and Extra-Hippocampal NR2B-Containing NMDA Receptors to Performance on Spatial Learning Tasks. *Neuron* 60:846–860.
- Wallace DG, Hines DJ, Pellis SM, Whishaw IQ (2002) Vestibular Information Is Required for Dead Reckoning in the Rat. *J Neurosci* 22:10009–10017.
- Warren Jr WH, Blackwell AW, Morris MW (1989) Age differences in perceiving the direction of self-motion from optical flow. *Journal of*

gerontology 44:P147–P153.

- Weintraub S, Wicklund AH, Salmon DP (2012) The neuropsychological profile of Alzheimer disease. *Cold Spring Harbor perspectives in medicine*:a006171.
- Wenger E, Schaefer S, Noack H, Kühn S, Måartensson J, Heinze H-J, Düzel E, Bäckman L, Lindenberger U, Lövdén M (2012) Cortical thickness changes following spatial navigation training in adulthood and aging. *Neuroimage* 59:3389–3397.
- West GL, Drisdelle BL, Konishi K, Jackson J, Jolicoeur P, Bohbot VD (2015) Habitual action video game playing is associated with caudate nucleus-dependent navigational strategies. *Proceedings of the Royal Society B: Biological Sciences* 282:20142952–20142952.
- West RL (1996) An application of prefrontal cortex function theory to cognitive aging. *Psychological bulletin* 120:272.
- Wiegand J-PL, Gray DT, Schimanski LA, Lipa P, Barnes CA, Cowen SL (2016) Age is associated with reduced sharp-wave ripple frequency and altered patterns of neuronal variability. *Journal of Neuroscience* 36:5650–5660.
- Wiener JM, Büchner SJ, Hölscher C (2009) Taxonomy of human wayfinding tasks: A knowledge-based approach. *Spatial Cognition & Computation* 9:152–165.
- Wiener JM, de Condappa O, Harris MA, Wolbers T (2013) Maladaptive Bias for Extrahippocampal Navigation Strategies in Aging Humans. *Journal of Neuroscience* 33:6012–6017.
- Wiener JM, Kmecova H, de Condappa O (2012) Route repetition and route retracing: effects of cognitive aging. *Front Ag Neurosci* 4:7.
- Wiener SI, Taube JS (2005) *Head direction cells and the neural mechanisms of spatial orientation*. MIT Press.
- Wikenheiser AM, Redish AD (2011) Changes in reward contingency modulate the trial-to-trial variability of hippocampal place cells. *Journal of neurophysiology* 106:589–598.
- Wikenheiser AM, Redish AD (2015a) Hippocampal theta sequences reflect current goals. *Nat Neurosci* 18:289–294.
- Wikenheiser AM, Redish AD (2015b) Decoding the cognitive map: ensemble hippocampal sequences and decision making. *Current Opinion in Neurobiology* 32:8–15.

- Wilkniss SM, Jones MG, Korol DL, Gold PE, Manning CA (1997) Age-related differences in an ecologically based study of route learning. *Psychology and aging* 12:372.
- Wilson HR, Cowan JD (1972) Excitatory and inhibitory interactions in localized populations of model neurons. *Biophysical journal* 12:1–24.
- Wilson HR, Cowan JD (1973) A mathematical theory of the functional dynamics of cortical and thalamic nervous tissue. *Kybernetik* 13:55–80.
- Wilson IA, Gallagher M, Eichenbaum H, Tanila H (2006) Neurocognitive aging: prior memories hinder new hippocampal encoding. *Trends in neurosciences* 29:662–670.
- Wilson IA, Ikonen S, Gallagher M, Eichenbaum H, Tanila H (2005) Age-Associated Alterations of Hippocampal Place Cells Are Subregion Specific. *Journal of Neuroscience* 25:6877–6886.
- Wilson IA, Ikonen S, McMahan RW, Gallagher M, Eichenbaum H, Tanila H (2003) Place cell rigidity correlates with impaired spatial learning in aged rats. *Neurobiology of aging* 24:297–305.
- Wilson MA, McNaughton BL (1993) Dynamics of the hippocampal ensemble code for space. *Science* 261:1055–1058.
- Wilson MA, McNaughton BL (1994) Reactivation of hippocampal ensemble memories during sleep. *Science* 265:676–679.
- Winter JC (1997) The Effects of Age on Continuous Learning in the Radial Maze. *Physiology & Behavior* 61:609–612.
- Witter MP, Amaral DG (2004) Hippocampal Formation. In: *The Rat Nervous System (Third Edition)* (Paxinos G, ed), pp 635–704. Burlington: Academic Press.
- Wolbers T, Büchel C (2005) Dissociable retrosplenial and hippocampal contributions to successful formation of survey representations. *Journal of Neuroscience* 25:3333–3340.
- Wolbers T, Wiener JM (2014) Challenges for identifying the neural mechanisms that support spatial navigation: the impact of spatial scale. *Front Hum Neurosci* 8:571.
- Wolbers T, Wiener JM, Mallot HA, Büchel C (2007) Differential Recruitment of the Hippocampus, Medial Prefrontal Cortex, and the Human Motion Complex during Path Integration in Humans. *J*

Neurosci 27:9408–9416.

- Woodruff-Pak DS, Chi J, Li Y-T, Pak MH, Fanelli RJ (1997) Nimodipine Ameliorates Impaired Eyeblink Classical Conditioning in Older Rabbits in the Long-Delay Paradigm. *Neurobiology of Aging* 18:641–649.
- Wörtwein G, Saerup LH, Charlottenfeld-Stapov D, Mogensen J (1995) Place Learning by Fimbria-Fornix Transected Rats in a Modified Water Maze. *International Journal of Neuroscience* 82:71–81.
- Yang Z, Krause M, Rao G, McNaughton BL, Barnes CA (2008) Synaptic Commitment: Developmentally Regulated Reciprocal Changes in Hippocampal Granule Cell NMDA and AMPA Receptors Over the Lifespan. *Journal of Neurophysiology* 99:2760–2768.
- Yartsev MM, Witter MP, Ulanovsky N (2011) Grid cells without theta oscillations in the entorhinal cortex of bats. *Nature* 479:103+.
- Yassa MA, Mattfeld AT, Stark SM, Stark CEL (2011) Age-related memory deficits linked to circuit-specific disruptions in the hippocampus. *Proceedings of the National Academy of Sciences* 108:8873–8878.
- Yassa MA, Stark CEL (2011) Pattern separation in the hippocampus. *Trends in Neurosciences* 34:515–525.
- Yoganarasimha D, Knierim JJ (2004) Coupling between place cells and head direction cells during relative translations and rotations of distal landmarks. *Experimental Brain Research* 160:344–359.
- Yoganarasimha D, Yu X, Knierim JJ (2006) Head direction cell representations maintain internal coherence during conflicting proximal and distal cue rotations: comparison with hippocampal place cells. *The Journal of neuroscience* 26:622–631.
- Young JJ, Shapiro ML (2009) Double dissociation and hierarchical organization of strategy switches and reversals in the rat PFC. *Behavioral neuroscience* 123:1028.
- Zeidman P, Bullinaria JA (2008) Neural models of head-direction cells. In: *From associations to rules: Connectionist models of behavior and cognition*, pp 165–177. World Scientific.
- Zhang K (1996) Representation of spatial orientation by the intrinsic dynamics of the head-direction cell ensemble: a theory. *Journal of Neuroscience* 16:2112–2126.
- Zhang S-J, Ye J, Miao C, Tsao A, Cerniauskas I, Ledergerber D, Moser

- M-B, Moser EI (2013) Optogenetic Dissection of Entorhinal-Hippocampal Functional Connectivity. *Science* 340:1232627.
- Zhao X, Rosenke R, Kronemann D, Brim B, Das SR, Dunah AW, Magnusson KR (2009) The effects of aging on N-methyl-D-aspartate receptor subunits in the synaptic membrane and relationships to long-term spatial memory. *Neuroscience* 162:933–945.
- Zhong JY, Moffat SD (2016) Age-related differences in associative learning of landmarks and heading directions in a virtual navigation task. *Frontiers in aging neuroscience* 8:122.
- Zinyuk L, Kubik S, Kaminsky Y, Fenton AA, Bures J (2000) Understanding hippocampal activity by using purposeful behavior: Place navigation induces place cell discharge in both task-relevant and task-irrelevant spatial reference frames. *PNAS* 97:3771–3776.
- Ziv Y, Burns LD, Cocker ED, Hamel EO, Ghosh KK, Kitch LJ, Gamal AE, Schnitzer MJ (2013) Long-term dynamics of CA1 hippocampal place codes. *Nature Neuroscience* 16:264–266.
- Zugaro MB, Arleo A, Berthoz A, Wiener SI (2003) Rapid spatial reorientation and head direction cells. *The Journal of neuroscience* 23:3478–3482.